TESTING OF FUEL/OXIDIZER-RICH, HIGH-PRESSURE PREBURNERS

AEROJET LIQUID ROCKET CO.
SACRAMENTO, CA

MAY 1982

N82-24353

1. Report No.	2. Government Accession No.	3. Recipient's Catalog No.
NASA CR-165609		

4. Title and Subtitle	5. Report Date
TESTING OF FUEL/OXIDIZER-RICH, HIGH-PRESSURE PREBURNERS	May 1982
	6. Performing Organization Code

7. Author(s)	8. Performing Organization Report No.
B. R. Lawver	
	10. Work Unit No.

9. Performing Organization Name and Address	11. Contract or Grant No.
Aerojet Liquid Rocket Company P.O. Box 13222 Sacramento, California 95813	NAS 3-22647
	13. Type of Report and Period Covered
12. Sponsoring Agency Name and Address	Contractor Report, Final
National Aeronautics and Space Administration Washington, D.C. 20546	14. Sponsoring Agency Code

15. Supplementary Notes

Project Manager, H. Price
NASA-Lewis Research Center
Cleveland, Ohio 44135

16. Abstract

This report presents the results of an evaluation of high-pressure combustion of fuel-rich and oxidizer-rich LOX/RP-1 propellants using 4.0-inch-diameter prototype preburner injectors and chambers. Testing covered a pressure range from 8.9 to 17.5 MN/m^2 (1292 to 2540 psia). Fuel-rich mixture ratios ranged from 0.238 to 0.367; oxidizer-rich mixture ratios ranged from 27.2 to 47.5.

Presented are performance, gas temperature uniformity, and stability data for two fuel-rich and two oxidizer-rich preburner injectors: a conventional like-on-like (LOL) design; the other a platelet design injector.

Kinetically limited combustion is shown by the excellent agreement of measured fuel-rich gas composition and C* performance data with kinetic model predictions. The oxidizer-rich test results support previous equilibrium combustion predictions.

17. Key Words (Suggested by Author(s))	18. Distribution Statement
LOX/RP-1; LOX-Rich; RP-1-Rich; Fuel-Rich Kinetics; Preburners; Gas Composition; Combustion; High Pressure.	Unclassified - Unlimited

19. Security Classif. (of this report)	20. Security Classif. (of this page)	21. No. of Pages	22. Price*
Unclassified	Unclassified	243	

* For sale by the National Technical Information Service, Springfield, Virginia 22161

NASA-C-168 (Rev. 10-75)

FOREWORD

This final report, submitted in fulfillment of Contract NAS 3-22647, document the results of high-pressure testing of fuel-rich and oxidizer-rich preburners using LOX/RP-1 propellants. Presented are fuel-rich test data for chamber pressures from 8.9 to 17.5 MN/m^2 (1292 to 2540 psia) and mixture ratios from 0.238 to 0.367, oxidizer-rich test data for chamber pressures from 12.7 to 17.2 MN/m^2 (1844 to 2497 psia) and mixture ratios from 27.2 to 47.5.

The NASA-Lewis Research Center project manager was H. Price. R. L. Friedman was the ALRC program manager, and B. R. Lawver was the ALRC project engineer.

TABLE OF CONTENTS

LIST OF TABLES

LIST OF FIGURES

LIST OF FIGURES (cont.)

LIST OF FIGURES (cont.)

LIST OF FIGURES (cont.)

LIST OF FIGURES (cont.)

LIST OF FIGURES (cont.)

I. INTRODUCTION

A. BACKGROUND

During the past several years, increasing priority has been given to the development of an economical space transportation system. Numerous NASA-sponsored studies have identified that high-pressure liquid oxygen/hydrocarbon (LOX/HC) booster engines have significant envelope, weight, and payload advantages over current booster systems.

The Advanced High-Pressure Engine Study (Contract NAS 3-19727), conducted by the Aerojet Liquid Rocket Company (ALRC) during 1975-76, resulted in a definition of required technology and engine design criteria for various high-pressure booster LOX/hydrocarbon engine cycles. This study identified the need for both fuel-rich and oxidizer-rich preburners to power their respective flow circuit turbopumps in order to achieve the required pump discharge pressures approaching 48.3 MN/m^2 (7000 psia). To preclude failure, these preburners must deliver thermally uniform flows to the turbine inlets; additionally, they must be designed to have the high life cycle that is required of an economical, reusable advanced booster engine.

Previous development experience has highlighted the need for advanced LOX/hydrocarbon preburner technology. Fuel-rich hydrocarbon preburners have consistently evidenced low combustion efficiency due to nonequilibrium reaction kinetics and carbon deposition that fouls and reduces the efficiency of the gas turbine. Experimental oxidizer-rich preburners have experienced combustion chamber metal wall ignition and reaction in the oxidizing environment due to nonuniform temperature distribution. This test program was undertaken to address these technical issues and to develop a technology base for LOX/HC preburner development.

B. PROGRAM SCOPE

The purpose and scope of this program was to test two fuel-rich and two oxidizer-rich preburner injectors to generate performance, stability and gas temperature uniformity data over a chamber pressure range from 8.9 MN/m^2 to 17.5 MN/m^2 (1292 to 2540 psia). The injectors, chambers, and ancillary hardware were designed and fabricated by ALRC on Contract NAS 3-21753. A kinetically limited Fuel-Rich Combustion Computer Model (FRCM) for predicting the performance of fuel-rich preburners was also developed on that contract.

The specific objective of the fuel-rich testing was to generate fuel-rich performance and carbon deposition data for comparison with the FRCM predictions. The chamber was fitted with instrumentation probes for taking gas samples and measuring gas temperature uniformity. The gas samples were used to define combustion gas composition for verification of the FRCM predictions. Carbon formation data was taken by measuring the pressure drop across a turbine simulator flow device. The fuel-rich testing was planned to cover a mixture ratio range from 0.238 to 0.367.

I, B, Program Scope (cont.)

The specific objective of the oxidizer-rich testing was to demonstrate the feasibility of oxidizer-rich preburners and to obtain performance, stability, and gas temperature uniformity data. The oxidizer-rich testing was planned to cover a mixture ratio range from 27 to 47.

II. SUMMARY

A total of 20 fuel-rich preburner tests were run over the range of operating conditions listed in Table I. Sixty-two (62) data points were obtained by running multiple points during the 14-sec duration tests. Oxidizer and fuel flow control valves were used to vary mixture ratio and chamber pressure. The test results acquired included C* performance, gas temperature uniformity, stability, gas composition, and material compatibility data.

The contract goal was to achieve an Energy Release Efficiency (ERE) of >98% of ODE. Energy release efficiencies (ERE) were found to vary from 62 to 81% of ODE. The measured C* and gas composition data are in accord with predicted values of the Fuel-Rich Combustion Model (FRCM) previously developed on Contract NAS 3-21753, indicating that fuel-rich combustion is both kinetically and vaporization limited. The measured C* varied from 92 to 99% of the FRCM-predicted values for ambient-temperature fuel, indicating that significantly greater C* efficiencies are not achievable. Injector influences, unlike the effects of turbulence rings and contraction ratio, were shown to be minor.

When no turbulence rings were used, the gas temperature uniformity of the platelet injector was found to be better than that of the electrical-discharge-machined (EDM) injector. With use of turbulence rings, equivalent gas temperature uniformities of better than $\pm$ 5.5°K ($\pm$ 10°F) were achieved with both injectors. The contract goal was to achieve a gas temperature uniformity of $\pm$ 27.8°K ($\pm$ 50°F).

Combustion instabilities in the 1st and 2nd longitudinal modes were encountered with use of the platelet injector. These instabilities were effectively damped and controlled by adding turbulence rings and changing combustor length. No high-frequency instabilities were incurred since the injectors had been provided with tuned acoustic resonators.

Gas composition measurements were made and then compared to those predicted with the FRCM. Agreement was excellent, except for the CH_4 and H_2 constituents. A minor modification to one reaction rate constant was required to achieve agreement. The impact on predicted C* performance and gas temperature was small.

Carbon deposition data are inconclusive due to severe erosion of the turbine simulator blades. The cause of the erosion appears to result from chemical attack of the interstitial carbon by the hydrogen-rich ($\sim$20%) exhaust gases. The reaction appears to be aggravated by high gas velocity and unburned fuel droplet impingement. A materials compatibility study needs to be made to define materials acceptable for high-pressure, fuel-rich LOX/HC preburners and turbines.

TABLE I

SUMMARY OF TEST POINTS

FUEL-RICH

INJECTOR:	L' mm (in.)	Turbulence Ring	Igniter MR	Test Duration (sec)	MR	Pc MN/m^2 (psia)	No. Tests	No. Data Points
EDM-LOL	787 (31)	No	3.5	0.5-14	0.25-0.35	13.1-17.2 (1900-2540)	5	15
PLATELET-SWIRLER	787 (31)	No	3.5&40	1-14	0.25-0.35	13.1-17.2 (1900-1500)	3	11
PLATELET-SWIRLER	533 (21)	No	40	14	0.25-0.35	13.1-17.2 (1900-2500)	2	10
PLATELET-SWIRLER	787 (31)	Yes (3.0 in.)	40	14	0.25-0.35	13.1-17.2 (1900-2500)	7	11
EDM-LOL	787 (31)	Yes (3.0 in.)	3.5	14	0.25-0.35	13.1-17.2 (1900-2500)	2	10
EDM-LOL	483 (19)	Yes (3.0 in.)	3.5	14	0.25-0.35	13.1-17.2 (1292-2500)	1	5
				162			20	62
OXIDIZER-RICH								
EDM-LOL	457 (18)	No	40	1	37	13.1 (1900)	1	1
PLATELET-SWIRLER	457 (18)	86 mm (3.4 in.)	40	0.5	37	No Ignition	1	1
PLATELET-SWIRLER	457 (18)	86 mm (3.4 in.)	3.5	0.5	37	12.7 (1840)	1	1
PLATELET-SWIRLER	457 (18)	76 mm (3.0 in.)	1.2	0.5	36	12.9 (1870)	1	1
EDM-LOL	457 (18)	76 mm (3.0 in.)	40	1	48	13.9 (2023)	1	1
EDM-LOL	457 (18)	76 mm (3.0 in.)	40	0.5	35	Delayed Ignition	1	1
EDM-LOL	406 (16)	76 mm (3.0 in.)	1.2	0.5-1	33-28	16.0 (2402)	2	2
							8	8

II, Summary (cont.)

Eight oxidizer-rich tests were completed as listed in Table I, and eight data points were acquired. Due to material compatibility problems, test durations were limited to 1 second. The C* performance data indicate that equilibrium combustion is achieved with oxidizer-rich preburners as had been predicted. C* performances of up to 99% of ODE were achieved. Longitudinal instabilities were incurred but were stabilized with turbulence rings and by shortening the chamber length. Due to failure of the thermocouple rake, gas temperature uniformity could not be measured. Uncoated stainless steel does not appear to be compatible with oxygen-rich gases at these pressures and temperatures, whereas nickel and Rokide-Z-coated nickel were compatible. A materials compatibility study needs to be made to define other metals acceptable for high-pressure, high-velocity oxygen-rich preburner gases.

III. CONCLUSIONS AND RECOMMENDATIONS

Following below is a summary of the conclusions and recommendations to be drawn from the test program.

Conclusions:

- Fuel-rich Energy Release Efficiencies (ERE) of 62-81% of ODE were achieved.
- Fuel-rich ERE is limited by slow fuel decomposition kinetics and vaporization.
- Fuel-rich combustion gas properties and C* performance are predictable with the Fuel-Rich Combustion Model.
- The gas temperature uniformity goal ($\pm$ 27.7°K [$\pm$ 50°F]) is achievable with a low pressure loss turbulence ring -- $\pm$ 5.5°K ($\pm$ 10°F) demonstrated.
- Longer test durations and over a broader mixture ratio range are required to define fuel-rich carbon deposition effects.
- Fuel-rich turbine and main injector simulator erosion is unacceptably high with type of metal used.
- Longitudinal stability with either fuel-rich or oxidizer-rich operation can be achieved with proper turbulence ring design.
- Oxidizer-rich preburner operation is difficult but believed to be feasible with proper material selection and operating conditions.

Recommendations:

- Run fuel-rich tests over broader mixture ratio range to define carbon deposition.
- Conduct long-duration fuel-rich turbopump assembly tests to define carbon deposition.
- Run materials tests to define fuel-rich gas metal erosion mechanism.
- Run material reactivity tests with flowing high-pressure and high-temperature oxygen to define metal ignition temperatures.

IV. TECHNICAL DISCUSSION

This section of the report is organized into four major subsections: (A) Hot-fire Testing; (B) Test Results; (C) Data Analysis; and (D) Fuel-Rich Combustion Model Update.

A. HOT-FIRE TESTING

This subsection of the report describes the test conditions and logic, the test hardware, the test facility, and the test instrumentation used.

1. Test Conditions and Logic

The fuel-rich testing was conducted ahead of the oxidizer-rich testing. It followed the sequence shown in Figure 1. Testing began with igniter checkout and valve sequencing tests, followed by preburner sequencing tests with the EDM injector. The injector screening tests were begun with the EDM injector. Two successful hot firings were made to conclude screening of the EDM injector.

Initial platelet screening tests with a 787-mm (31-in.) length chamber revealed the platelet injector to be unstable in the 1st longitudinal (1L) mode at certain operating conditions. It was mutually agreed upon by ALRC and NASA that three additional tests be run to define the effects of chamber length and turbulence rings on longitudinal stability. The results of these tests show that use of turbulence rings improves the longitudinal stability characteristics. With the installation of the turbulence ring in the 787-mm (31-in.) chamber, the platelet injector was stabilized over the entire operating range.

The platelet injector was mutually selected by ALRC and NASA for the carbon deposition test series. Its selection was made on the basis of its superior gas temperature uniformity without the turbulence ring. It was also agreed that only one heated fuel test rather than two would be run. Five tests, in all, were added, and three tests were deleted. Added funding was provided by NASA for two additional tests with the EDM injector to evaluate chamber length and turbulence ring effects.

The planned and completed fuel-rich test conditions are listed in Table II. Test objectives and hardware used are also included.

The oxidizer-rich testing followed the sequence shown in Figure 2. Oxidizer-rich testing was started with the EDM injector. Three tests were planned, but only one hot firing was completed due to damage caused by a hot-gas leak at the igniter inlet line. The platelet injector was installed, and three hot-firings were made. No ignition occurred on the first test. The igniter mixture ratio was changed from 40 to 3.5 to achieve

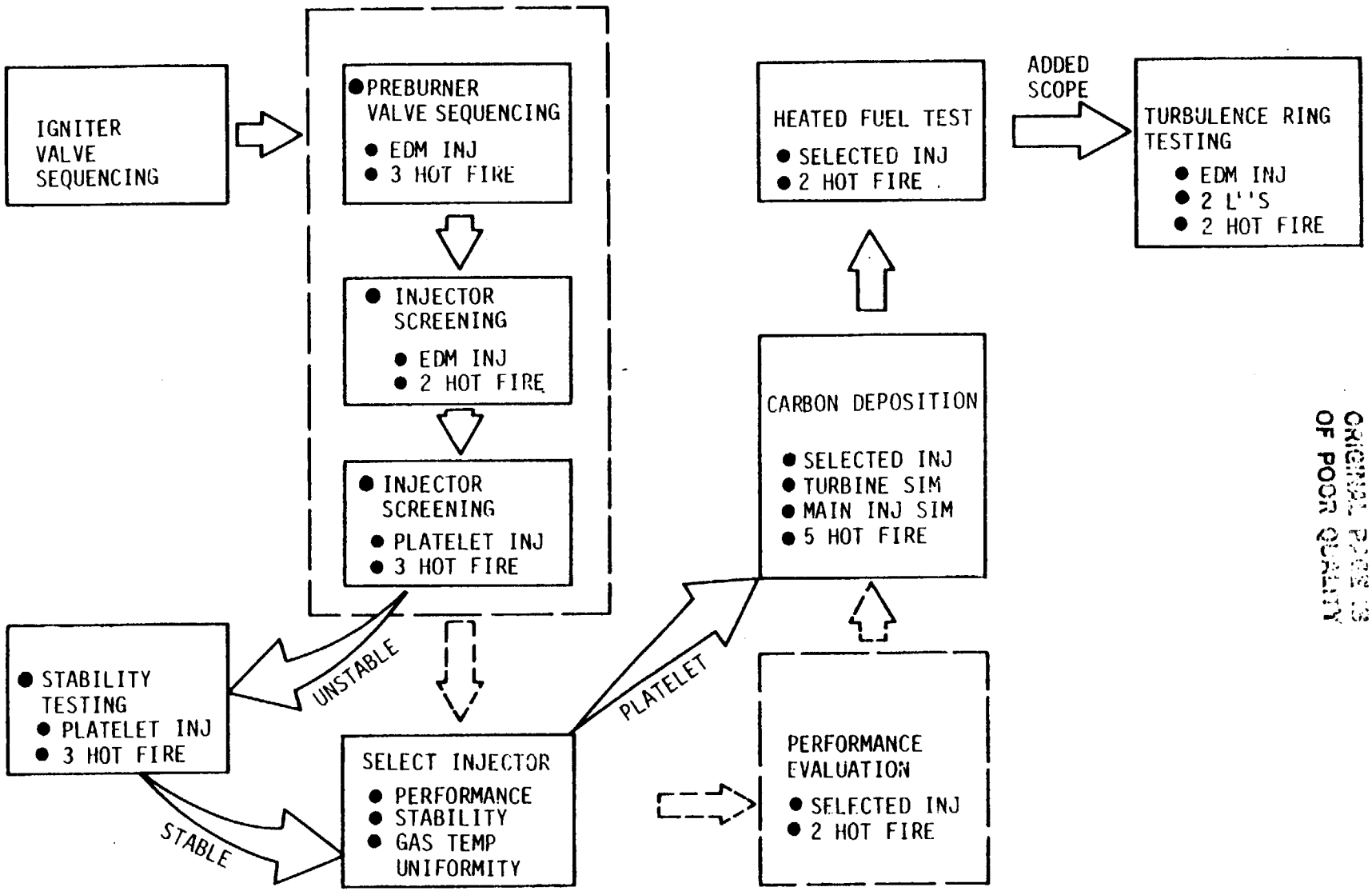

Figure 1. Fuel-Rich Testing Sequence

TABLE II

TEST MATRIX FOR THE FUEL-RICH PREBURNER

Status	Task	Test Objective	Test Points	Duration (sec)	Pc MN/m² (psia)	MR	Injector	Test Hardware: Chamber Sections	Turbulator	Turbine Simul.	Main Inj. Simul.	Instr. Rake	Gas Sample
Complete	III-1	Establish igniter valve sequencing and verify repeatability	4 Cold Flow 3 Hot Fire	0.4	1.7 (250)	3.5	N.A.	Lined 394 mm (15.5 in.) & Unlined 292 mm (11.5 in.)	No	No	No	No	No
Complete	III-2	Determine igniter and preburner valve sequencing for safe startup & shutdown	3	1/2-1	15.2 (2200)	0.3	EDM	Lined 394 mm (15.5 in.) & Unlined 292 mm (11.5 in.)	No	No	No	No	No
Complete		Screen injector for performance & stability	10 (2 firings)	2 1/2 sec/pt	13.1-17.2 (1900-2500)	0.3 ±15%	EDM	Lined 394 mm (15.5 in.) & Unlined 292 mm (11.5 in.)	No	No	No	Yes	Yes (3)
Complete		Checkout start sequence with injector	1	3 sec	15.2 (2200)	0.3	Platelet	Lined 394 mm (15.5 in.) & Unlined 292 mm (11.5 in.)	No	No	No	No	No
Complete		Screen injector for performance & stability	10 (2 firings)	2 1/2 sec/pt	13.1-17.2 (1900-2500)	0.3 ±15%	Platelet	Lined 394 mm (15.5 in.) & Unlined 292 mm (11.5 in.)	No	No	No	Yes	Yes (3)
Deleted	III-3	Checkout test	1	1.5	15.2 (2200)	0.3	Platelet	TBD	TBD	No	No	No	No
Deleted		Evaluate performance and temperature uniformity	5 (1 firing)	2 1/2 sec/pt	13.1-17.2 (1900-2500)	0.3 ±15%	Platelet	TBD	TBD	No	No	Yes	Yes (1)
Complete	III-4	Evaluate the effects of carbon deposition on turbine blades & main injector	5 (5 firings)	14	13.1-17.2 (1900-2500)	0.3 ±15%	Platelet	Lined 394 mm (15.5 in.) & Unlined 292 mm (11.5 in.) & Lined 292 mm (11.5 in.)	Yes	Yes	Yes	Yes	Yes (5)
Complete (1 test deleted)	III-5	Evaluate the effect of heated fuel on performance and carbon formation & deposition	1 (2 planned)	14	15.2 (2200)	0.3	Platelet	Lined 394 mm (15.5 in.) & Unlined 292 mm (11.5 in.) & Lined 292 mm (11.5 in.)	Yes	Yes	Yes	Yes	Yes (1)

TABLE II (cont.)

Status	Task	Test Objective	Test Points	Duration (sec)	Pc MN/m^2 (psia)	MR	Injector	Test Hardware: Chamber Sections	Turbulator	Turbine Simul.	Main Inj. Simul.	Instr. Rake	Gas Sample
ADDED SCOPE TESTING													
Complete	III-2A	Determine effect of short chamber on stability	5 (1 firing)	2 1/2 sec/pt	13.1-17.2 (1900-2500)	0.3 ·15	Platelet	Lined 394 mm (15.5 in.)	No	No	No	Yes	Yes (1)
Complete	III-2B	Determine effect of turbulence ring on stability	5 (1 firing)	2 1/2 sec/pt	13.1-17.2 (1900-2500)	0.3 · 15	Platelet	Lined 394 mm (15.5 in.)	Yes	No	No	Yes	Yes (1)
Complete	III-2C	Determine effect of chamber length on stability with turbulence ring	5 (1 firing)	2 1/2 sec/pt	13.1-17.2 (1900-2500)	0.3 ·15	Platelet	Lined 394 mm (15.5 in.) & Unlined 292 mm (11.5 in.)	Yes	No	No	Yes	Yes (1)
Complete	III-6A	Evaluate effect of turbulence ring on temp. uniformity & stability	5 (1 firing)	2 1/2 sec/pt	13.1-17.2 (1900-2500)	0.3 ·15	EDM	Lined 394 mm (15.5 in.) & Unlined 292 mm (11.5 in.)	Yes	No	No	Yes	No
Complete	III-6B	Evaluate effect of turbulence ring on temp. uniformity & stability	5 (1 firing)	2 1/2 sec/pt	13.1-17.2 (1900-2500)	0.3 ·15	EDM	Lined 394 mm (15.5 in.)	Yes	No	No	Yes	No

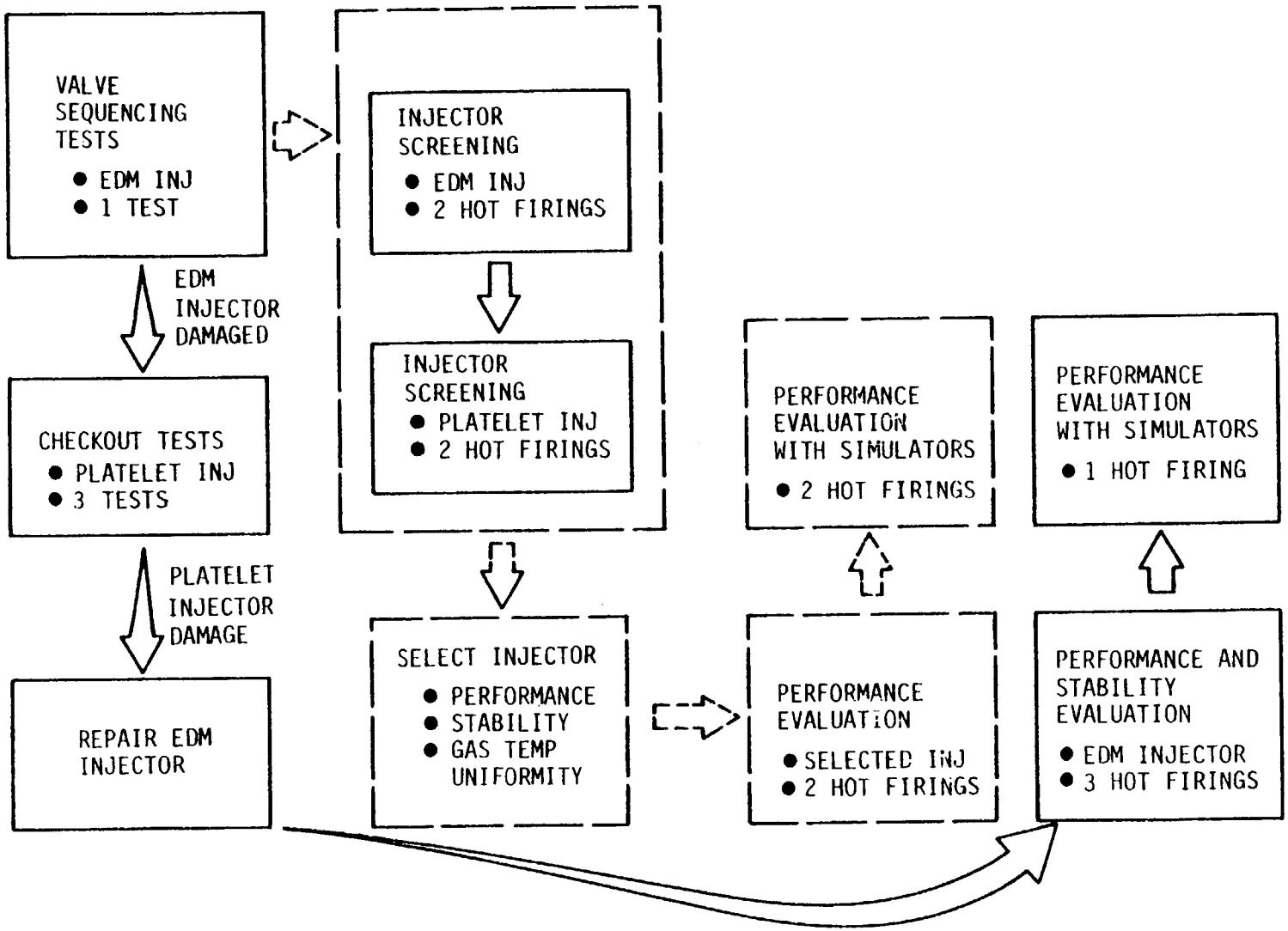

Figure 2. Oxidizer-Rich Testing Sequence

ignition on the second test. The injector suffered internal manifold damage on the third test due to a hard start. It was mutually agreed upon by NASA and ALRC to repair the EDM injector and attempt to complete the planned testing. NASA provided the added funding necessary to make the injector repairs.

Three hot-firings were made to check out the performance and stability. The first hot-fire test was unstable in the 1L mode, causing some minor damage to the injector face. After the injector had been repaired on the stand, a second firing was made with a shorter chamber at high Pc and low MR. A delayed ignition occurred on this test, and no data were acquired. The third test was stable and high-performing.

A final firing was made after the turbine simulator and instrumentation rakes had been installed. The rakes failed on start and precipitated failure of the turbine simulator and nozzle; consequently, no valid temperature rake data were obtained. Of the nine oxidizer-rich firings planned, eight were accomplished. The planned and completed oxidizer-rich test conditions are listed in Table III.

2. Test Hardware

The fuel-rich and oxidizer-rich test hardware was designed and fabricated by ALRC on Contract NAS 3-21753. The hardware includes the components listed in Table IV. Since complete and detailed dimensional descriptions are provided in the final report for Contract NAS 3-21753, only functional descriptions are provided herein.

A preburner assembly schematic is shown in Figure 3 to illustrate component assembly. The major components include igniter, injector assembly, acoustic resonator ring, lined and unlined chamber segments, turbulence rings, chamber liners, instrumentation rakes, turbine simulators, main injector simulators, and nozzle throat flanges and reducers. All of the hardware is interchangeable between fuel-rich and oxidizer-rich assemblies, with the exception of injectors, turbine simulator blades, main injector simulators, and nozzle throat flanges and reducers.

This hardware permits a complete simulation of the preburner gas flow path from preburner injector to main combustor injector. The relative positions of all components downstream of the resonator flange are mechanically interchangeable for test versatility. Components can be omitted or interchanged as desired. Photographs of a preburner assembly and components are shown in Figure 4 to illustrate component design features.

TABLE III

TEST MATRIX FOR THE OXIDIZER-RICH PREBURNER

Status	Task	Test Objective	Test Points	Duration (sec)	Pc MN/m^2 (psia)	MR	Injector	Test Hardware: Chamber Sections	Turbulator	Turbine Simul.	Main Injector Simul.	Instr. Rake
1 Firing	IV-1	Evaluate valve sequencing	3	1/2-1	15.2 (2200)	40	EDM	Lined 394 mm (15.5 in.)	No	No	No	No
3 Firings completed w/o rake	IV-2	Screen EDM injector for performance & temperature uniformity	10 (2 firings)	2 sec/pt	13.1-17.2 (1900-2500)	35-45	EDM	Lined 394 mm (15.5 in.)	No	No	No	Yes
3 Firings completed w/o rake		Screen platelet injector for performance & temperature uniformity	10 (2 firings)	2 sec/pt	13.1-17.2 (1900-2500)	35-45	Platelet	Lined 394 mm (15.5 in.)	No	No	No	Yes
N/A	IV-3	Checkout Test	1	1	15.2 (2200)	40	TBD	TBD	TBD	No	No	No
1 Firing Attempted		Evaluate performance and gas temperature uniformity	5 (1 firing)	2 sec/pt	13.1-17.2 (1900-2500)	35-45	TBD	TBD	TBD	No	No	Yes
N/A	IV-4	Checkout Test	1	1	15.2 (2200)	40	TBD	TBD	TBD	Yes	Yes	No
1 Firing completed		Evaluate performance with simulators installed	3 (1 firing)	12	13.1-17.2 (1900-2000)	TBD	TBD	TBD	TBD	Yes	Yes	Yes
8 Firings completed			9 firings planned									

TABLE IV

PREBURNER PARTS LIST

	ITEM	PART NO.	NO.
1.	Injector Manifold Assembly	1191404	2
2.	Oxidizer-Rich Injector Assembly (Platelet)	1191403-29	1
3.	Fuel-Rich Injector Assembly (Platelet)	1191403-39	1
4.	Oxidizer-Rich Injector Assembly (EDM)	1193105-19	1
5.	Fuel-Rich Injector Assembly (EDM)	1193105-9	1
6.	Lined Chamber 292 mm (11.5 in.)	1191401-9	1
7.	Lined Chamber 394 mm (15.5 in.)	1191401-29	1
8.	Unlined Chamber 292 mm (11.5 in.)	1191401-19	1
9.	Unlined Chamber 394 mm (15.5 in.)	1191401-39	1
10.	Instrumentation Rake Assembly	1191411-19	1 + Two extra probes
11.	Oxidizer-Rich Turbine Simulator	1191521-9	1
12.	Fuel-Rich Turbine Simulator	1191521-19	1
13.	Igniter Assembly	1191522	2
14.	Oxidizer Throat	1191402-2	1
15.	Fuel Throat	1191402-1	1
16.	Oxidizer Main Injector Simulator	1191402-11	1
17.	Fuel Main Injector Simulator	1191402-10	1
18.	Injector Simulator Flange	1191402-8	1
19.	Resonator Flange	1191402-3	1
20.	Resonator Cavity	1191402-4	1
21.	Throat Reducer	None	2
22.	Turbulence Ring	None	2

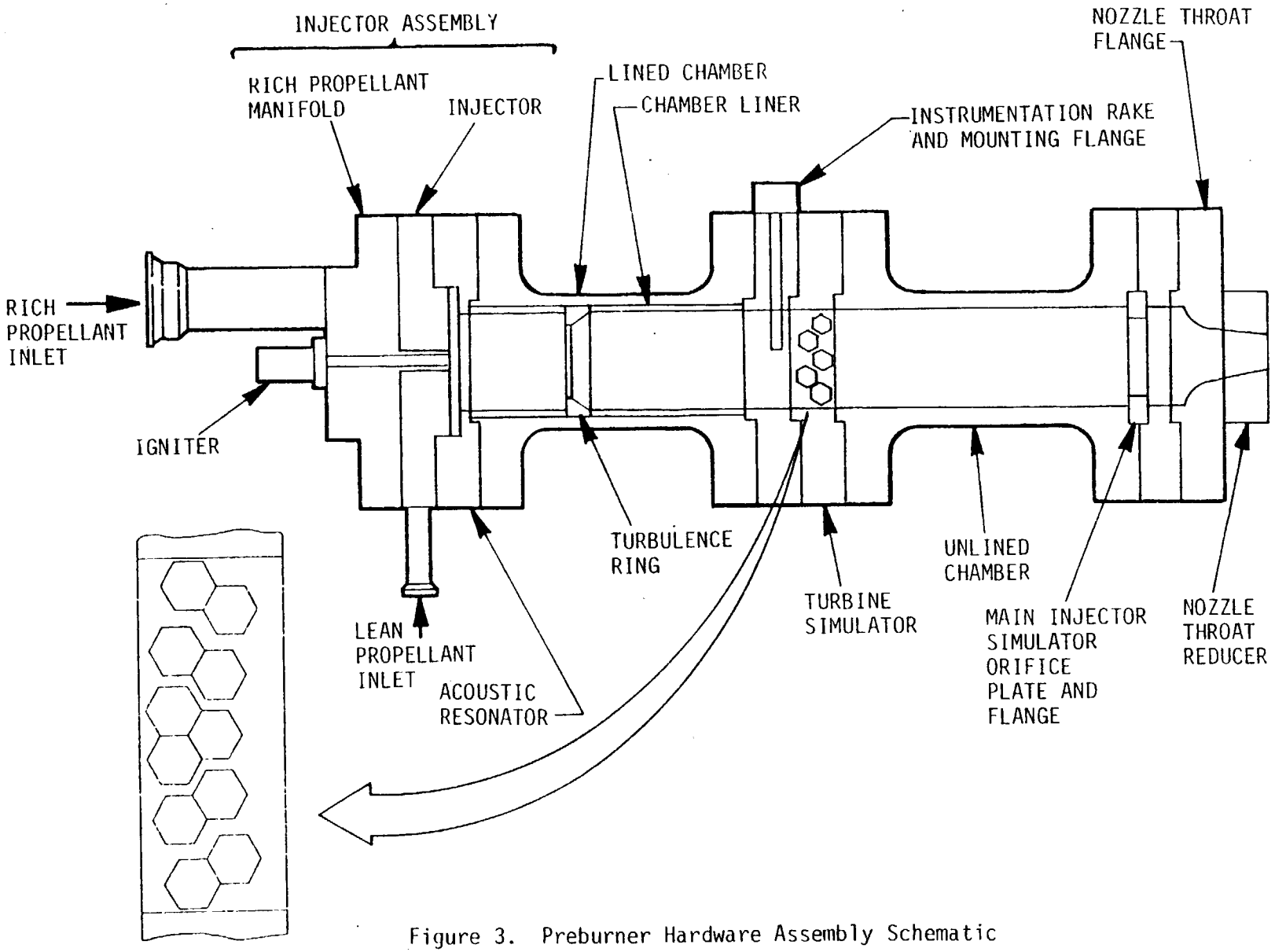

Figure 3. Preburner Hardware Assembly Schematic

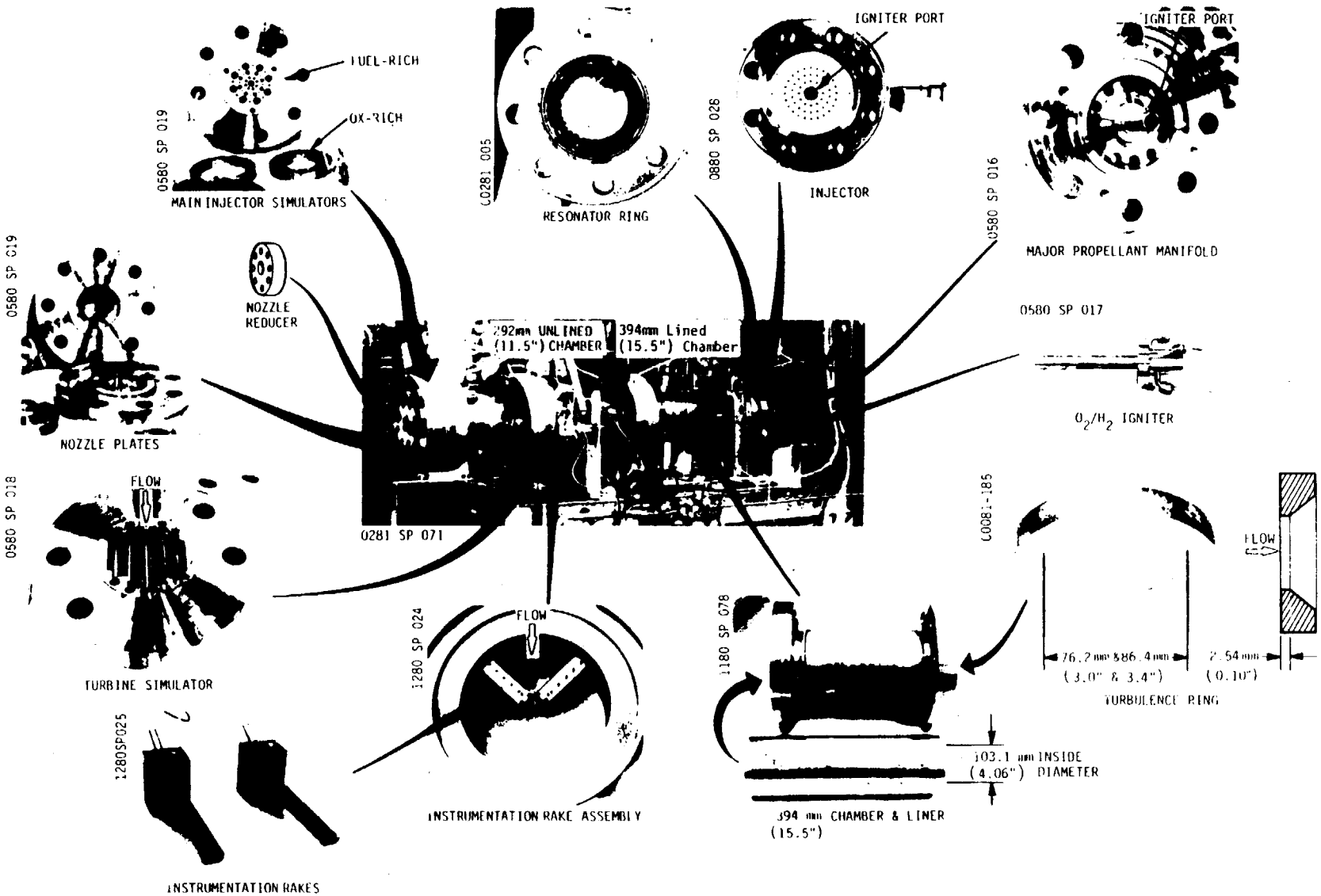

Figure 4. Preburner Assembly and Component Features

Igniter

The igniter is a spark-ignited GO_2/GH_2 torch igniter. The uncooled copper torch chamber has a limited firing duration of 0.400 seconds. The igniter can be fired either fuel-rich or oxidizer-rich by proper orificing of the inlets. The design and operating conditions for the igniter are summarized in Table V.

Injectors

Two platelet swirler coaxial element injectors and two EDM Like-On-Like (LOL) element injectors were tested. The injector design conditions are listed in Table VI. The predicted and measured hydraulic characteristics are listed in Table VII.

The platelet swirler injectors are shown in Figure 5 along with their design and operating characteristics. These injectors produce concentric cones of rich and lean propellant. As illustrated in Figure 5, the lean propellant is shrouded by the larger cone of the rich propellant.

The EDM LOL injectors are shown in Figure 6. These injectors atomize the rich propellant with self-impinging like-on-like (LOL) elements to form spray fans. As illustrated in the figure, the lean propellants are injected through small showerhead elements between the fans.

Acoustic Resonator

The acoustic resonator used is a radial inlet quarterwave tube design with 12 equally spaced cavities. Tuning blocks provide adjustable cavity depths. Cavity depths of 17 and 11 mm (0.65 and 0.45 in.) were used for the fuel-rich and oxidizer-rich tests, respectively.

Combustion Chamber Segments

Two sets of chamber segments were provided: one set without and one set with nickel liners. The nickel liners were flame-sprayed with Rokide Z coatings prior to the oxidizer-rich testing. Each chamber set has one 292-mm (11.5-in.) and one 394-mm (15.5-in.) long chamber. The lined chambers are provided with ports for mounting Kistler transducers and/or thermocouple plugs. The chambers are assembled to the other components with studs and nuts.

Turbine Simulator

One turbine simulator flange and two sets of blades were provided. The turbine simulator blade spacings are adjustable with spacers

TABLE V

GO_2/GH_2 IGNITER SPECIFICATIONS

	Fuel-Rich	Ox-Rich
Oxidizer Flowrate	31.75 g/s (0.070 lb/sec)	100.9 g/s (0.220 lb/sec)
Fuel Flowrate	9.07 g/s (0.020 lb/sec)	2.5 g/s (0.0055 lb/sec)
Mixture Ratio	3.5	40
Chamber Pressure	3.1 MN/m^2 (450 psia)	3.1 MN/m^2 (450 psia)
Oxidizer Orifice Inlet Pressure	16.5 MN/m^2 (2400 psia)	16.5 MN/m^2 (2400 psia)
Fuel Orifice Inlet Pressure	17.2 MN/m^2 (2500 psia)	17.2 MN/m^2 (2500 psia)
Spark Voltage	40,000 volts	
Spark Energy	30 millijoules	
Spark Rate	500 spks/sec	
Maximum Firing Duration	0.400 sec	

TABLE VI

PREBURNER DESIGN CONDITIONS

Parameter	Fuel-Rich	Oxidizer-Rich
Chamber Pressure	15.2 MN/m^2 (2200 psia)	15.2 MN/m^2 (2200 psia)
Mixture Ratio	0.30	40
Performance	>98% ERE	
Combustion Length	292-686 mm (11.5-27 inches)	
Effluent Gas		
Temperature	921-1088°K (1200-1500°F)	
Temperature Uniformity	± 27.7°K (± 50°F)	
Combustion Pressure		
Stability	< ± 5% Pc Variation	
Total Propellant Flow	16.8 kg/s (37 lb/sec)	39.9 kg/s (88 lb/sec)

TABLE VII

INJECTOR HYDRAULIC CHARACTERISTICS

Injector	Injector Admittance - kg/s - $kN/m^2)^{1/2}$ ($KW\ lb/sec\text{-}psi^{1/2}$) Predicted	Cold Flow	Hot Fire
Fuel-Rich EDM LOL-Fuel	0.304 (1.76)	0.314 (1.82)	0.311 (1.80)
Fuel-Rich EDM LOL-Ox	0.056 (0.326)	0.052 (0.300)	0.060 (0.350)
Fuel-Rich Platelet Swirler - Fuel	0.314 (1.82)	0.309 (1.79)	0.311 (1.80)
Fuel-Rich Platelet Swirler - Ox	0.080 (0.461)	0.068 (0.395)	0.068 (0.395)
Ox-Rich EDM LOL - Fuel	0.015 (0.089)	0.015 (0.088)	0.017 (0.098)
Ox-Rich EDM LOL-Ox	0.689 (3.99)	0.691 (4.0)	0.657 (3.80)
Ox-Rich Platelet Swirler - Fuel	0.024 (0.137)	0.020 (0.117)	0.023 (0.133)
Ox-Rich Platelet Swirler - Ox	0.805 (4.66)	0.645 (3.73)	0.677 (3.92)

0880 SP 328

FUEL-RICH PLATELET CONCENTRIC VORTEX INJECTOR

$\dot{w}_o$ = 3.86 kg/s (8.5 LB/SEC)

$\dot{w}_f$ = 12.93 kg/s (28.5 LB/SEC)

P_o = 2.83 MN/m^2 (410 PSIA)

P_f = 2.16 MN/m^2 (313 PSIA)

Kw_o = 0.395

Kw_f = 1.79

54 ELEMENTS

0480 SP 045

OXIDIZER-RICH PLATELET CONCENTRIC VORTEX INJECTOR FACE

$\dot{w}_o$ = 38.92 kg/s (85.8 LB/SEC)

$\dot{w}_f$ = 0.97 kg/s (2.14 LB/SEC)

P_o = 3.23 MN/m^2 (468 PSIA)

P_f = 2.85 MN/m^2 (413 PSIA)

Kw_o = 3.73

Kw_f = 0.117

54 ELEMENTS

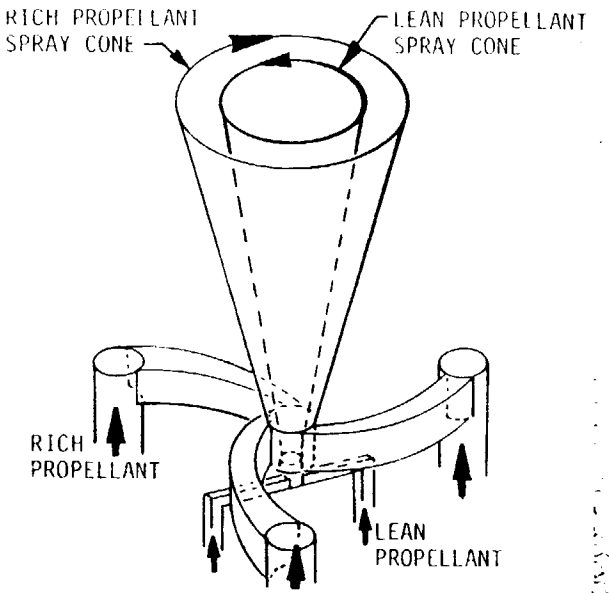

0680 SP 065

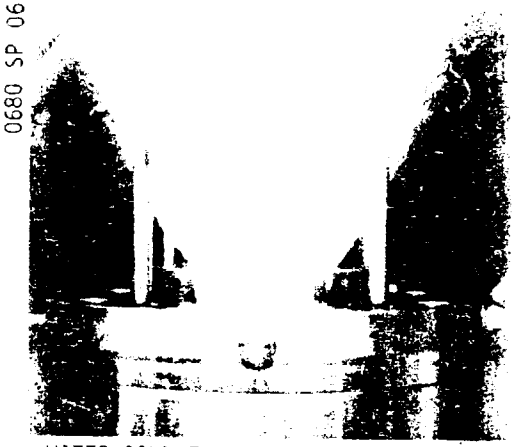

WATER COLD FLOW FUEL-RICH PLATELET CONCENTRIC VORTEX INJECTOR

Figure 5. Platelet Swirler Injectors

C1180 001

$\dot{W}_o$ = 3.86 kg/s (8.5 lb/sec)

$\dot{W}_f$ = 12.93 dg/s (28.5 lb/sec)

ΔP_o = 4.90 Mn/m^2 (710 psia)

ΔP_f = 2.08 Mn/m^2 (302 psia)

KW_o = 0.300

KW_f = 1.82

D_o = 1.016 mm (0.040")

D_f = 1.422 mm (0.056")

80 ELEMENTS

FUEL-RICH EDM LOL INJECTOR FACE PLATE

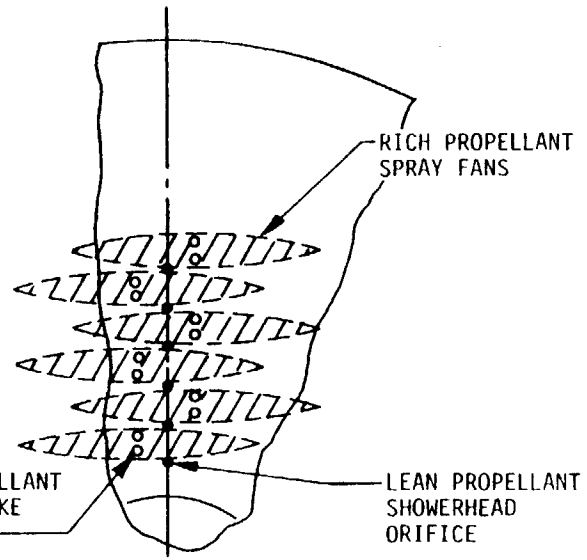

0381 SP 024

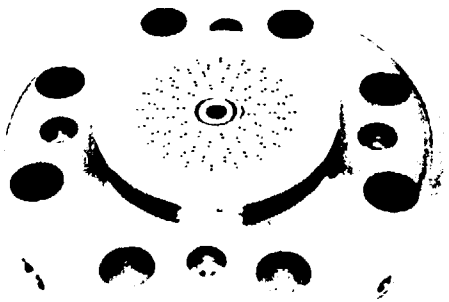

$\dot{W}_o$ = 38.92 kg/s (85.8 lb/sec)

$\dot{W}_f$ = 0.97 kg/s (2.14 lb/sec)

ΔP_o = 2.81 Mn/m^2 (407 psia)

ΔP_f = 5.03 Mn/m^2 (730 psia)

KW_o = 4.0

KW_f = 0.088

D_o = 2.286 mm (0.090")

D_f = 0.559 mm (0.022")

70 ELEMENTS

OX-RICH EDM LOL INJECTOR

480 SP 038

WATER COLD FLOW FUEL-RICH LOL INJECTOR

Figure 6. EDM Like-on-Like Injectors

under the blades to permit control of the simulator pressure drop. Using data obtained from GN_2 cold flow, both the fuel-rich and oxidizer-rich blades were adjusted prior to hot firing to provide the desired pressure drops. The oxidizer-rich blades were sprayed with a Rokide Z coating prior to testing.

Main Injector Simulators

Two main injector simulators and one simulator flange were provided. The fuel-rich main injector simulator consists of a flat plate with various size drilled orifices. The intent of the simulator is to represent the pressure drop of the main combustor injector and to evaluate the effects of carbon deposition and erosion on the inlet of main injector orifices. The oxidizer-rich main injector simulator is a flat plate with a single orifice to simulate pressure drop.

Turbulence Rings

Two turbulence rings were provided to improve gas-phase mixing and gas temperature uniformity. One has an orifice diameter of 76 mm (3.0 in.); the other an orifice diameter of 86 mm (3.4 in.). These rings were flame-sprayed with Rokide Z coatings prior to oxidizer-rich testing.

Nozzle Throat Flanges and Reducers

Two nozzle throat flanges and two nozzle throat reducers were provided for achieving the desired chamber pressures. The nozzle throat reducer is used for performance testing prior to insertion of the turbine and main injector simulators. The oxidizer-rich nozzle throat flange and throat reducer were flame-sprayed with Rokide Z coatings.

Instrumentation Rakes

Four instrumentation rakes and one mounting flange were provided. Two of the rakes are mounted as shown in Figure 4; the other two are spares. Each rake contains two (2) gas sample ports and five (5) thermocouple probes. The gas sample ports are manifolded together as described in Section IV.A.4. The gas temperature probe design is shown in Figure 7.

3. Test Facility

The testing was conducted on ALRC test stand J-1A, shown in Figure 8. A schematic of the test setup is shown in Figure 9. The propellants are fed from high-pressure intensifiers through flow control valves. The flow control valves are throttled during the test to permit multiple

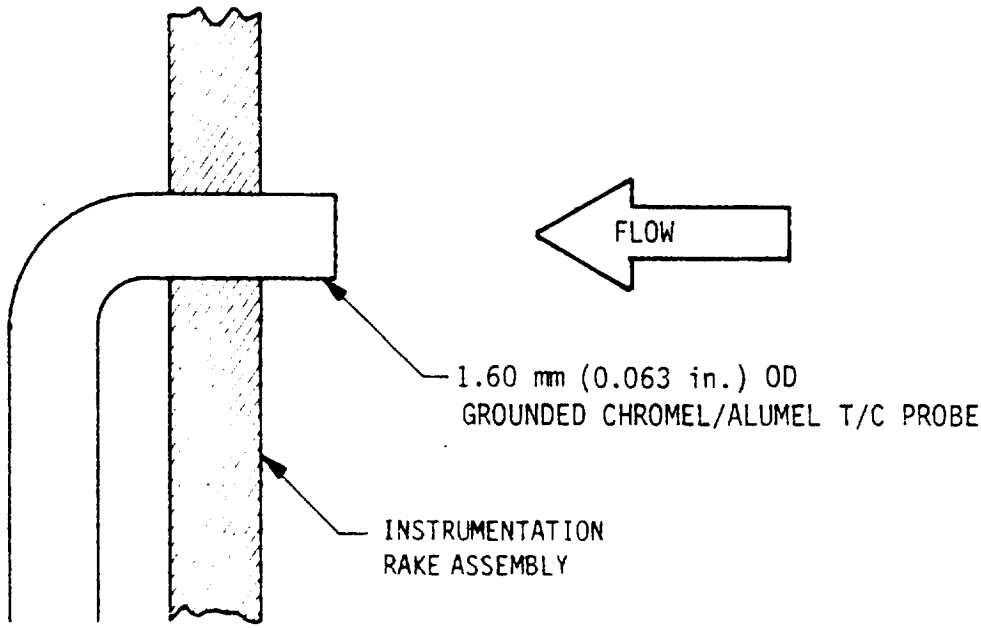

Figure 7. Gas Temperature Probe design

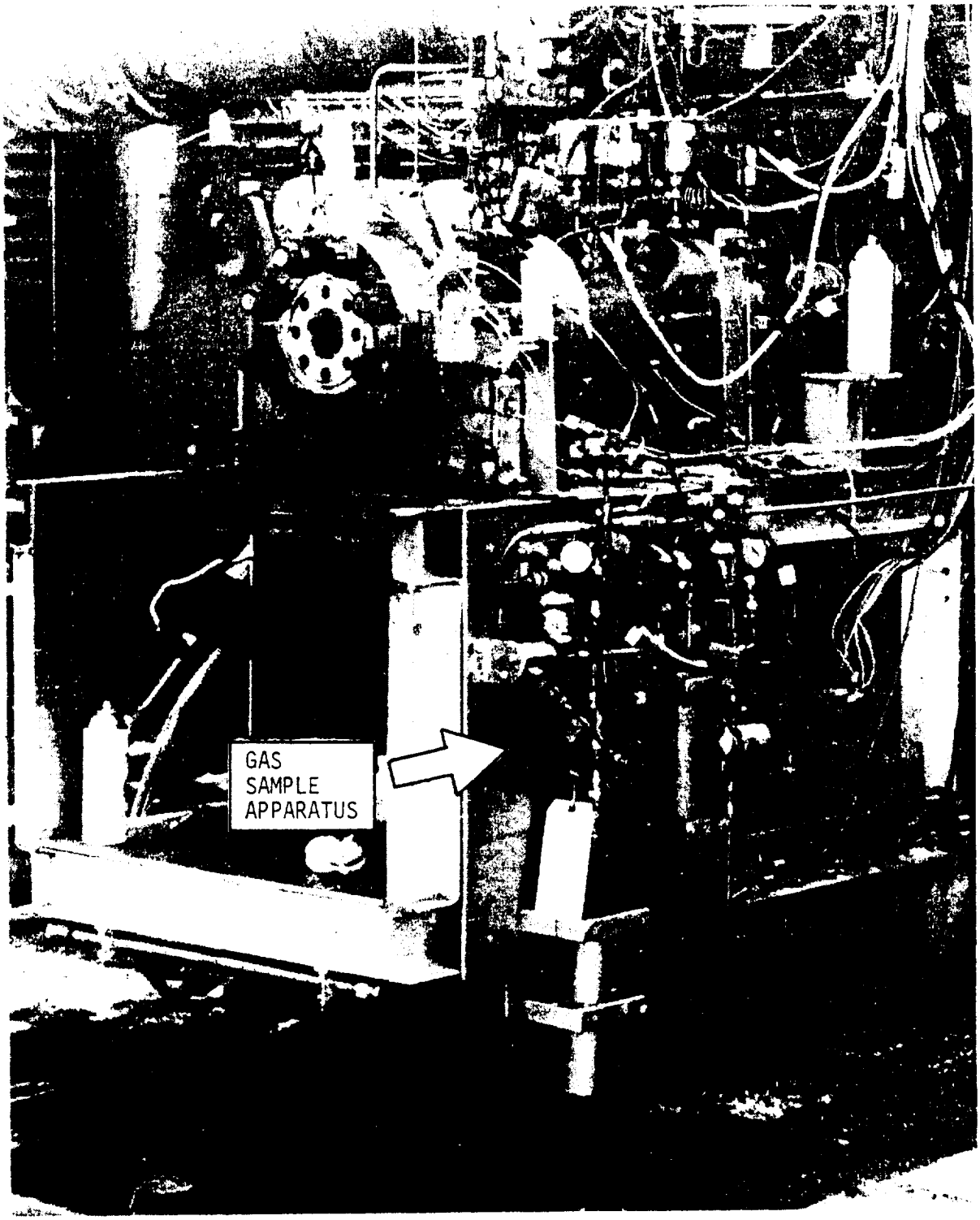

Figure 8. Fuel-Rich Preburner Test Setup - J-1A Test Stand

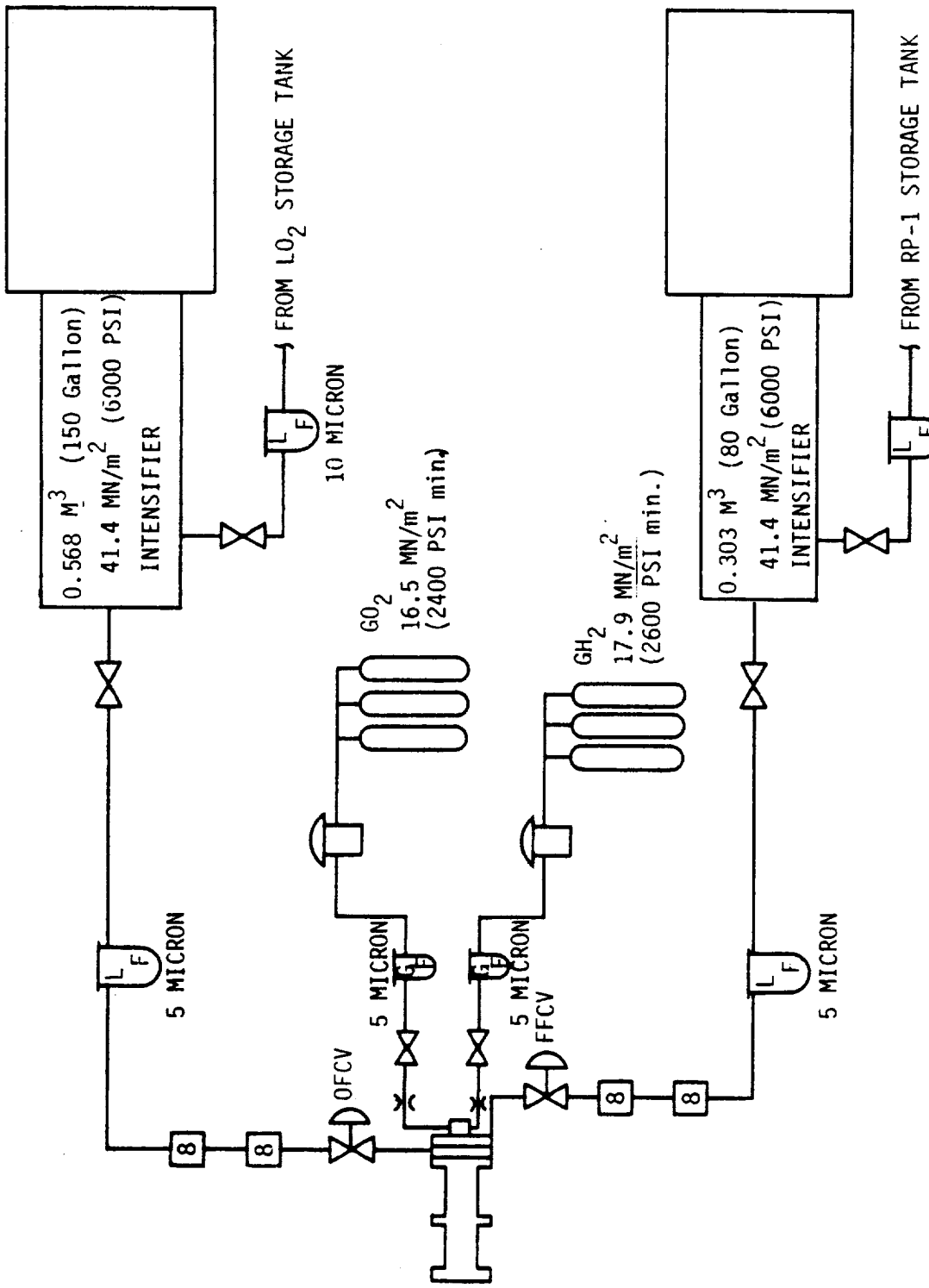

Figure 9. J-1A Preburner Test Setup Schematic

MR/Pc test points. The oxygen and the RP-1 are supplied from a .568 M^3 (150-gallon) and a .303 M^3 (80-gallon) intensifier, respectively. The propellants are passed through 10 micron filters before entering the intensifiers. 5 micron filters are used upstream of the flowmeter. Dual flowmeters are used to ensure flow measurement accuracy.

4. Instrumentation and Measurement Methods

Both preburners were instrumented to measure C* performance, stability, and gas temperature uniformity. The fuel-rich preburner was also instrumented to measure preburner gas compositions and turbine simulator carbon deposition. Instrumentation probe locations for the fuel-rich preburner are shown in Figure 10. A complete list of measured parameters is shown in Table VIII.

C* Measurement

The measured C* was determined from the following equation:

$$C^*_{meas} = Pc\ C_D\ A_t\ g/W_T$$

where:

Pc = Throat stagnation pressure (N/m^2 [$lb/in.^2$])

C_D = Nozzle discharge coefficient

A_t = Throat area (mm^2 [$in.^2$])

g = Gravitational constant (m/s^2 [ft/sec^2])

W_T = Total weight (g/s [lb/sec])

The injector face pressure (Pc-1) was used when no turbulence rings or turbine simulators were installed. The pressure downstream of the turbulence ring (Pc-2) was used when applicable. The pressure at the nozzle inlet (Pc-4) was used when the turbine simulator and main injector simulator were installed. The measured pressures were taken to be the throat stagnation pressure since the static-to-stagnation-pressure correction factor is small (1.005% for the fuel-rich preburner, and 1.020% for the oxidizer-rich preburner).

The nozzle discharge coefficients were determined by cold-flow test to be 0.99. The total flowrate is the sum of the measured oxidizer and fuel flowrates. To determine the fuel and oxidizer flowrates, the average of two series flowmeters was used. The throat area was determined by taking the average of six post-test throat diameter measurements.

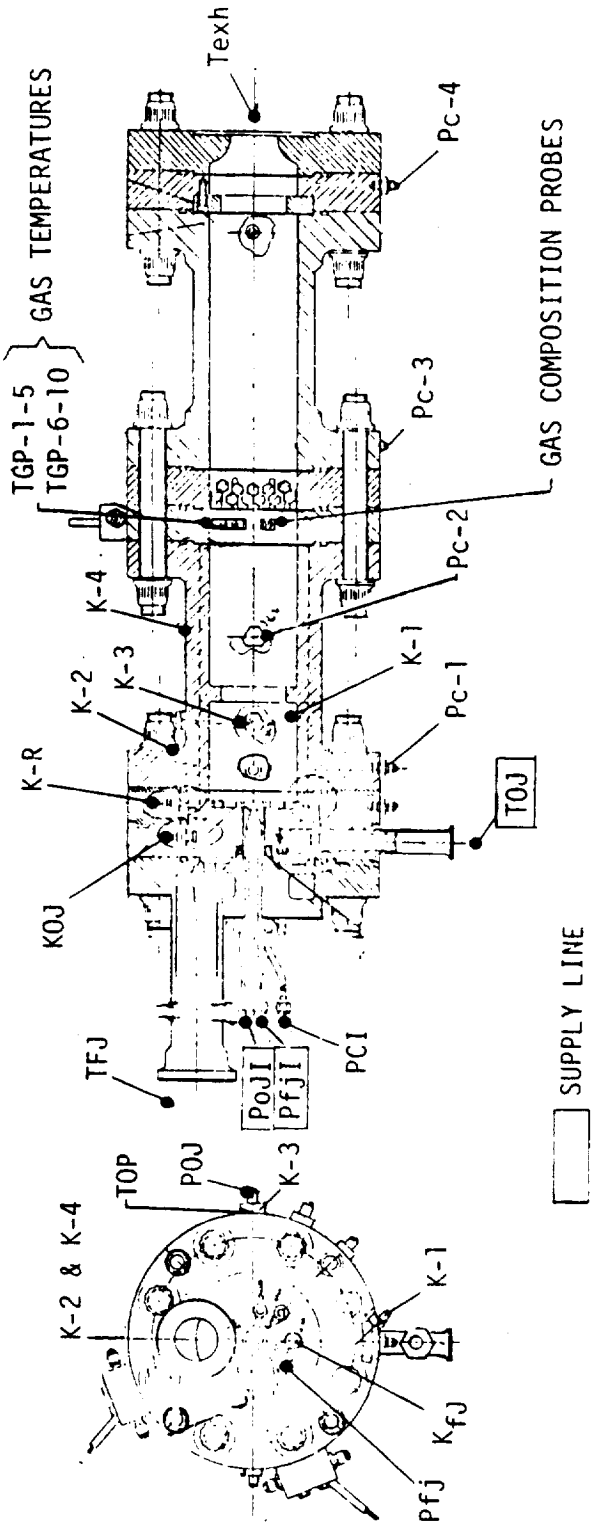

Figure 10. Instrumentation Locations

TABLE VIII

INSTRUMENTATION LIST

Parameter	Symbol	Units	Range	Recording: Digital	Recording: O'Graph R_1	Recording: O'Graph R_2	Recording: FM
PREBURNER							
Ox Valve Position	LOV	in.	0-100%	X	X		
Fuel Valve Position	LFV	in.	0-100%	X	X		
Ox Pilot Valve Current	IOV	Amps	S/T		X		
Fuel Pilot Valve Current	IFV	Amps	S/T		X		
Ox Flowrate	FMO-1	kg/s (lb/sec)	5.44 (0-12)	X		X	
	FMO-2	kg/s (lb/sec)	5.44 (0-12)	X		X	
Fuel Flowrate	FMF-1	kg/s (lb/sec)	15.88 (0-35)	X		X	
	FMF-2	kg/s (lb/sec)	15.88 (0-35)	X		X	
Ox Flowmeter Press.	PoFM	MN/m^2 (psia)	24.1 (0-3500)	X			
Fuel Flowmeter Press.	PFFM	MN/m^2 (psia)	24.1 (0-3500)	X			
Ox Flowmeter Temp.	ToFM	°C (°F)	-160 + -3.9 (-320 + 25)	(2)			
Fuel Flowmeter Temp.	TFFM	°C (°F)	38 (0-100)	X			
Chamber Pressure	PC-1	MN/m^2 (psia)	17.2 (0-2500)	X	X	X	X
Chamber Pressure	PC-2	MN/m^2 (psia)	17.2 (0-2500)	X	X		
Ox Injector Manifold Press.	PoJ	MN/m^2 (psia)	24.1 (0-3500)	X		X	
Fuel Injector Manifold Press.	PfJ	MN/m^2 (psia)	24.1 (0-3500)	X		X	
Ox Injector Manifold Temp.	ToJ	°C (°F)	-160 to 38 (-320 to +100)	X			
Fuel Injector Inlet Temp.	TfJ	°C (°F)	204 (0-400)	X			
Turbine Discharge Press.	PC-3	MN/m^2 (psia)	17.2 (0-2500)	X		X	
Main Chamber Press.	PC-4	MN/m^2 (psia)	17.2 (0-2500)	X		X	
Ox Manifold Kistler	KOJ	MN/m^2 (psia)	0.69 (0-100) PK-PK		•		X(A/C Only)
Resonator Kistler	K-R	MN/m^2 (psia)	0.69 (0-100) PK-PK				X(A/C Only)
Chamber Kistler (He Bleed)	K-1,4	MN/m^2 (psia)	0.69 (0-100) PK-PK				(4) (A/C Only)
Gas Probe Temp.	TGP-1,10	°C (°F)	1371 (0-2500)	(10)			
Chamber Wall Temp.	TCW-1,4	°C (°F)	1371 (0-2500)	(4)			
Gas Sample Valve Current	EGSV	Amps	S/T		X		
Gas Sample Purge Valve Current	EGSPV	Amps	S/T		X		
Gas Sample Pressure	PGS	MN/m^2 (psia)	17.2 (0-2500)	X			
Turbine Simulator Press. Drop	DPTS	MN/m^2 (psid)	6.9 (0-1000)	X	(PC-1-PC-2)		
Exhaust Gas Temp.	TEXH	°C (°F)	1371 (0-2500)	X		X	
Mainstage Injector Simulator Press. Drop	DPMS	MN/m^2 (psid)	6.9 (0-1000)	X	(PC-2-PC-3)		
Gas Sample Temp.	TGS	°C (°F)	1371 (0-2500)	X	X		
Ox Purge Valve Current	IOPV	Amps	S/T		X		
Fuel Purge Valve Current	IFPV	Amps	S/T		X		
IGNITER							
Ox Igniter Pilot Valve Current	IOIV	Amps	S/T		X		
Fuel Igniter Pilot Valve Current	IFIV	Amps	S/T		X		
Ox Igniter Valve Position	LOIV	In.	0-100%		X		
Fuel Igniter Valve Position	LFIV	In.	0-100%		X		
Spark Trace	SPK	N/A	N/A			X	
Ox Orifice Inlet Pressure	POIV	MN/m^2 (psia)	20.7 (0-3000)	X			
Fuel Orifice Inlet Pressure	PFIV	MN/m^2 (psia)	27.6 (0-4000)	X			
Igniter Chamber Pressure	PCI	MN/m^2 (psia)	20.7 (0-3000)	X	X	X	
Ox Igniter Injector Press.	POJI	MN/m^2 (psia)	20.7 (0-3000)	X		X	
Fuel Igniter Injector Press.	PFJI	MN/m^2 (psia)	27.6 (0-4000)	X		X	

Stability

Combustion stability was determined by using helium bleed Kistler pressure transducers. The Model 614A Kistlers are mounted in adaptors as shown in Figure 11. This mounting with helium bleed provides thermal compatibility and a flat frequency response of about 10,000 Hz. After being recorded on magnetic tape, the transducer output is examined for stability by playing it back on an oscillograph at a 16/1 speed reduction. The output is also fed through a Combustion Stability Monitor (CSM) for automatic engine shutdown. The shutdown limits were set as follows:

Frequency	> 1,000 Hz
Amplitude	> 10% of Pc, PK-PK
Duration	> 30 ms

No CSM shutdown occurred since the observed instabilities were longitudinal modes with frequencies of 600 to 700 Hz.

Gas Temperature Uniformity

The gas temperature uniformity was measured by using the instrumentation rakes shown in Figure 12. Two rakes with five probes each were used to measure radial gas temperature profiles and define gas temperature uniformity.

Gas Composition Measurement

The gas composition was measured by using the gas sample probes shown in Figure 12. These probes were plumbed to a gas sample apparatus as shown in the schematic of Figure 13. Each of the four 1.6-mm (1/16-in.) probes (two on each rake) were manifolded into a 3.2-mm (1/8-in.) tubing connected to a 300-cc CRES bomb. The bomb has a screw-on top for disassembly and cleaning.

The probes are isolated from the bomb by a hand valve and a remote-control hot-gas valve. A GH_e bleed was provided to purge the probes prior to sampling. A GN_2 bleed was provided for post-test purging. Pressure and temperature measuring ports were provided to monitor the sample bomb temperature and pressure.

The gas sampling test procedures used were as follows:

(1) The bomb is cleaned, evacuated, and filled with GH_e to 10.3 MN/m^2 (1500 psia) pressure for leak check.

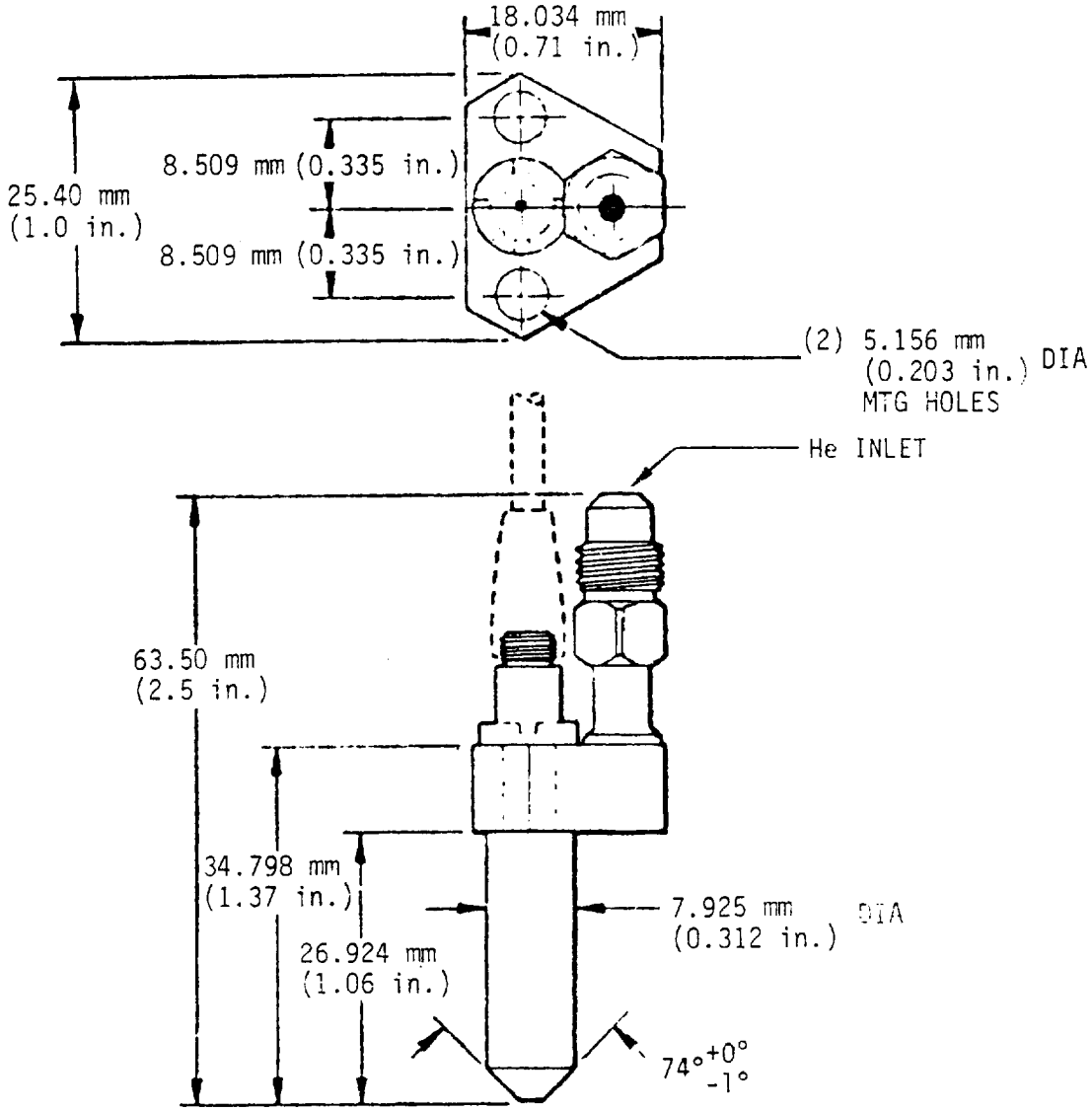

Figure 11. Model 614A Kistler Transducer

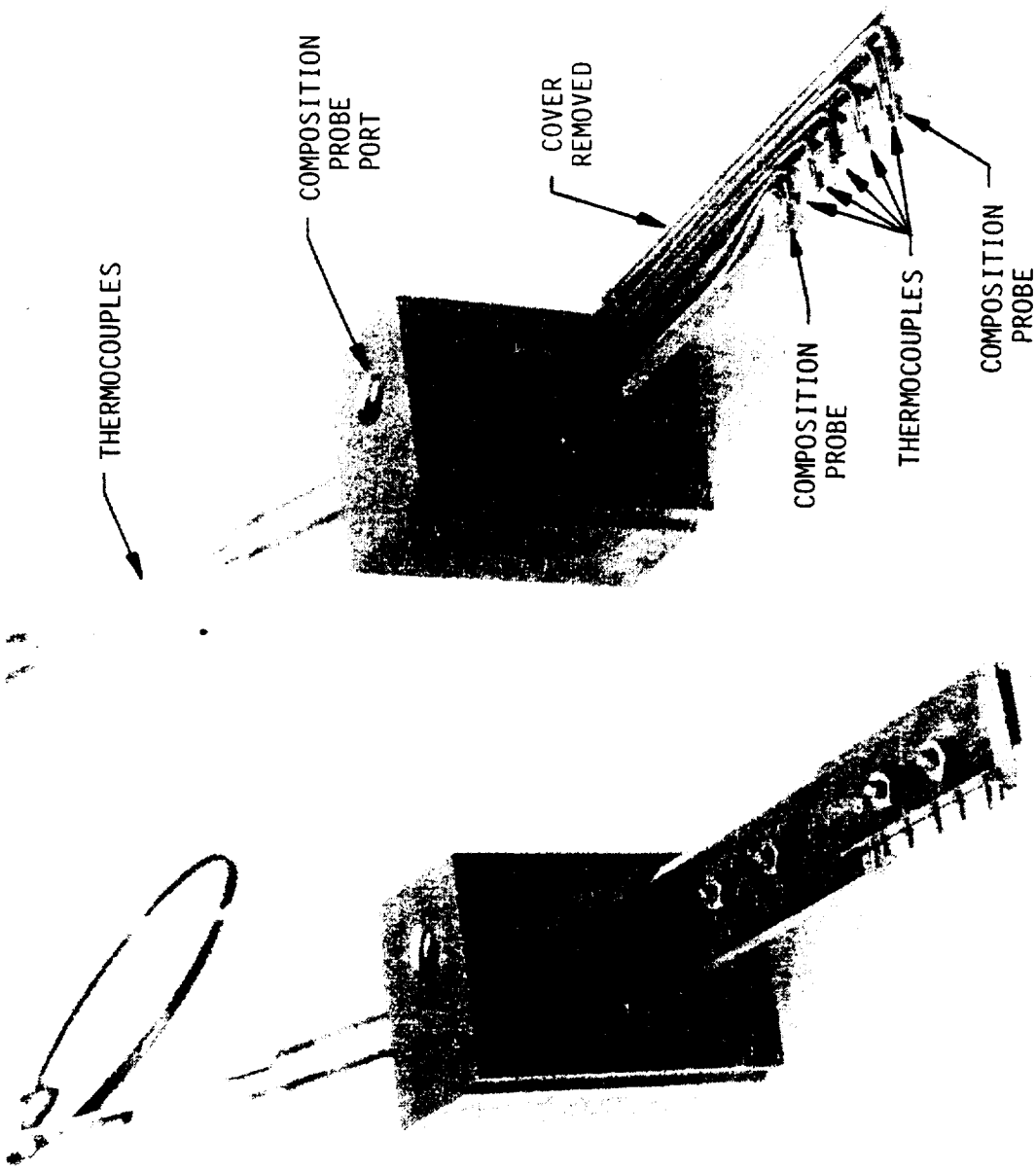

1280 SP 025

Figure 12. Instrumentation Rake Assemblies

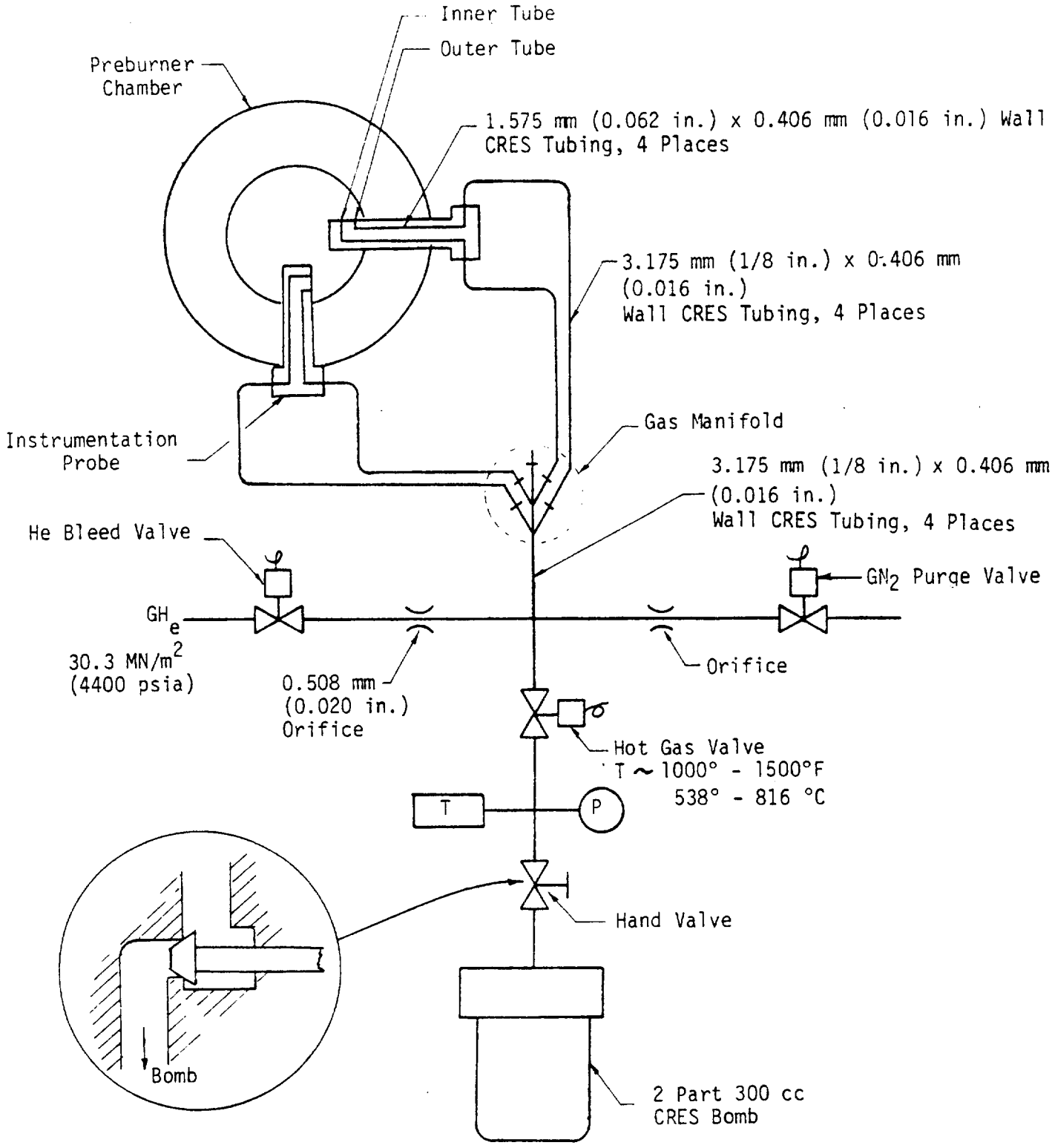

Figure 13. Gas Sample Apparatus Schematic

(2) The pressure is vented to 1.4 MN/m^2 (200 psia), and the bomb is installed in the apparatus.

(3) The sample line hand valve is opened at the 10-minute warning signal.

(4) The GH_e purge flow is started 5 seconds before fire switch 1 (FS-1).

(5) The GH_e purge valve is closed 50 ms ahead of opening the hot-gas sample valve.

(6) Sample gas flows for 2 seconds and is shut down at FS-2.

(7) The GN_2 purge flow is started, and the GH_e purge flow is stopped at FS-2 +5 seconds.

(8) The hand valve is closed as soon as possible after test termination (usually within 5 minutes).

(9) The pressure and temperature are recorded, and a pressure cap is placed on the hand valve outlet to prevent leakage.

(10) The bomb pressure and temperature are checked prior to gas analysis to ensure that no leakage has occurred.

The gas samples were analyzed for composition by using a Hewlitt-Packard Model 5830A Gas-Liquid Chromatograph. A water-heated bath was used to analyze the liquid condensate for vapor pressure. The solid condensate was measured by collecting the solids on filter paper.

B. TEST RESULTS

This subsection of the report presents a summary of the fuel-rich and oxidizer-rich test data via a test-by-test description of all tests conducted for this study.

1. Fuel-Rich Testing

The fuel-rich injector test results are summarized in Table IX. The fuel-rich test series is designated 2351-D01-0G-XXX.

TABLE IX
FUEL-RICH PREBURNER TEST DATA SUMMARY

Test No.	Date	Injector	Test Objective	Duration (sec)	Pc MN/m² (psia)	MR	$\dot{w}_o$ kg/s (lb/sec)	$\dot{w}_f$ kg/s (lb/sec)	T_G C (F)	C* m/s (ft/sec)	Stability	Gas Sample	Remarks
-008	1/08/81	EDM	Sequence Checkout	0.4	-	-	-	-	-	-	Stable	-	Test terminated prematurely due to T4 kill
-009	1/09/81	EDM	Sequence Checkout	0.1	17.5 (2540)	0.305	3.62 (7.97)	11.83 (26.09)	-	792 (2598)	Stable	-	Minor erosion of the throat. Due to ox. valve shutdown
-010	1/16/81	EDM	Balance Point Checkout	5.0	-	-	-	-	-	-	-	-	Test terminated prematurely due to igniter spark malf.
-011	1/16/81	EDM	Balance Point Checkout	5.0	15.6 (2265)	0.331	4.13 (9.1)	12.43 (27.4)	593 (1100)	838 (2750)	Stable	-	Good Test
-012	1/26/81	EDM	Injector Screening	9.7									Good Test
			Data Point 1	5	13.5 (1960)	0.238	3.52 (7.75)	14.70 (32.4)	499 (930)	655 (2150)	Stable	Yes	
			Data Point 2	2.25	16.7 (2424)	0.318	4.38 (9.65)	13.83 (30.5)	643 (1190)	815 (2675)	Stable	-	
			Data Point 3	2.25	16.4 (2381)	0.239	4.26 (9.40)	17.83 (39.3)	513 (955)	659 (2163)	Stable	-	
-013	1/27/81	EDM	Injector Screening	14									Good Test
			Data Point 1	5	15.6 (2257)	0.327	4.06 (8.95)	12.43 (27.4)	657 (1215)	834 (2737)	Stable	Yes	
			Data Point 2	2.25	15.2 (2201)	0.271	3.99 (8.80)	14.70 (32.4)	554 (1030)	718 (2355)	Stable	-	
			Data Point 3	2.25	16.0 (2320)	0.367	4.13 (9.10)	11.20 (24.7)	743 (1370)	915 (3002)	Stable	-	
			Data Point 4	2.25	17.5 (2535)	0.332	4.54 (10.0)	13.74 (30.3)	688 (1270)	844 (2770)	Stable	-	
			Data Point 5	2.25	13.6 (1972)	0.312	3.62 (7.97)	11.57 (25.5)	638 (1180)	794 (2605)	Stable	-	
-014	1/30/81	Platelet	Injector Checkout Test	3	15.1 (2185)	0.303	4.00 (8.81)	13.15 (29.0)	-	777 (2551)	Stable	-	Hard start - 20 MS Delay from ox manifold fill
-015	2/02/81	Platelet	Injector Screening	14									Hard start - Resonator ring seal damaged & rake damaged - 2L instability observed
			Data Point 1	4	15.1 (2193)	0.300	4.01 (8.85)	13.38 (29.5)	654 (1210)	768 (2521)	Stable	Yes	
			Data Point 2	2.5	17.2 (2492)	0.350	4.53 (9.98)	12.93 (28.5)	774 (1425)	871 (2858)	Stable	-	
			Data Point 3	2.5	17.3 (2513)	0.263	4.53 (9.98)	17.19 (37.9)	610 (1130)	706 (2318)	Low Amplitude 2L Oscillations	-	

TABLE IX (cont.)

Test No.	Date	Injector	Test Objective	Duration (sec)	P_c MN/m² (psia)	MR	$\dot{w}_o$ kg/s (lb/sec)	$\dot{w}_f$ kg/s (lb/sec)	T_G C (°F)	C* m/s (ft/sec)	Stability	Gas Sample	Remarks
-015	2/02/81	Platelet	Data Point 4	2.5	13.5 (1968)	0.255	3.56 (7.85)	13.97 (30.8)	552 (1026)	679 (2228)	unstable - 2L Oscillations	-	
			Data Point 5	2.5	12.9 (1881)	0.320	3.47 (7.65)	10.80 (23.8)	685 (1265)	803 (2636)	Stable	-	
-016	2/04/81	Platelet	Injector Screening	1s									Smooth Start with ox rich Igniter - No hardware damage - 2L instability observed
			Data Point 1	4	15.1 (2204)	0.305	4.04 (8.90)	13.20 (29.1)	660 (1220)	778 (2552)	Stable	Yes	
			Data Point 2	4	15.3 (2208)	0.255	4.00 (8.81)	15.65 (34.5)	566 (1050)	687 (2255)	Unstable 2L Oscillations	-	
			Data Point 3	2.5	15.1 (2197)	0.319	4.71 (8.85)	11.52 (25.4)	749 (1380)	863 (2830)	Stable	-	
			Data Point 4	3.5	17.4 (2520)	0.319	4.58 (10.10)	14.33 (31.6)	704 (1300)	826 (2645)	Stable	-	TCw Term Kill - chamber
-017	2/06/81	Platelet	Determine effect of short chamber on stability	0.5	-	-	-	-	-	-	-	-	Premature shutdown due to TCw kill - T/C protruding into chamber
-018	2/09/81	Platelet	Determine effect of short chamber on stability	14									
			Data Point 1	4	15.1 (2208)	0.304	4.38 (9.30)	13.29 (29.3)	657 (1215)	723 (2535)	Unstable 1L Oscillations	Yes	Short chamber exhibits 1L instability
			Data Point 2	2.5	17.2 (2502)	0.365	4.62 (10.19)	12.66 (27.9)	782 (1440)	888 (2915)	Unstable 1L Oscillations	-	
			Data Point 3	2.5	17.5 (2545)	0.271	4.60 (10.14)	16.96 (37.4)	610 (1130)	723 (2372)	Stable	-	
			Data Point 4	2.5	13.7 (1991)	0.261	3.62 (7.97)	13.79 (30.4)	582 (1080)	698 (2296)	Unstable 1L Oscillations	-	

TABLE IX (cont.)

Test No.	Date	Injector	Test Objective	Duration (sec)	P_c MN/m² (psia)	MR	$\dot{w}_o$ kg/s (lb/sec)	$\dot{w}_f$ kg/s (lb/sec)	T_G °C (°F)	C* m/s (ft/sec)	Stability	Gas Sample	Remarks
-018	2/09/81	Platelet	Data Point 5	2.5	12.7 (1842)	0.335	3.51 (7.73)	10.48 (23.1)	682 (1260)	805 (2641)	Unstable 1L Oscillations	-	
-019	2/10/81	Platelet	Determine effect of turbulence ring on 1L stability	14									
			Data Point 1	4	15.2 (2200)	0.303	4.04 (8.90)	13.31 (29.35)	649 (1200)	751 (2465)	Stable	Yes	Turbulence ring improves 1L Stability
			Data Point 2	2.5	17.2 (2490)	0.353	4.58 (10.10)	12.99 (28.63)	749 (1380)	841 (2760)	Stable	-	
			Data Point 3	2.5	17.3 (2515)	0.269	4.56 (10.06)	17.06 (37.63)	591 (1095)	693 (2273)	Stable		
			Data Point 4	2.5	13.6 (1972)	0.257	3.57 (7.86)	13.86 (30.63)	568 (1055)	673 (2209)	Stable	-	
			Data Point 5	2.5	12.8 (1851)	0.327	3.57 (7.66)	10.61 (23.4	677 (1253)	751 (2464)	Unstable 1L Oscillations	-	
-020	2/11/81	Platelet	Determine effect of chamber length on stability with turbulence	14									Long chamber with turbulence ring is stable
1				4	14.9 (2158)	0.299	3.98 (8.77)	13.34 (29.4	635 (1175)	735 (2411)	Stable	Yes	
2				2.5	17.0 (2470)	0.354	4.57 (10.07)	12.88 (28.4)	743 (1370)	842 (2762)	Stable	-	
3				2.5	17.3 (2506)	0.264	4.55 (10.02)	17.19 (37.9)	588 (1090)	685 (2249)	Stable	-	
4				2.5	13.5 (1964)	0.260	3.57 (7.88)	13.76 (30.34)	574 (1065)	675 (2214)	Stable	-	
5				2.5	12.8 (1860)	0.330	3.50 (7.71)	10.58 (23.33)	688 (1270)	787 (2581)	Stable	-	
-021	2/12/81	Platelet	Determine effect of operating PT on carbon formation	14	14.6 (2115)	0.301	4.17 (9.19)	13.83 (30.5)	646 (1195)	798 (2617)	Stable	Yes	Light carbon build-up on turbine simulator - Thickness .001 - .002"
-022	2/13/81	Platelet	Determine effect of operating PT on carbon formation	14	15.8 (2292)	0.350	4.87 (10.74)	13.93 (30.7)	735 (1355)	883 (2897)	Stable	Yes	Some hard carbon buildup on T/S inlet - 1/32"

TABLE IX (cont.)

Test No.	Date	Injector	Test Objective	Duration (sec)	P_c MN/m² (psia)	MR	$\dot{w}_o$ kg/s (lb/sec)	$\dot{w}_f$ kg/s (lb/sec)	T_G °C (°F)	C* m/s (ft/sec)	Stability	Gas Sample	Remarks
-023	2/14/81	Platelet	Determine effect of operating PT on carbon formation	0.5	-	-	-	-	-	-	-	-	Premature shutdown due to facility parameter kill
-024	2/16/81	Platelet	Determine effect of operating PT on carbon formation	0.5	-	-	-	-	-	-	-	-	Premature shutdown due to Pc transducer malfunction
-025	2/17/81	Platelet	Determine effect of operating PT on carbon formation	10.	16.2 (2351)	0.262	4.88 (10.75)	18.67 (41.15)	582 (1080)	723 (2373)	Stable	Yes	Pc Ign Transducer Line ruptured during test - T/S erosion noted
-026	2/19/81	Platelet	Determine effect of operating PT on carbon formation	0.5	-	-	-	-	-	-	-	-	Premature shutdown due to low Pc kill
-027	2/20/81	Platelet	Determine effect of operating PT on carbon formation	14	12.3 (1786)	0.256	3.72 (8.21)	14.52 (32.0)	563 (1045)	715 (2346)	Stable	Yes	Erosion of turbine & inj. simulators
-028	2/21/81	Platelet	Determine effect of operating PT on carbon formation	16	12.1 (1748)	0.369	3.86 (8.51)	10.46 (23.06)	746 (1375)	898 (2945)	Stable	Yes	
-029	2/24/81	Platelet	Determine effect of heated fuel on carbon formation	14	13.9 (2015)	0.350	4.23 (9.32)	12.07 (26.62)	763 (1405)	913 (2995)	Stable	Yes	No noticeable effect of heated fuel - MR increased during test data taken at 13.5 sec

TABLE IX (cont.)

Test No.	Date	Injector	Test Objective	Duration (sec)	P_c MN/m² (psia)	MR	$\dot{w}_o$ kg/s (lb/sec)	$\dot{w}_f$ kg/s (lb/sec)	T_G °C (°F)	c* m/s (ft/sec)	Stability	Gas Sample	Remarks
-030	2/28/81	EDM	Determine effect of turbulence ring on temp. uniformity and stability	12									
1				4	11.1 (1615)	0.283	4.56 (10.05)	16.10 (35.5)	602 (1115)	752 (2468)	Stable	No	Nozzle adapter not installed
2				2.5	13.7 (1984)	0.343	5.69 (12.54)	16.56 (36.5)	719 (1326)	863 (2830)	Stable	No	
3				2.5	14.0 (2026)	0.262	5.67 (12.50)	21.59 (47.6)	571 (1059)	714 (2343)	Stable	No	
4				2.5	9.1 (1325)	0.243	3.71 (8.18)	15.24 (33.6)	528 (983)	675 (2214)	Stable	No	
5				0.5	8.9 (1292)	0.332	3.73 (8.23)	11.25 (24.8)	674 (1245)	828 (2718)	Stable	No	
-031	4/29/81	EDM	Same as -030	14									
1				4	14.6 (2112)	0.288	3.92 (8.65)	13.59 (29.96)	621 (1150)	729 (2392)	Stable	No	Very uniform temperatures
2				2.5	17.3 (2504)	0.355	4.59 (10.11)	12.88 (28.4)	765 (1409)	867 (2844)	Stable	No	
3				2.5	17.3 (2505)	0.271	4.61 (10.17)	17.01 (37.5)	601 (1113)	700 (2298)	Stable	No	
4				2.5	12.5 (1806)	0.240	3.30 (7.27)	13.74 (30.3)	534 (993)	641 (2102)	Stable	No	
5				2.5	12.2 (1775)	0.321	3.34 (7.36)	10.39 (22.9)	674 (1246)	782 (2565)	Stable	No	
-032	4/30/81	EDM	Same as -030 with short chamber	14									
1				4	14.9 (2155)	0.298	3.99 (8.79)	13.38 (29.5)	632 (1170)	743 (2439)	Stable	No	
2				2.5	17.5 (2534)	0.360	4.63 (10.2)	12.84 (28.3)	782 (1440)	869 (2852)	Stable	No	
3				2.5	17.5 (2540)	0.278	4.67 (10.3)	16.83 (37.1)	609 (1128)	708 (2322)	Stable	No	
4				2.5	12.8 (1861)	0.254	3.41 (7.52)	13.43 (29.6)	559 (1038)	661 (2169)	Stable	No	
5				2.5	12.6 (1834)	0.341	3.45 (7.60)	10.12 (22.3)	709 (1309)	810 (2656)	Stable	No	

Test -008

This was the first full preburner checkout test. The preburner test setup is shown in Figure 14. The set conditions were for a chamber presure of 16.6 MN/m^2 (2409 psia) and a mixture ratio of 0.254, using a nozzle throat diameter of 30 mm (1.18 in.). The run duration was set for 0.5 second; however, a premature shutdown occurred at FS-1 + 0.4 seconds due to the T4 timer kill as shown in Figure 15. Ignition had occurred and chamber pressure was rising rapidly; however, the time to reach a chamber pressure of 6.9 MN/m^2 (1000 psia) from FS-1 had been underestimated, and the T4 timer initiated the shutdown. There was no evidence of hardware damage.

Test -009

The set conditions for this test were the same as for Test -008. Based on the Test -008 results, the T4 timer was extended from 130 to 205 ms. The T2 timer was extended from 60 to 85 ms to delay the oxidizer filling and achieve a smoother start. The T6 timer was increased to 1.0 second to permit longer test duration.

Data plots of the test parameters are shown in Figure 16. The actual operating point was Pc = 17.5 MN/m^2 (2540 psia) and MR = 0.305 due to a higher-than-anticipated oxidizer flow. The higher oxidizer flow is a result of a lower-than-expected oxidizer valve pressure drop. It appears that the flow through the valve reattached downstream of the poppet, resulting in a valve discharge coefficient of 0.8 compared to a design value of 0.6.

Two anomalies occurred on the test, requiring test system modifications. The first anomaly was an oxidizer valve malfunction that resulted in an oxidizer-rich shutdown, causing minor nozzle throat erosion. The oxidizer valve trace shown in Figure 16 indicates the abnormal shutdown. Post-test examination of the valve actuator hydraulic system identified actuation pressure interactions between the fuel and oxidizer valve servoactuators to be the cause of the problem. Replumbing of the servovalve discharges solved the interaction problem.

Post-test examination of the high-speed movies taken clearly shows the throat erosion occurring during the oxidizer-rich shutdown. Based on Test -009 C* data, the throat diameter was subsequently enlarged to 33.6 mm (1.322 in.) to achieve the design point conditions of Pc = 15.2 MN/m^2 (2200 psia), MR = 0.3, and W_T = 16.78 kg/s (37 lb/sec).

The second anomaly involved backflow of fuel-rich combustion gases into the igniter GO_2 feed line, resulting in minor damage to the

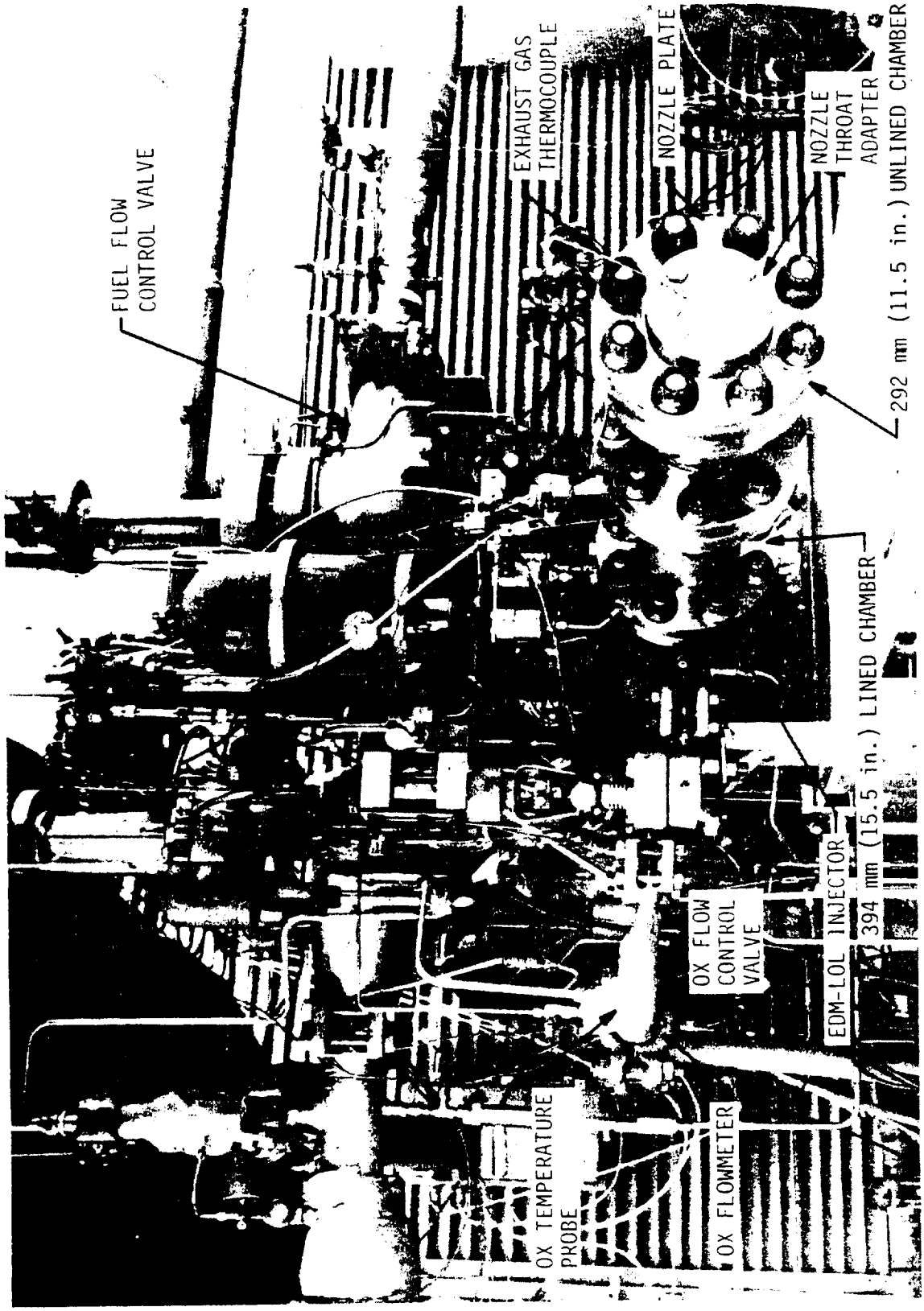

Figure 14. Fuel-Rich Preburner Test Setup

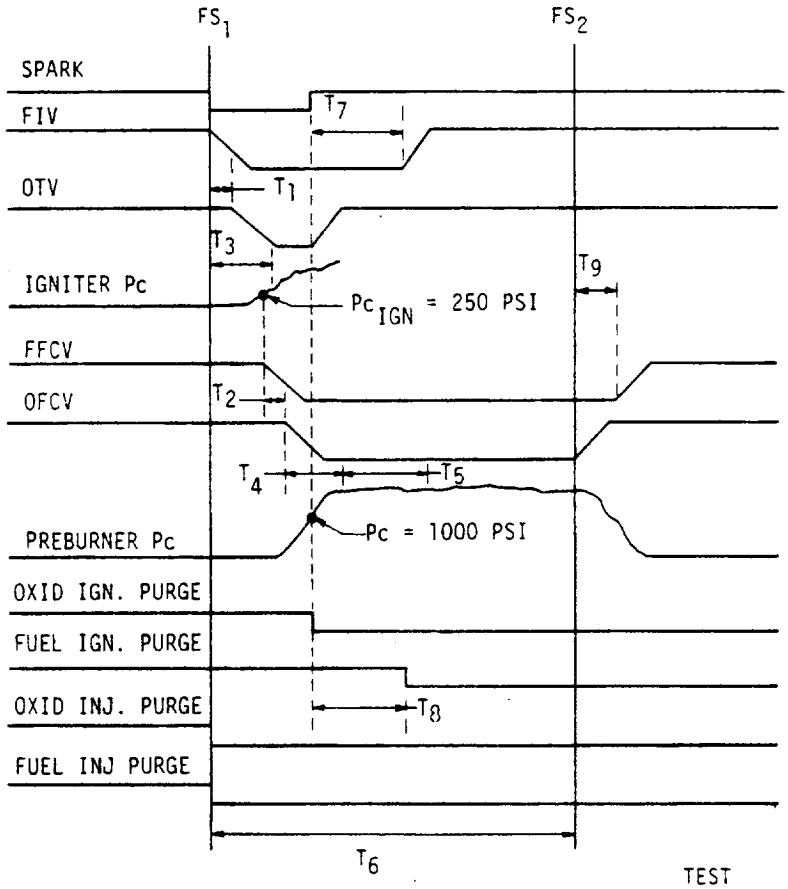

TIMER FUNCTIONS:	TIME	TEST -008	-009	-010	-011
T_1 - FUEL IGNITER VALVE OPENING DELAY. DELAYS VALVE OPENING FROM FS_1.	10 MS	10	10	10	
T_2 - OXIDIZER FLOW CONTROL VALVE DELAY. DELAYS VALVE OPENING FROM INITIAL OPENING SIGNAL TO FUEL FLOW CONTROL VALVE.	60 MS	85	100	100	
T_3 - IGNITER CHAMBER PRESSURE SHUTDOWN. IF IGNITER PRESSURE IS NOT UP TO 1.7 MN/m^2 (250 psi) PRESSURE BY T_3, A FS_2 SIGNAL IS OBTAINED.	250 MS	250	250	250	
T_4 - PREBURNER CHAMBER PRESSURE SHUTDOWN. IF PREBURNER PRESSURE IS NOT UP TO 6.9 MN/m^2 (1000 psi) BY T_4, A FS_2 SIGNAL IS OBTAINED.	130 MS	205	190	190	
T_5 - CSM SHUTDOWN LOCKOUT. THE CSM SHUTDOWN WILL NOT BE INITIATED UNTIL AFTER T_5, TO PRECLUDE ANY PRESSURE PERTURBATIONS DURING START TRANSIENTS.	30 MS	30	30	30	
T_6 - DURATION TIMER. GIVES THE TOTAL DURATION OF THE TEST.	500 MS	1000	5000	5000	
T_7 - FUEL IGNITER VALVE CLOSING DELAY	50 MS	50	50	50	
T_8 - FUEL IGNITER PURGE VALVE OPENING DELAY	50 MS	50	50	50	
T_9 - FUEL FLOW CONTROL VALVE CLOSING DELAY	50 MS	50	100	100	

Figure 15. Fuel-Rich Preburner Test Sequence

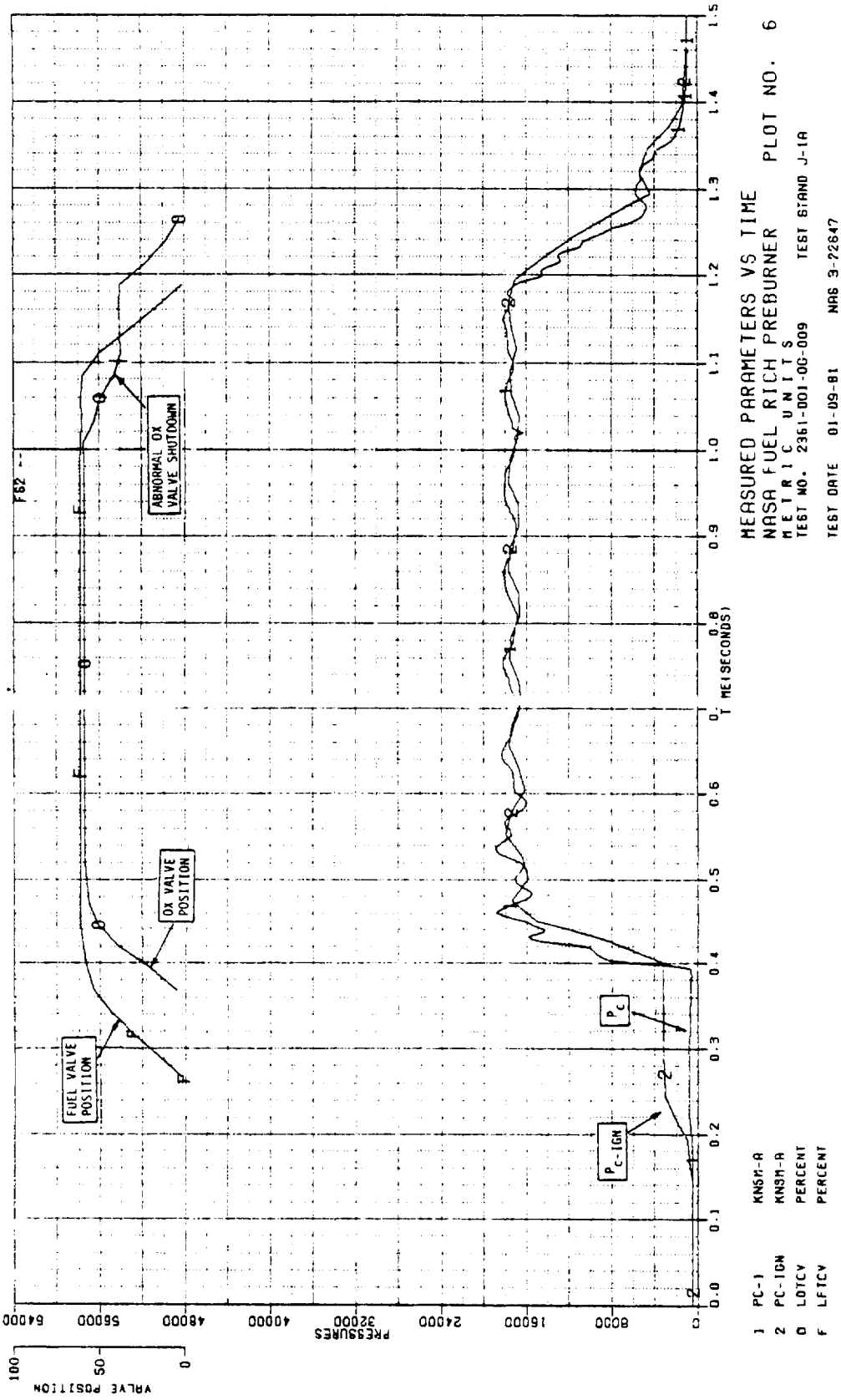

Figure 16. Fuel-Rich Preburner, Measured Parameters Versus Time, Test -009 (1 of 2)

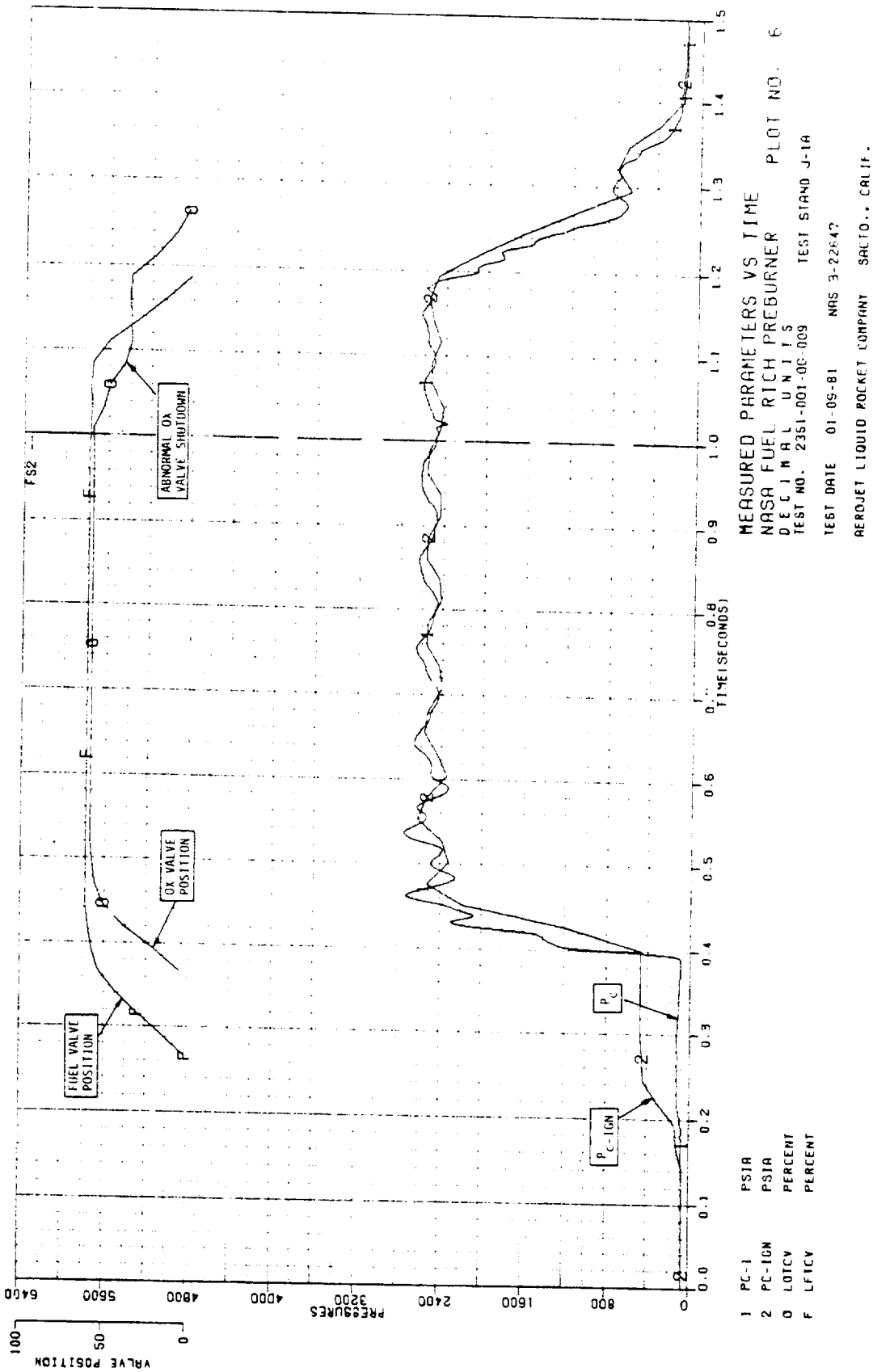

Figure 16. Fuel-Rich Preburner, Measured Parameters Versus Time, Test -009 (2 of 2)

igniter and feed line. Corrective action was taken by installing a check valve immediately at the igniter oxidizer inlet in addition to the original check valve located about 60.96 cm (2 ft) upstream of the igniter. The igniter oxidizer feed and purge pressures were also increased to provide added margin.

Test -010

The conditions were set for Pc = 15.2 MN/m^2 (2200 psia), MR = 0.3, and $\dot{W}_T$ = 16.78 kg/s (37 lb/sec). The test was terminated prematurely by the T3 timer. Post-test analysis showed that the spark did not receive an electrical signal from the computer sequence.

Test -011

The test conditions for Test -011 were the same as for Test -010. The firing was successful, with no anomalies occurring. Data plots of key test parameters are shown in Figure 17.

The actual operating point was Pc = 15.6 MN/m^2 (2265 psia), MR = 0.331, and $\dot{W}_T$ = 16.56 kg/s (36.5 lb/sec). The test was stable, and there was no evidence of hardware damage.

Test -012

Test -012 was scheduled to obtain data at five operating points. However, only three operating points were obtained due to a low-Pc kill resulting from a lower-than-desired mixture ratio on Point 4. Difficulty in achieving the desired set conditions resulted from uncertainties in the oxidizer valve Kw at low valve openings.

The test was stable at all operating conditions. Key test parameters are plotted in Figures 18, 19 and 20. Prior to testing, the instrumentation probes had been installed, as shown in Figure 21, and temperature and gas sample data were taken.

Test -013

Test -013 ran the scheduled duration, and five operating points were obtained, as planned. Test data are shown in Figures 22, 23, and 24.

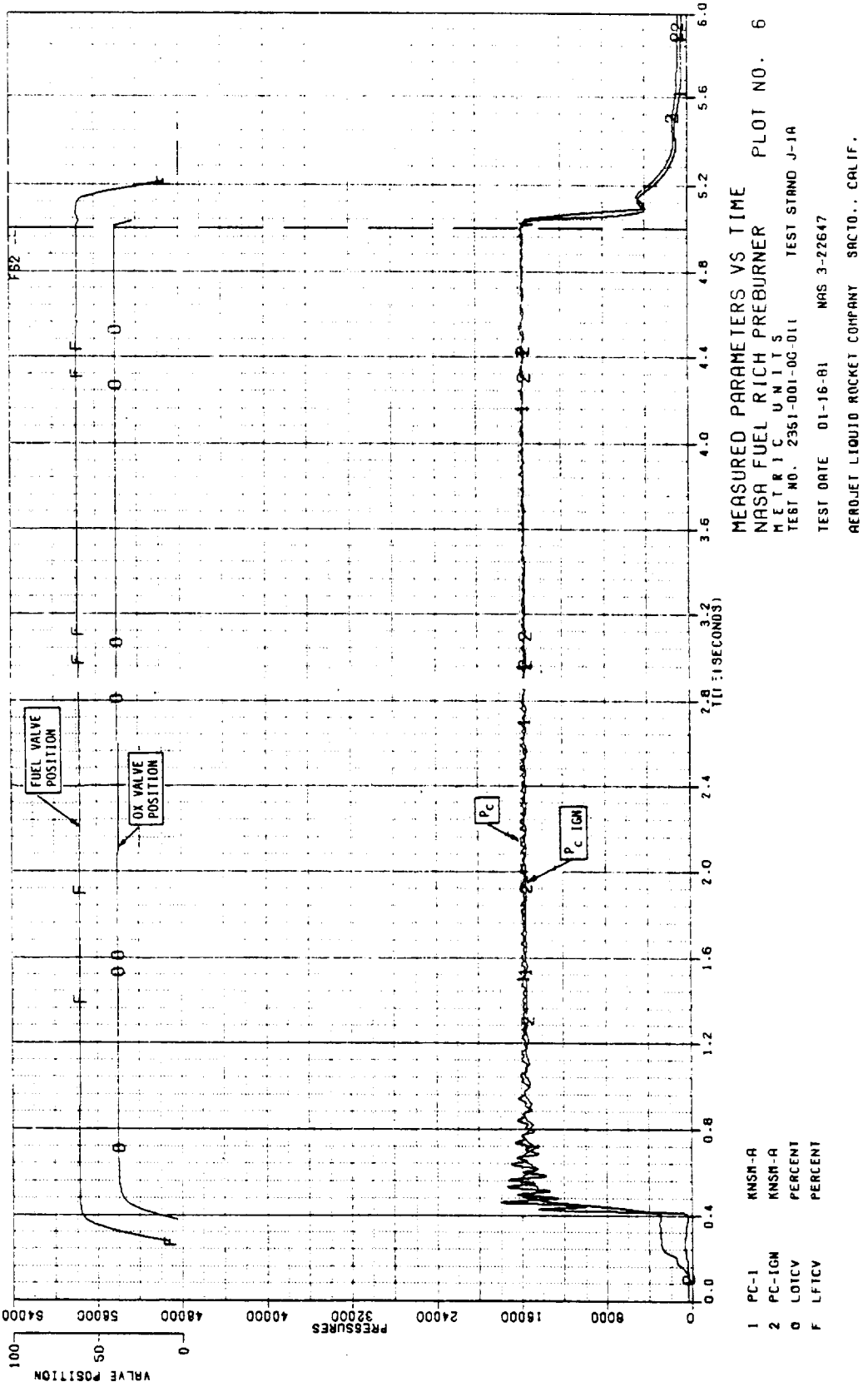

Figure 17. Fuel-Rich Preburner, Measured Parameters Versus Time, Test -011 (1 of 2)

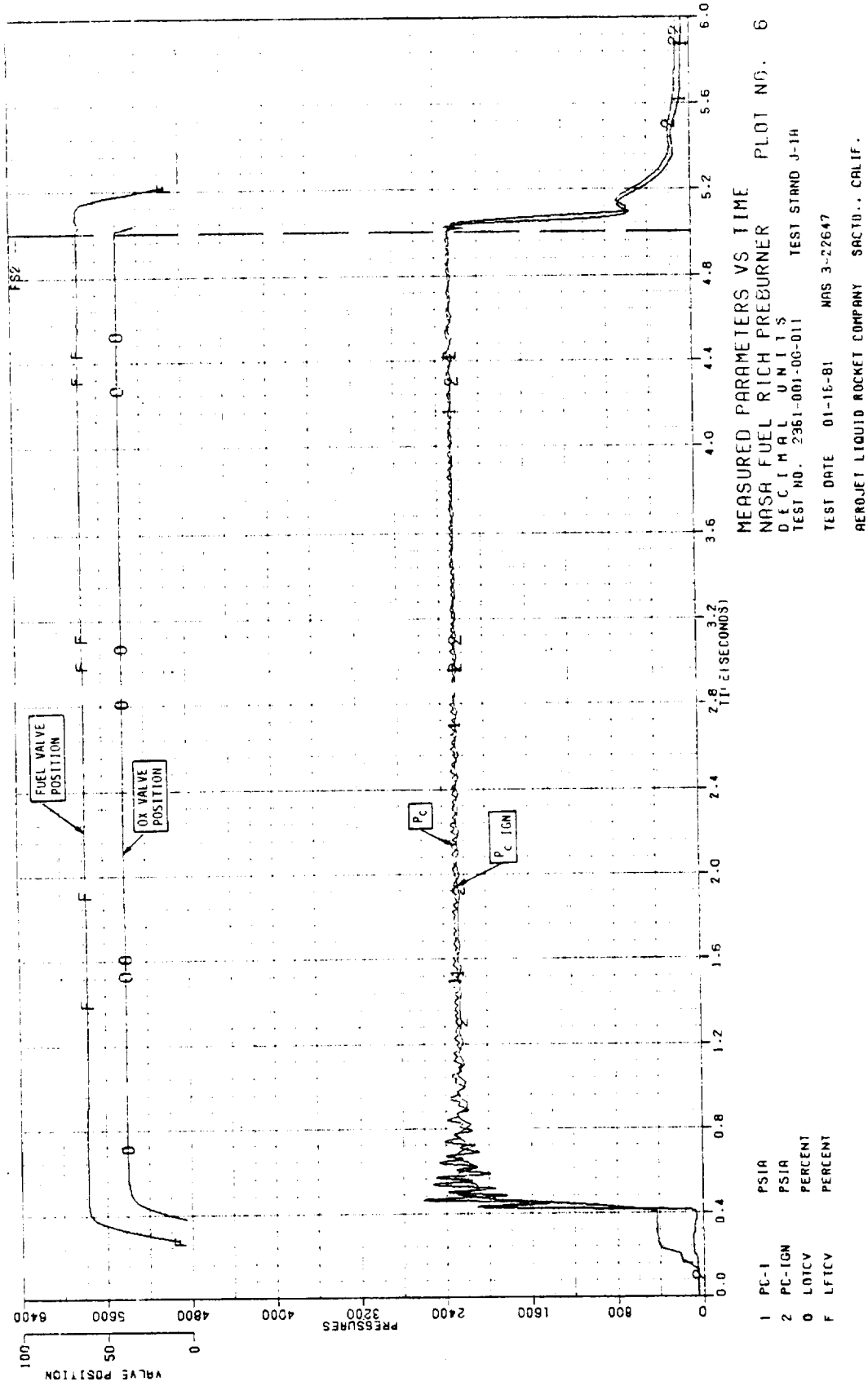

Figure 17. Fuel-Rich Preburner, Measured Parameters Versus Time, Test -001 (2 of 2)

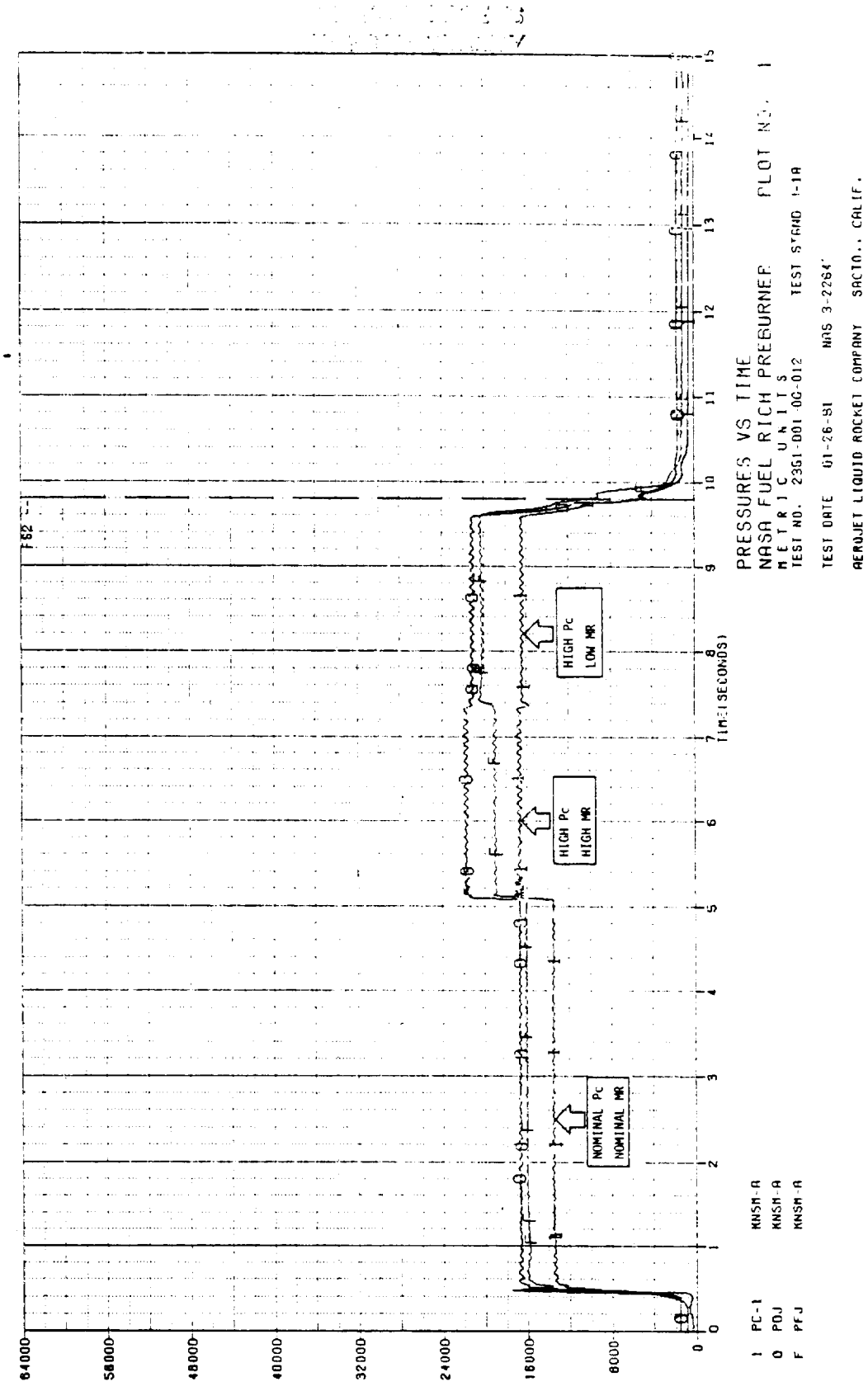

Figure 18. Fuel-Rich Preburner, Pressures Versus Time, Test -012 (1 of 2)

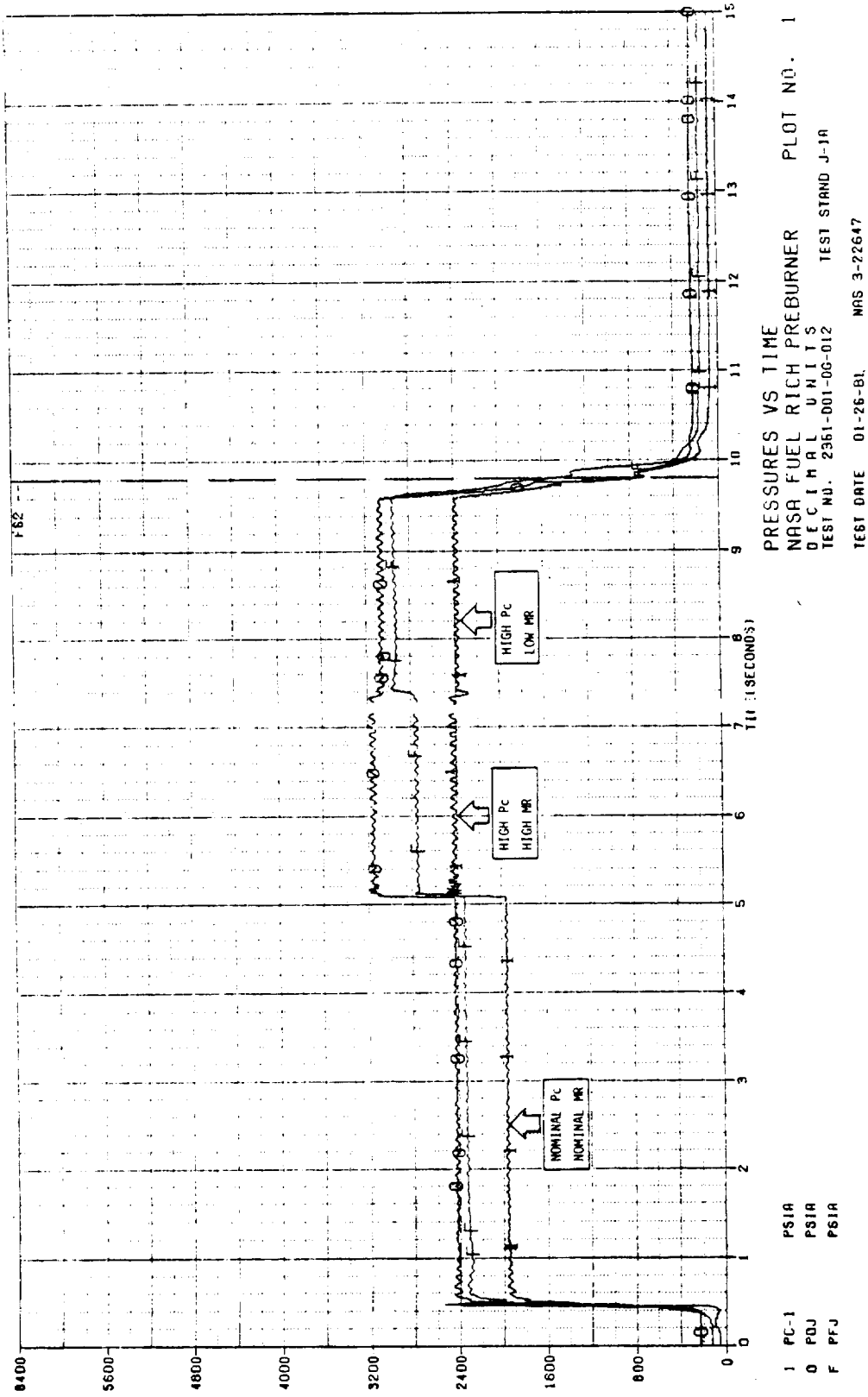

Figure 18. Fuel-Rich Preburner, Pressures Versus Time, Test -012 (2 of 2)

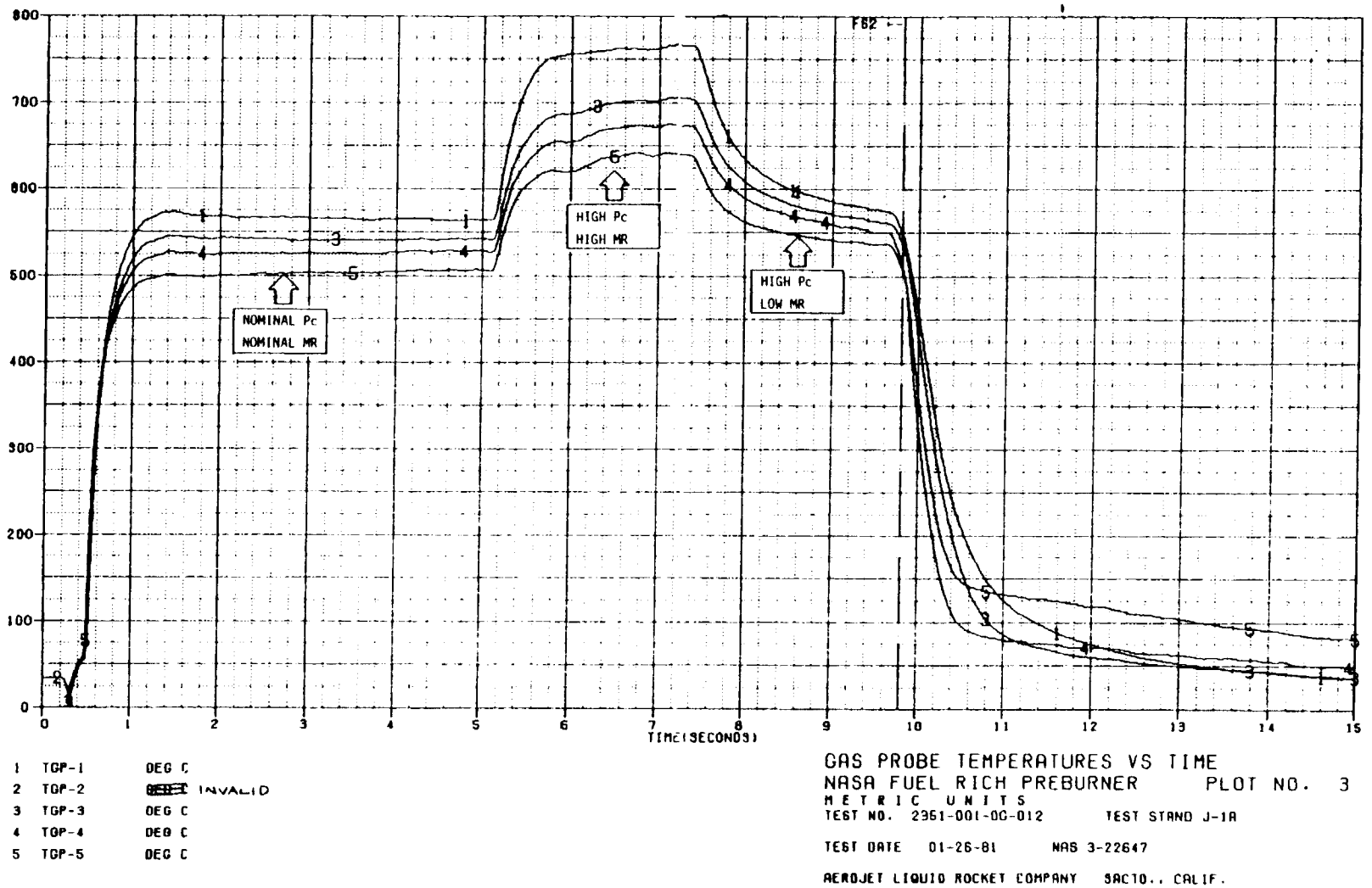

Figure 19. Fuel-Rich Preburner, Gas Probe Temperatures Versus Time, Test -012 (1 of 2)

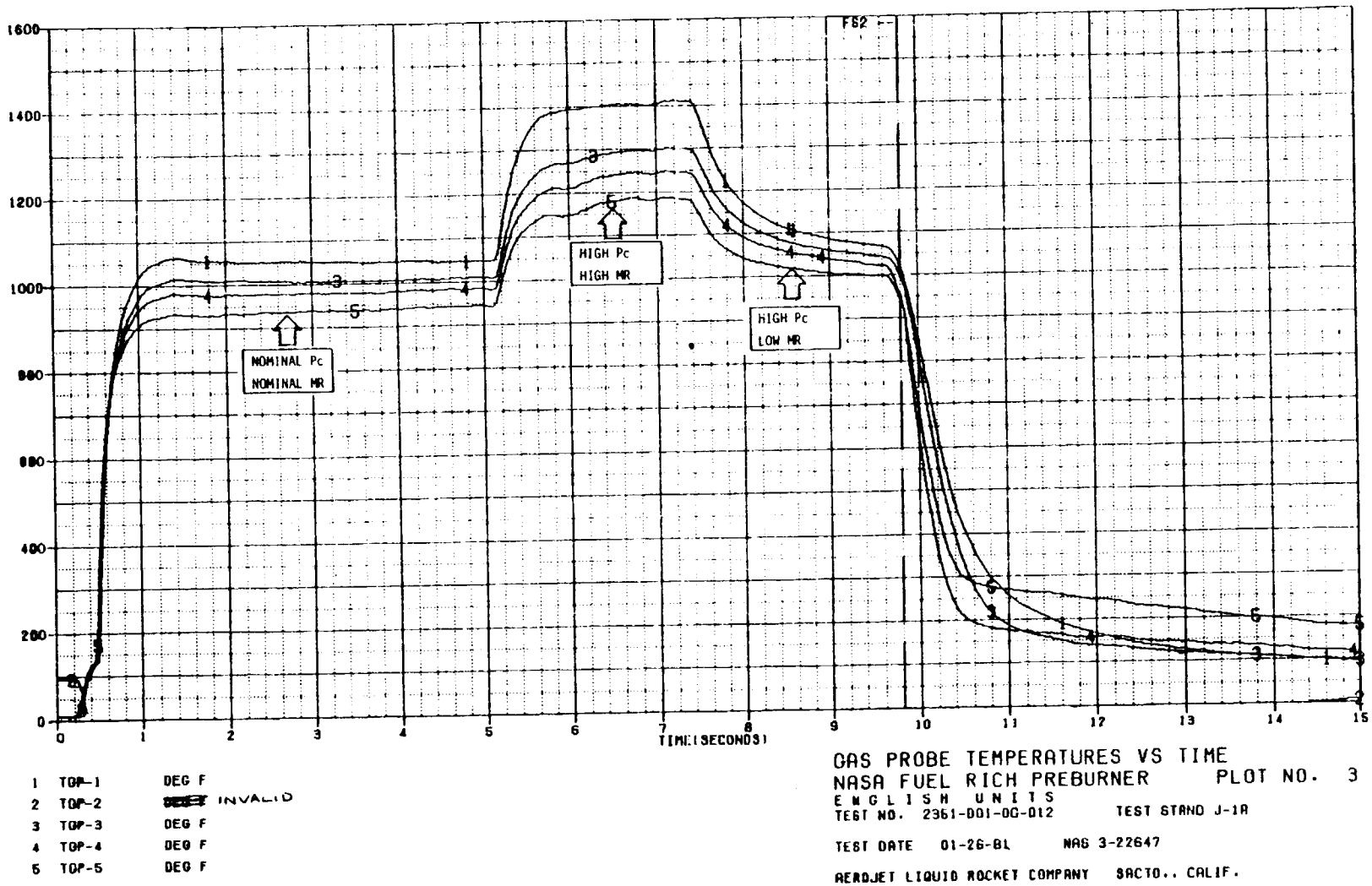

Figure 19. Fuel-Rich Preburner, Gas Probe Temperatures Versus Time, Test -012 (2 of 2)

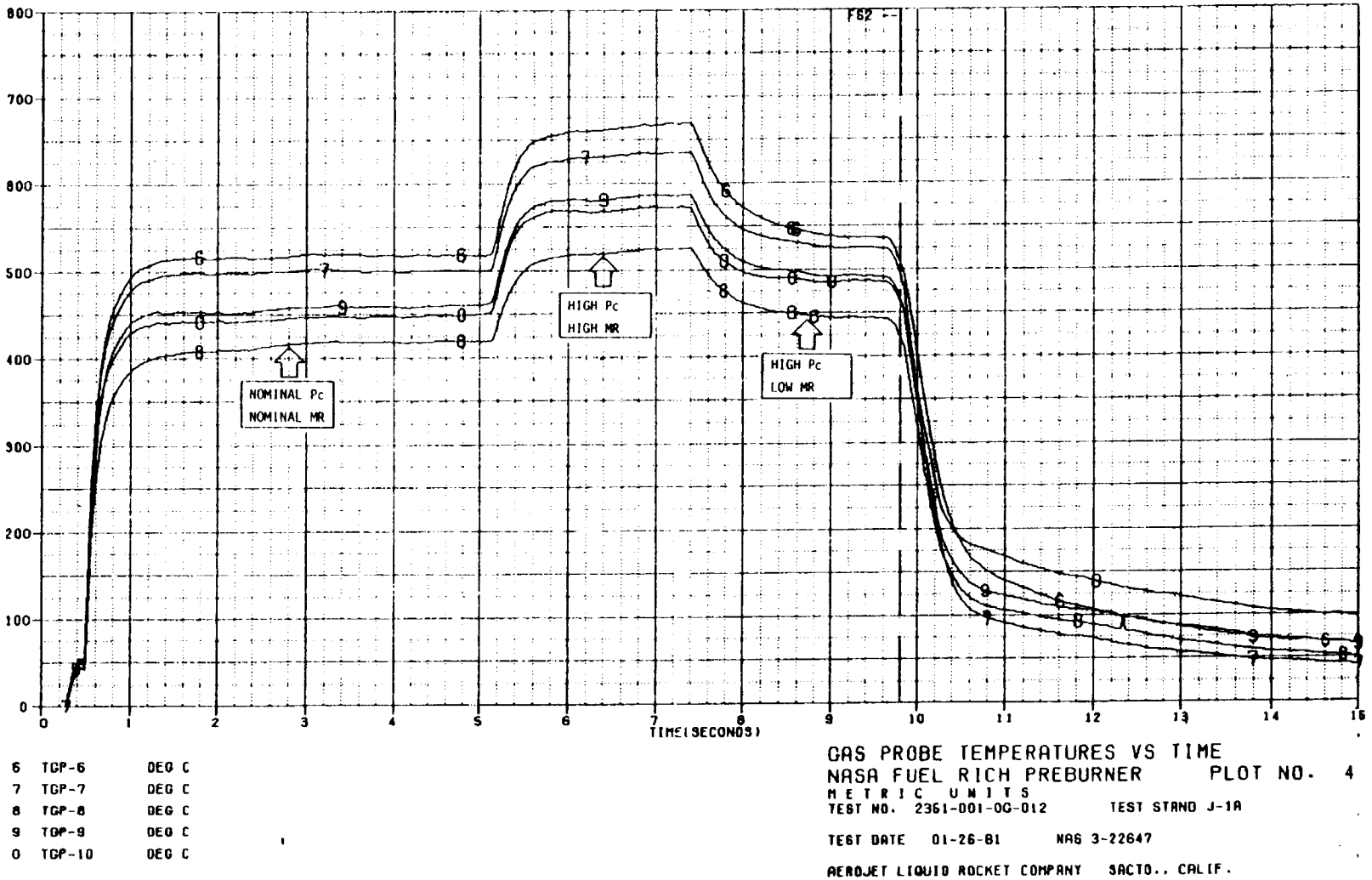

Figure 20. Fuel-Rich Preburner, Gas Probe Temperatures Versus Time, Test -012 (1 of 2)

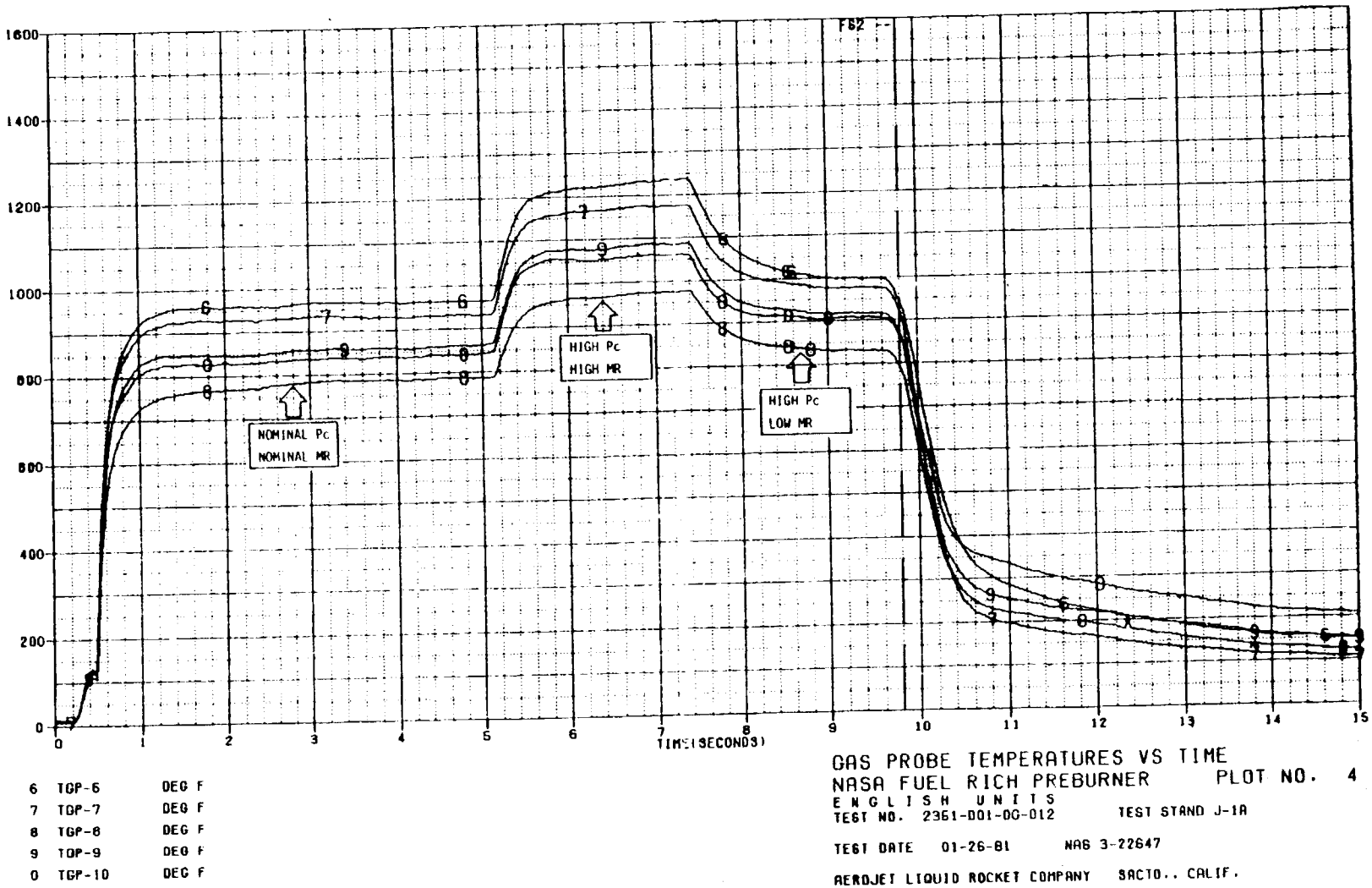

Figure 20. Fuel-Rich Preburner, Gas Probe Temperatures Versus Time, Tes -012 (2 of 2)

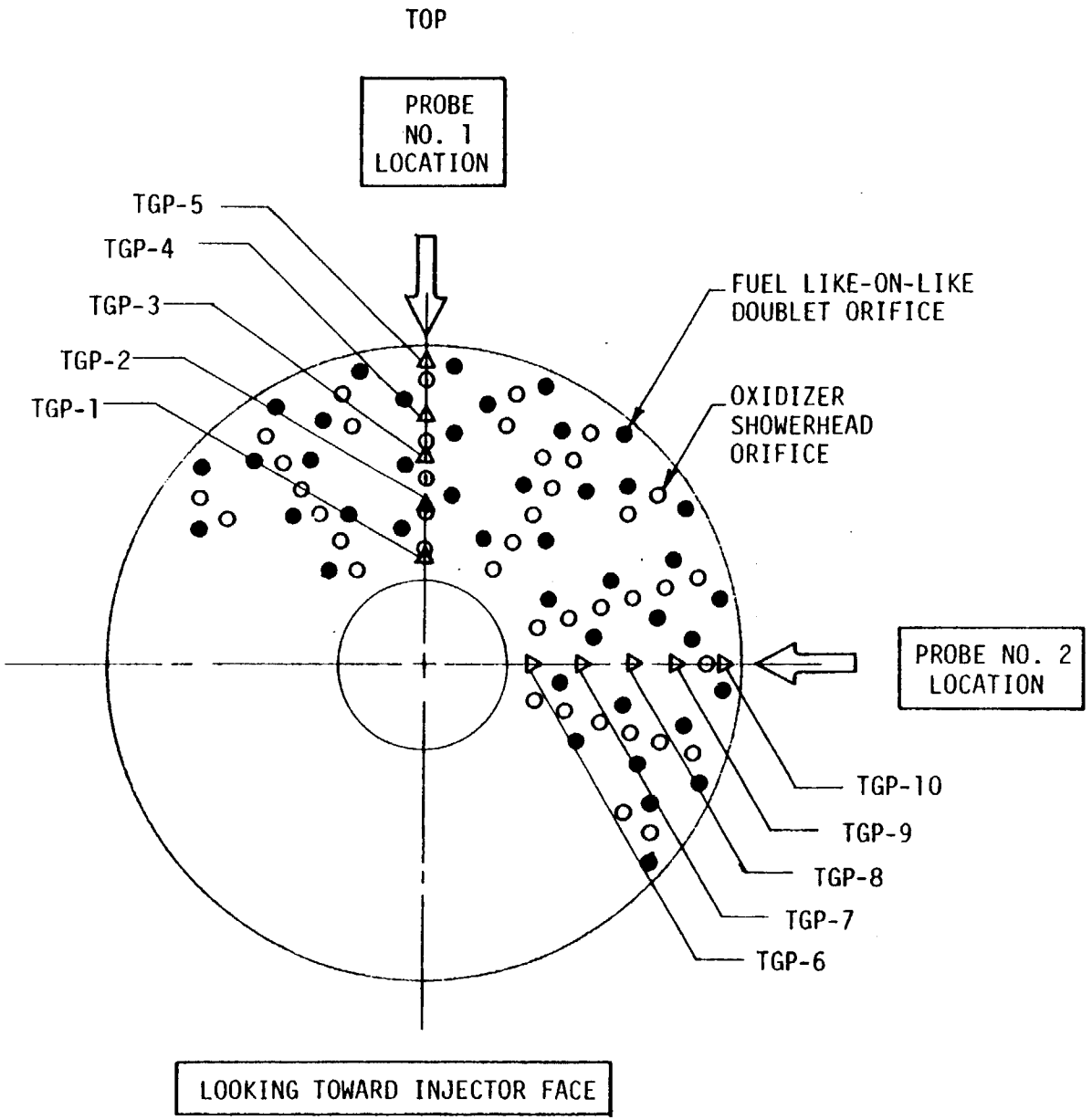

Figure 21. Temperature Probe Locations in Relation to the EDM-LOL Injector Pattern

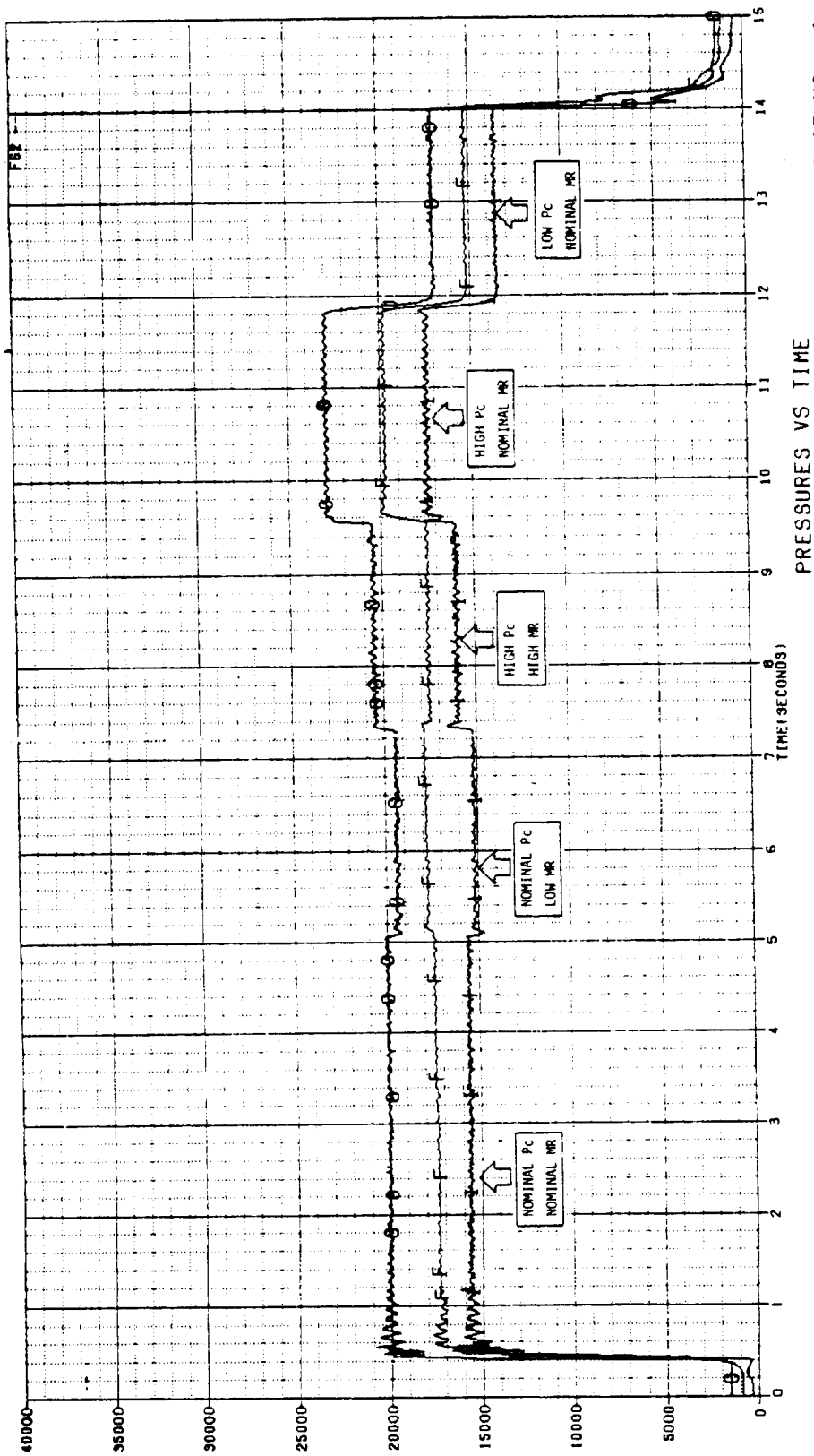

Figure 22. Fuel-Rich Preburner, Pressures Versus Time, Test -013 (1 of 2)

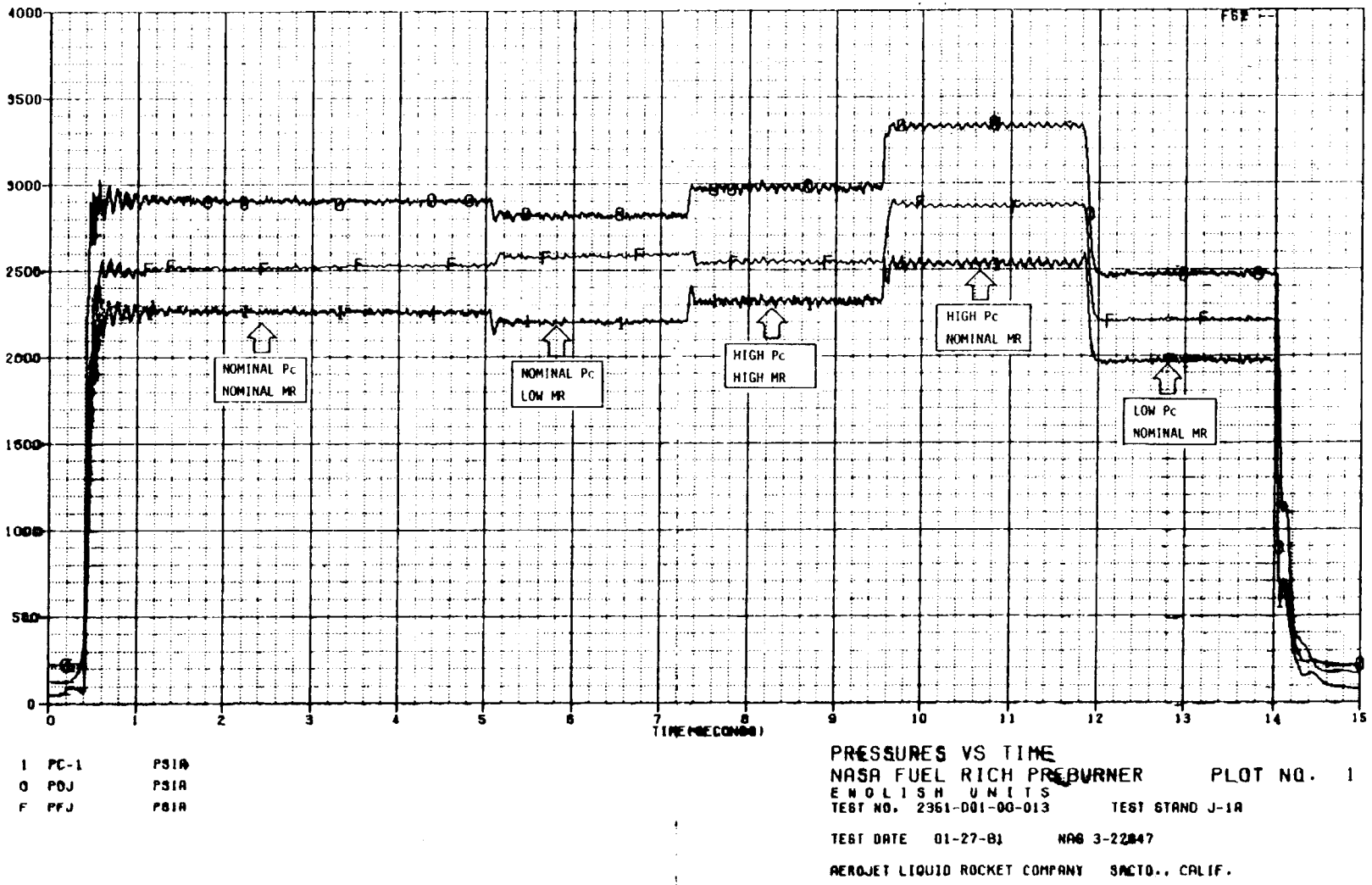

Figure 22. Fuel-Rich Preburner, Pressures Versus Time, Test -013 (2 of 2)

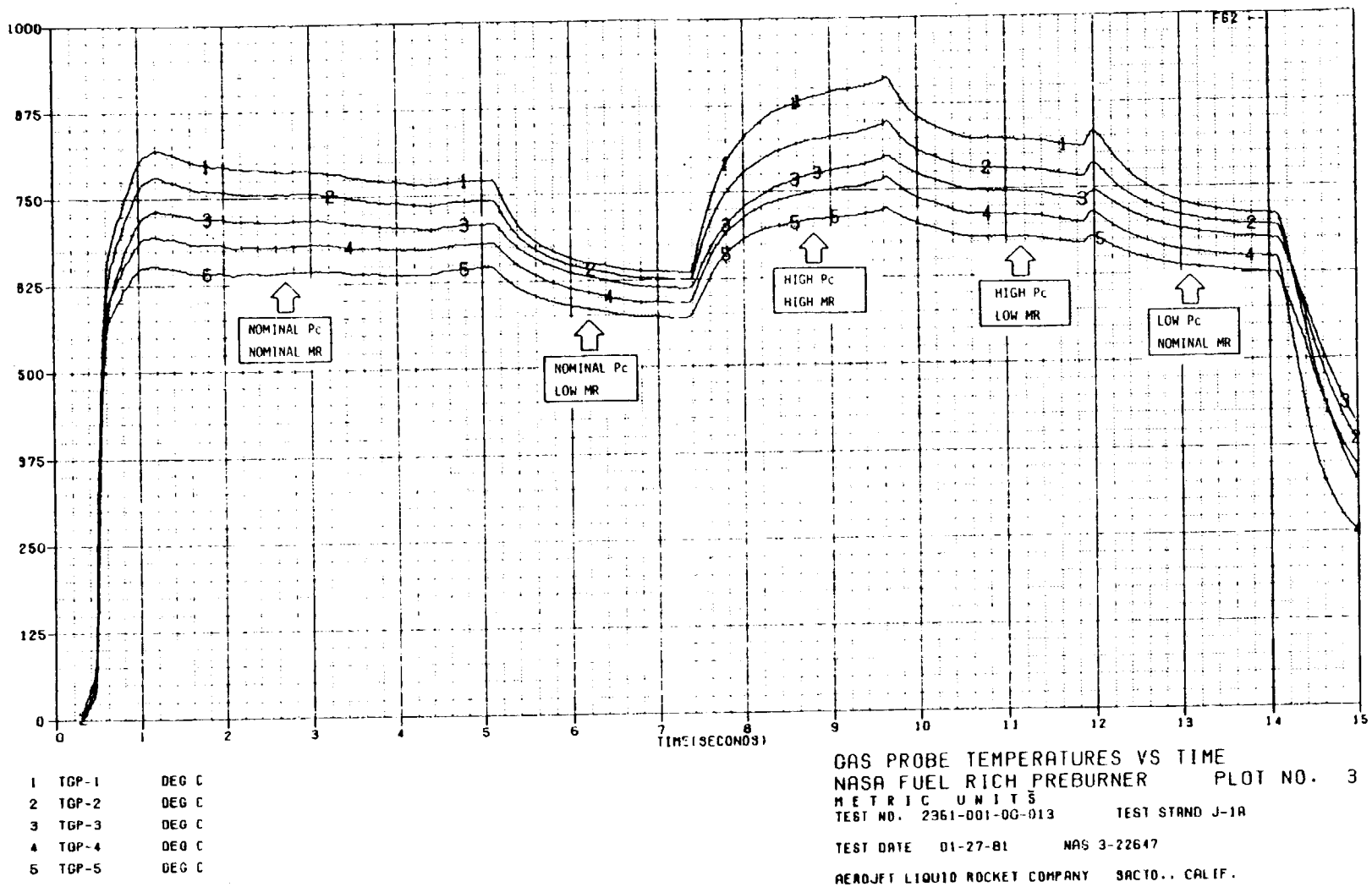

Figure 23. Fuel-Rich Preburner, Gas Probe Temperatures Versus Time, Test -013 (Page 1 of 2)

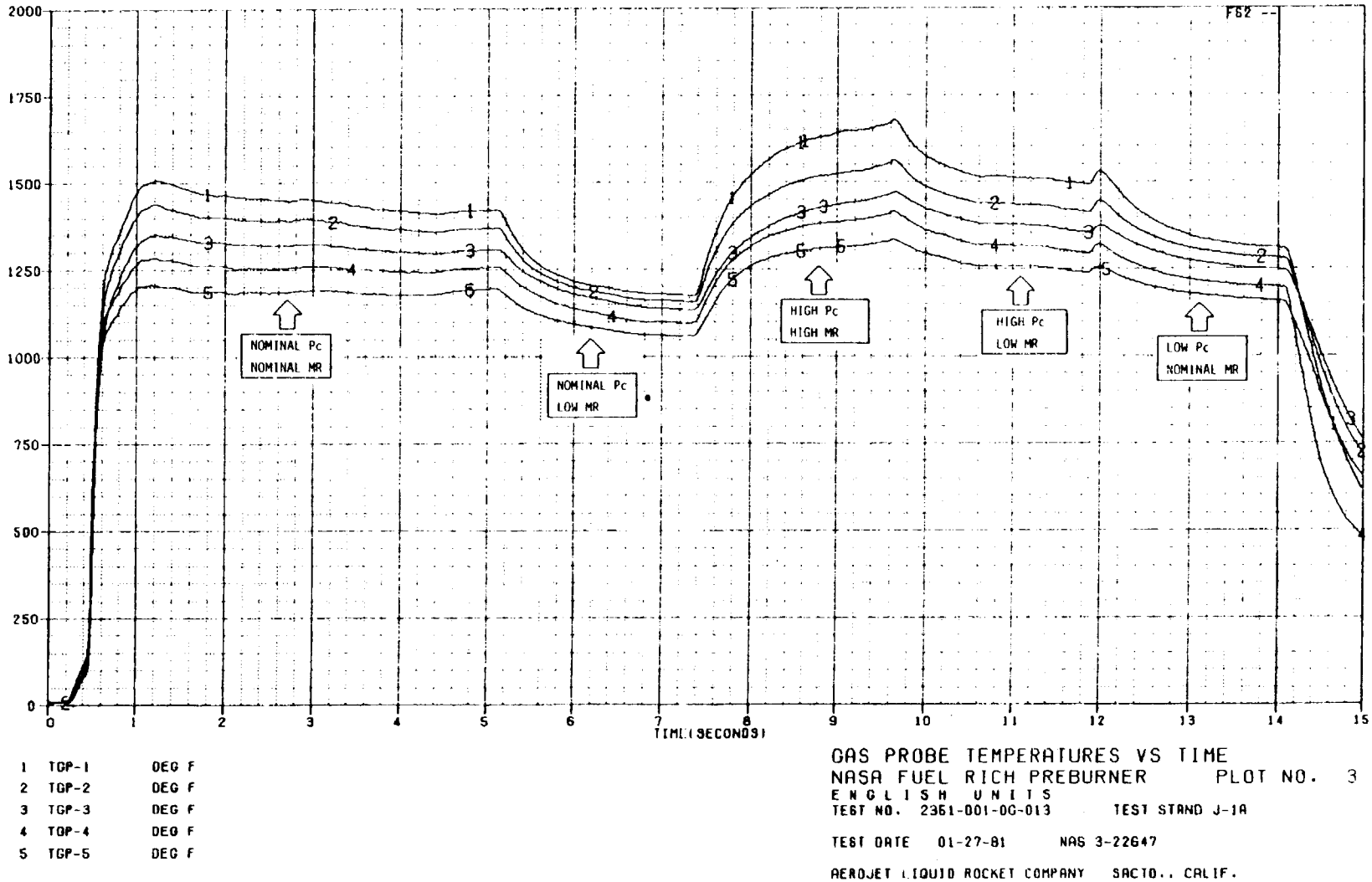

Figure 23. Fuel-Rich Preburner, Gas Probe Temperatures Versus Time, Test -013 (Page 2 of 2)

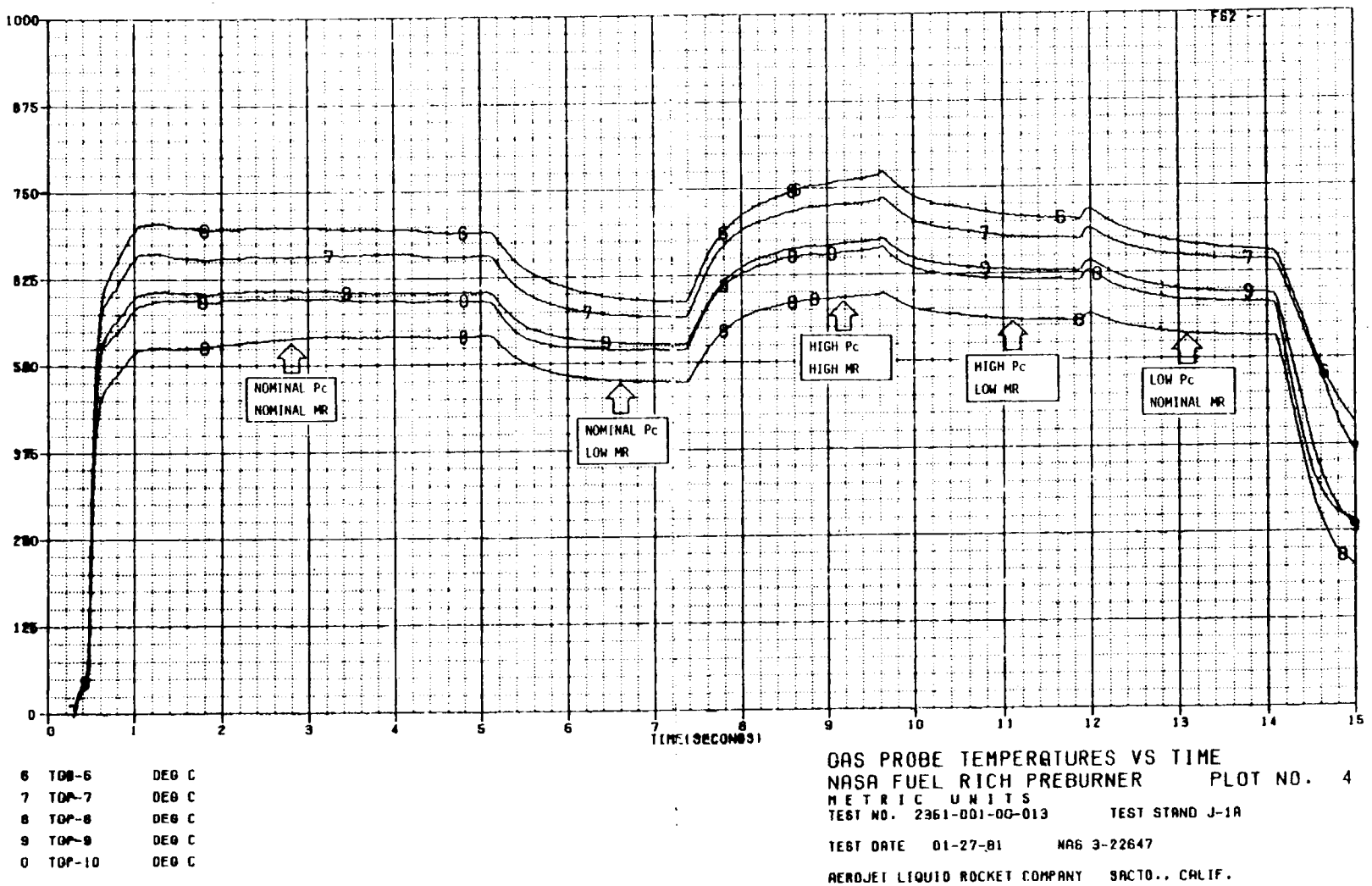

Figure 24. Fuel-Rich Preburner, Gas Probe Temperatures Versus Time, Test -013 Probe 2 (1 of 2)

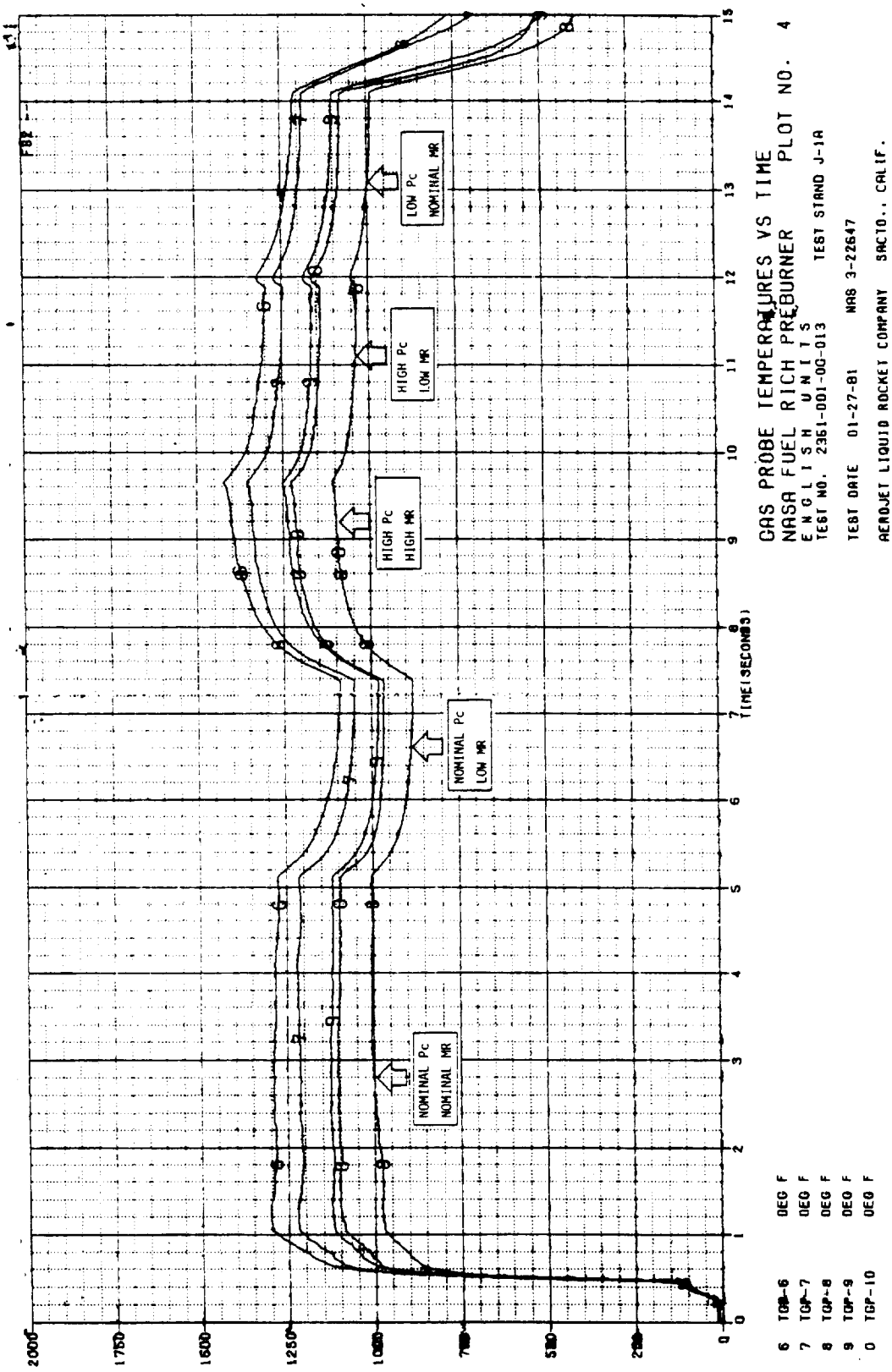

Figure 24. Fuel-Rich Preburner, Gas Probe Temperatures Verus Time, Test -013 Probe 2 (2 of 2)

Test -014

This was the first test conducted with the platelet injector. The objective of this test was to check out ignition and valve timing before proceeding to the injector screening test. Ignition was delayed about 20 ms, resulting in a large overpressure, as shown in Figure 25. The delayed ignition was initially thought to be due to a slower oxidizer manifold fill than that experienced with the EDM injector. Consequently, the start sequence was modified prior to Test -015 to advance the oxidizer valve opening by 15 ms.

The steady-state combustion and shutdown transient were normal. No hardware damage was incurred.

Test -015

Test -015 was the first platelet injector screening test. Five Pc-MR operating points were achieved. Ignition was again delayed by about 20 ms, resulting in an overpressure as shown in Figure 26. Post-test examination of the hardware showed damage to the resonator ring and the instrumentation rakes. These components were replaced prior to Test -016.

The hard start was found to be a consequence of the platelet swirler injector mixing and igniter torch characteristics. As illustrated in Figure 27, the inability of the oxidizer spray fan to penetrate the fuel spray fan near the injector face causes an extreme fuel-rich mixture ratio to be exposed to the fuel-rich igniter torch. Consequently, there is not enough oxygen in contact with the hot torch to cause ignition until the spray fans mix in the throat. The result is that ignition occurs in the throat. The flame propagates via a detonation wave to the injector face, causing the overpressure. The 20-ms delay correlates well with the calculated gas residence time.

The solution to the delayed ignition was to reorifice the igniter to operate oxidizer-rich at a mixture ratio of 40:1. This change was made prior to Test -016, with the result that smooth ignition was achieved on Test -016 and all subsequent platelet injector tests.

The hard start problem was not encountered with the EDM injector. Oxidizer orifices were purposely placed in the EDM injector face near the igniter exit to react with the fuel-rich torch. This induces ignition near the injector face, thus avoiding large overpressures.

Combustion instability was experienced at the low-Pc (13.1 MN/m^2 [1900 psia]), low-MR (0.25) operating point. The instability was

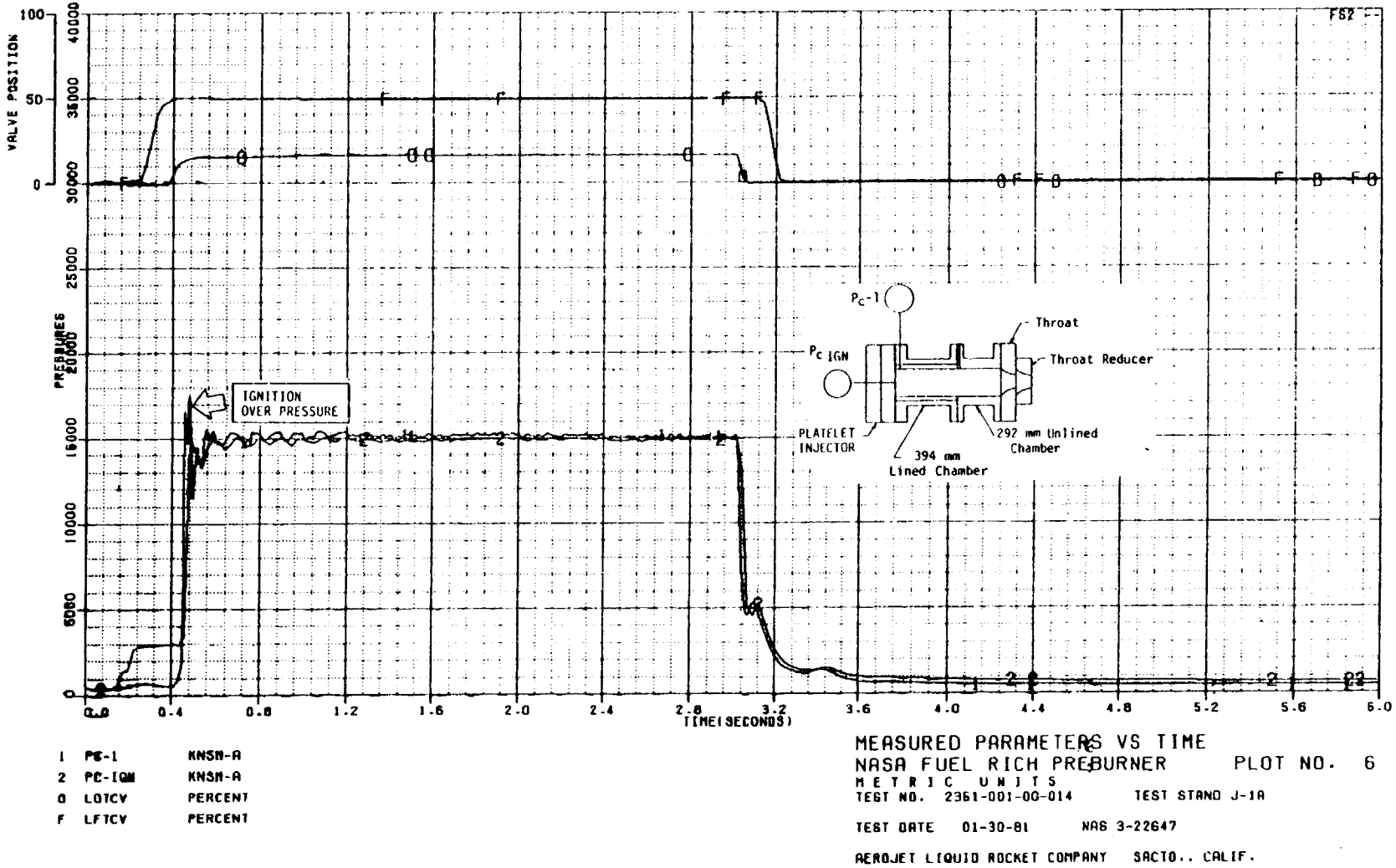

Figure 25. Fuel-Rich Preburner, Measured Parameters Versus Time, Test -014 (1 of 2)

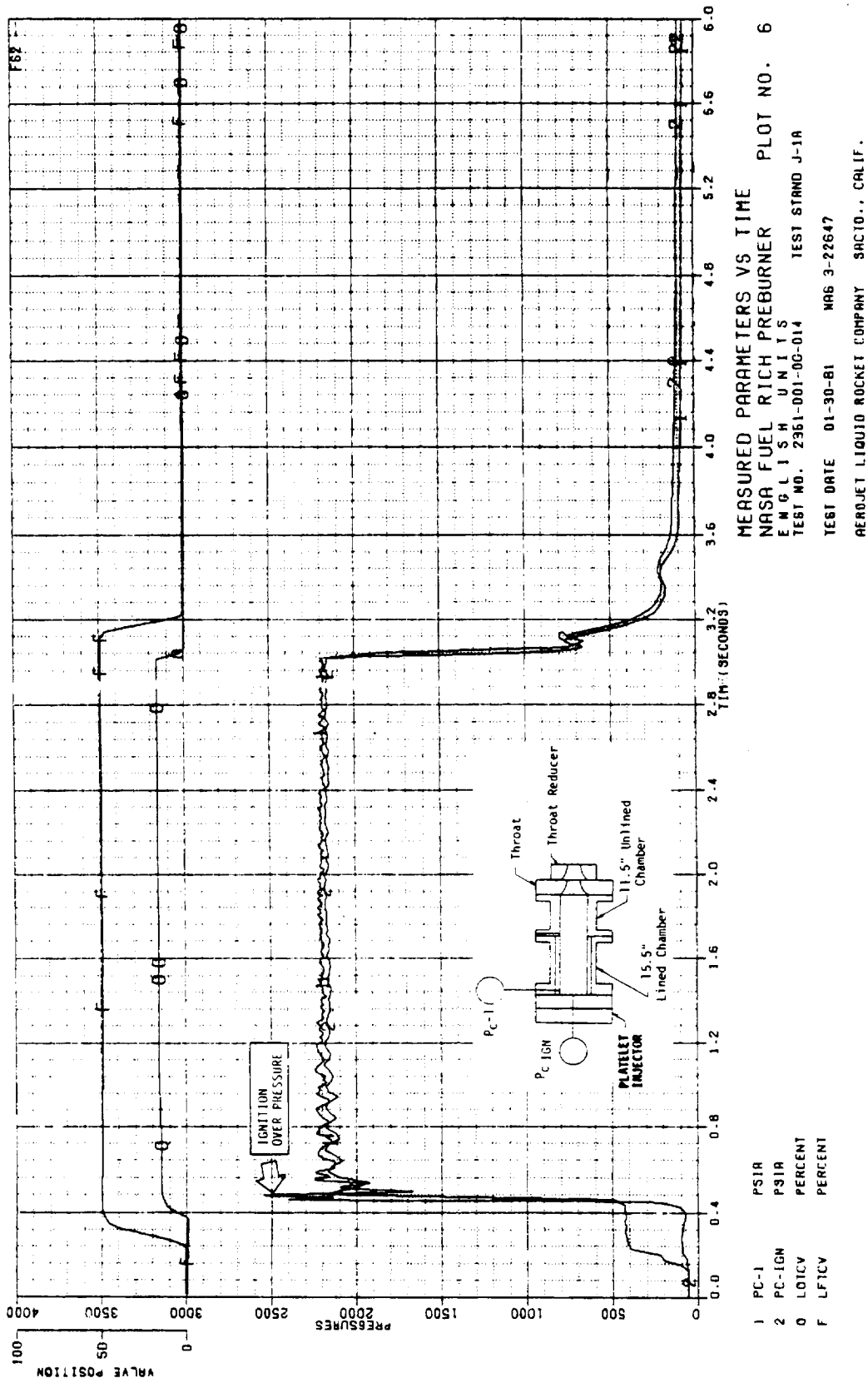

Figure 25. Fuel-Rich Preburner, Measured Parameters Versus Time, Test -014 (2 of 2)

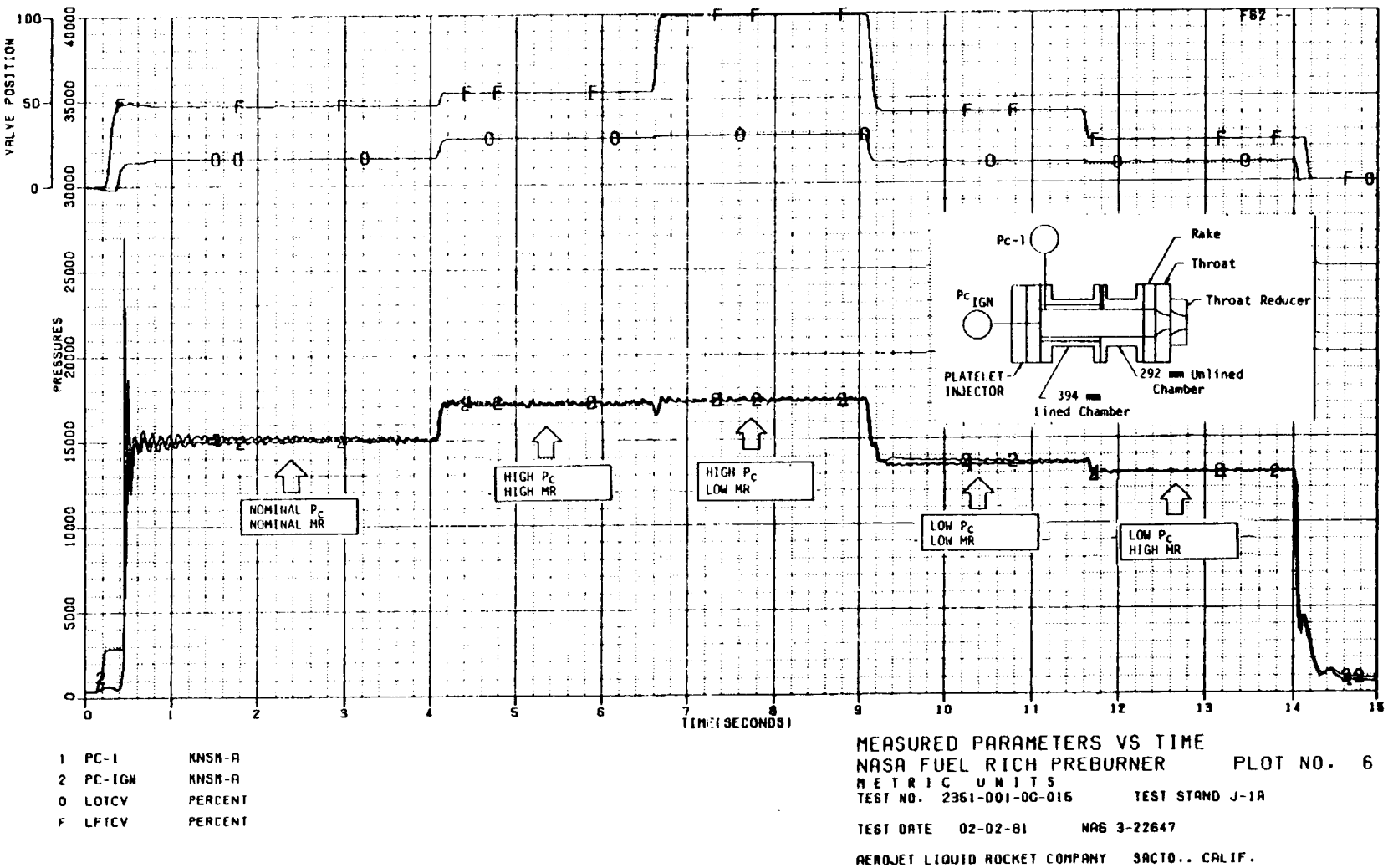

Figure 26. Fuel-Rich Preburner, Measured Parameters Versus Time, Test -015 (1 of 2)

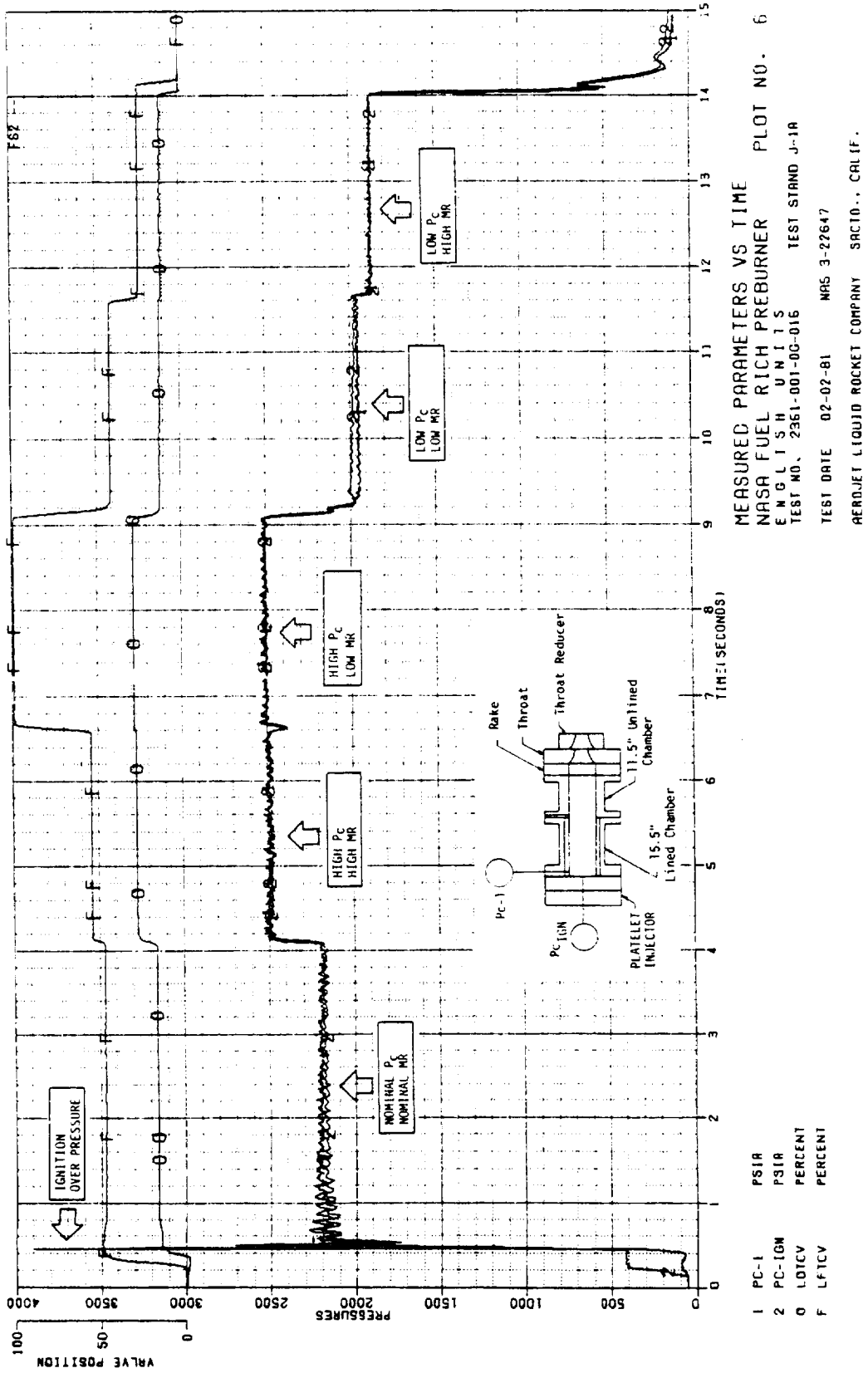

Figure 26. Fuel-Rich Preburner, Measured Parameters Versus Time, Test -015 (2 of 2)

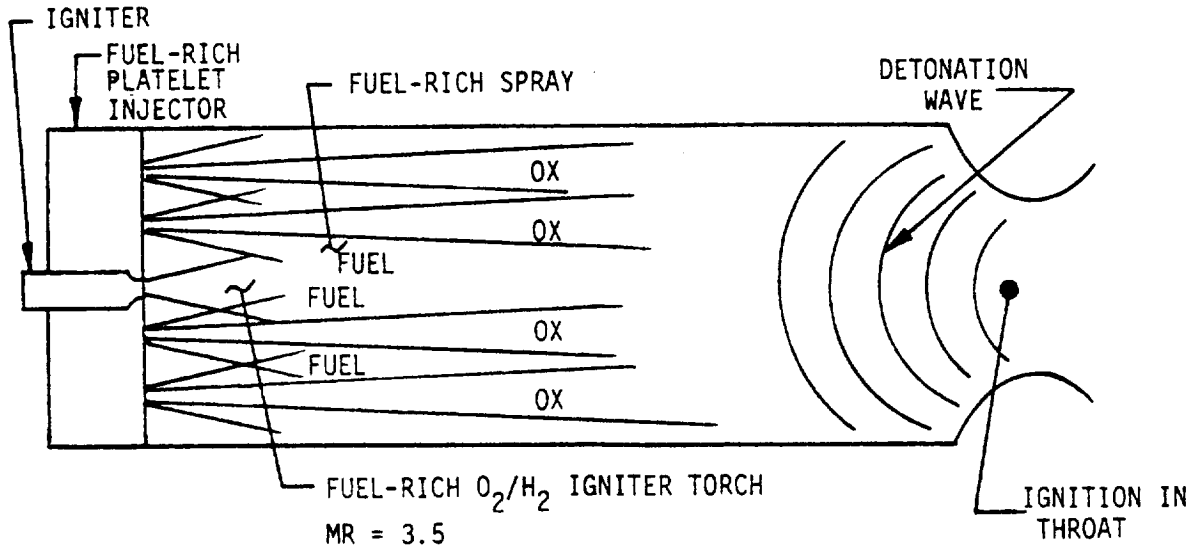

TEST -014 AND -015

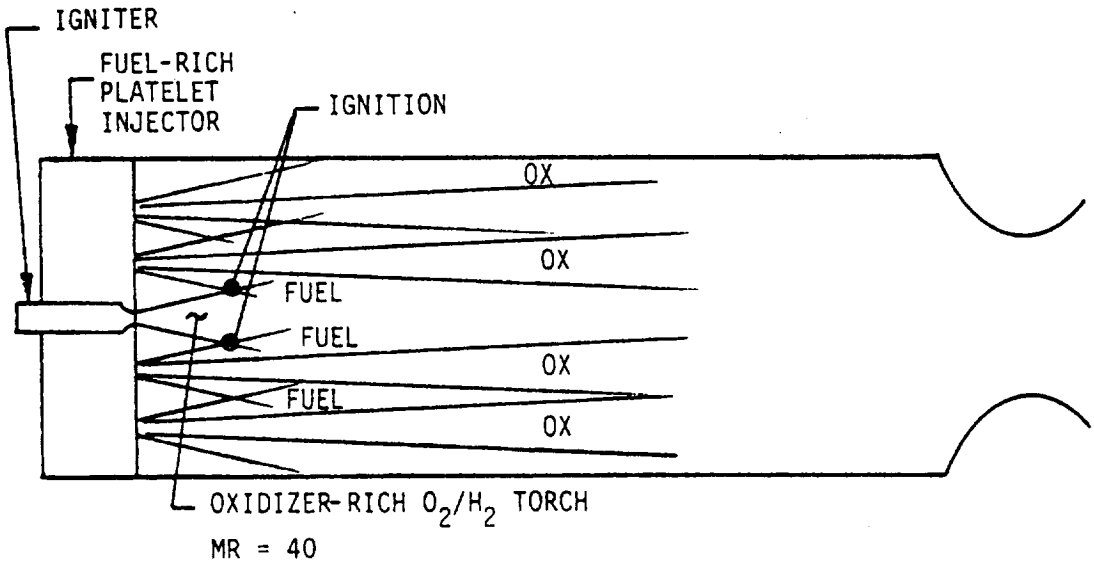

TEST -016 THROUGH -029

Figure 27. Effect of Igniter Torch Mixture Ratio on Fuel-Rich Platelet Injector Ignition

identified as being in the second longitudinal (2L) mode. The frequency of oscillation was 600 Hz, and the amplitude was .827 MN/m^2 (120 psia) PK-PK.

The gas temperatures are shown in Figures 28 and 29. The longitudinal combustion instability usually improves the gas temperature uniformity through improved mixing.

Test -016

Test -016 was the second platelet injector screening test. Four Pc-MR operating points were achieved. Five operating points were planned; however, a temperature probe kill terminated the test early in the fourth Pc-MR step.

The temperature kill occurred at the high-Pc (17.2 MN/m^2 [2500 psia]), nominal (0.3) MR condition on thermocouple wall 1 (TCW-1). The temperature kill was set for 1256°K (1800°F). Post-test examination showed the thermocouple to be protruding about 1.6 mm (1/16 in.) into the gas stream rather than flush with the wall, thus creating an erroneous shutdown. A new TCW-1 thermocouple was installed prior to Test -017.

Ignition was smooth, with a slight overpressure as shown in Figure 30. Unstable combustion was encountered at nominal Pc (15.2 MN/m^2 [2200 psia]) and low MR (0.25). The frequency of oscillation was 600 Hz, and the instability was identified as being the 2L mode. The gas temperatures are shown in Figures 31 and 32. The longitudinal combustion instability improves the gas temperature uniformity through improved mixing.

Test -017

Test -017 was to be the first of three added scope tests. The objective of this test was to verify the effect of reduced chamber length on the longitudinal mode stability. The 292-mm (11.5-in.) chamber section was removed. The main injector simulator flange, without injector simulator, was installed ahead of the instrumentation rake to achieve an overall length of about 533 mm (21 in.).

Ignition was smooth and normal; however, the test was terminated 50 ms after ignition by the TCW-1 thermocouple kill. Post-test examination showed that the new TCW-1 had been installed about 3.2 mm (1/8 in.) into the gas stream, causing the thermocouple (T/C) kill. TCW-1 was retracted to be flush with the wall, and the thermocouple kill was moved to the gas probe temperature 1 (TGP-1) thermocouple prior to Test -018.

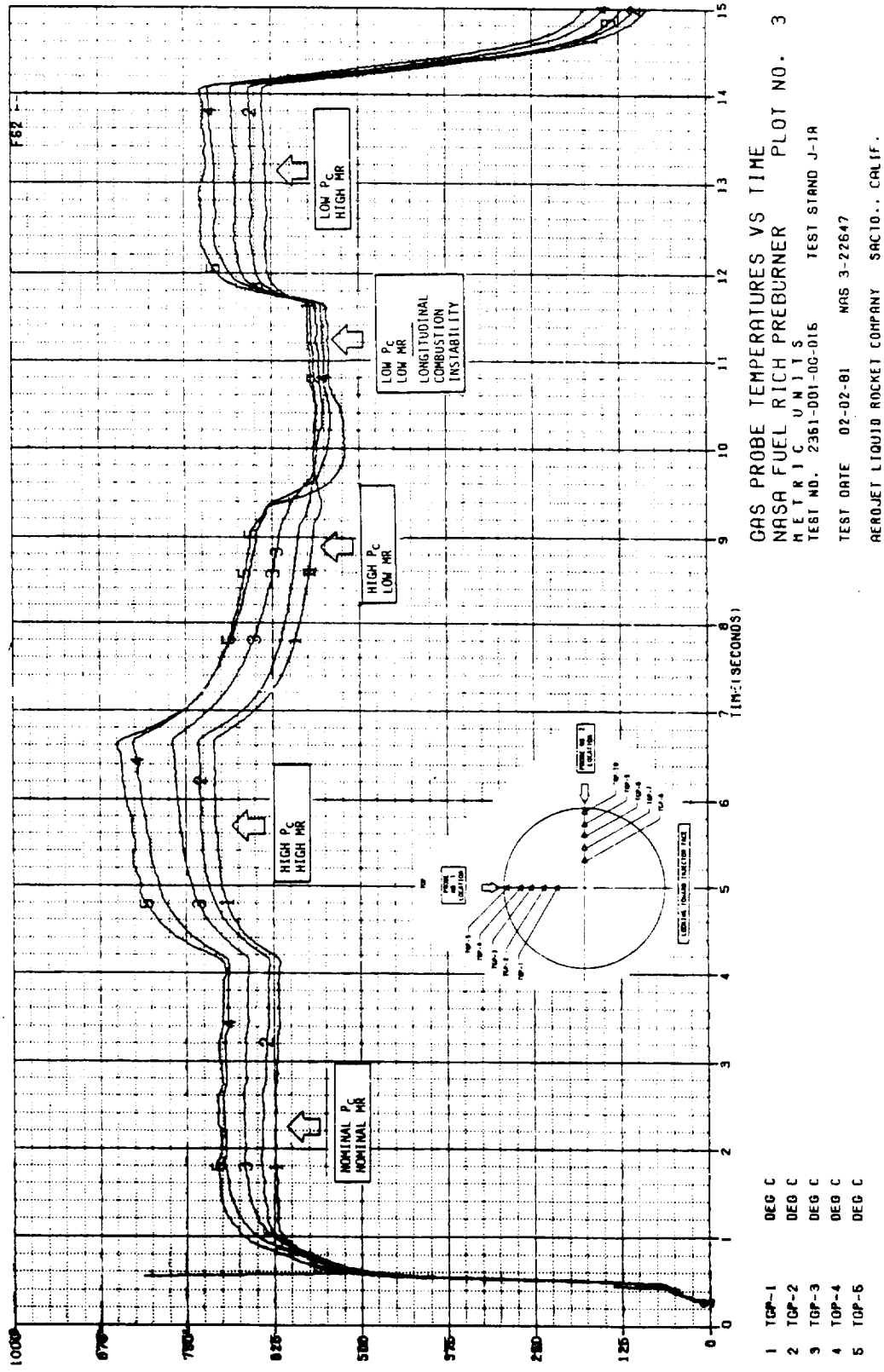

Figure 28. Fuel-Rich Preburner, Gas Probe Temperatures (TGP-1, -5) Versus Time, Test -015 (1 of 2)

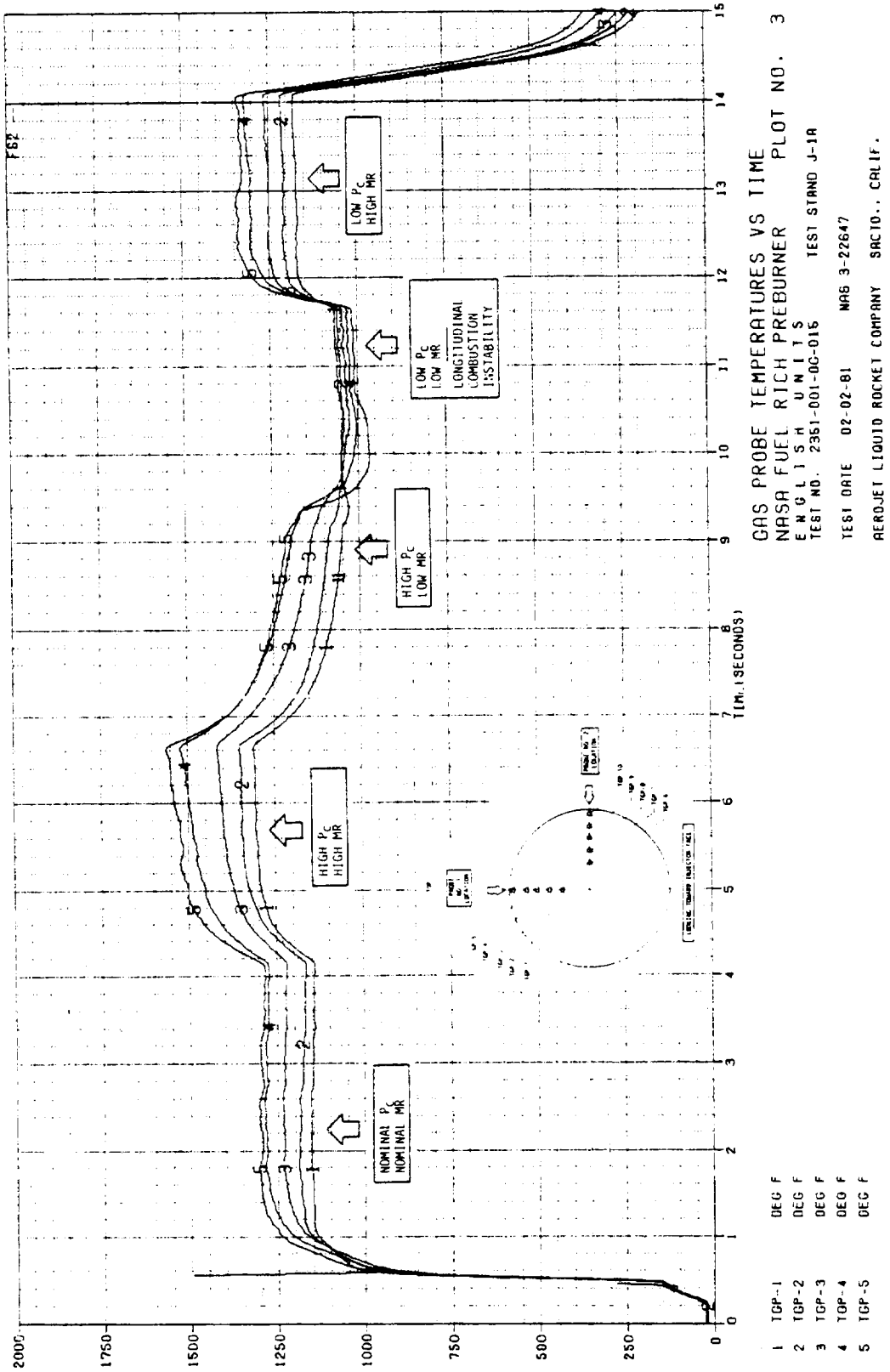

Figure 28. Fuel-Rich Preburner, Gas Probe Temperatures (TGP-1, -5) Versus Time, Test -015 (2 of 2)

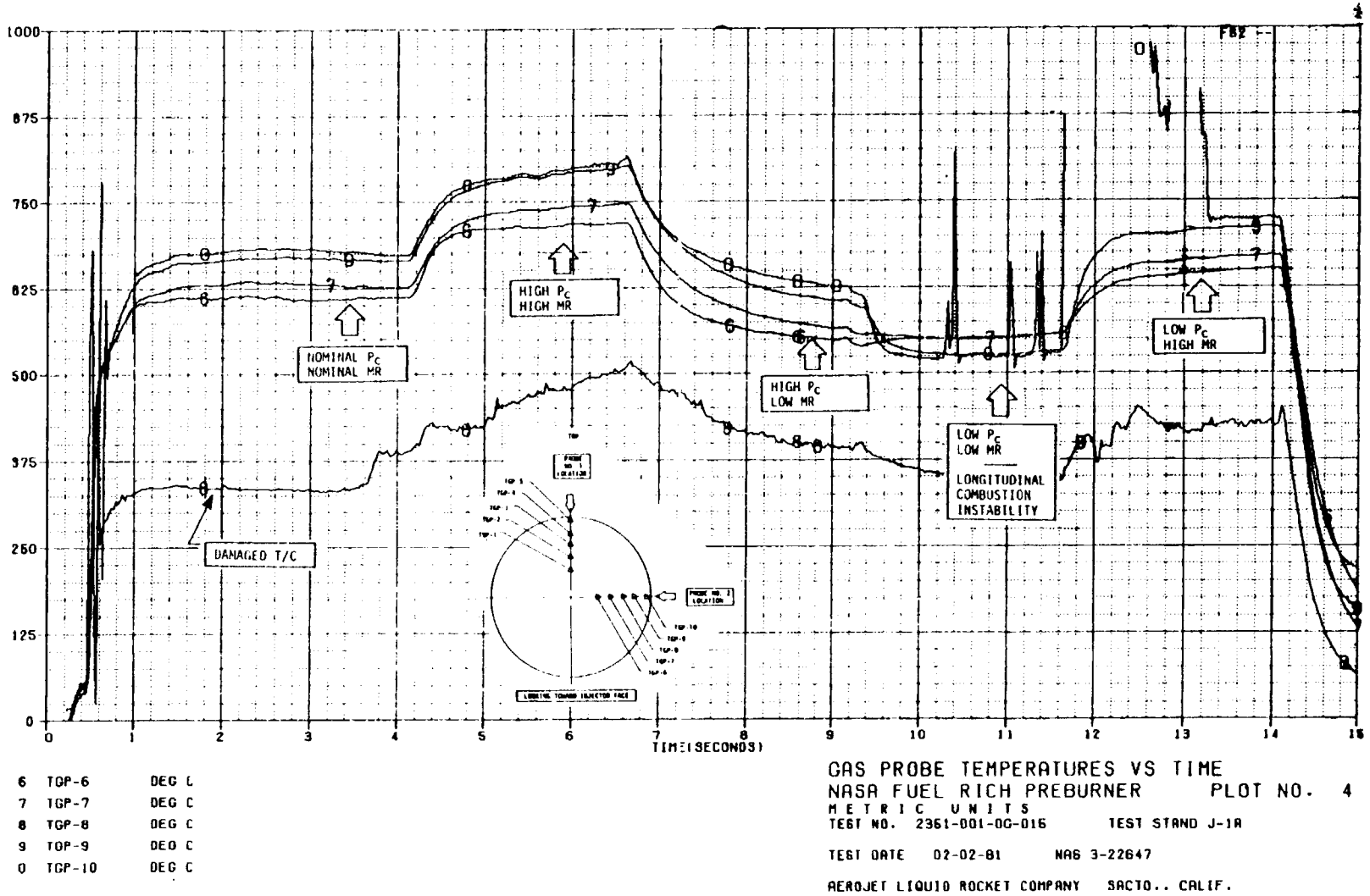

Figure 29. Fuel-Rich Preburner, Gas Probe Temperatures (TGP-6, -10) Versus Time, Test -015 (1 of 2)

ORIGINAL PAGE IS
OF POOR QUALITY

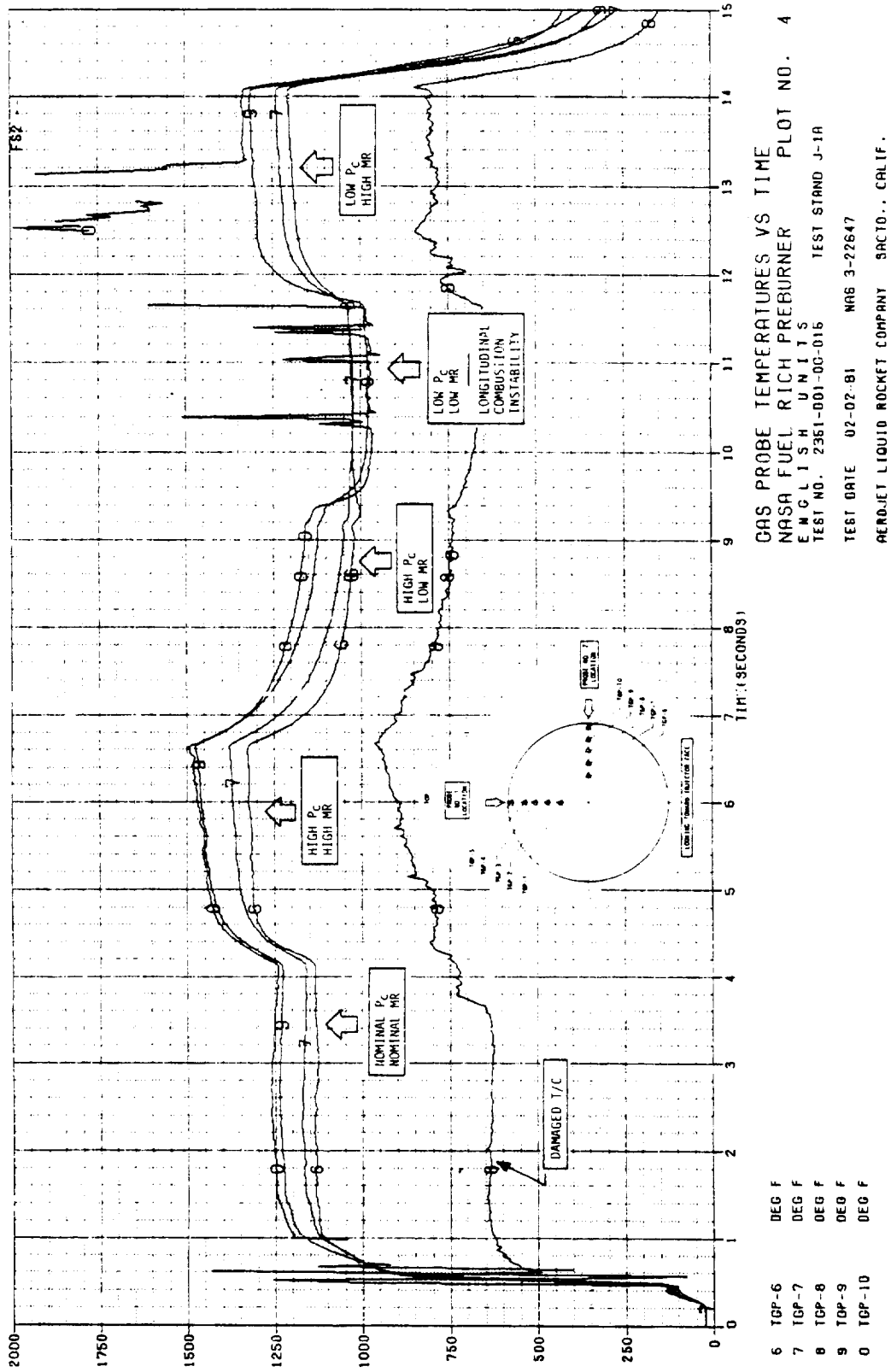

Figure 29. Fuel-Rich Preburner, Gas Probe Temperatures (TGP-6, -10) Versus Time, Test -015 (2 of 2)

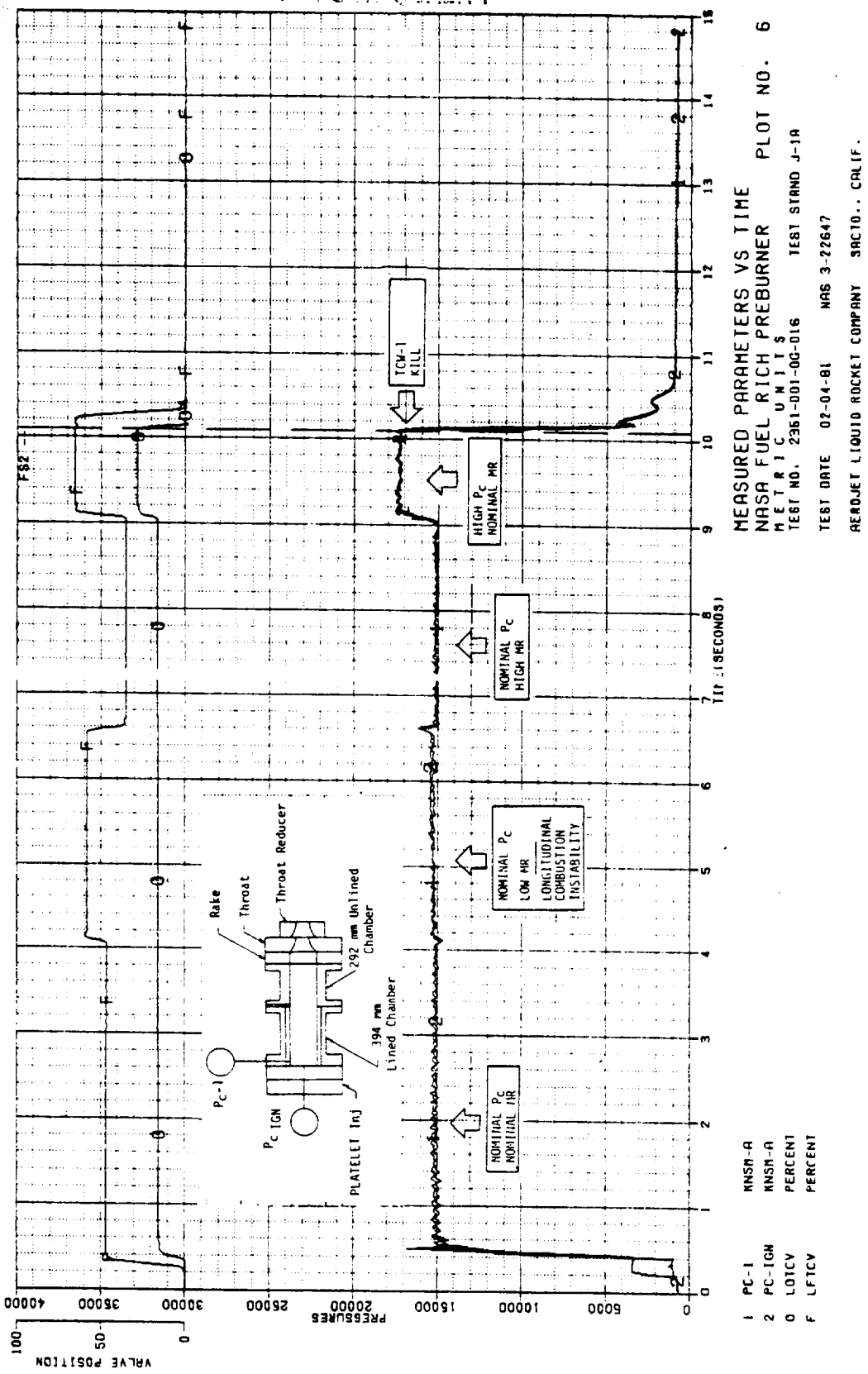

Figure 30. Fuel-Rich Preburner, Measured Parameters Versus Time, Test -016 (1 of 2)

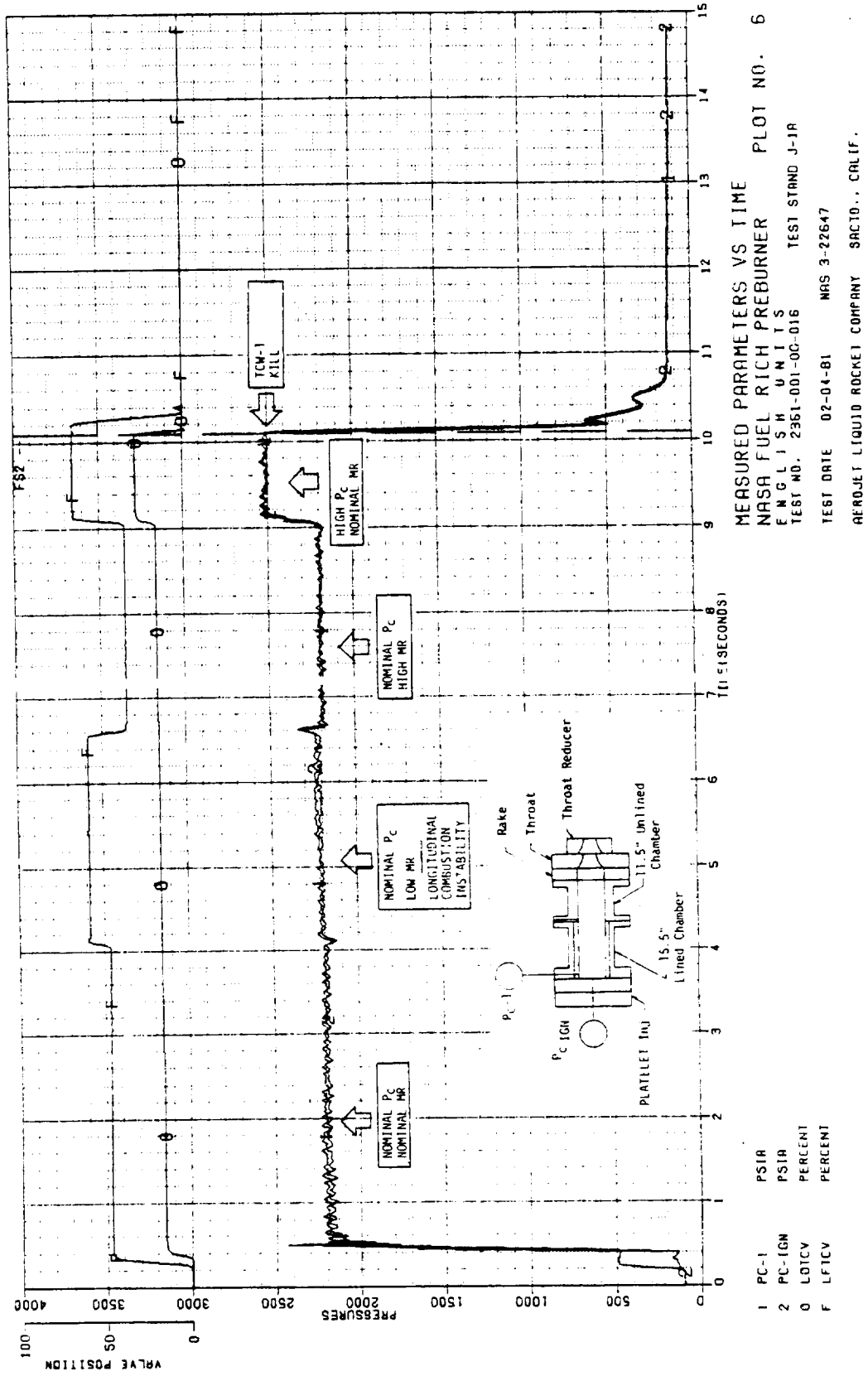

Figure 30. Fuel-Rich Preburner, Measured Parameters Versus Time, Test -016
(2 of 2)

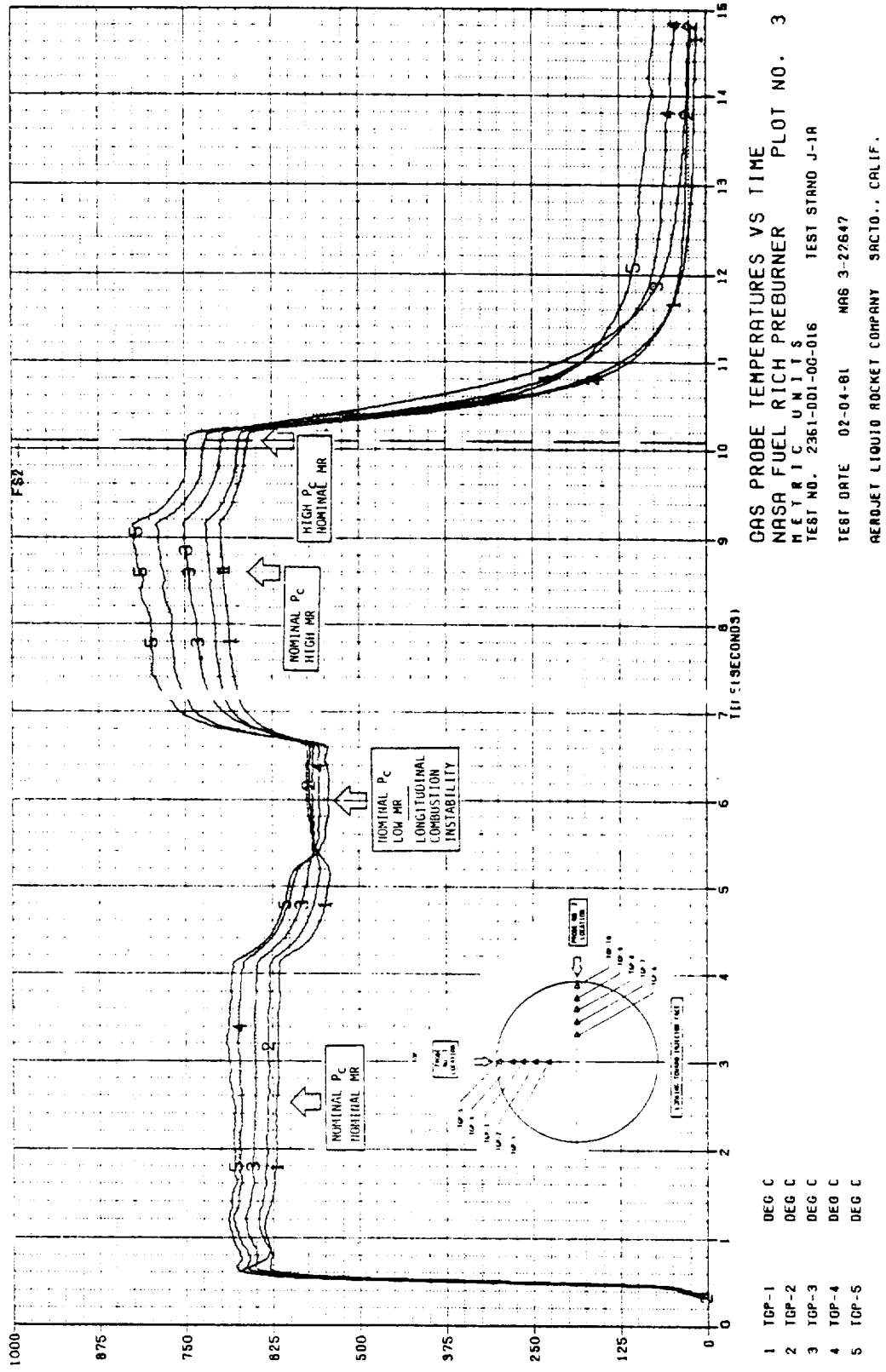

Figure 31. Fuel-Rich Preburner, Gas Probe Temperatures (TGP-1, -5) Versus Time, Test -016 (1 of 2)

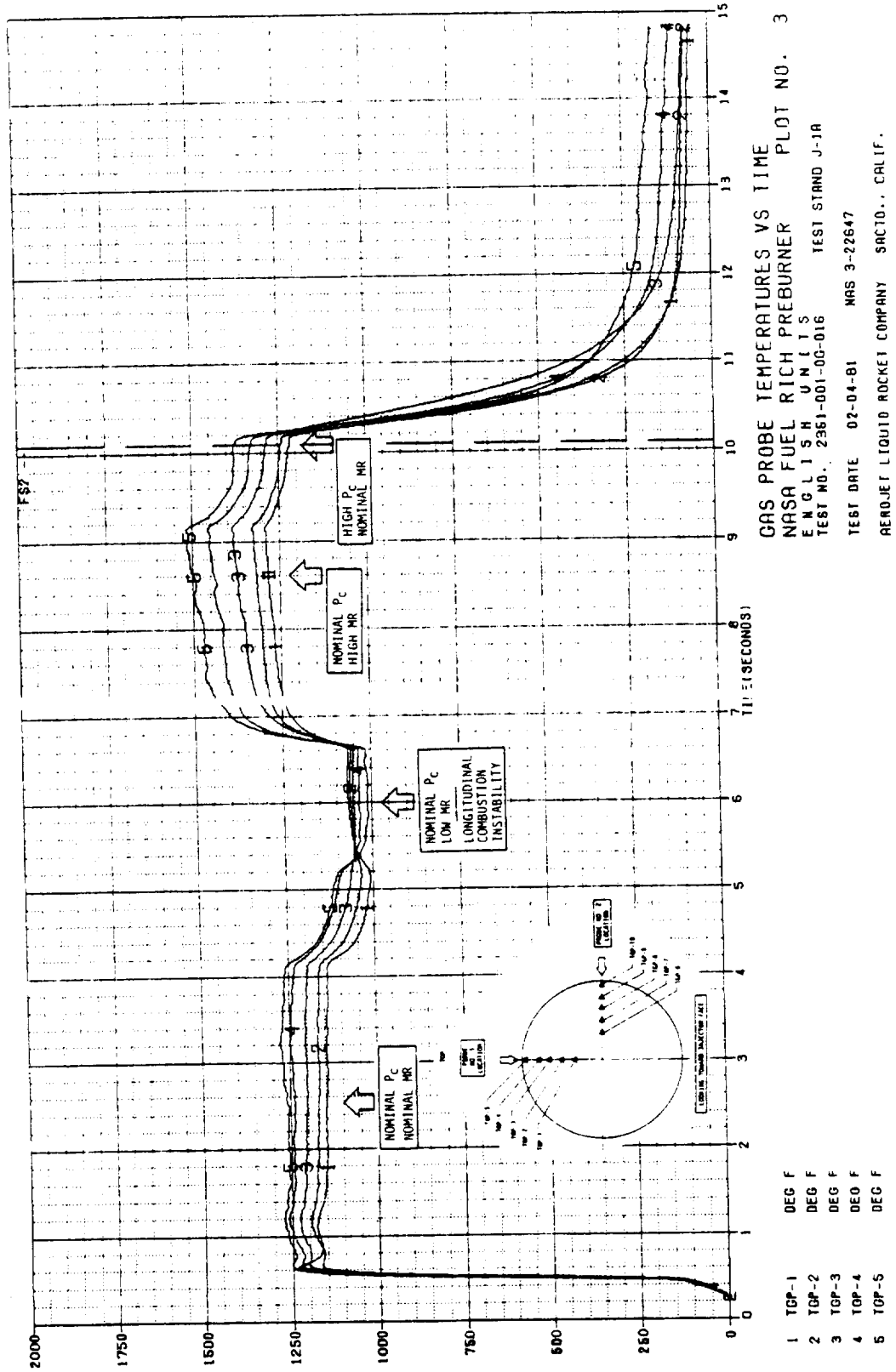

Figure 31. Fuel-Rich Preburner, Gas Probe Temperatures (TGP-1, -5) Versus Time, Test -016 (2 of 2)

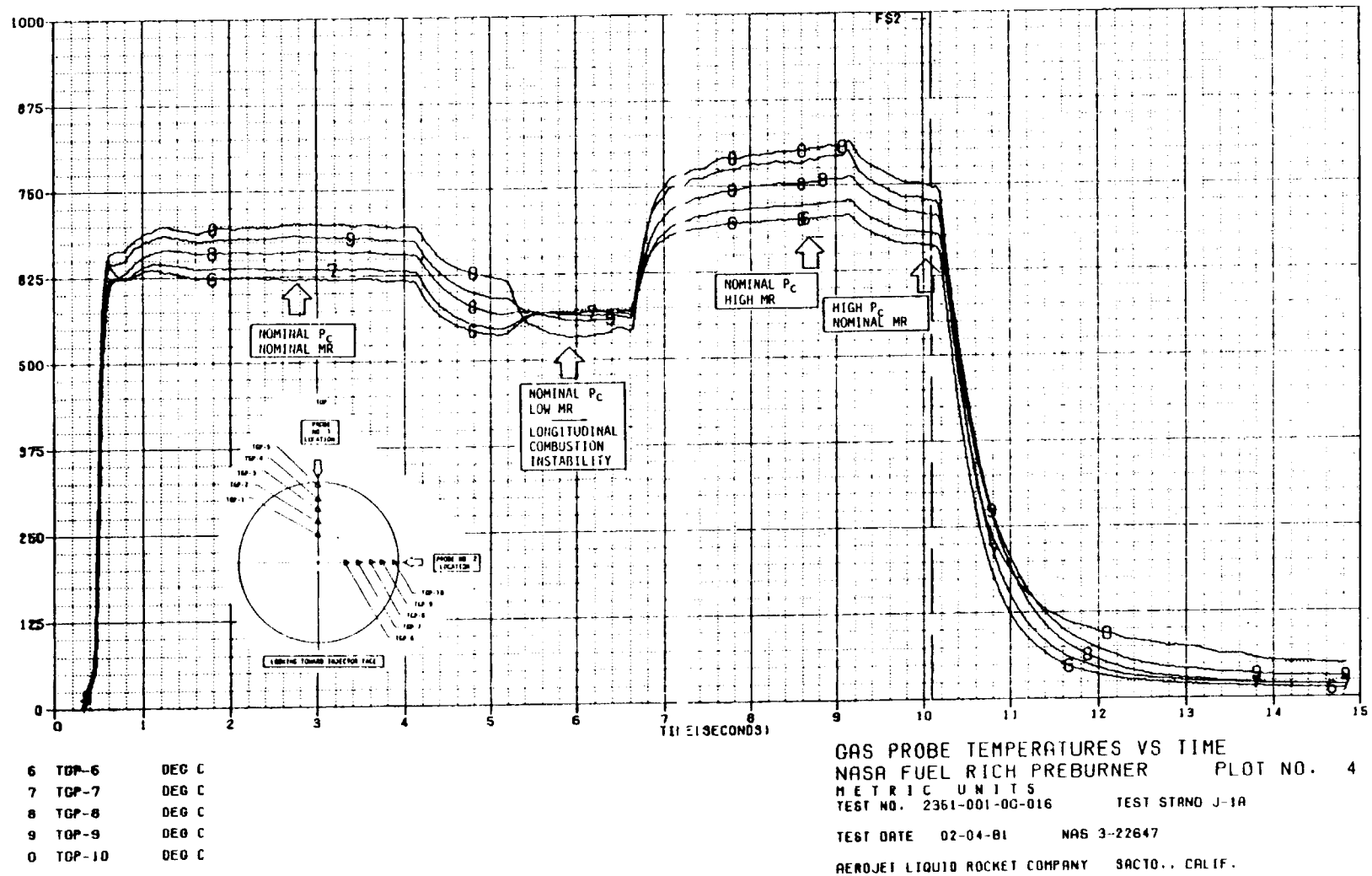

Figure 32. Fuel-Rich Preburner, Gas Probe Temperatures (TGP-6, -10) Versus Time, Test -016 (1 of 2)

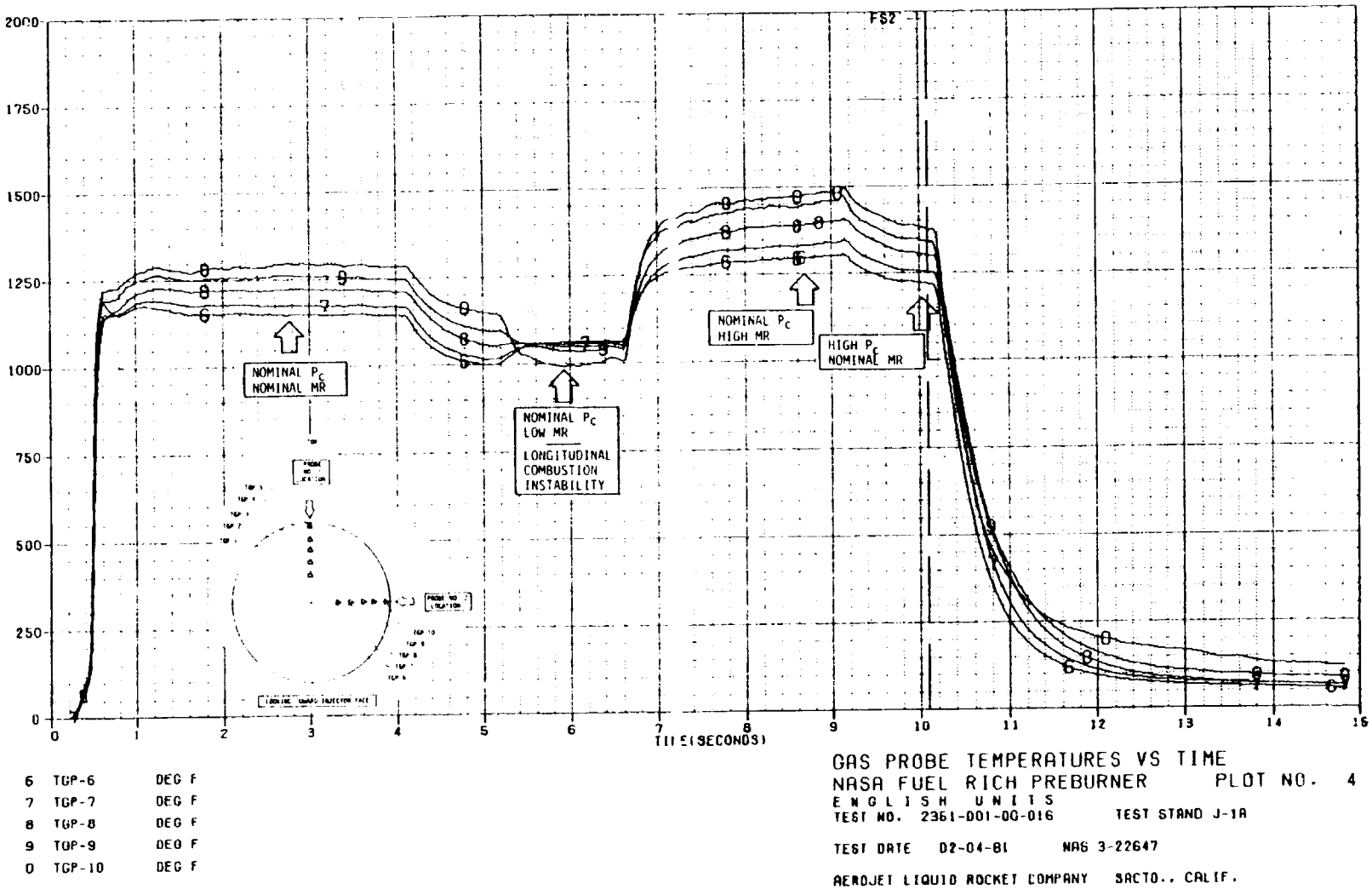

Figure 32. Fuel-Rich Preburner, Gas Probe Temperatures (TGP-6, -10) Versus Time, Test -016 (2 of 2)

IV, B, Test Results (cont.)

Test -018

Test -018 was a repeat of Test -017. Five operating points were successfully achieved. All operating points, except at high Pc (17.2 MN/m^2 (2500 psia)) and low MR (0.25), were unstable in the 1L mode, as indicated in Figure 33. The gas temperatures are shown in Figures 34 and 35.

Test -019

This was the second of three added scope tests. The objective was to determine the damping effect of the turbulence ring on the longitudinal mode stability. Analysis indicated that the turbulence ring should provide damping and improve stability. The 76.2 mm (3.0 in.) turbulence ring diameter was installed about 127 mm (5 in.) from the injector face. Selection of the turbulence ring location was based on thermal considerations as discussed in Section IV.C.1. Five operating points were achieved. All operating points, except at low Pc (3.1 MN/m^2 [1900 psia]) and high MR (0.35), were stable, as indicated in Figure 36.

The turbulence ring has a stabilizing effect on the 533-mm (21-in.) chamber length. It also has a significant effect on the temperature uniformity, as shown in Figures 37 and 38.

Test -020

This was the third added scope test. The objective was to verify the effect of the turbulence ring on the longitudinal stability with the longer (787-mm [31-in.]) chamber. The 292-mm (11.5 in.) chamber section was added to the 394-mm (15.5-in.) chamber section, with the turbulence ring in the same position as for Test -019.

Five operating points were achieved. All operating points were stable, as indicated in Figure 39. The gas temperatures are shown in Figures 40 and 41.

Test -021

This was the first test to determine the effect of operating point on carbon deposition. The platelet injector was selected for these tests. The test configuration was as shown in Figure 42. The turbine simulator blade openings were adjusted to the gap sizes shown in Figure 43.

Post-test examination showed light carbon buildup on the turbine and main injector simulators. The chamber pressure was found to rise during the entire test, as shown in Figure 42. A detailed evaluation of the

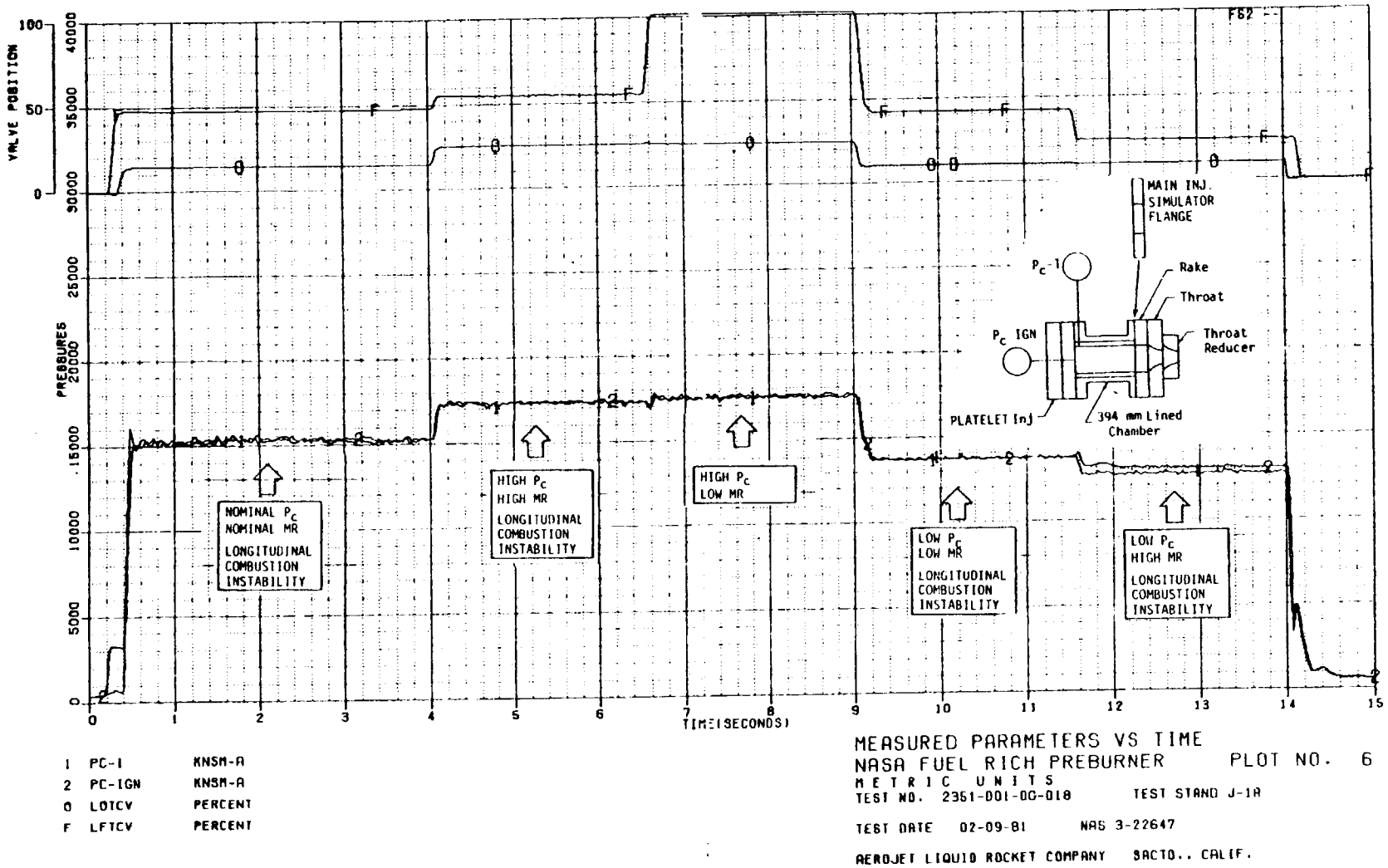

Figure 33. Fuel-Rich Preburner, Measured Parameters Versus Time, Test -018 (1 of 2)

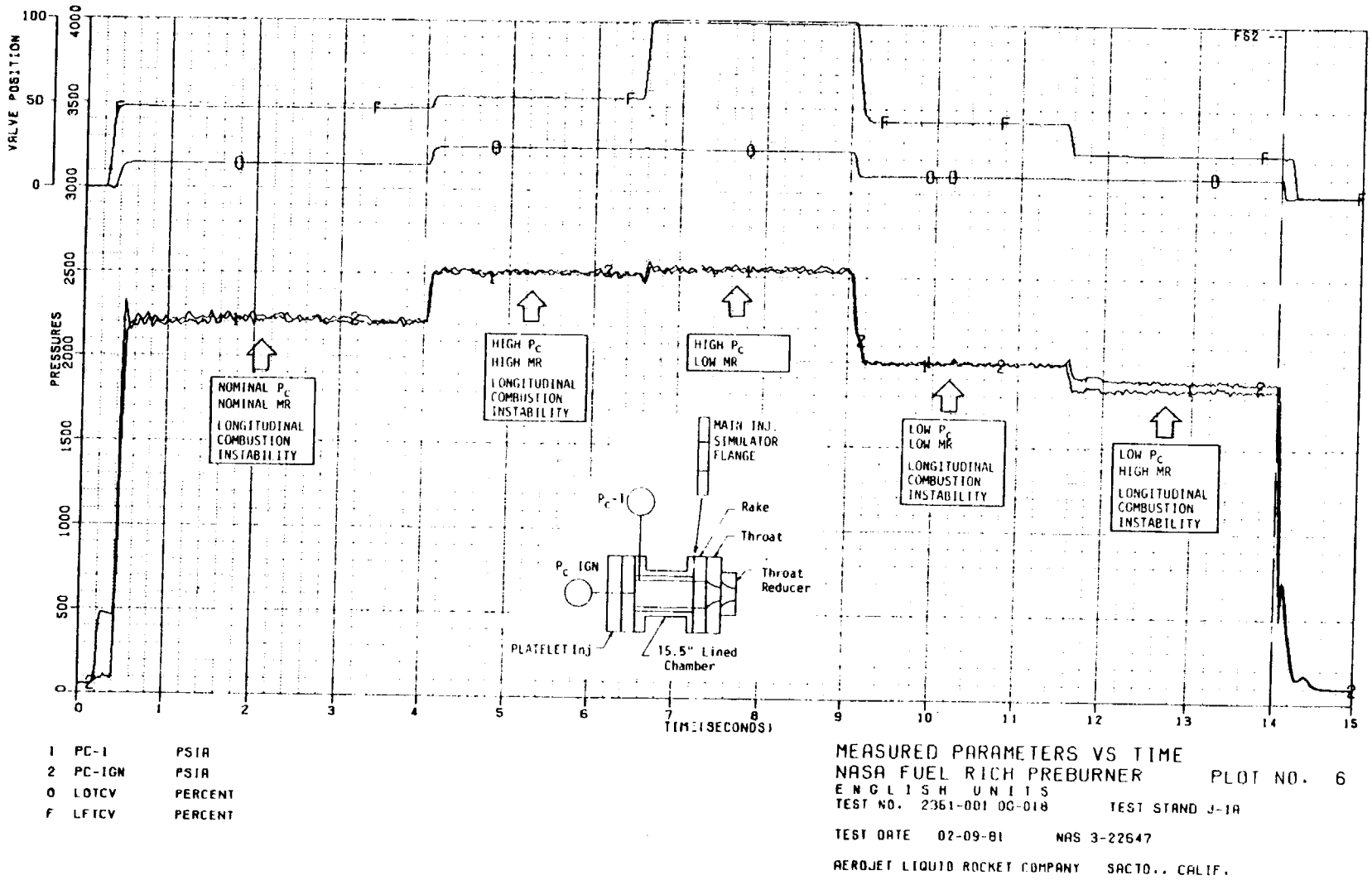

Figure 33. Fuel-Rich Preburner, Measured Parameters Versus Time, Test -018 (2 of 2)

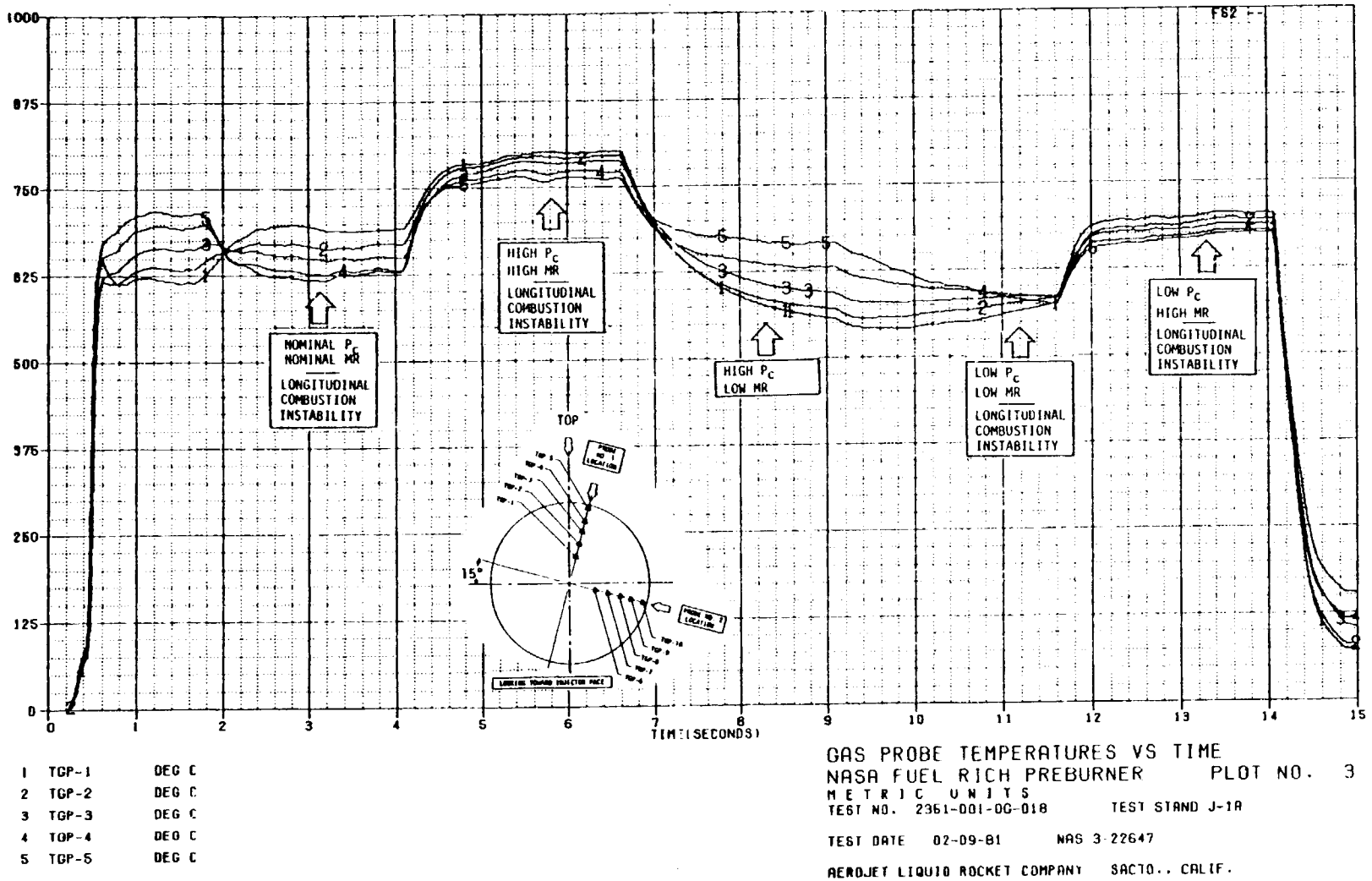

Figure 34. Fuel-Rich Preburner, Gas Probe Temperatures (TGP-1, -5) Versus Time, Test -018 (1 of 2)

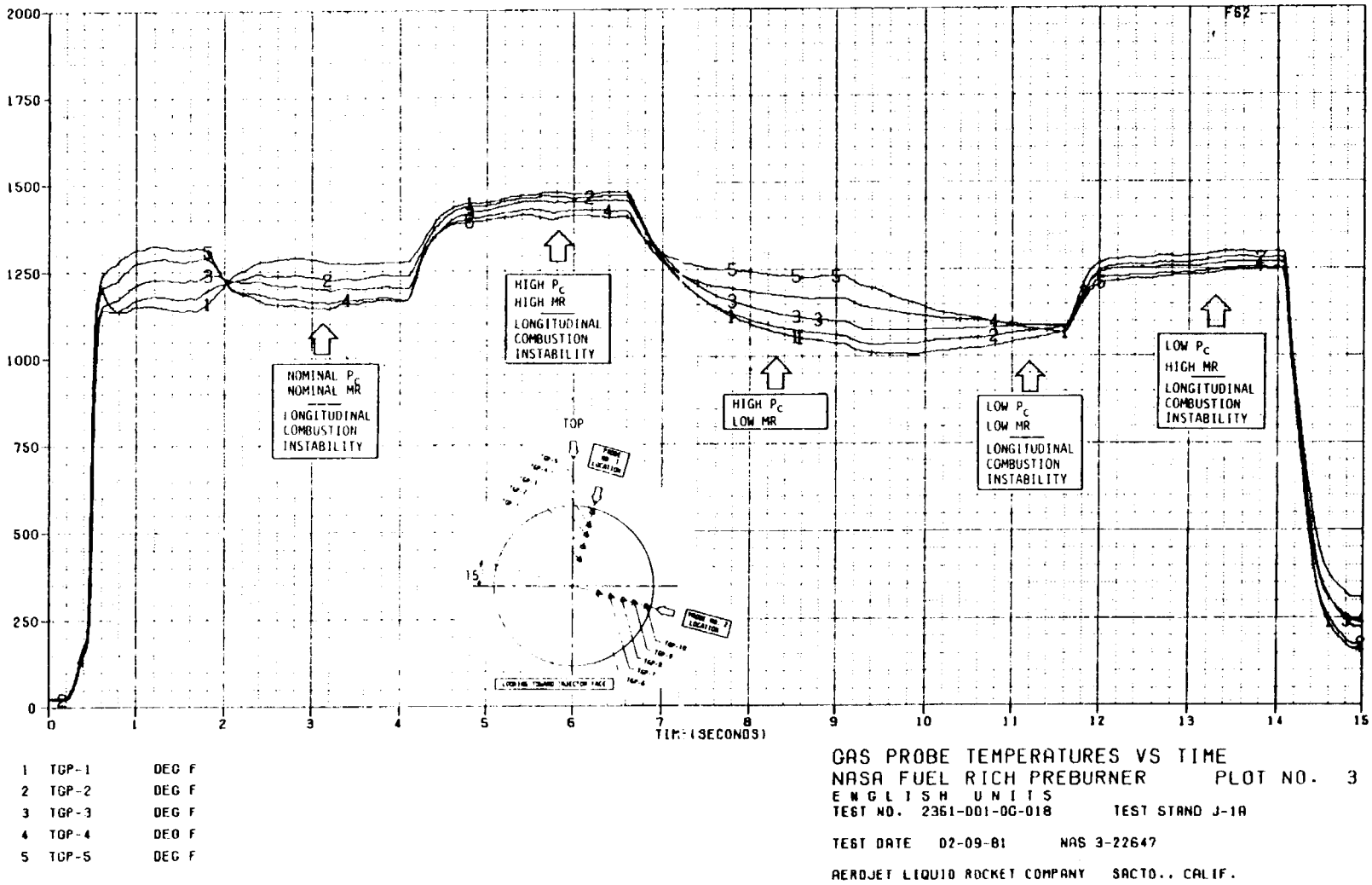

Figure 34. Fuel-Rich Preburner, Gas Probe Temperatures (TGP-1, -5) Versus Time, Test -018 (2 of 2)

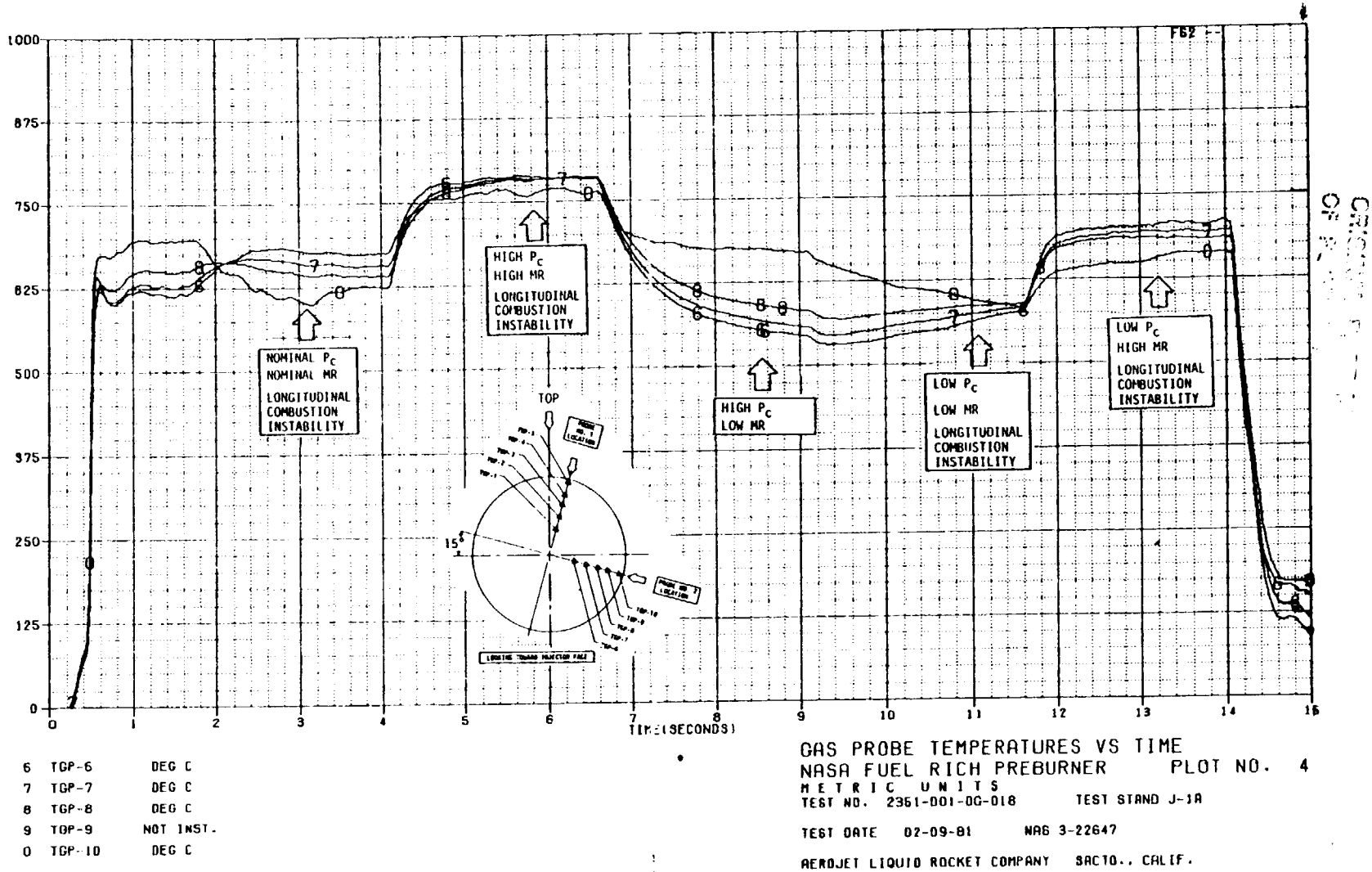

Figure 35. Fuel-Rich Preburner, Gas Probe Temperatures (TGP-6, -10) Versus Time, Test -018 (1 of 2)

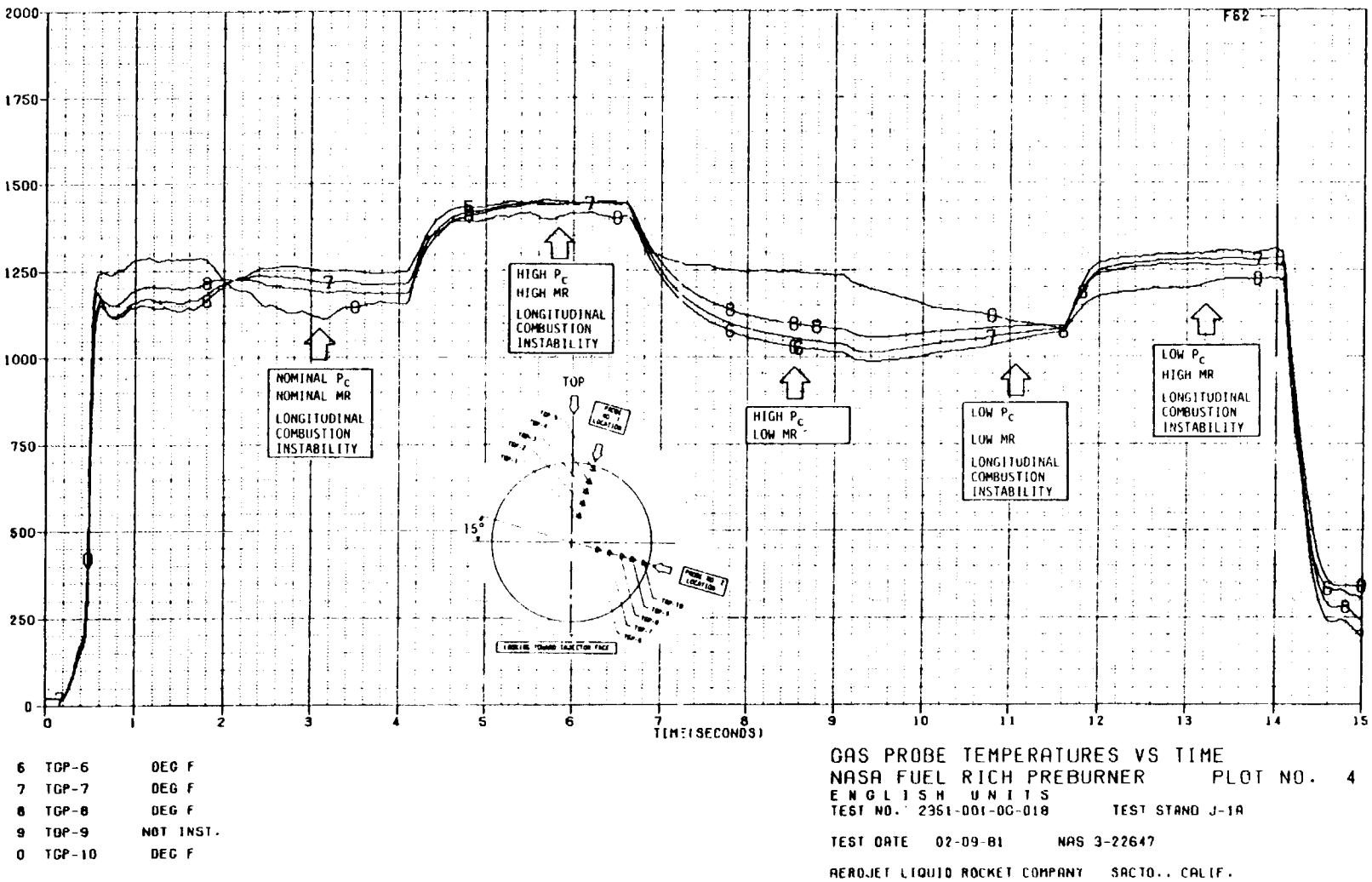

Figure 35. Fuel-Rich Preburner, Gas Probe Temperatures (TGP-6, -10) Versus Time, Test -018 (2 of 2)

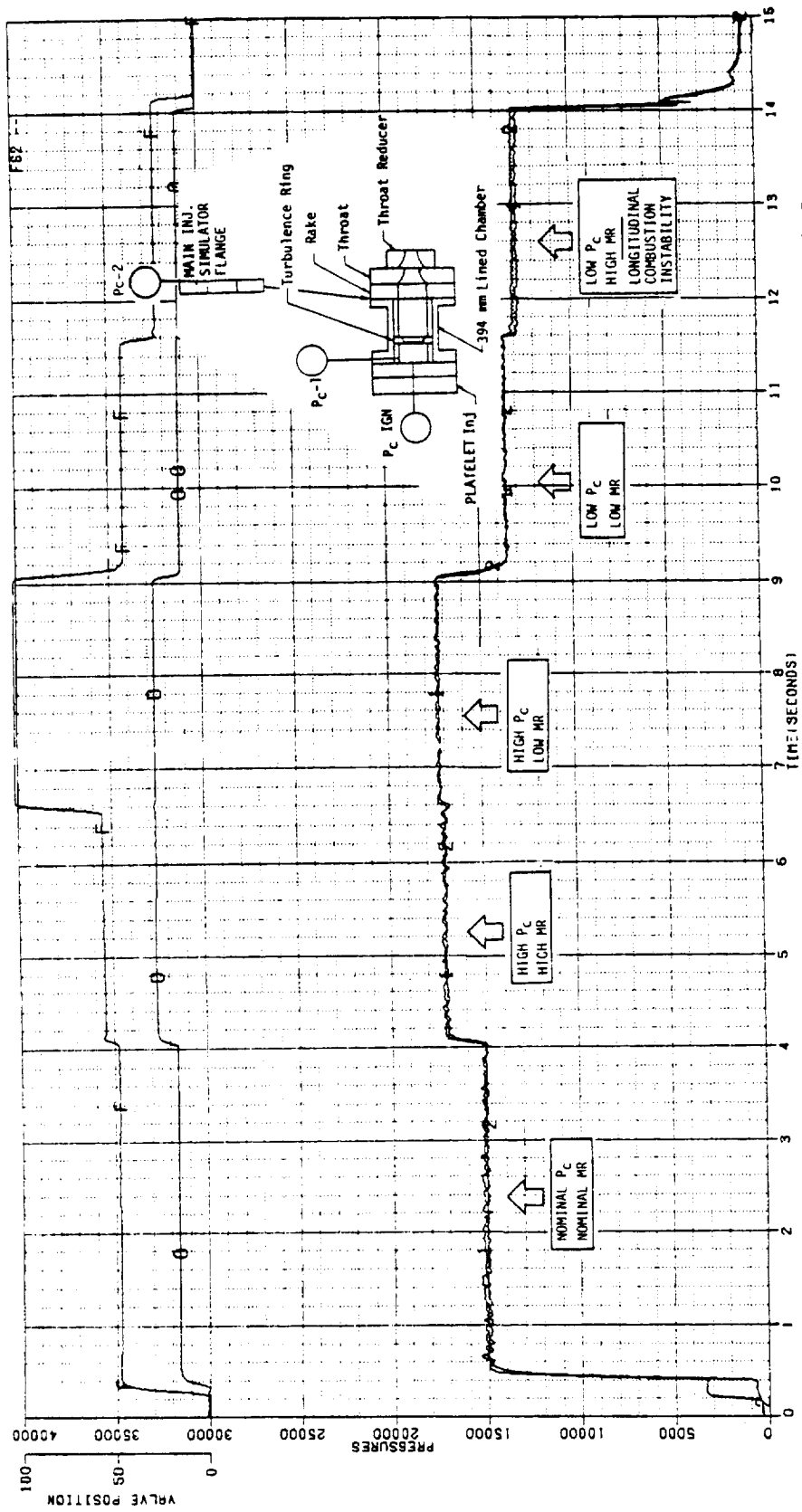

Figure 36. Fuel-Rich Preburner, Measured Parameters Versus Time, Test -019 (1 of 2)

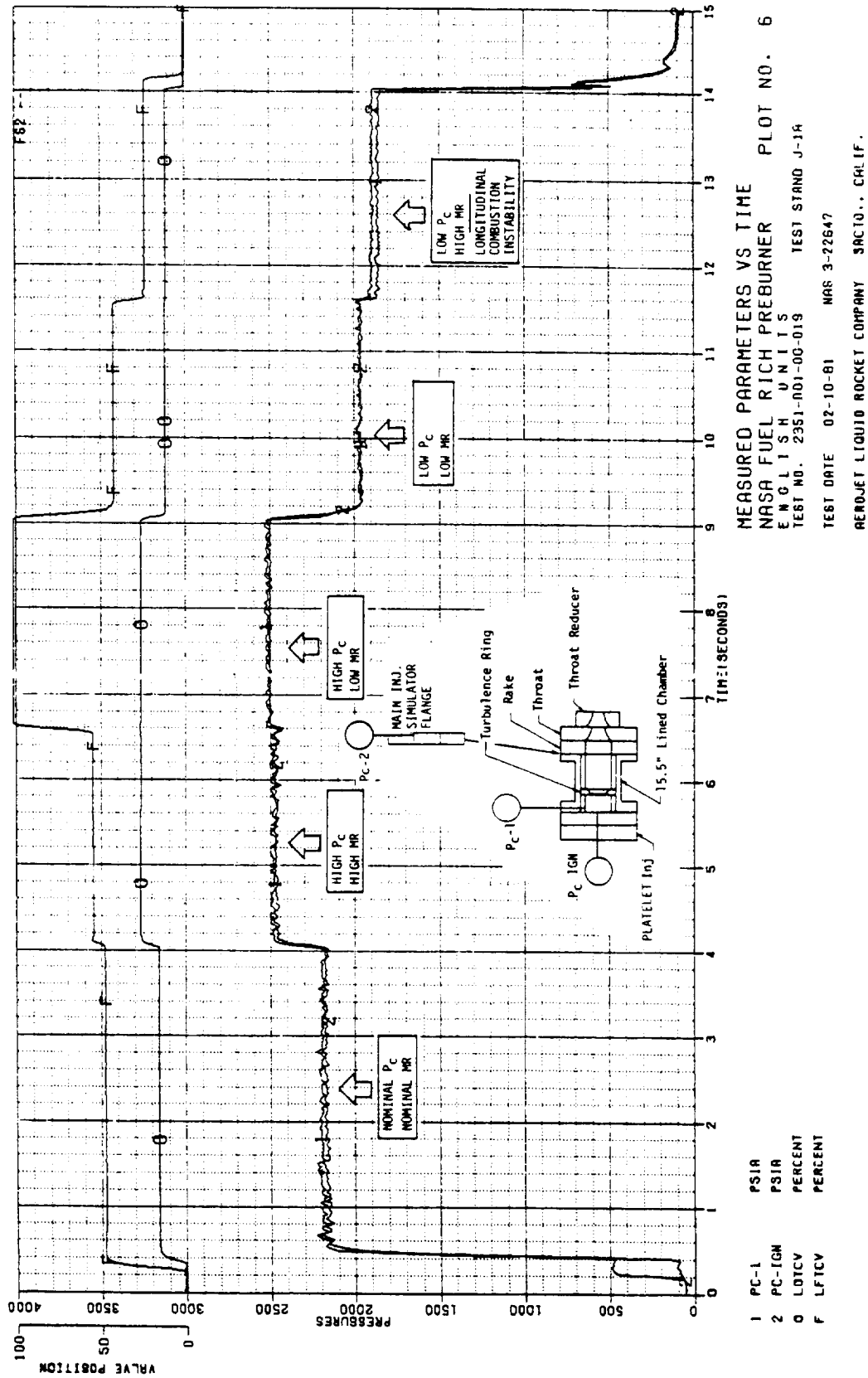

Figure 36. Fuel-Rich Preburner, Measured Parameters Versus Time, Test -019 (2 of 2)

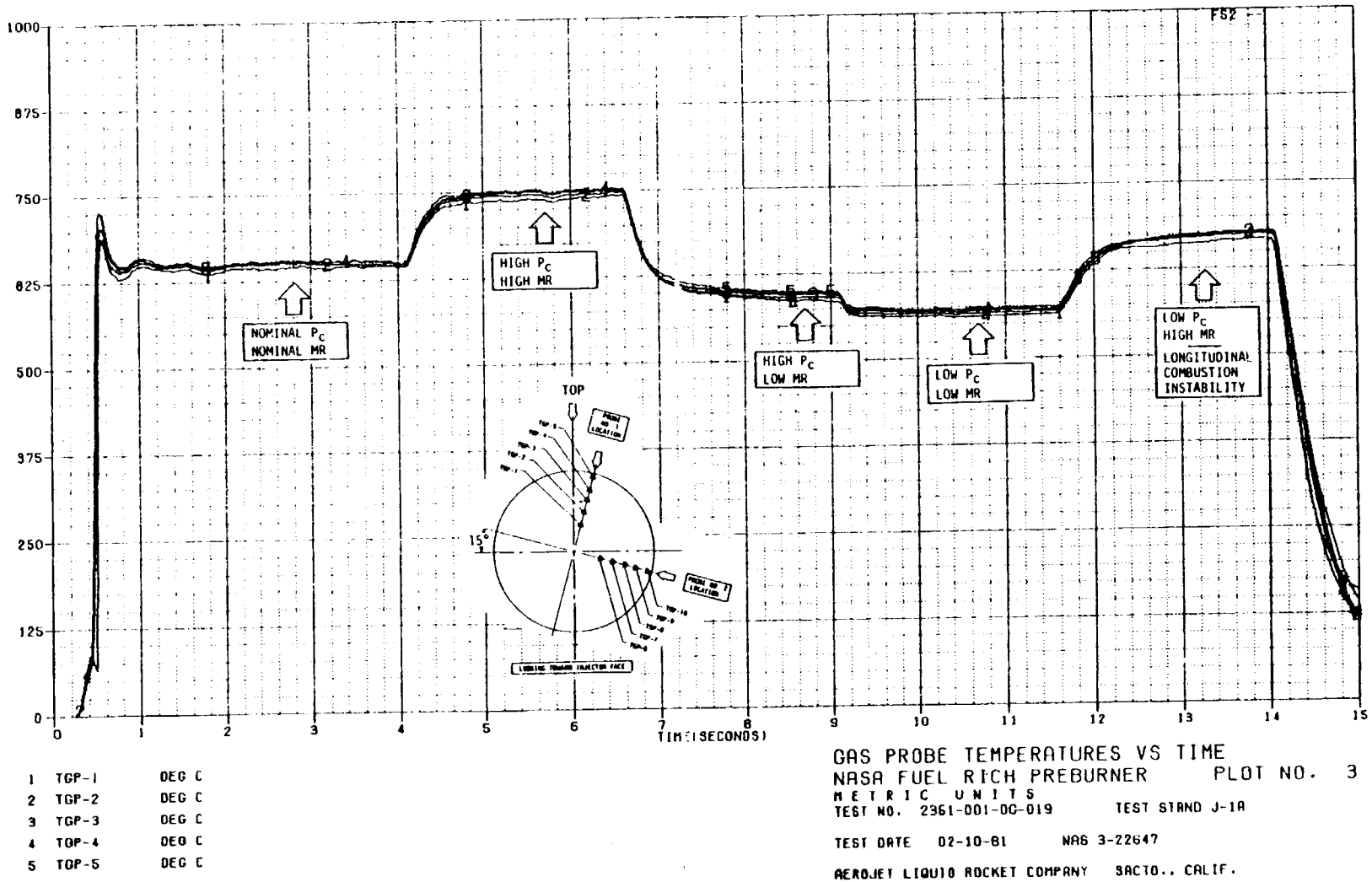

Figure 37. Fuel-Rich Preburner, Gas Probe Temperatures (TGP-1, -5) Versus Time, Test -019 (1 of 2)

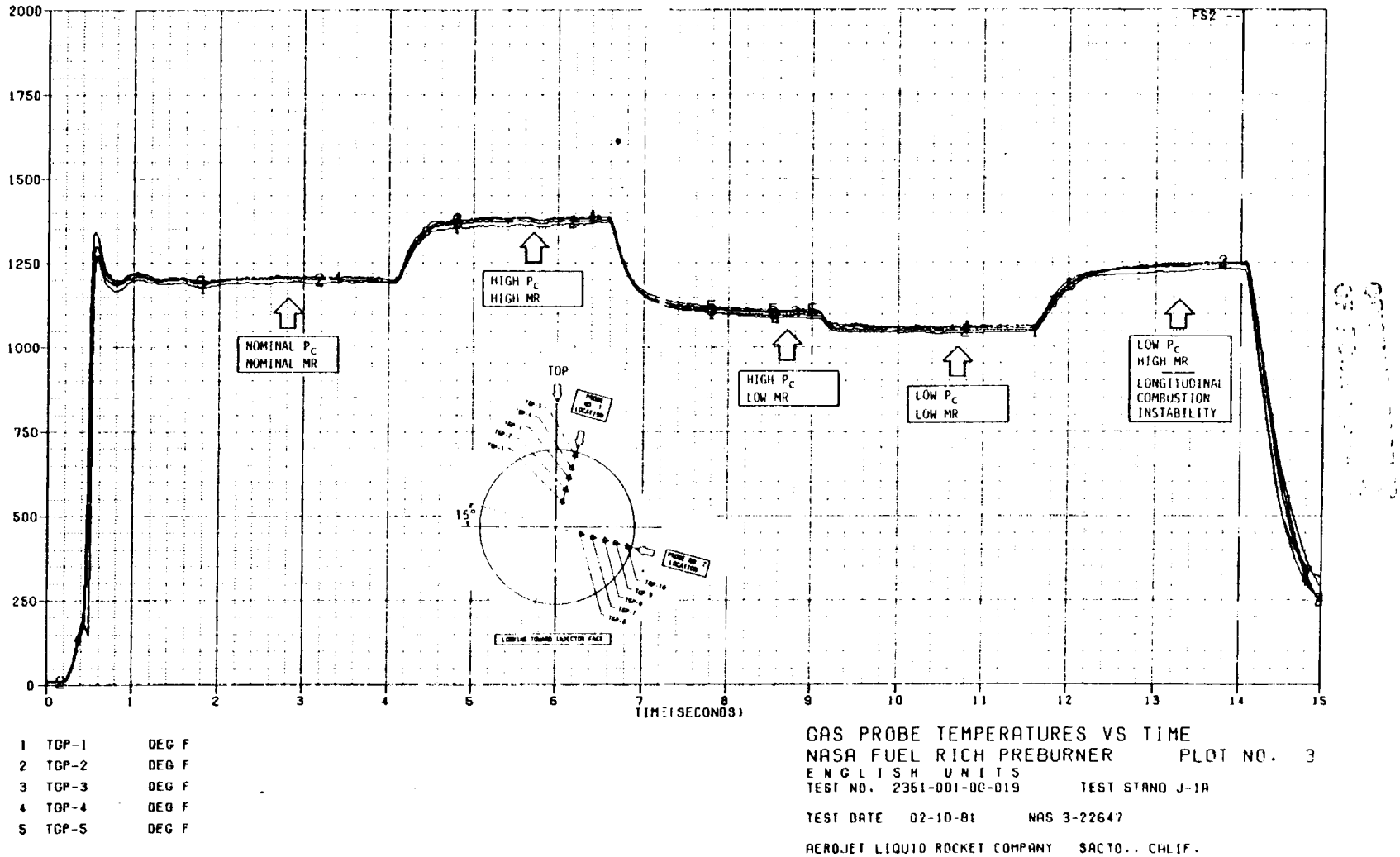

Figure 37. Fuel-Rich Preburner, Gas Probe Temperatures (TGP-1, -5) Versus Time, Test -019 (2 of 2)

ORIGINAL PAGE IS
OF POOR QUALITY

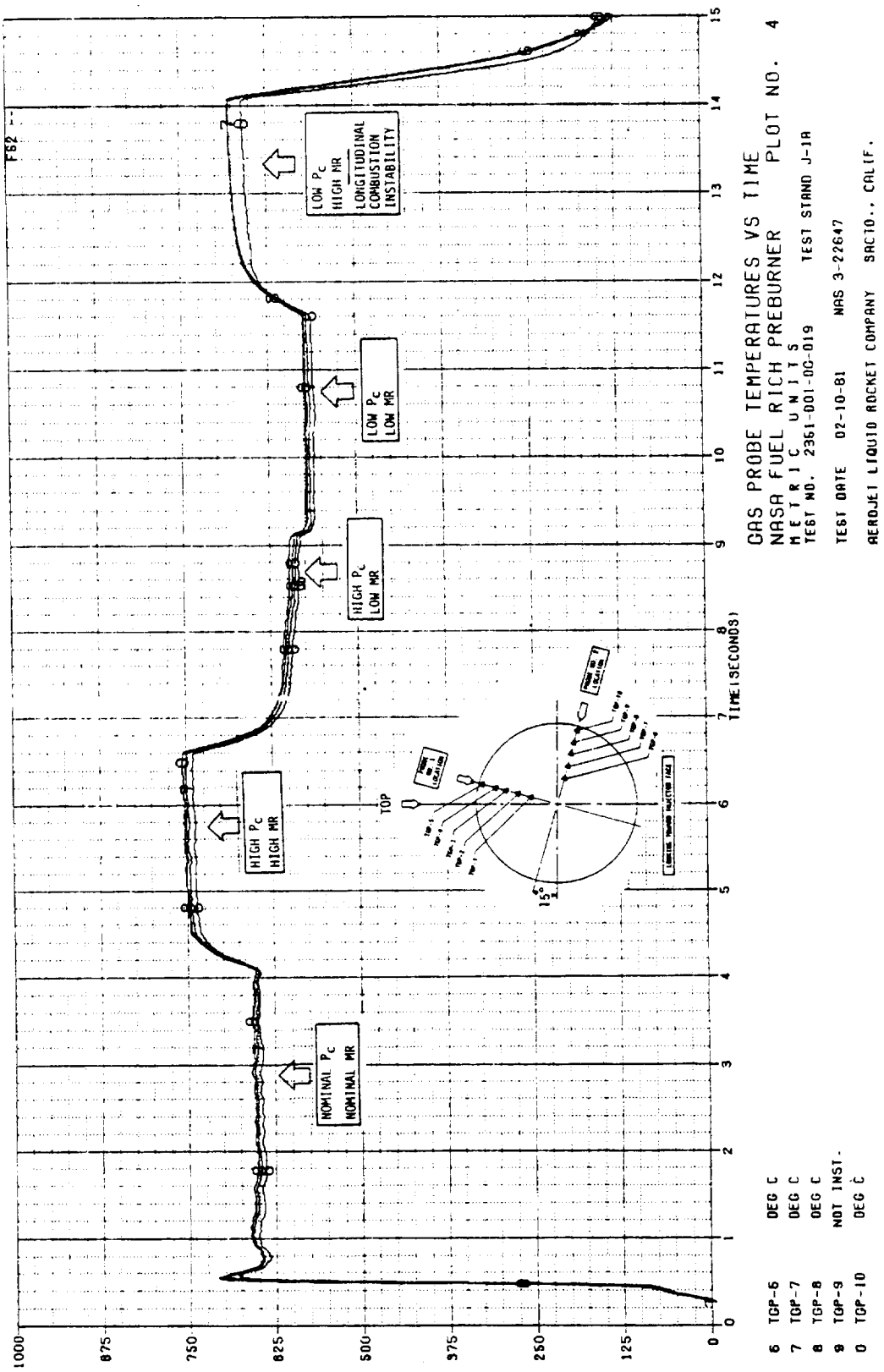

Figure 38. Fuel-Rich Preburner, Gas Probe Temperatures (TGP-6, -10) Versus Time, Test -019 (1 of 2)

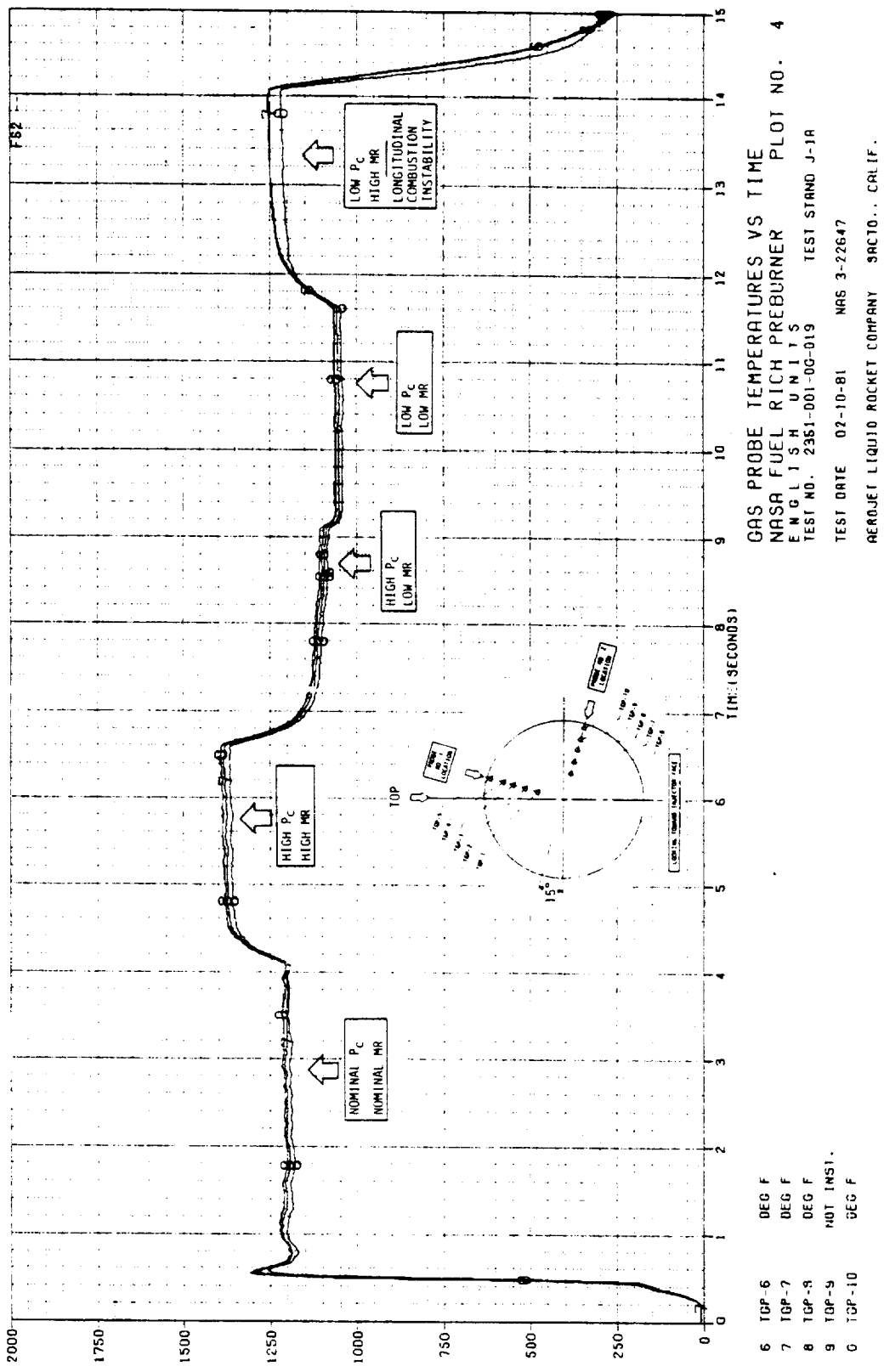

Figure 38. Fuel-Rich Preburner, Gas Probe Temperatures (TGP-6, -10) Versus Time, Test -019 (2 of 2)

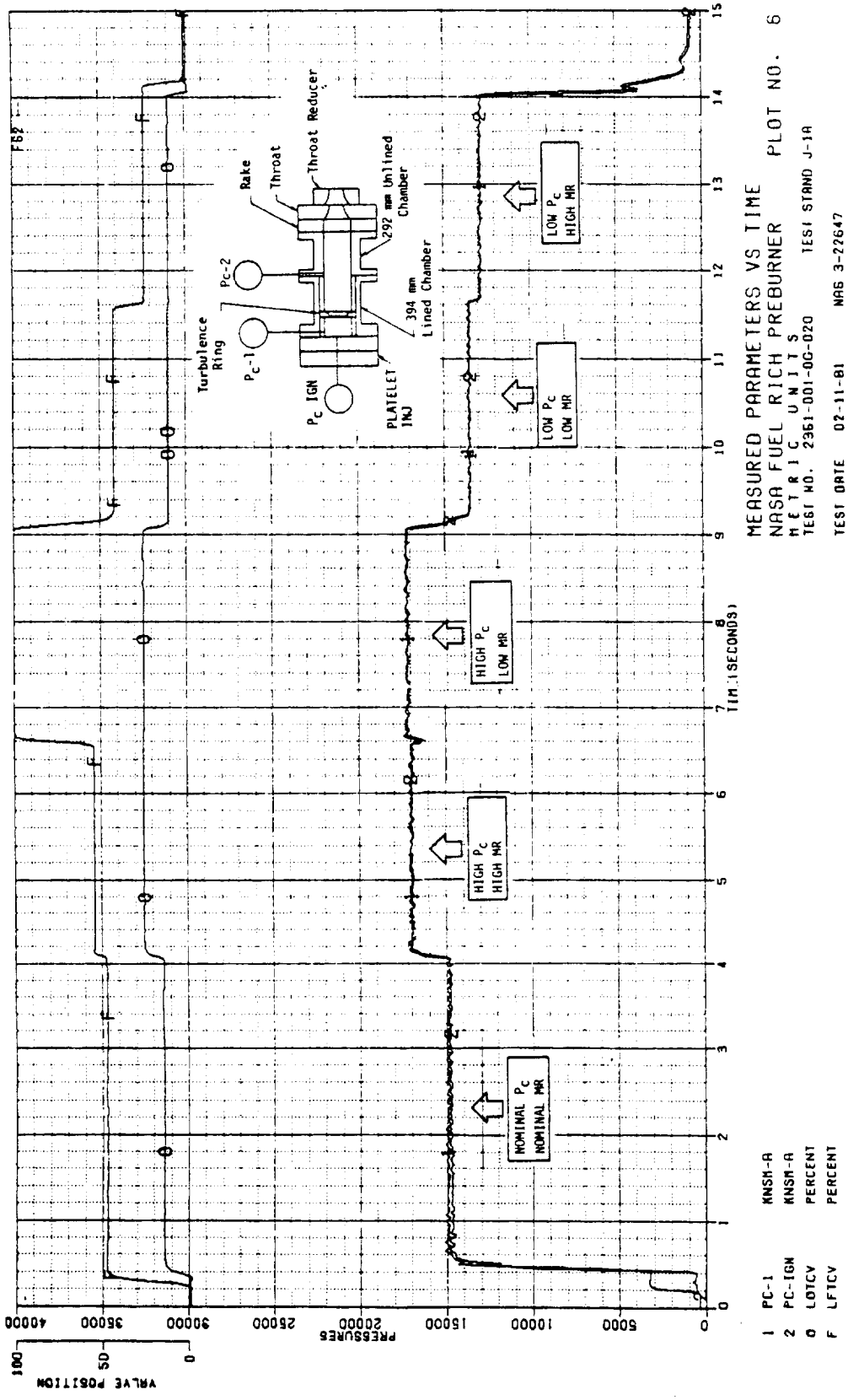

Figure 39. Fuel-Rich Preburner, Measured Parameters Versus Time, Test -020
(1 of 2)

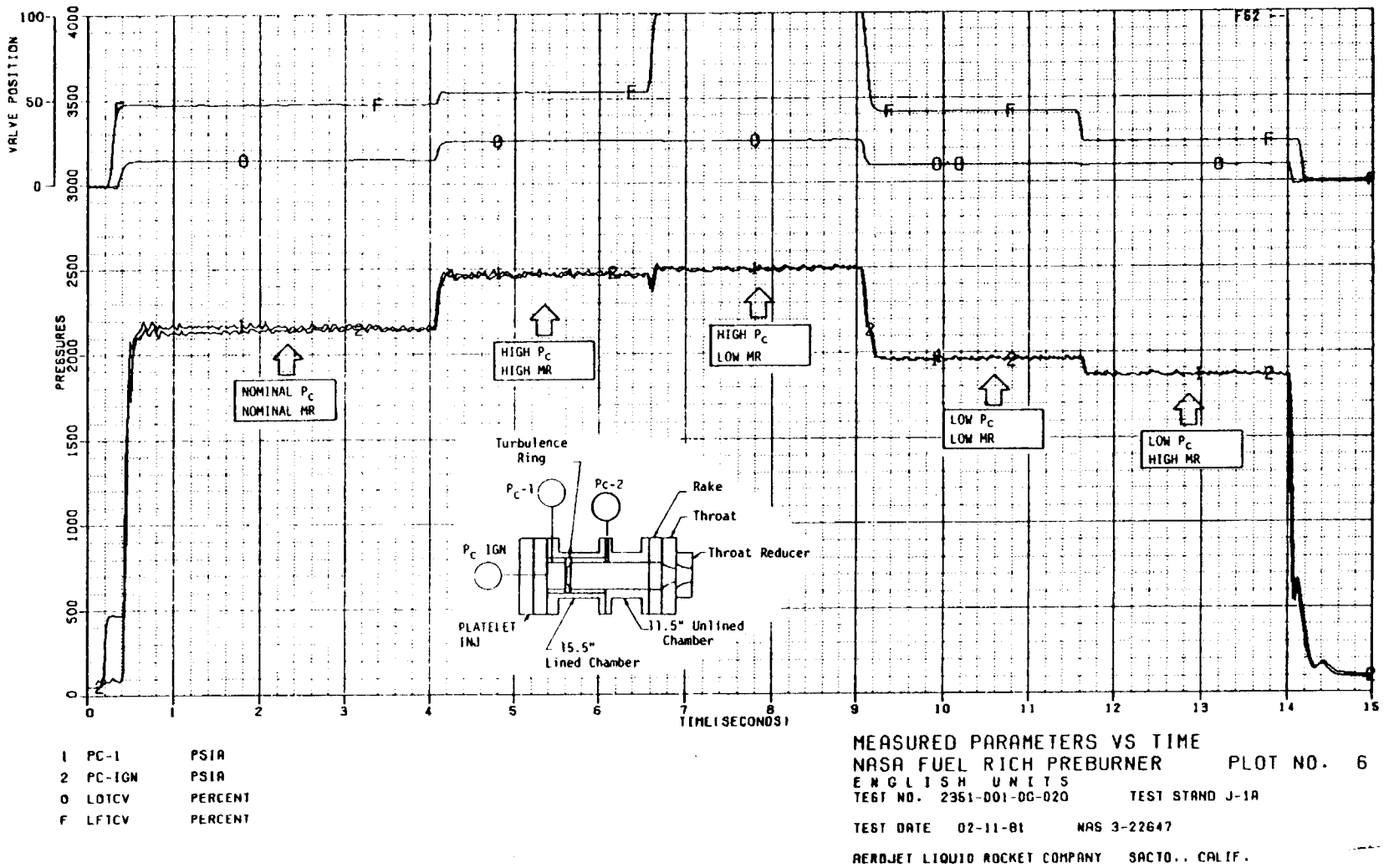

Figure 39. Fuel-Rich Preburner, Measured Parameters Versus Time, Test -020 (2 of 2)

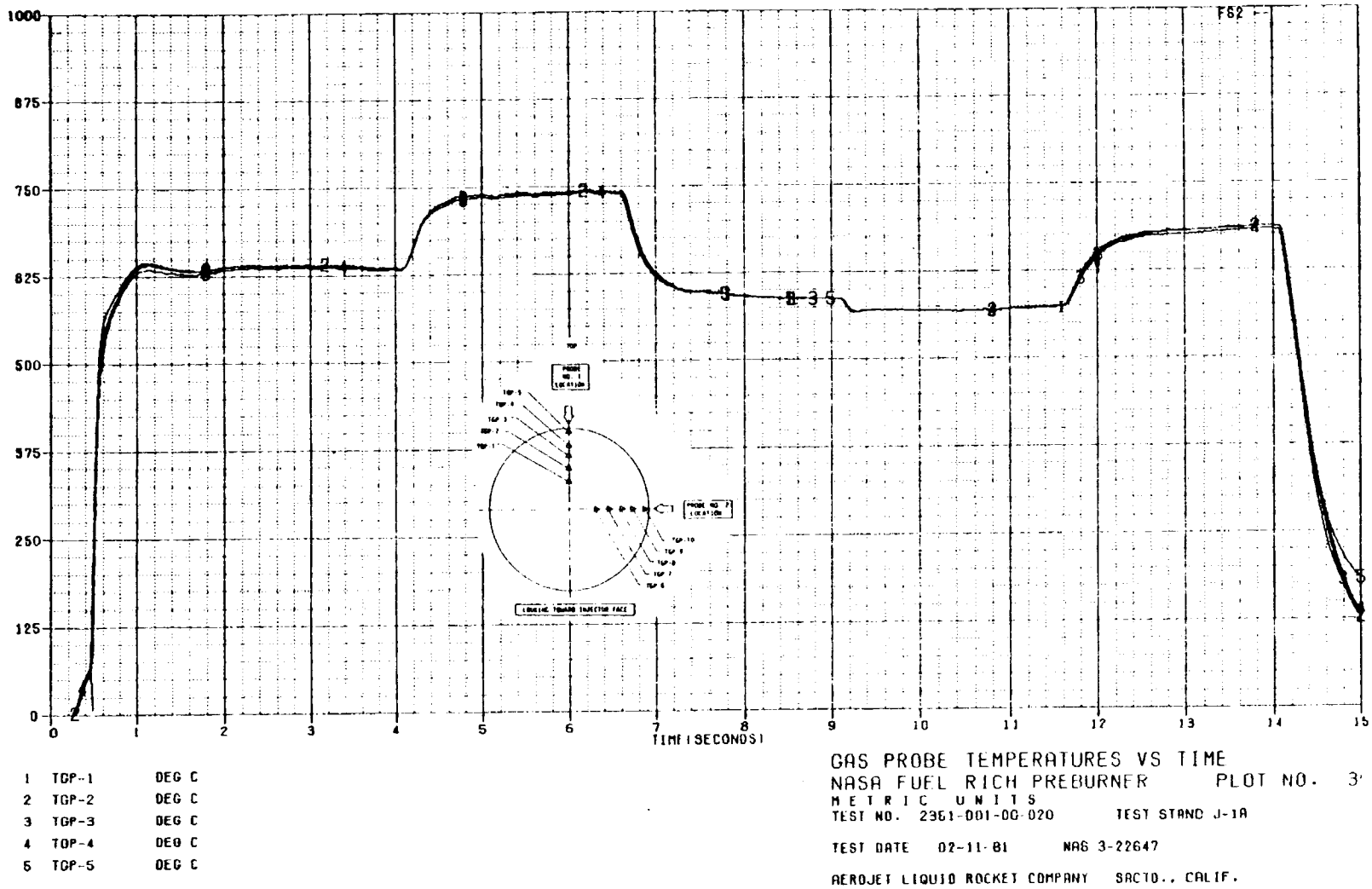

Figure 40. Fuel-Rich Preburner, Gas Probe Temperatures (TGP-1, -5) Versus Time, Test -020 (1 of 2)

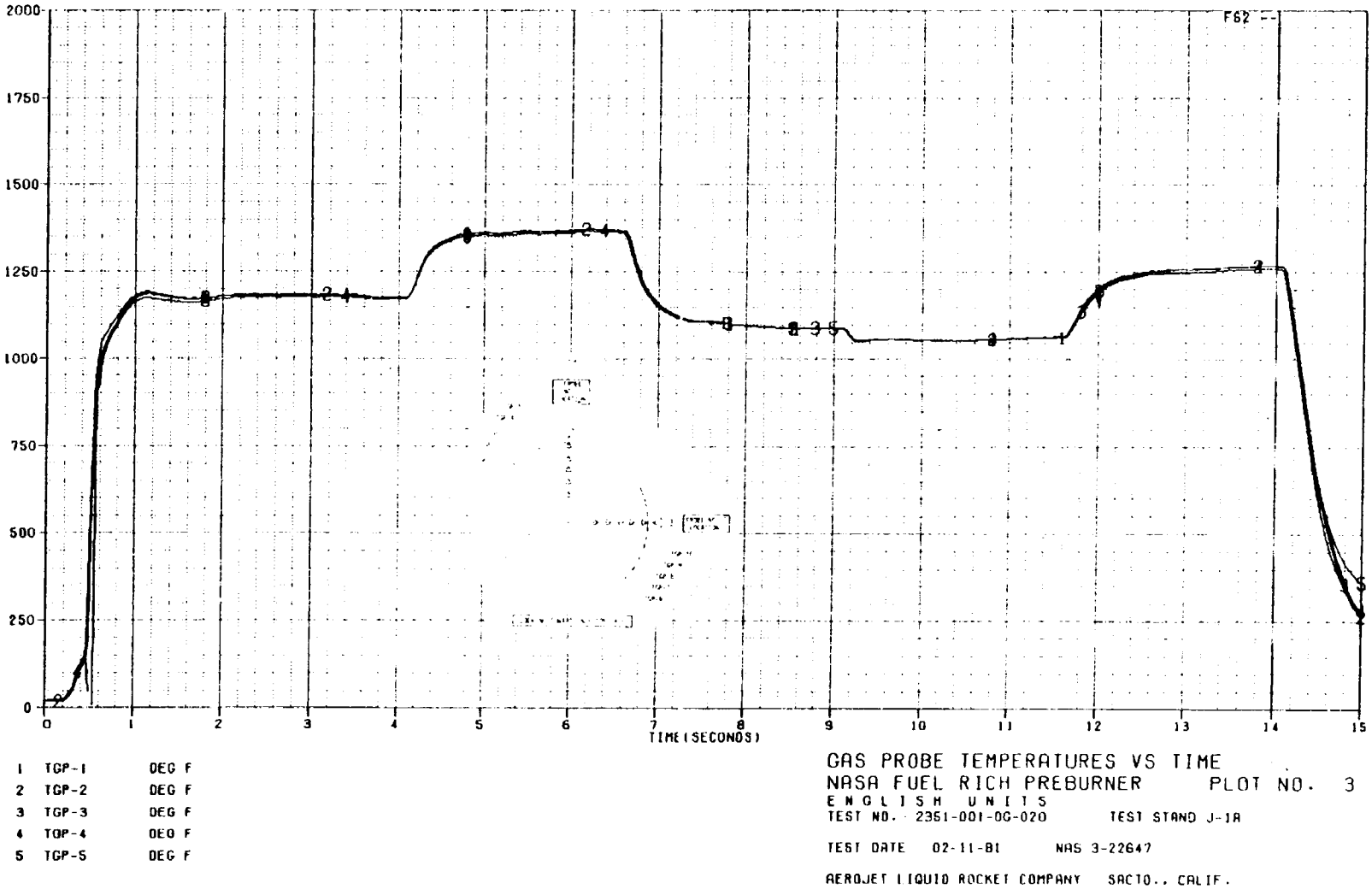

Figure 40. Fuel-Rich Preburner, Gas Probe Temperatures (TGP-1, -5) Versus Time, Test -020 (2 of 2)

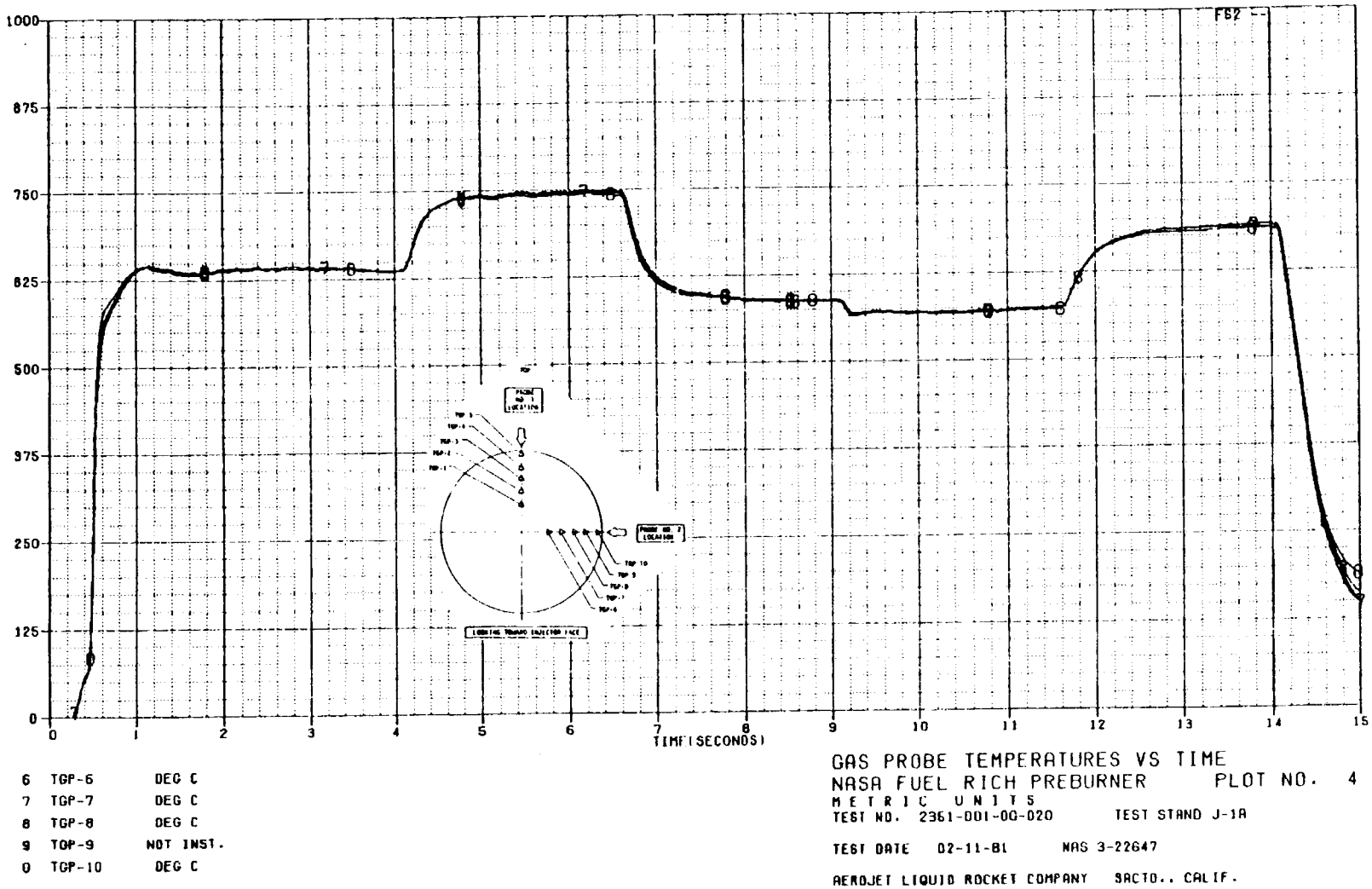

Figure 41. Fuel-Rich Preburner, Gas Probe Temperatures (TGP-6, -10) Versus Time, Test -020 (1 of 2)

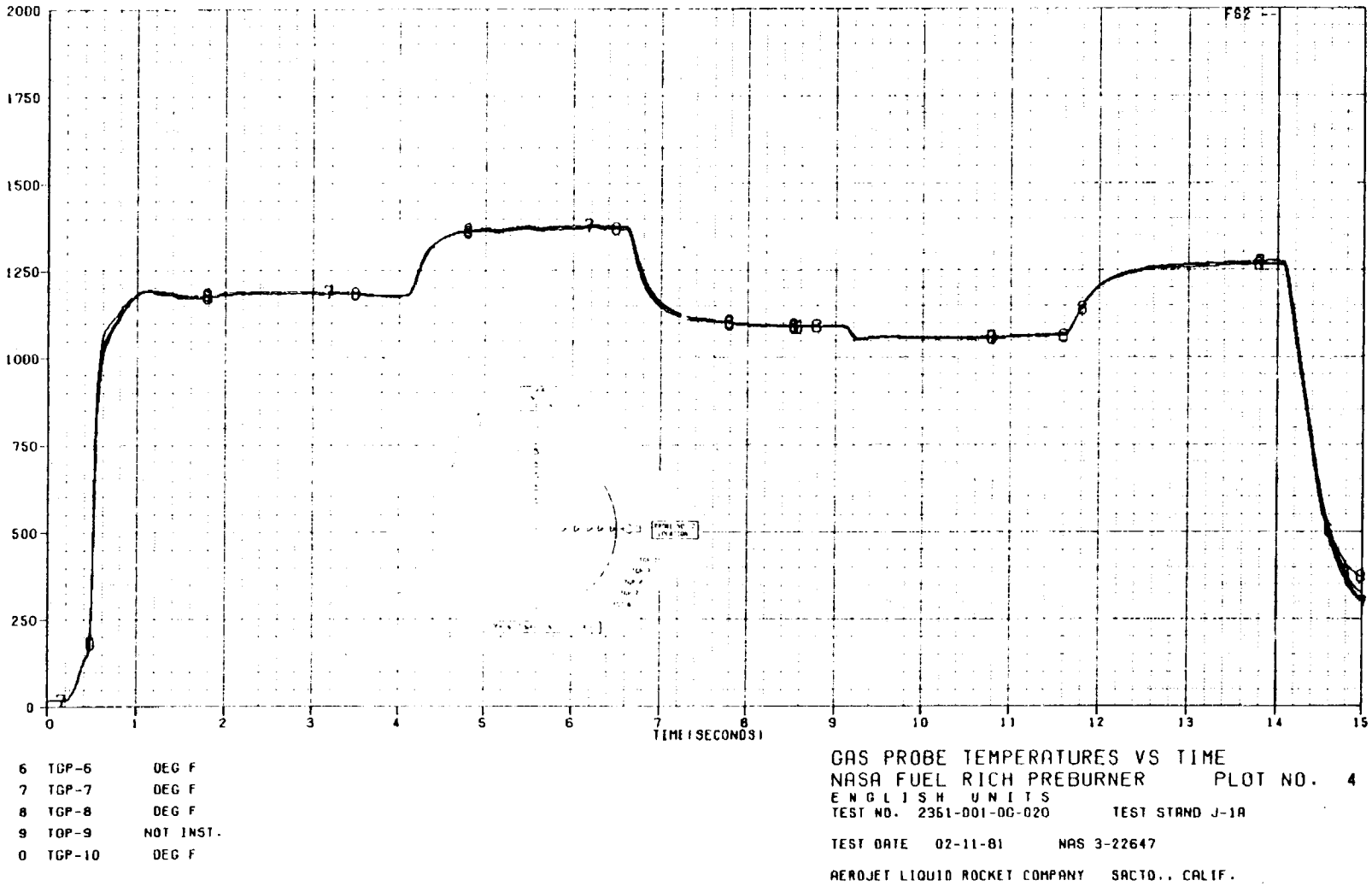

Figure 41. Fuel-Rich Preburner, Gas Probe Temperatures (TGP-6, -10) Versus Time, Test -020 (2 of 2)

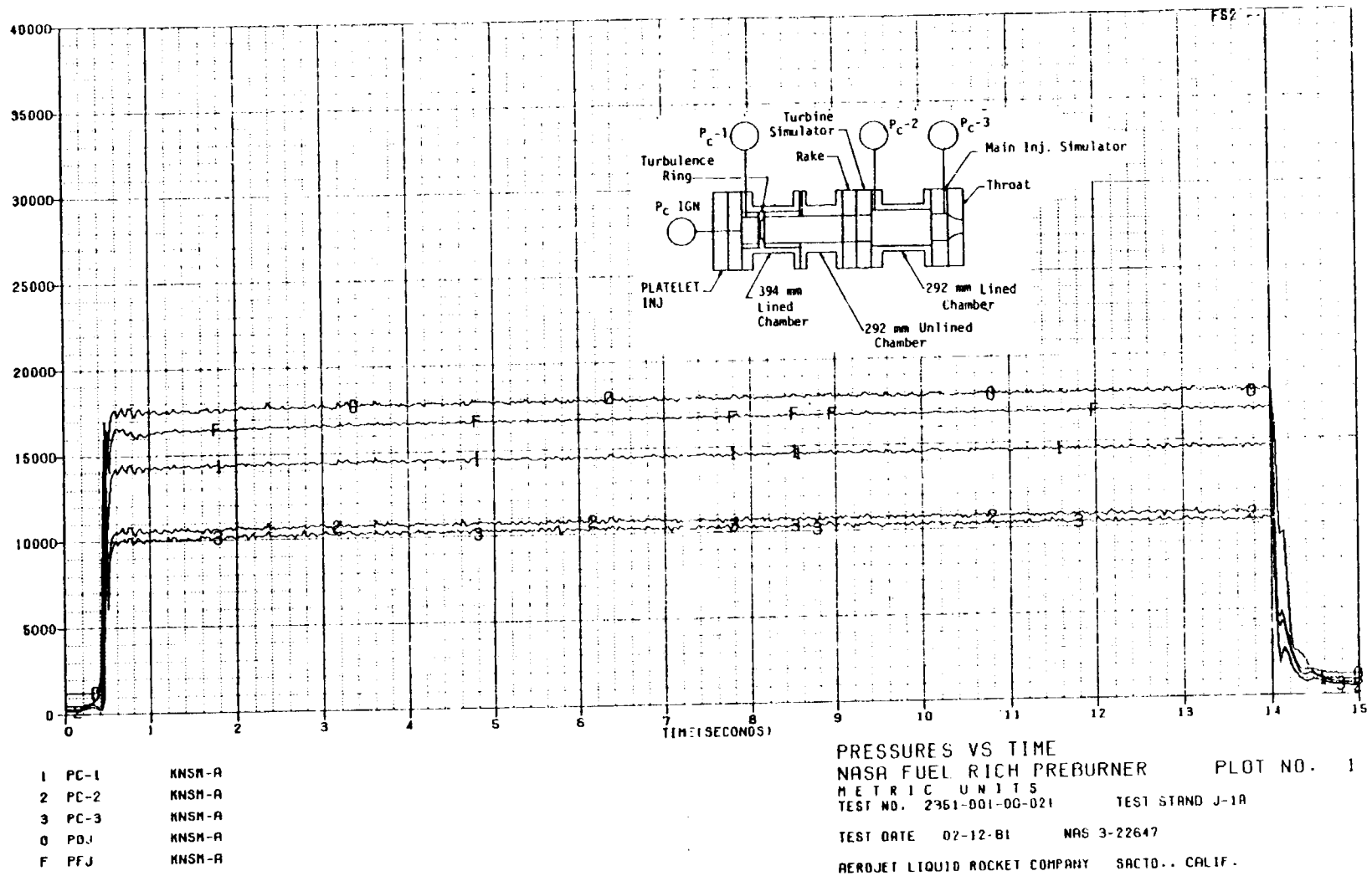

Figure 42. Fuel-Rich Preburner, Pressures Versus Time, Test -021 (1 of 2)

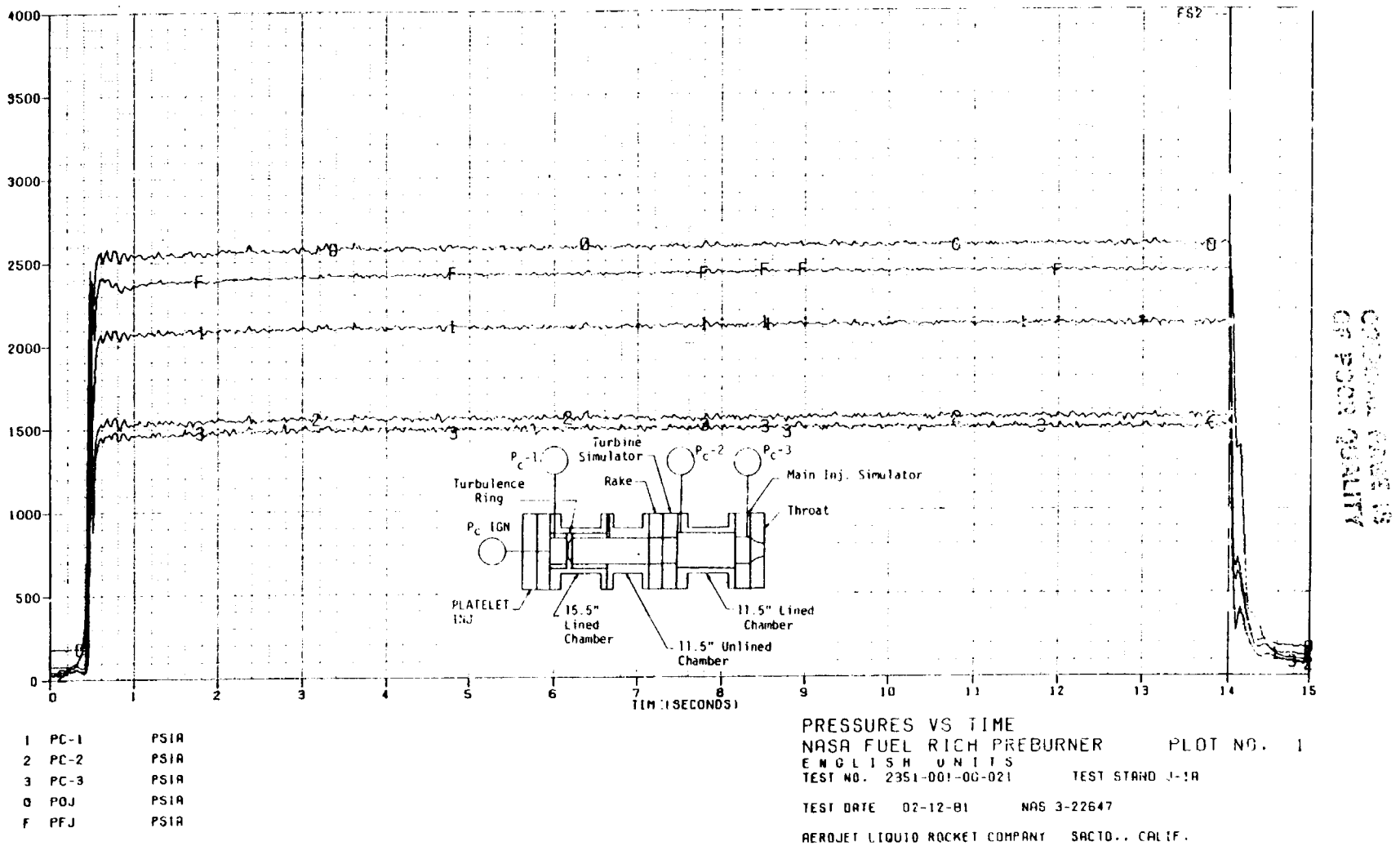

Figure 42. Fuel-Rich Preburner, Pressures Versus Time, Test -021 (2 of 2)

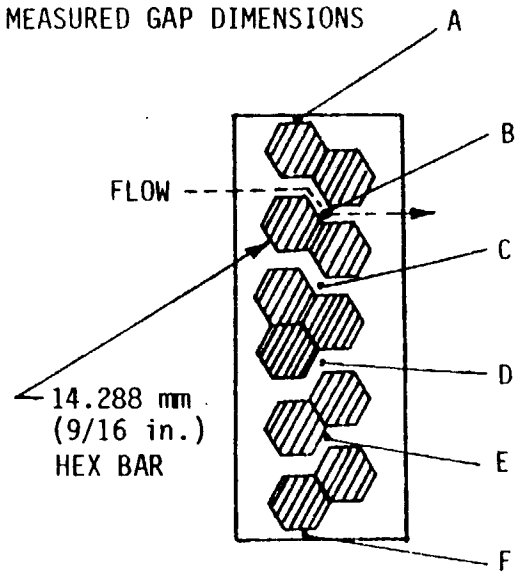

TEST	GAP WIDTH mm (in.) A	B	C	D	E	F
-021	0.127 (0.005)	4.877 (0.192)	3.531 (0.139)	3.556 (0.140)	4.699 (0.185)	0.762 (0.030)
-022,-029	0.127 (0.005)	3.683 (0.145)	3.531 (0.139)	3.556 (0.140)	3.683 (0.145)	0.762 (0.030)

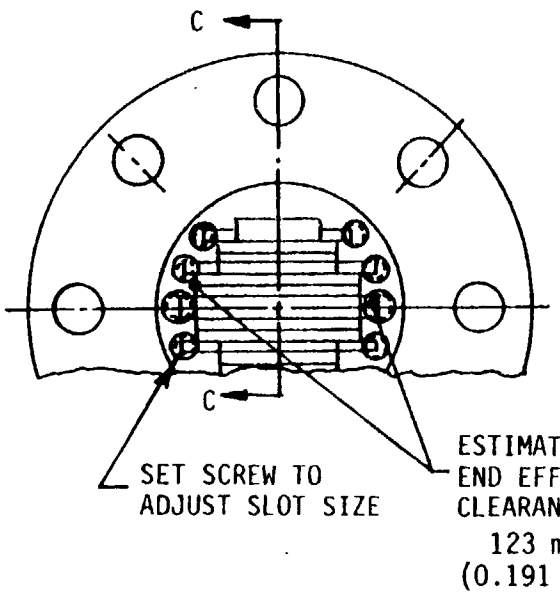

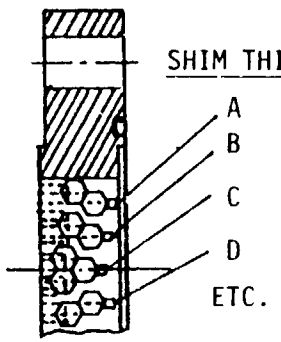

SECTION C - C

TEST	SHIM THICKNESS mm (in.) A	B	C	D	E
-021	0 0	0 0	1.676 (0.066)	0 0	0 0
-022,-029	1.905 (0.075)	0 0	1.676 (0.066)	0 0	1.905 (0.075)

Figure 43. Turbine Simulator Blade Spacing

chamber pressure rise with firing duration was made to determine how much was due to thermal effects and how much, if any, was due to carbon buildup. These results are discussed in Section IV.C.1 of this report.

The measured pressure ratio (Pc-1/Pc-2) was about 1.35. As shown in Figure 43, the blade spacing was adjusted prior to Test -022 to try to increase the pressure ratio to about 1.5. However, it was found that reducing the gap size changes the discharge coefficient (C_D) such that the overall discharge coefficient area product (C_{DA}) is larger than with the larger gap. This phenomenon was also observed during the cold-flow testing. It has been found that placing the blades close together causes the flow passage to behave as a supersonic nozzle rather than as an orifice. Consequently, the flow becomes supersonic in the blade and shocks up to the backpressure.

Test -022

This was the second test run to define the carbon buildup, at a planned chamber pressure of 17.2 MN/m^2 (2500 psia); however, due to the lower-than-desired pressure drop through the turbine simulator, this pressure could not be achieved.

The chamber pressure history is shown in Figure 44. Post-test examination showed minor hard carbon buildup on the turbine simulator inlet.

Test -023

This was to have been the third carbon buildup test; however, the test was terminated immediately after ignition due to a facility pressure kill parameter. The kill was initiated by the fuel inlet pressure transducer due to a waterhammer wave during the start transient. The wave resulted from the high fuel flow transient associated with starting at the high-Pc/high-MR condition. The pressure wave was nondamaging. The kill pressure was reset to a higher pressure for Test -024.

Test -024

This was a repeat of Test -023. It was terminated prematurely by a Pc-1 kill due to a transducer failure. Post-test examination showed a large pressure spike in the Pc transducer. Examination of other hot-gas transducers showed them to be contaminated with a black gunk. Subsequently, all hot-gas transducers were removed and flushed before each firing.

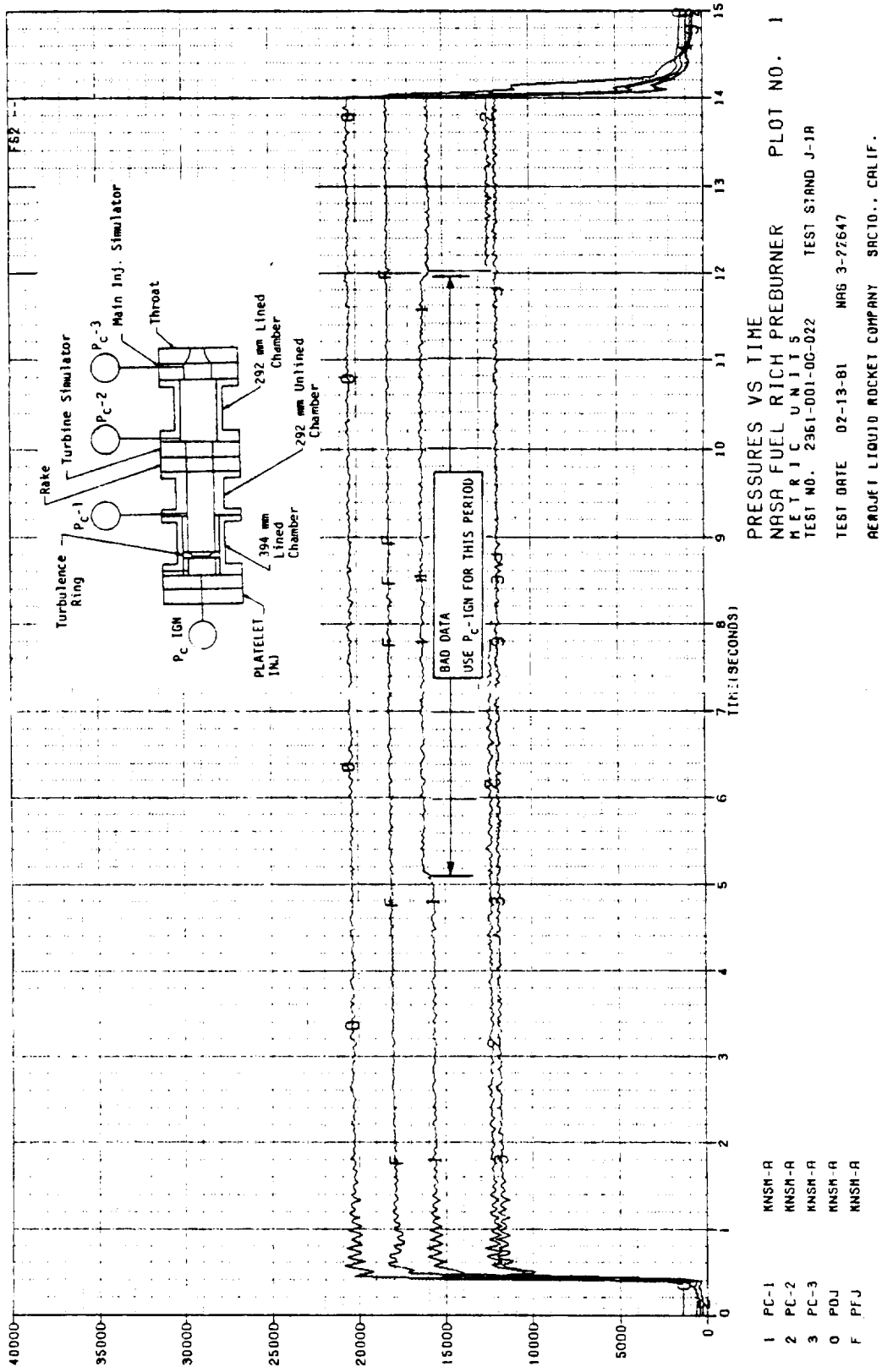

Figure 44. Fuel-Rich Preburner, Pressures Versus Time, Test -022 (1 of 2)

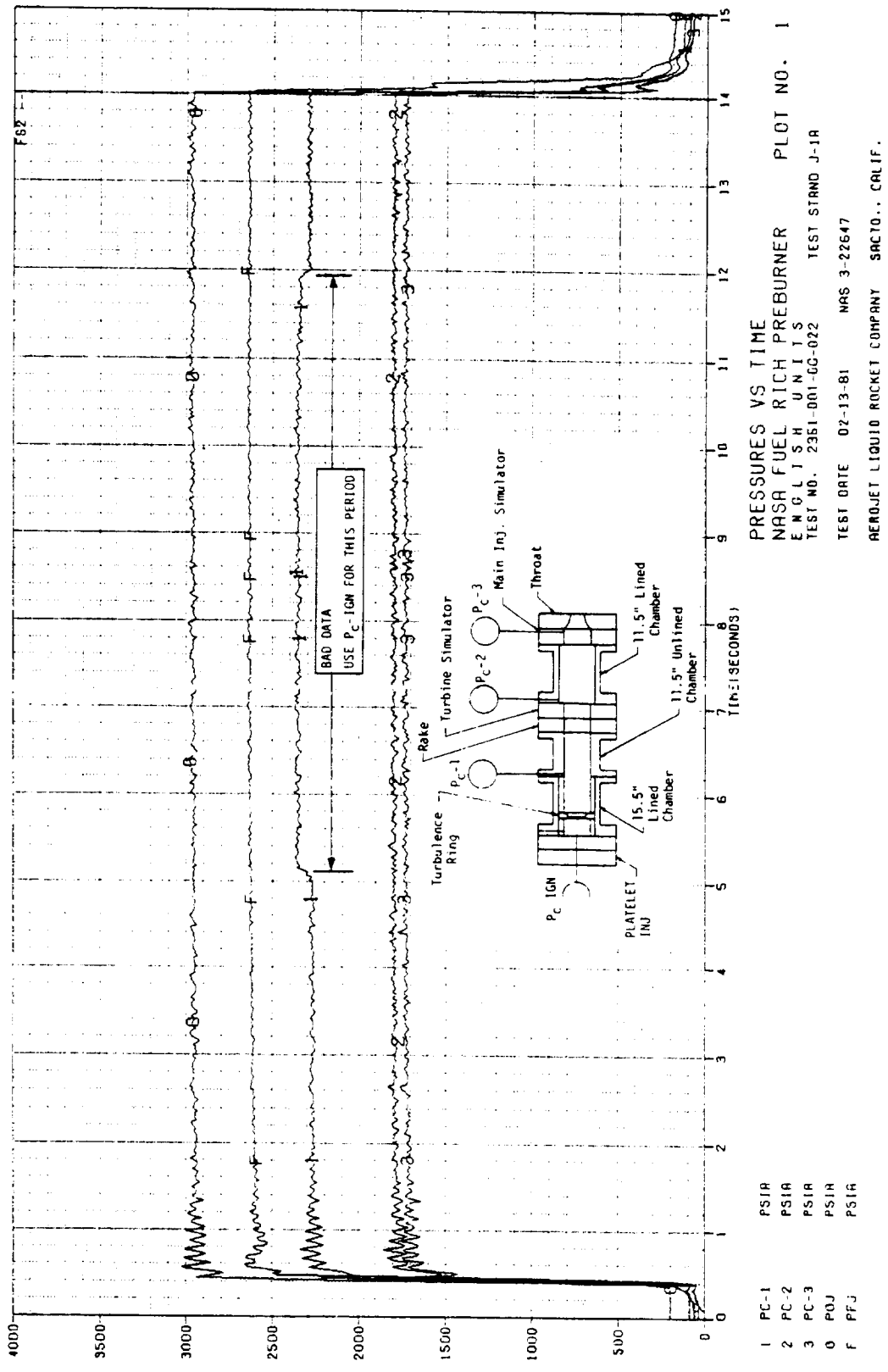

Figure 44. Fuel-Rich Preburner, Pressures Versus Time, Test -022 (2 of 2)

Test -025

This was the third carbon buildup test. It was run at the high-Pc/low-MR operating point. The test duration was limited to 10 seconds due to the high fuel flow at this operating point.

The Pc history is shown in Figure 45. The Pc-igniter transducer line ruptured during the test. No other hardware damage resulted. Post-test examination showed that the rupture occurred at a low point in the line. The line was replumbed to eliminate the low point and avoid material accumulation. A purge was also added to preclude fuel-rich combustion products from backing up into the line after igniter shutdown.

Examination of the hardware showed some hard carbon buildup and evidence of erosion of the turbine simulator blades.

Test -026

This test was shut down immediately after ignition by a low-Pc kill parameter. The Pc momentarily dipped lower than expected due to the feed system dynamics, causing the low-Pc kill to be activated. The low-Pc kill limit was reduced for Test -027.

Test -027

This was the fourth carbon buildup test. It was run at the low-Pc/low-MR operating point. The Pc history is shown in Figure 46. Post-test examination showed some hard carbon buildup on the turbine simulator. The turbine simulator blades and housing were noticeably eroded.

Test -028

This test was run at the low-Pc/high-MR operating point. The Pc history is shown in Figure 47.

Post-test examination showed progressive erosion of the turbine simulator and housing. Erosion was also evident on the main injector simulator and the nozzle. The erosion appears to be due to chemical reaction aggravated by high gas velocities and liquid droplet impact.

Test -029

The objective of this test was to determine the effect of fuel heating on carbon buildup, performance, and stability. The fuel temperature started at 320°K (117°F) and reached 379°K (223°F) before the end of the test. The fuel flowrate decayed during the test, causing the MR to shift from 0.3 at the start to 0.35 at the end of the test. The Pc history is shown in Figure 48.

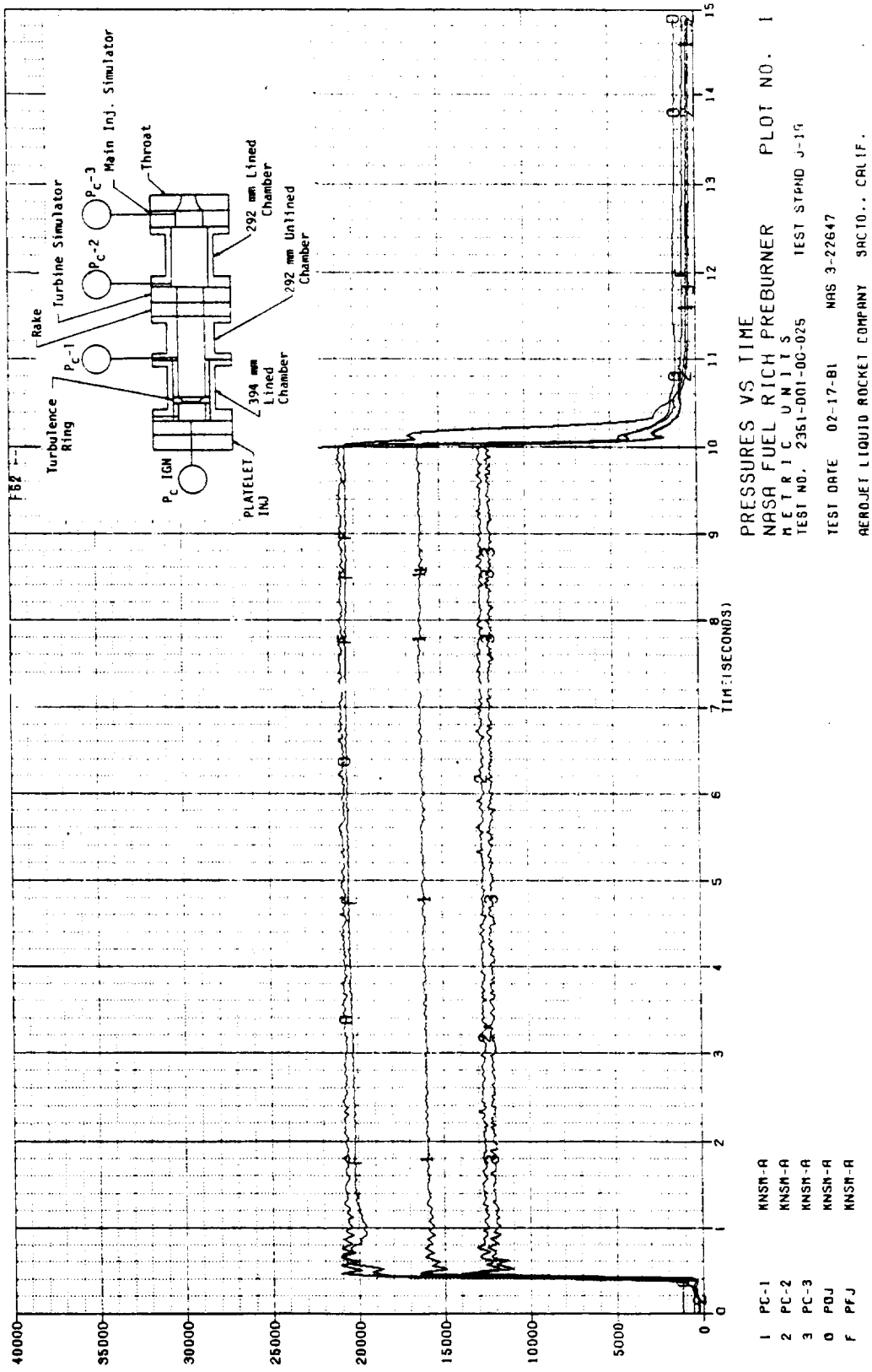

Figure 45. Fuel-Rich Preburner, Pressures Versus Time, Test -025 (1 of 2)

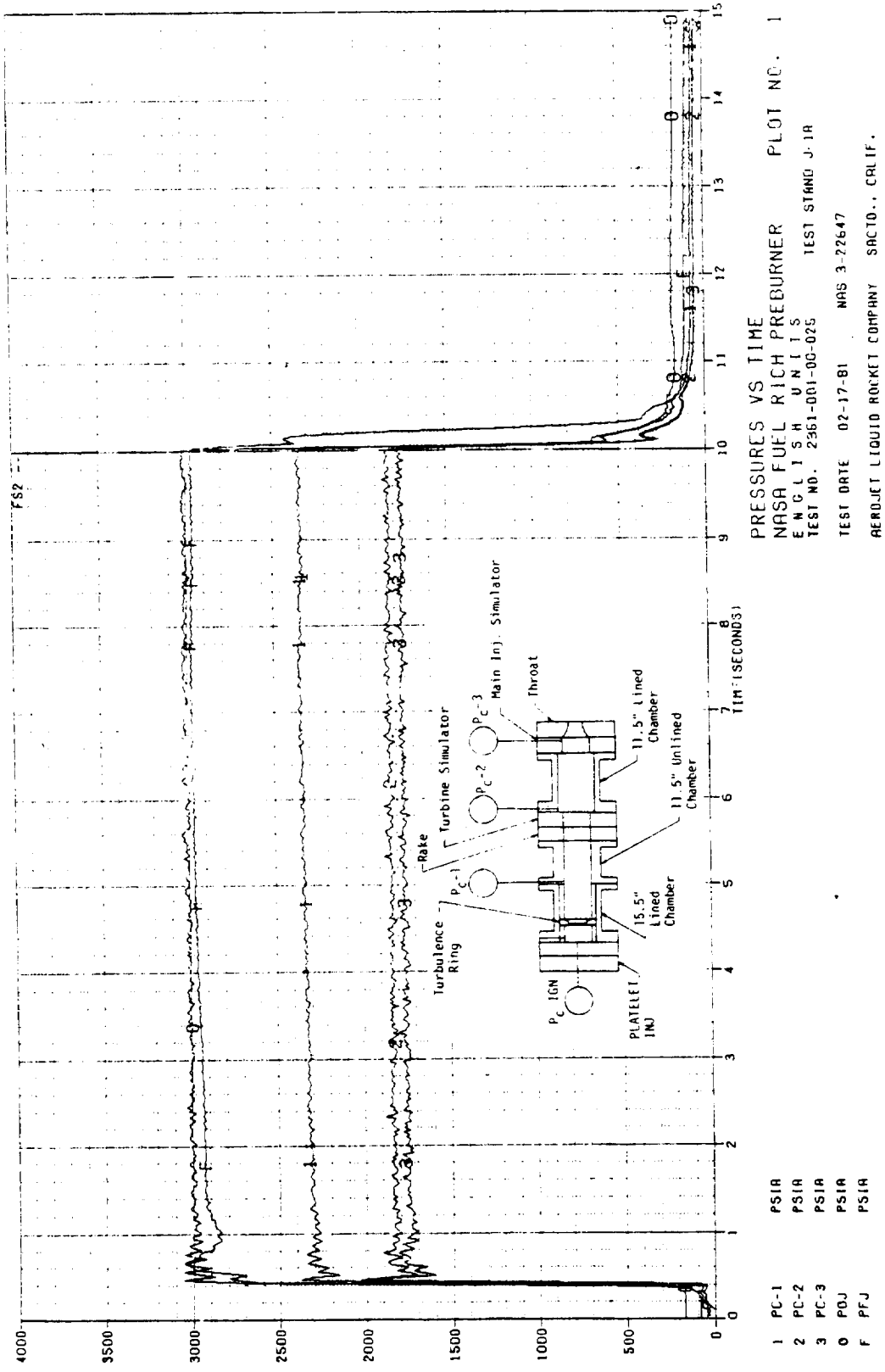

Figure 45. Fuel-Rich Preburner, Pressures Versus Time, Test -025 (2 of 2)

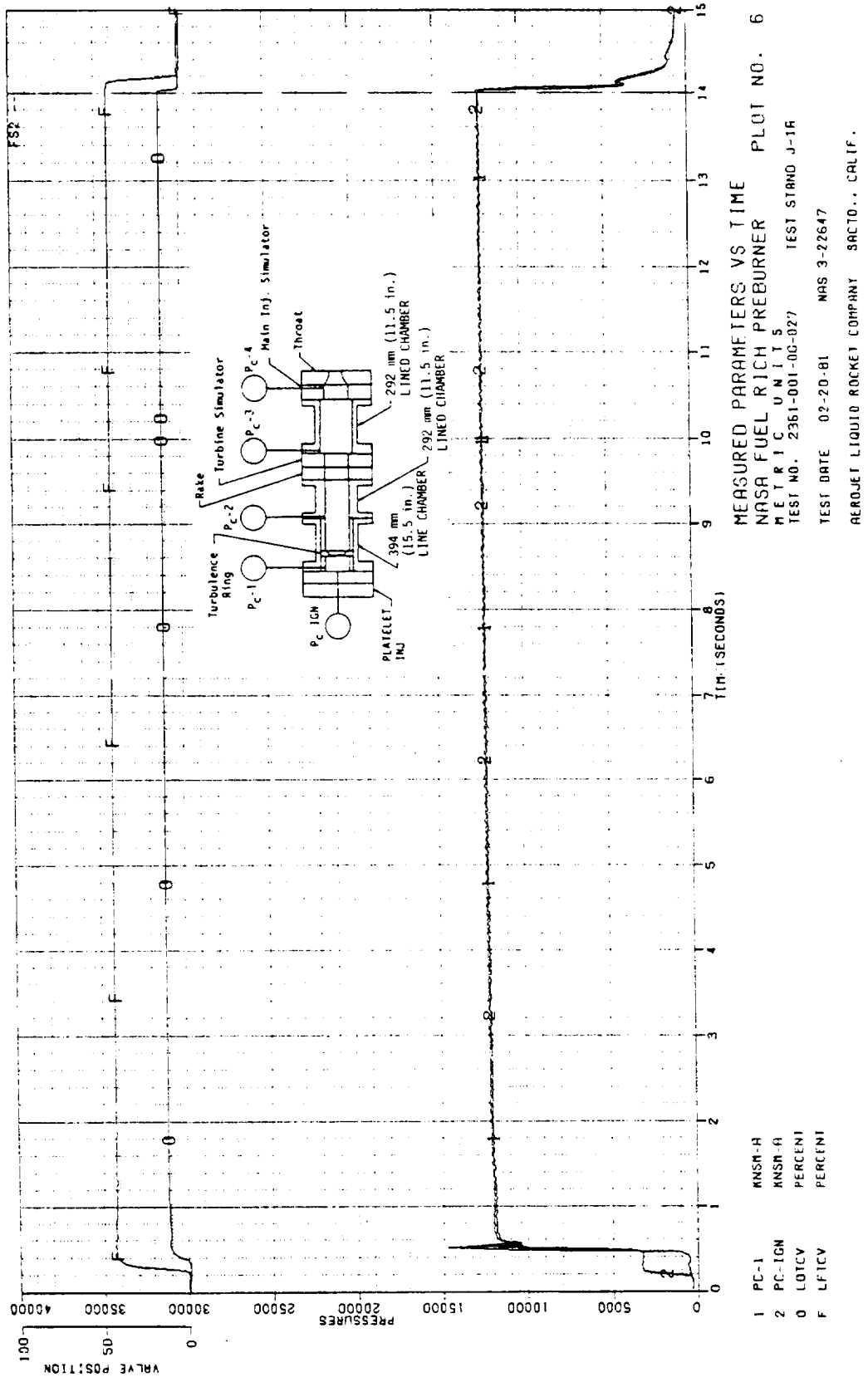

Figure 46. Fuel-Rich Preburner, Pressures Versus Time, Test -027 (1 of 2)

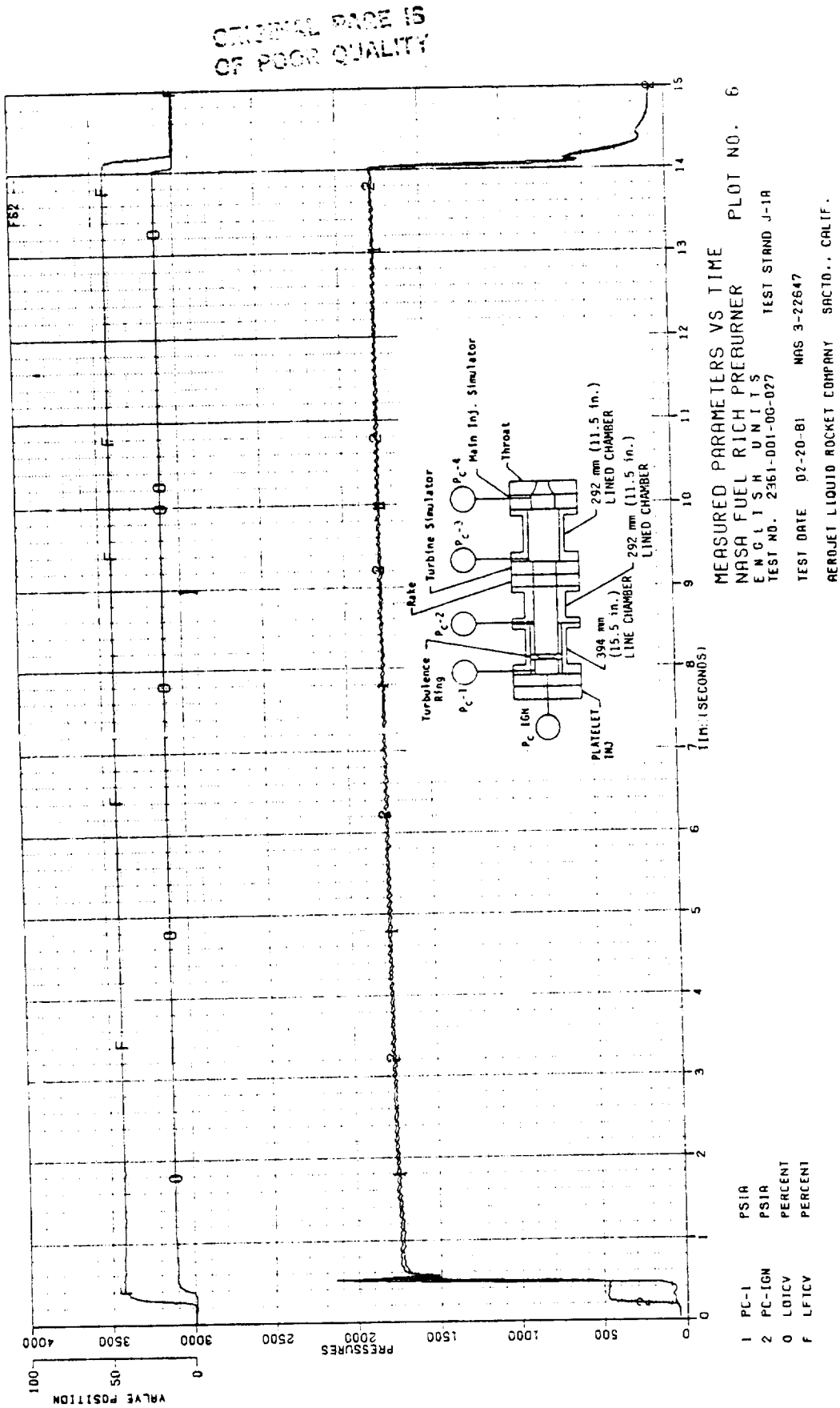

Figure 46. Fuel-Rich Preburner, Pressures Versus Time, Test -027 (2 of 2)

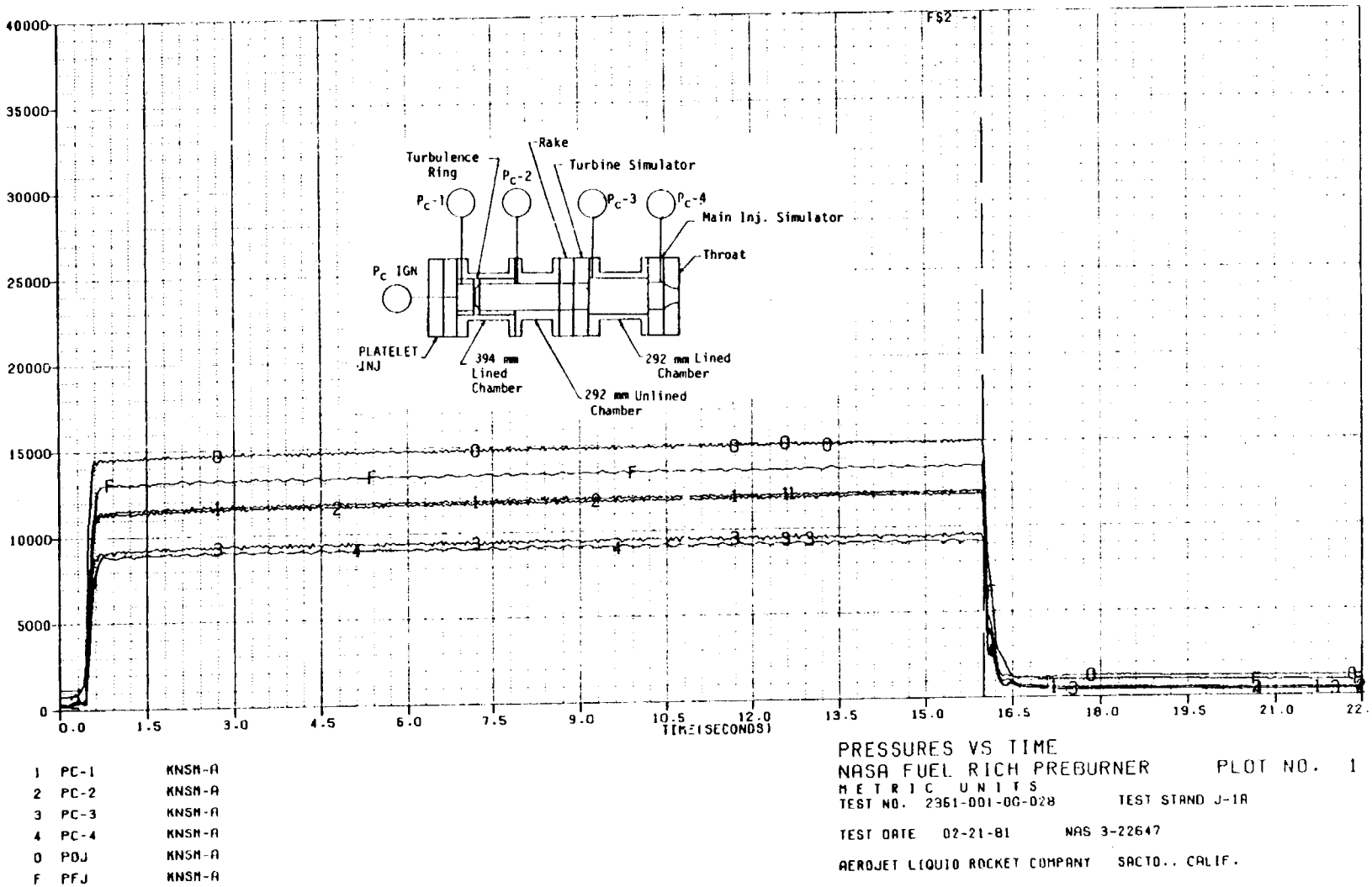

Figure 47. Fuel-Rich Preburner, Pressures Versus Time, Test -028 (1 of 2)

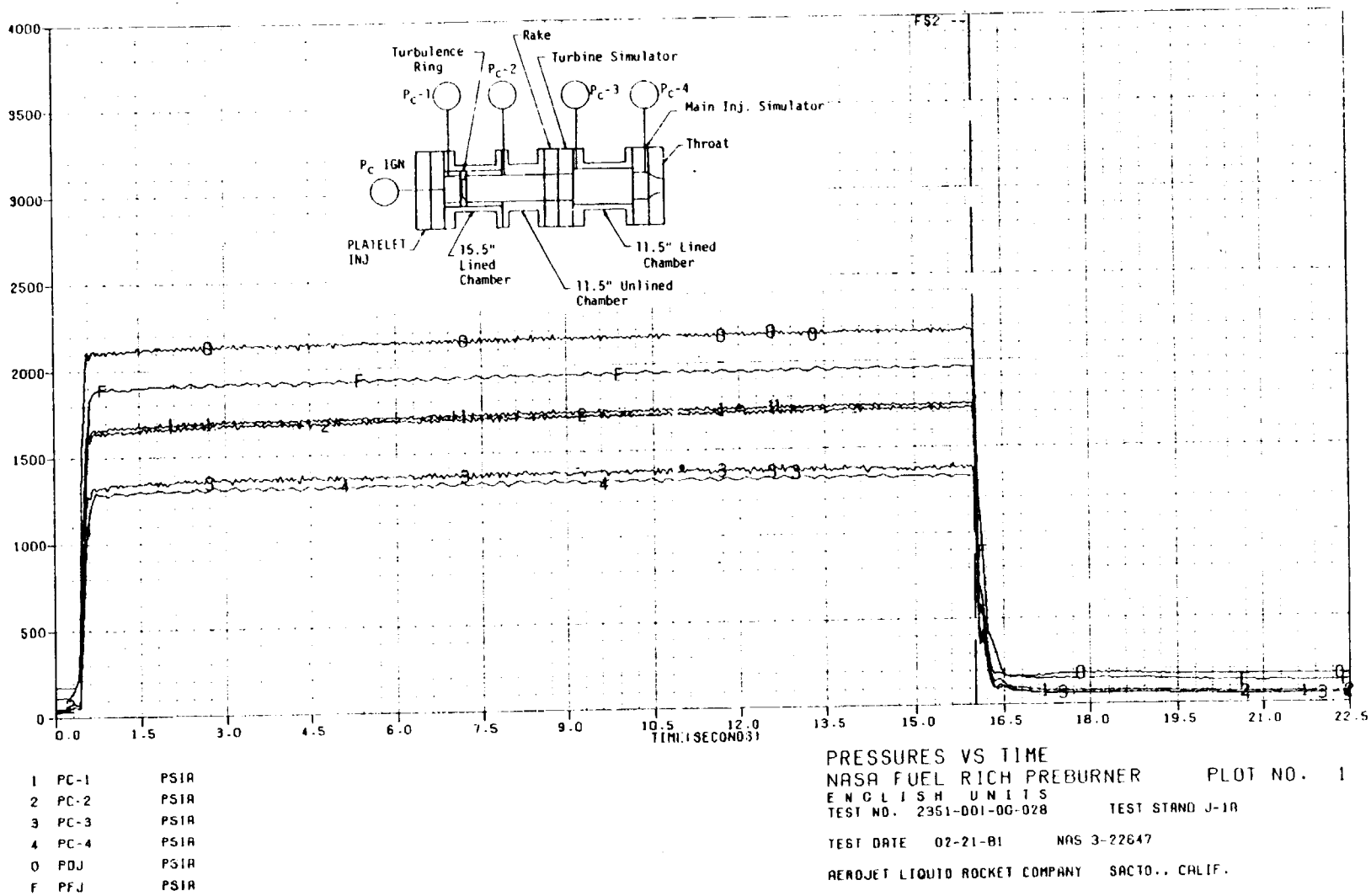

Figure 47. Fuel-Rich Preburner, Pressures Versus Time, Test -028 (2 of 2)

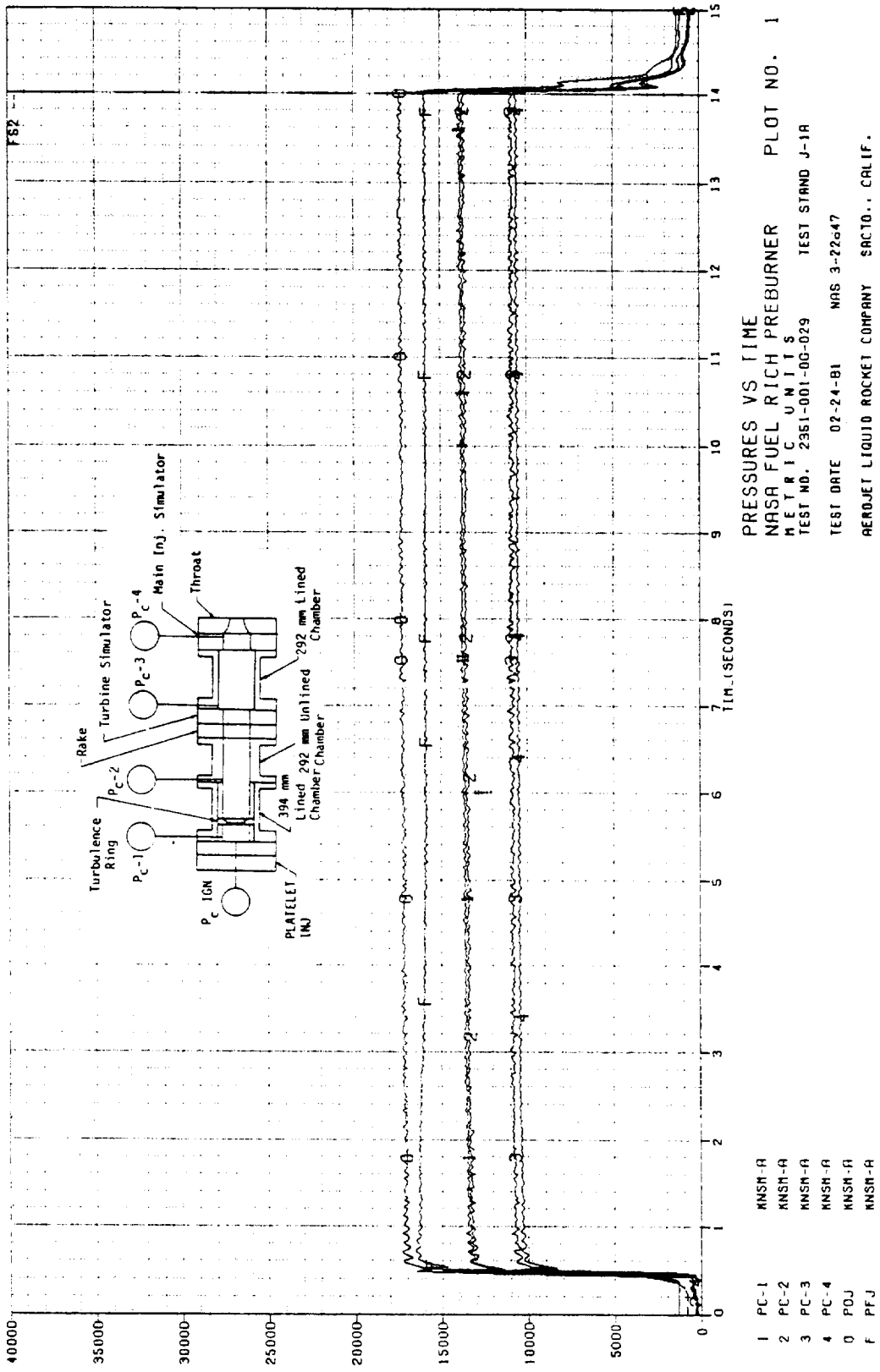

Figure 48. Fuel-Rich Preburner, Pressures Versus Time, Test -029 (1 of 2)

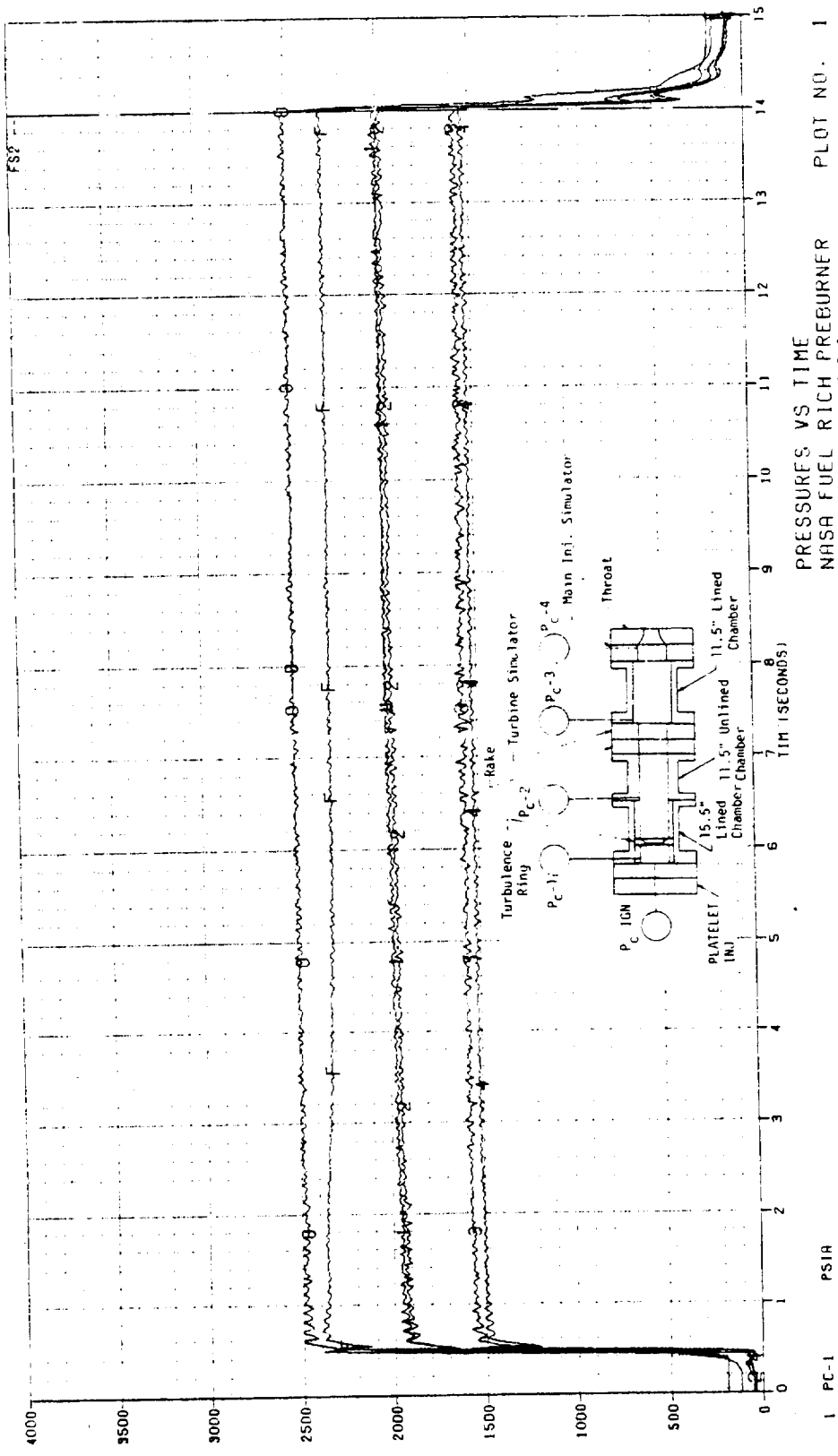

Figure 48. Fuel-Rich Preburner, Pressures Versus Time, Test -029 (2 of 2)

Test -030

This was the first of the add-on tests. The chamber configuration was as shown in Figure 49. The nozzle using the EDM injector with a turbulence ring throat reducer flange was left off, resulting in a lower chamber pressure than planned. The planned duration was 14 seconds; however, the test was terminated after 12 seconds by the fuel intensifier capacity limit kill due to the higher-than-planned fuel flowrates.

A chamber pressure versus time plot is given in Figure 49. The measured gas temperatures are shown in Figures 50 and 51. As can be seen, the temperature distribution is very uniform, indicating that use of the turbulence ring with the EDM injector is very effective.

Test -031

Test -031 is a repeat of Test -030, but with the nozzle throat reducer flange installed. The Pc-MR conditions are indicated in Figure 52. The gas temperatures are shown in Figures 53 and 54.

The temperatures are extremely uniform. Combustion was stable at all operating conditions. Post-test examination showed no evidence of erosion of the turbulence ring.

Test -032

Test -032 was run at the same Pc-MR point as Test -031 but with a shorter-length chamber. The operating points are shown in Figure 55. The gas temperatures are plotted in Figures 56 and 57.

2. Oxidizer-Rich Testing

Twenty-four (24) oxidizer-rich tests in all were run. Tests -001 through -012 were propellant cold-flow tests which were run to establish manifold fill times and injector and fuel valve Kw's. The final valve sequence is shown in Figure 58. The oxidizer preburner valve (OTCV) and the igniter are sequenced on with FS-1. The oxidizer manifold fills about 10 msec ahead of igniter ignition. This prevents backflow of igniter gases into the oxidizer injector manifold. The preburner fuel valve (FTCV) is not signaled to open until the igniter chamber pressure reaches 1.7 MN/m^2 (250 psia). If the igniter chamber pressure does not achieve 1.7 MN/m^2 (250 psia) within 250 msec, then FS-2 is initiated. The igniter is signaled off when the preburner chamber pressure reaches 6.9 MN/m^2 (1000 psia). The fuel valve is signaled closed by the duration timer (T6). The oxidizer valve is delayed 150 msec to provide an oxidizer lag on shutdown. This sequence

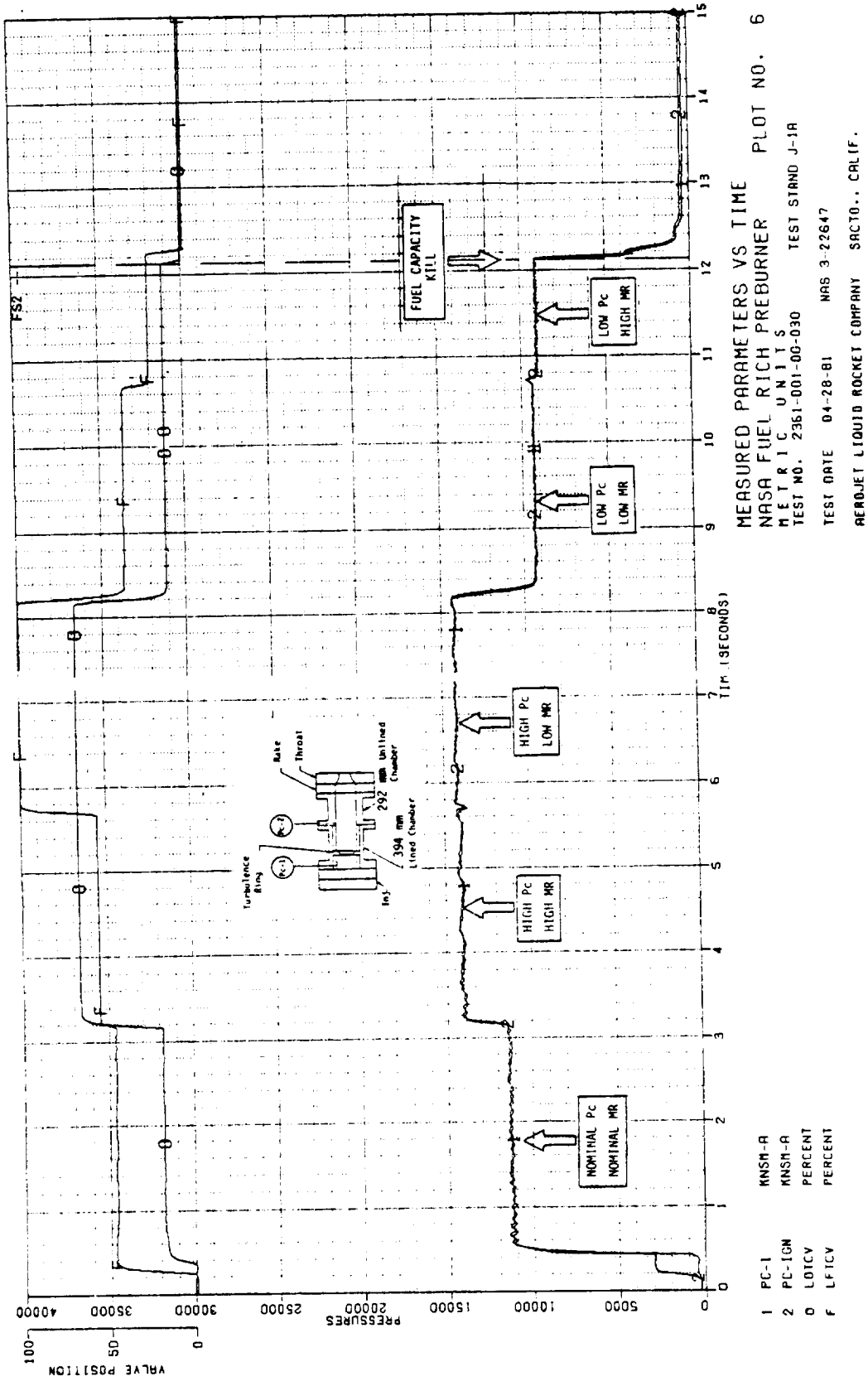

Figure 49. Fuel-Rich Preburner, Measured Parameters Versus Time, Test -030 (1 of 2)

ORIGINAL PAGE IS
OF POOR QUALITY

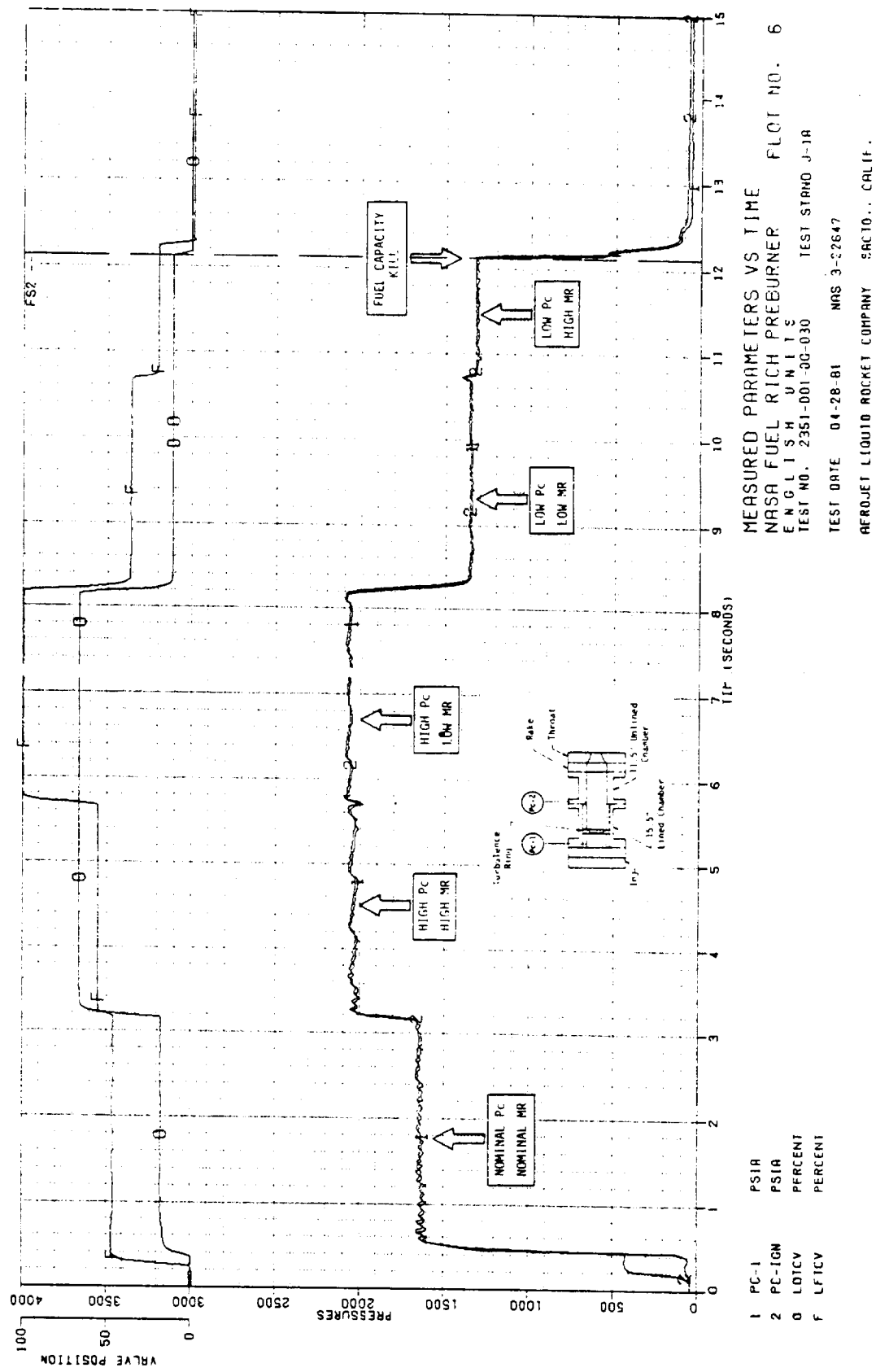

Figure 49. Fuel-Rich Preburner, Measured Parameters Versus Time, Test -030 (2 of 2)

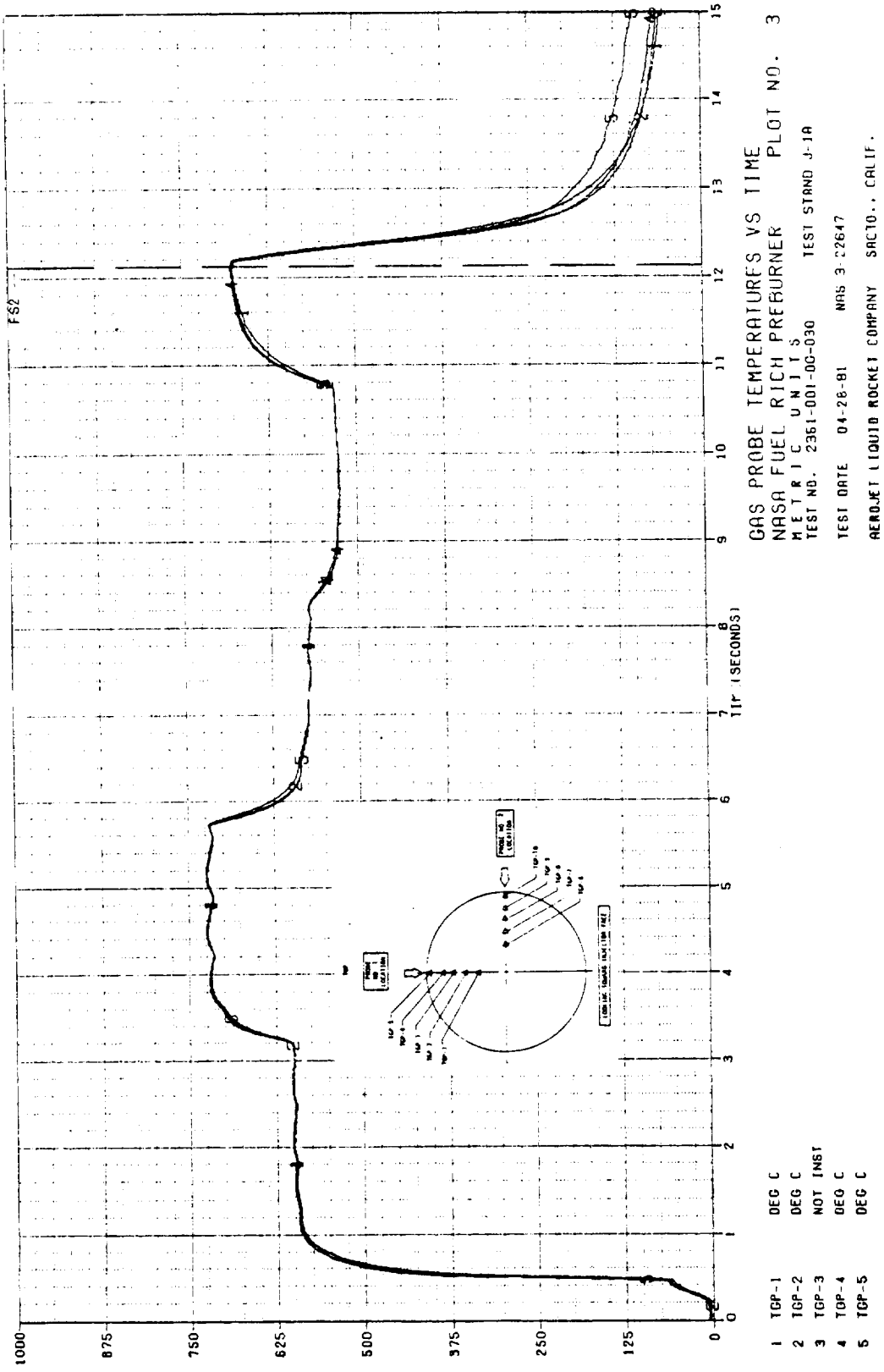

Figure 50. Fuel-Rich Preburner, Gas Probe Temperatures (TGP-1, -5) Versus Time, Test -030 (1 of 2)

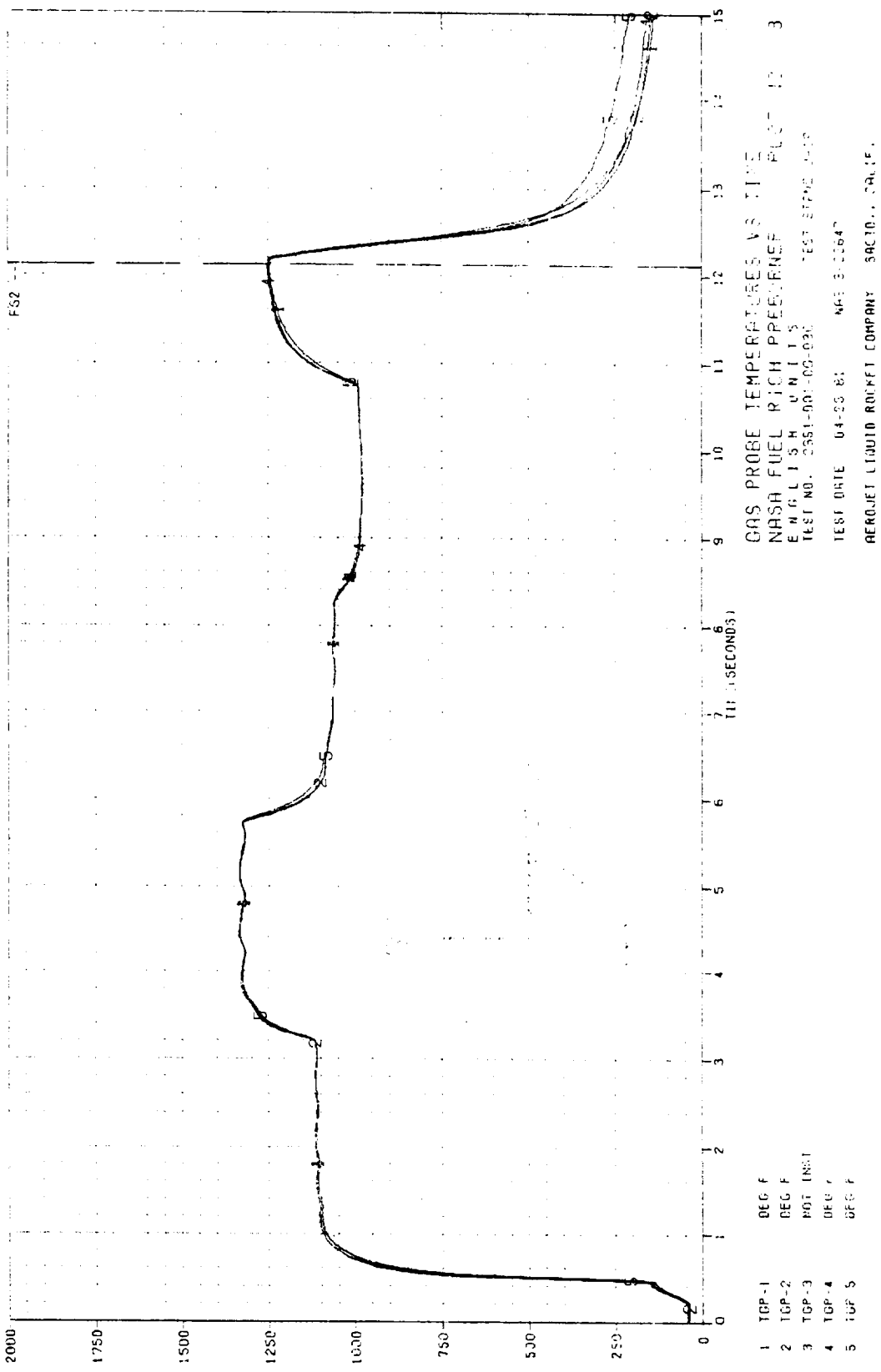

Figure 50. Fuel-Rich Preburner, Gas Probe Temperatures (TGP-1, -5) Versus Time, Test -030 (2 of 2)

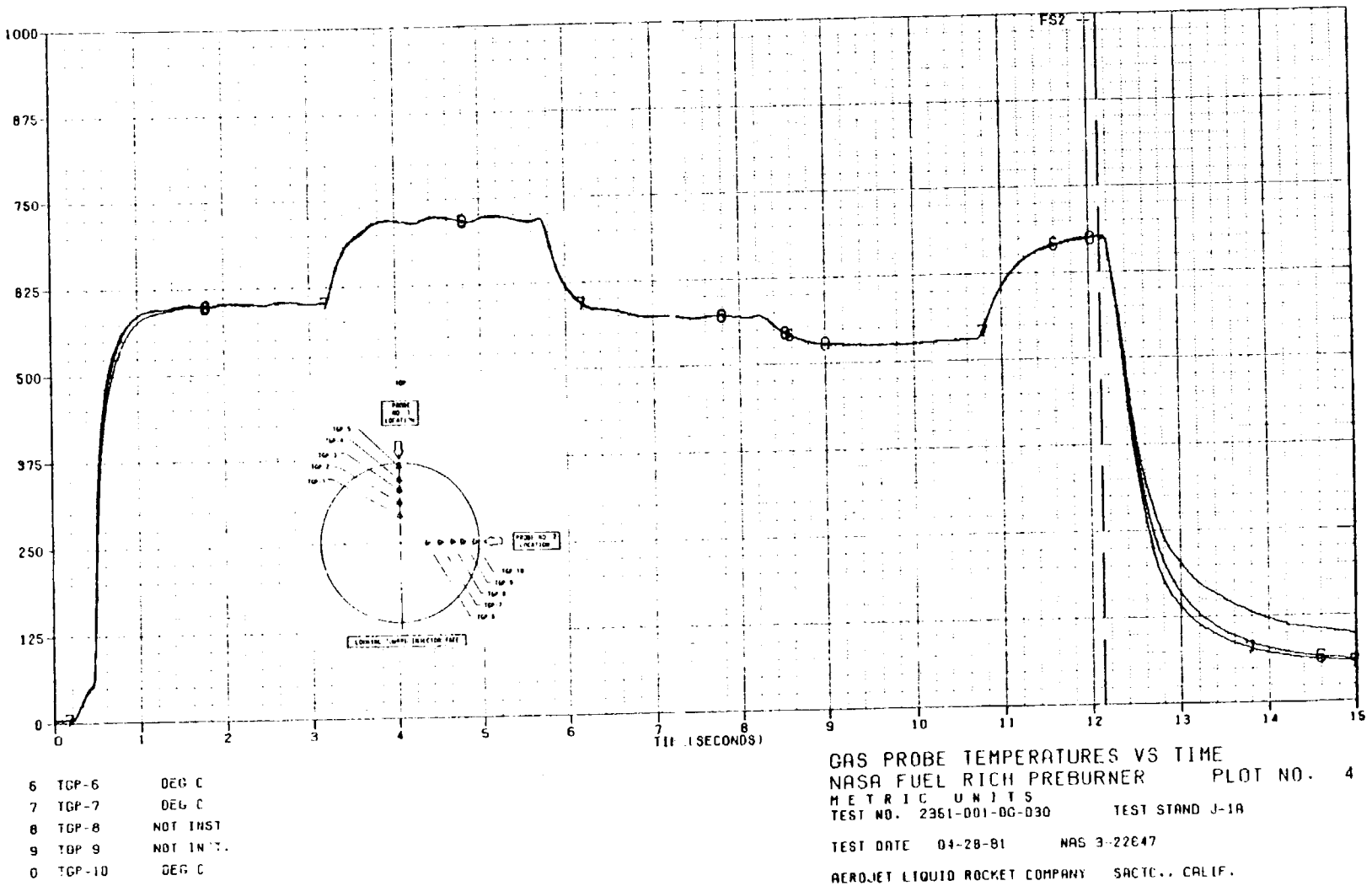

Figure 51. Fuel-Rich Preburner, Gas Probe Temperatures (TGP-6, -10) Versus Time, Test -030 (1 of 2)

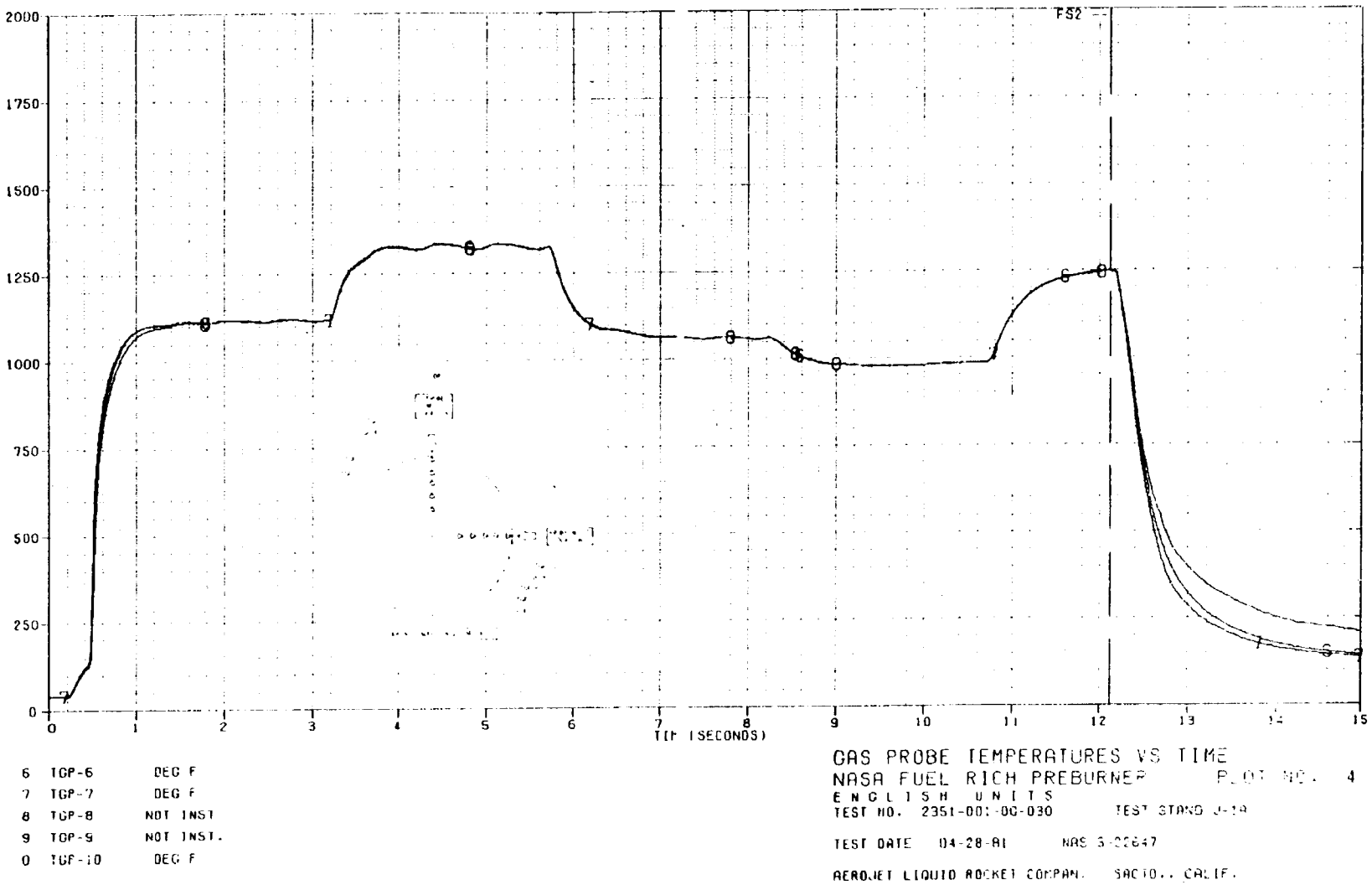

Figure 51. Fuel-Rich Preburner, Gas Probe Temperatures (TGP-6, -10) Versus Time, Test -030 (2 of 2)

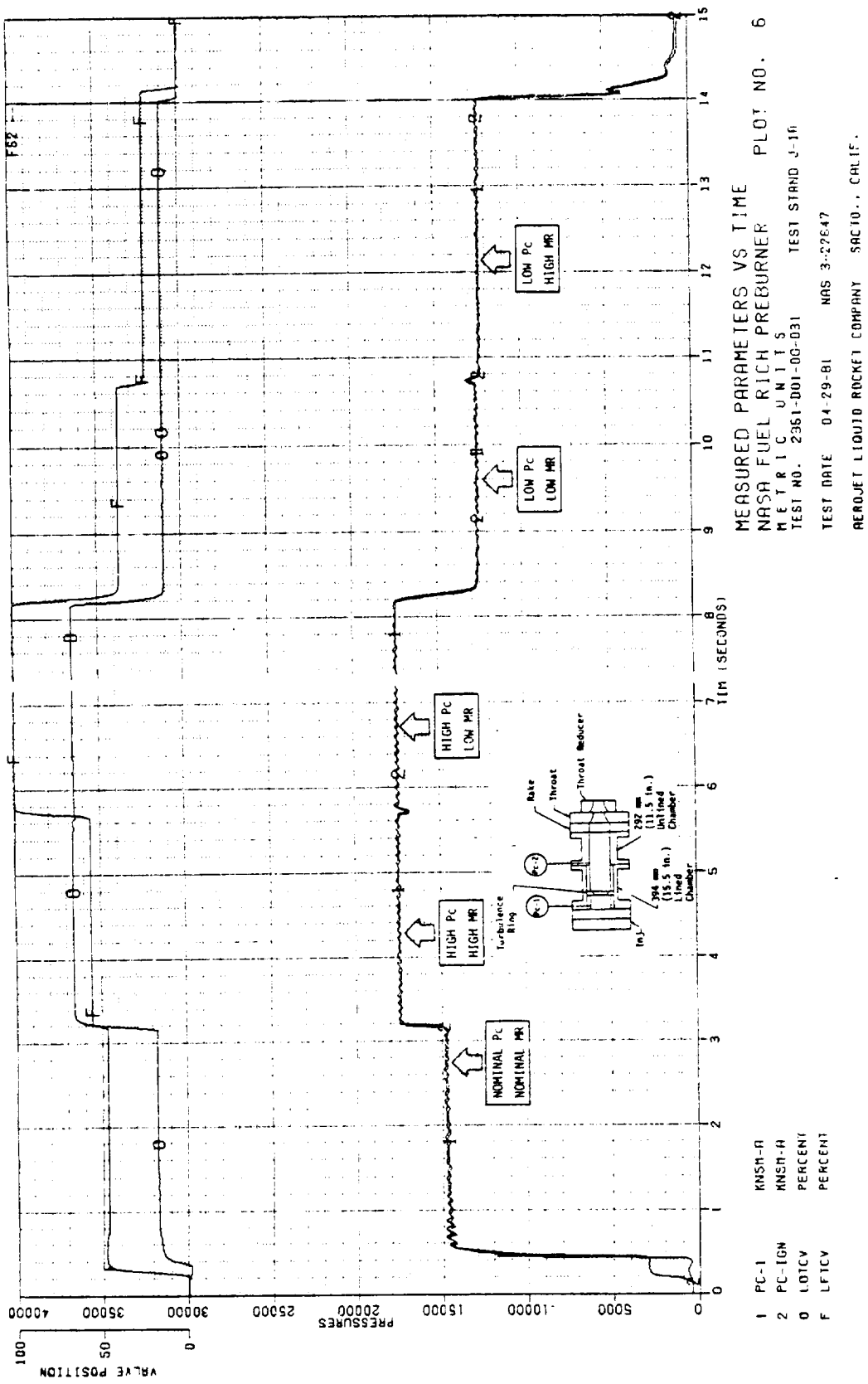

Figure 52. Fuel-Rich Preburner, Measured Parameters Versus Time, Test -031 (Page 1 of 2)

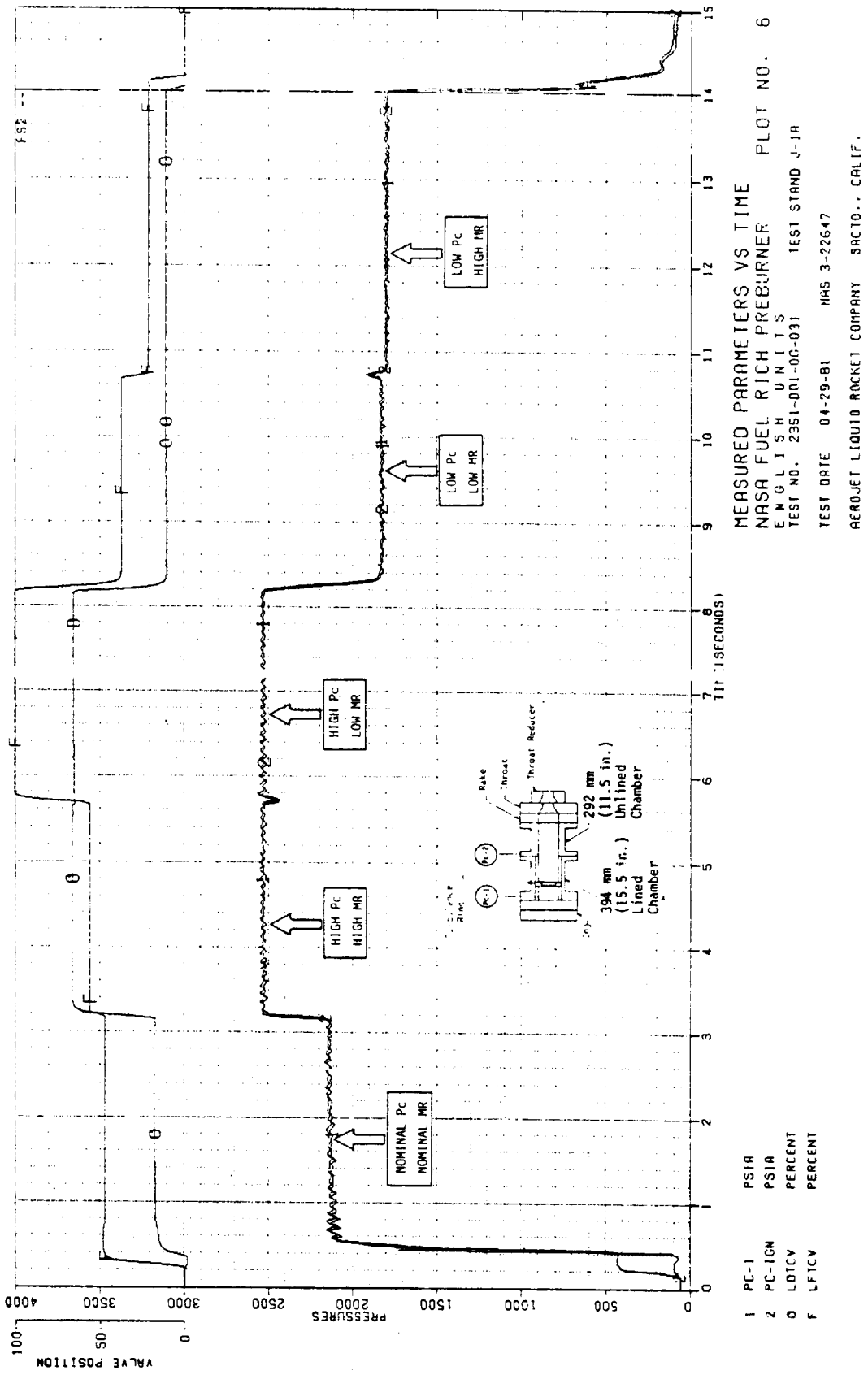

Figure 52. Fuel-Rich Preburner, Measured Parameters Versus Time, Test -031 (Page 2 of 2)

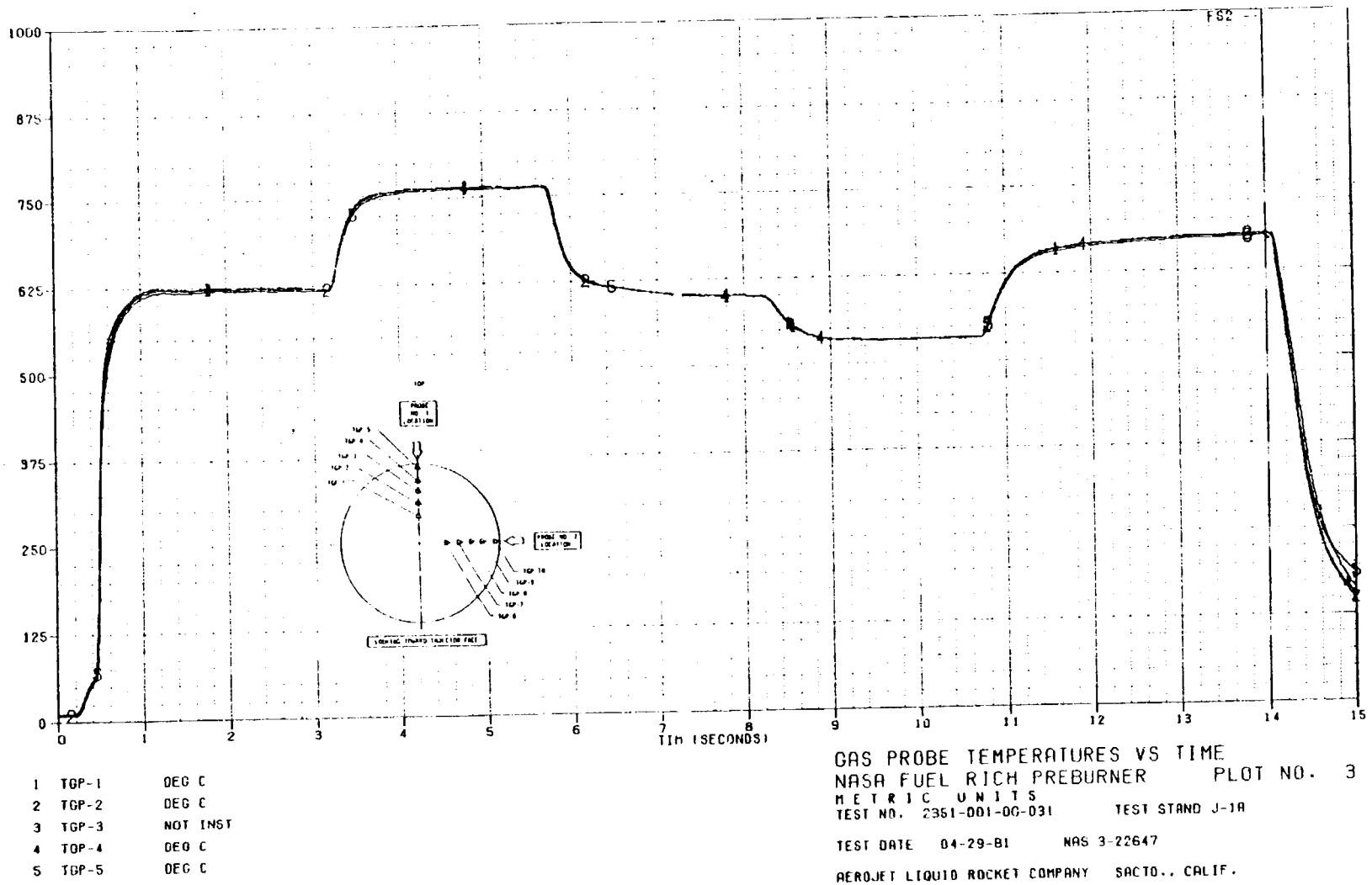

Figure 53. Fuel-Rich Preburner, Gas Probe Temperatures (TGP-1, -5), Test -031 (Page 1 of 2)

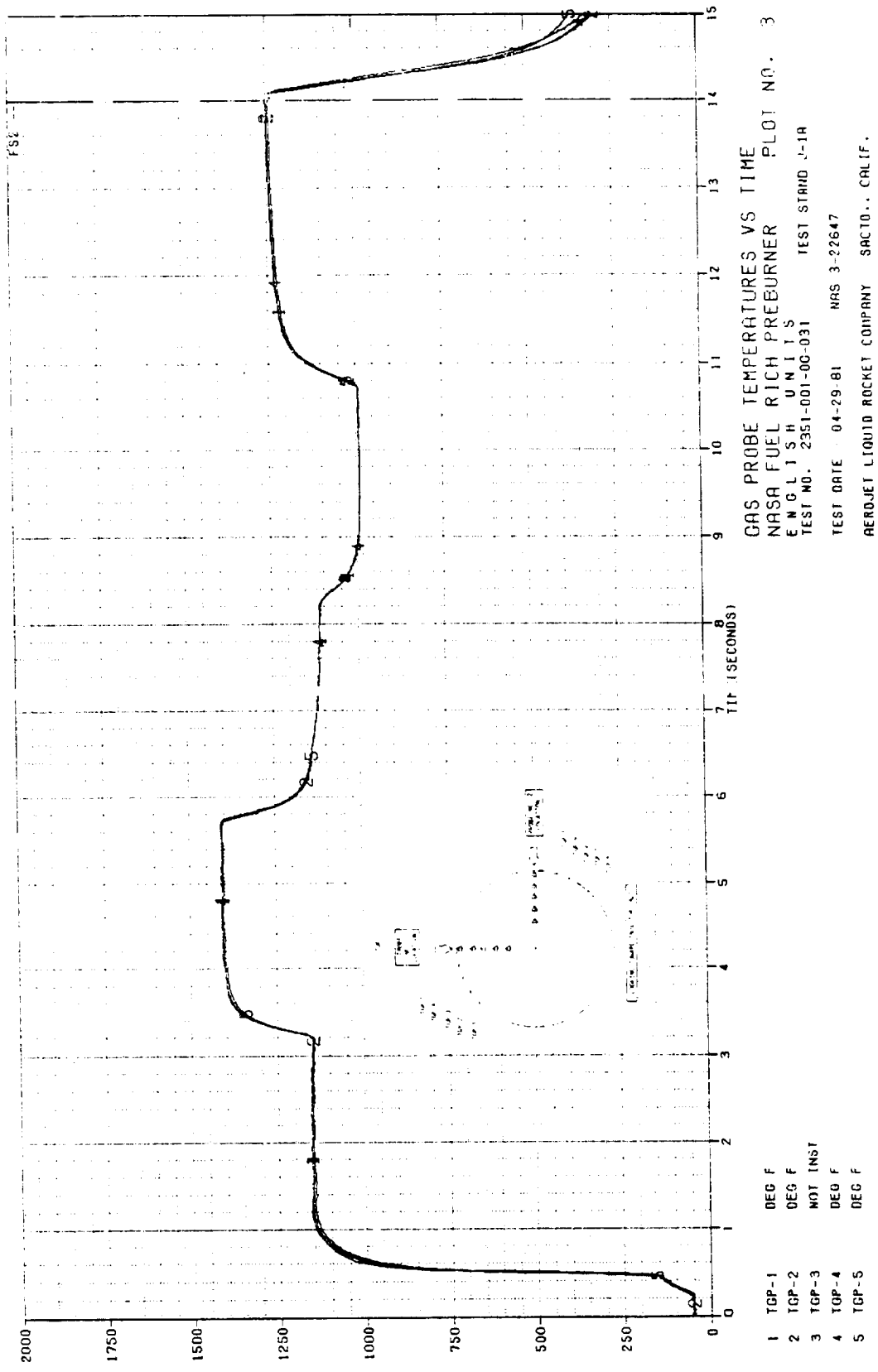

Figure 53. Fuel-Rich Preburner, Gas Probe Temperatures (TGP-1, -5), Test -031 (Page 2 of 2)

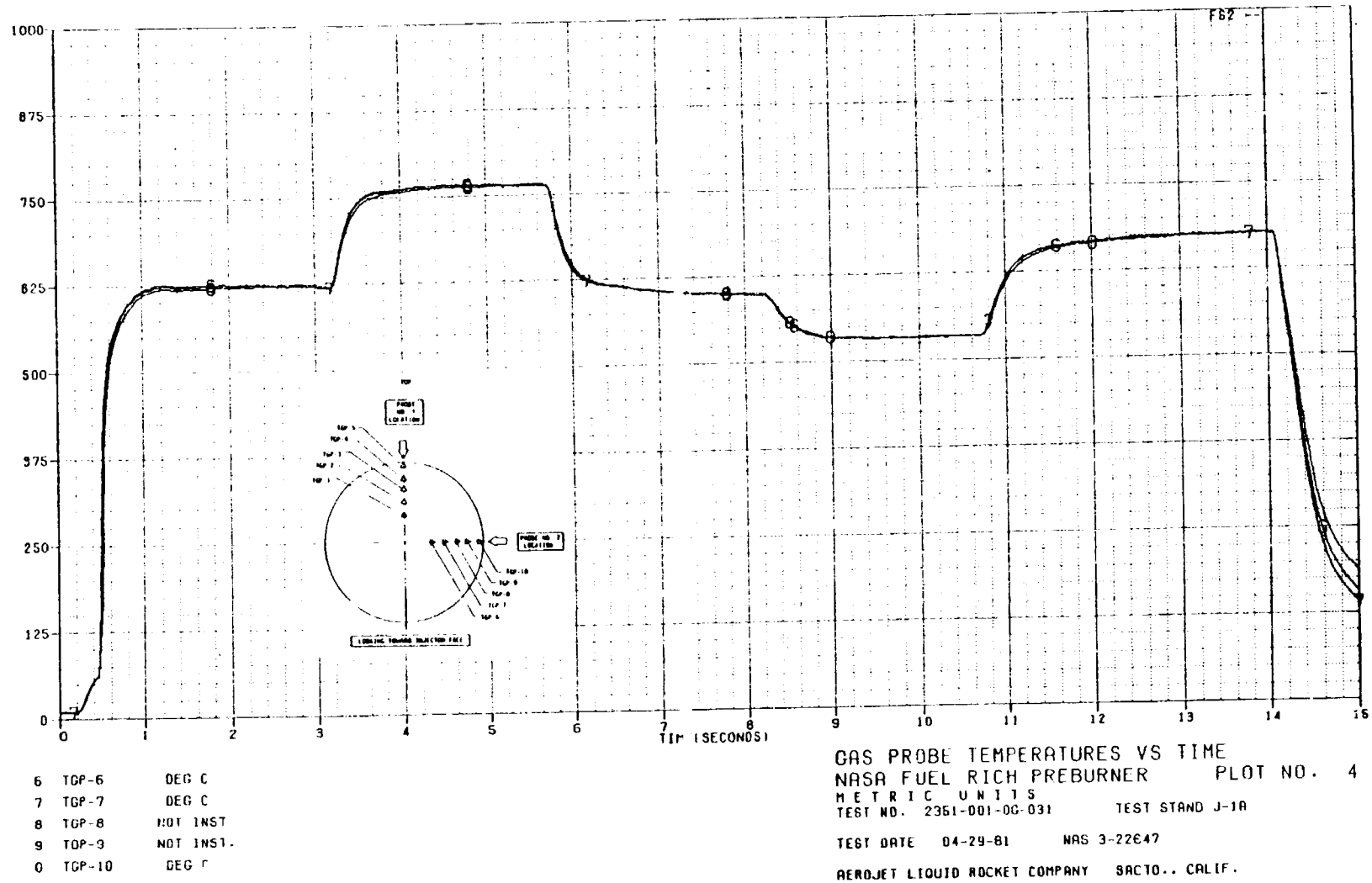

Figure 54. Fuel-Rich Preburner, Gas Probe Temperatures (TGP-6, -10) Versus Time, Test -031 (1 of 2)

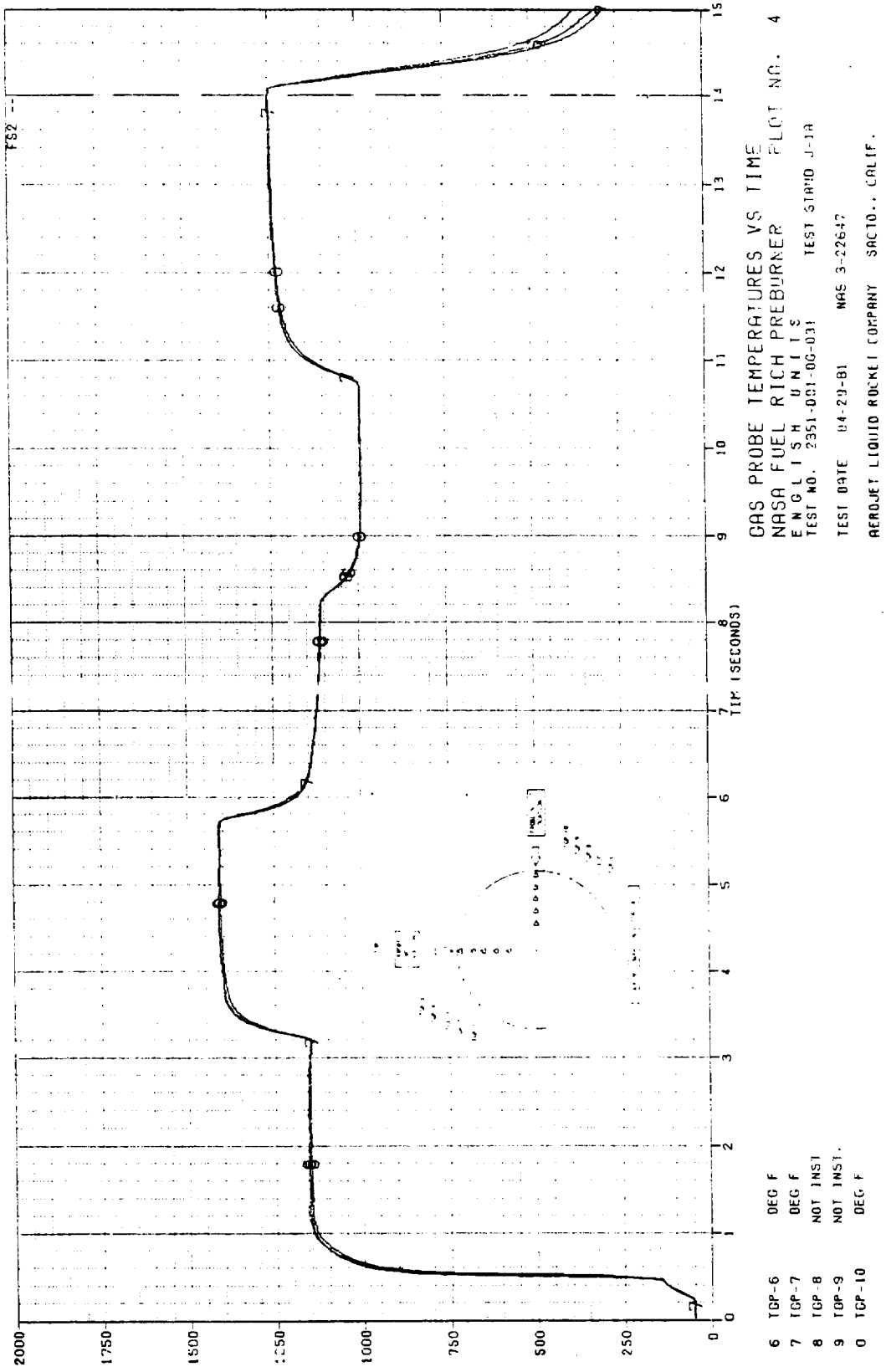

Figure 54. Fuel-Rich Preburner, Gas Probe Temperatures (TGP-6, -10) Versus Time, Test -031 (2 of 2)

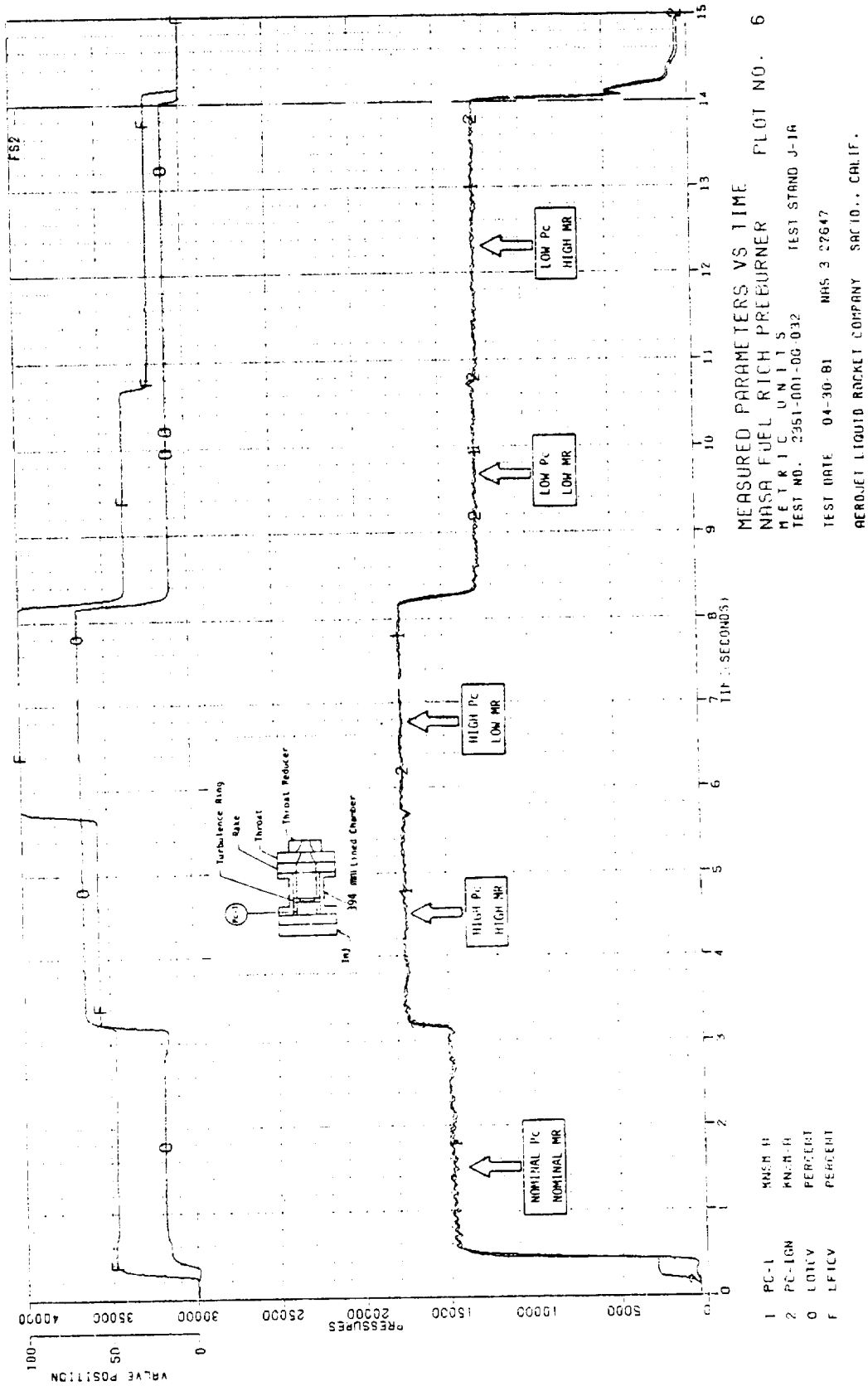

Figure 55. Fuel-Rich Preburner, Measured Parameters Versus Time, Test -032
(1 of 2)

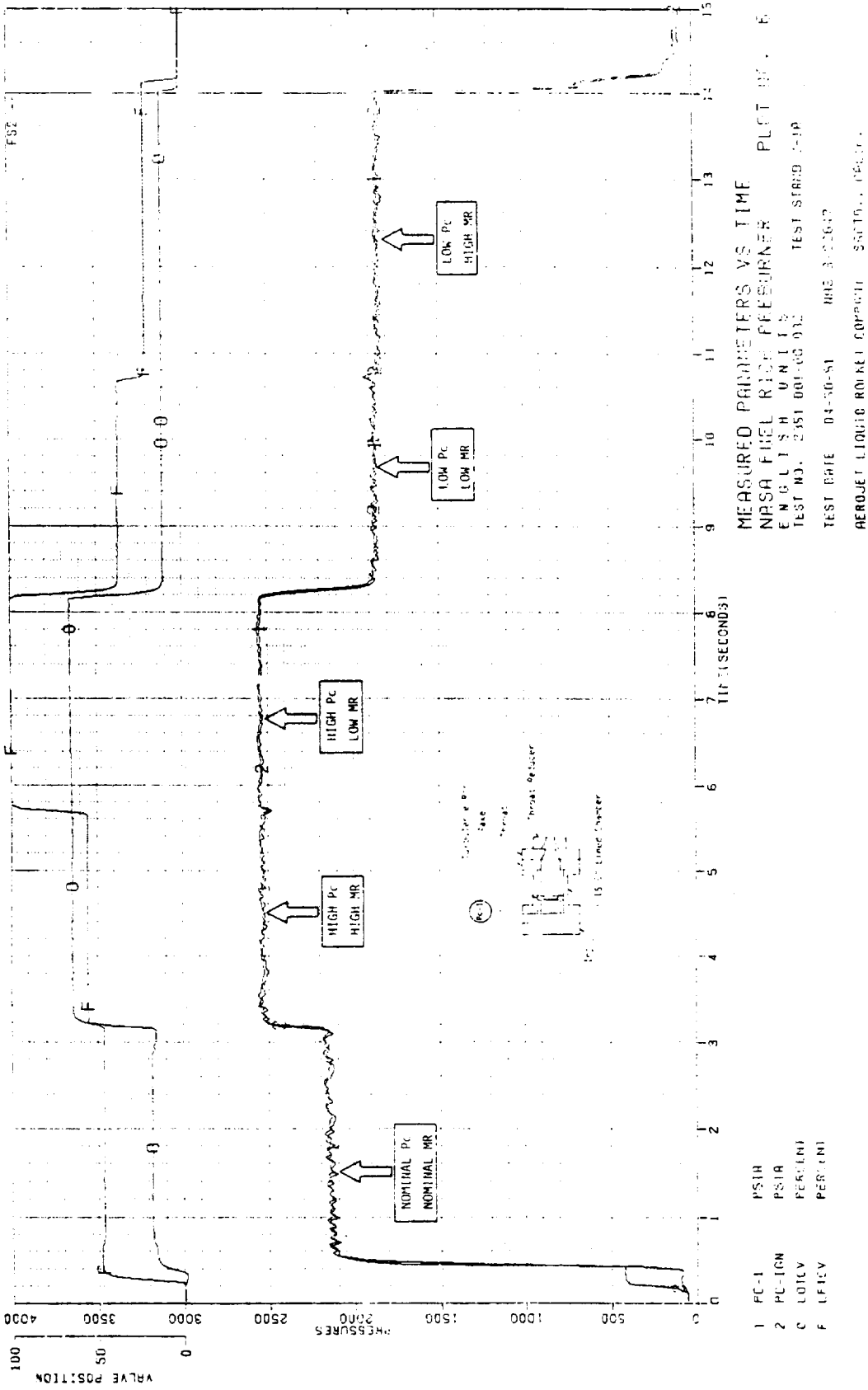

Figure 55. Fuel-Rich Preburner, Measured Parameters Versus Time, Test -032 (2 of 2)

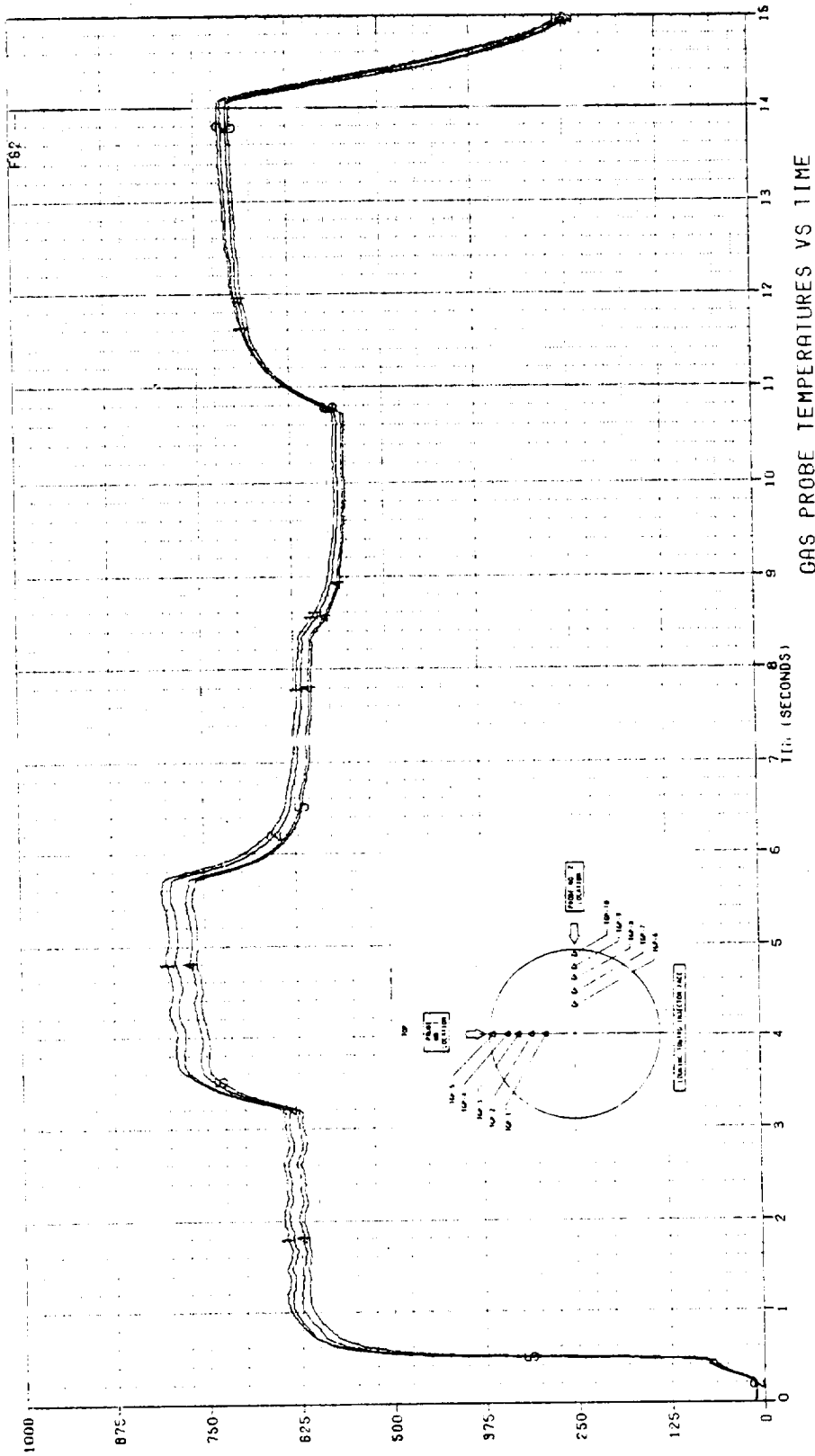

Figure 56. Fuel-Rich Preburner, Gas Probe Temperatures (TGP-1, -5) Versus Time, Test -032 (1 of 2)

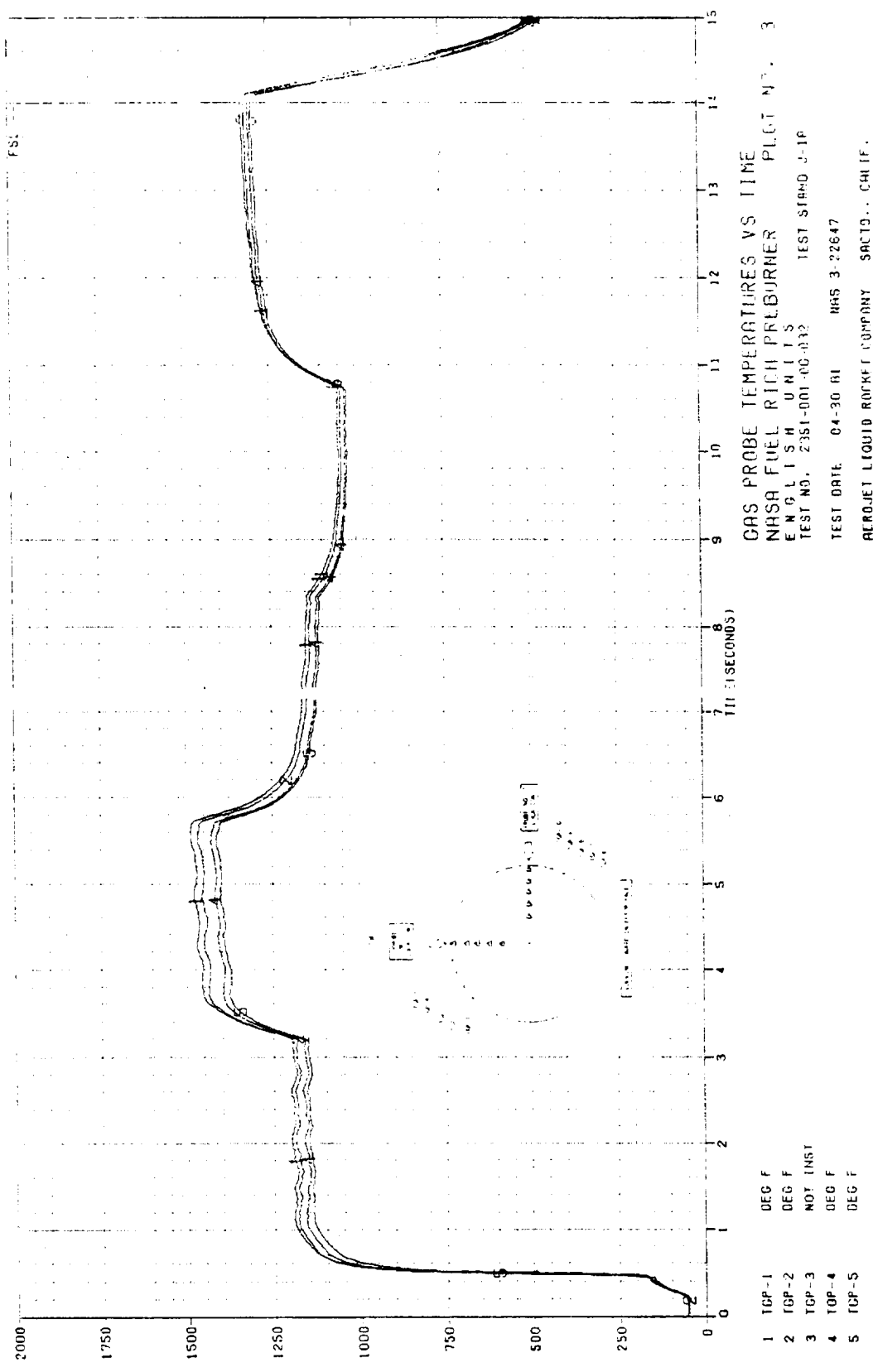

Figure 56. Fuel-Rich Preburner, Gas Probe Temperatures (TGP-1, -5) Versus Time, Test -032 (2 of 2)

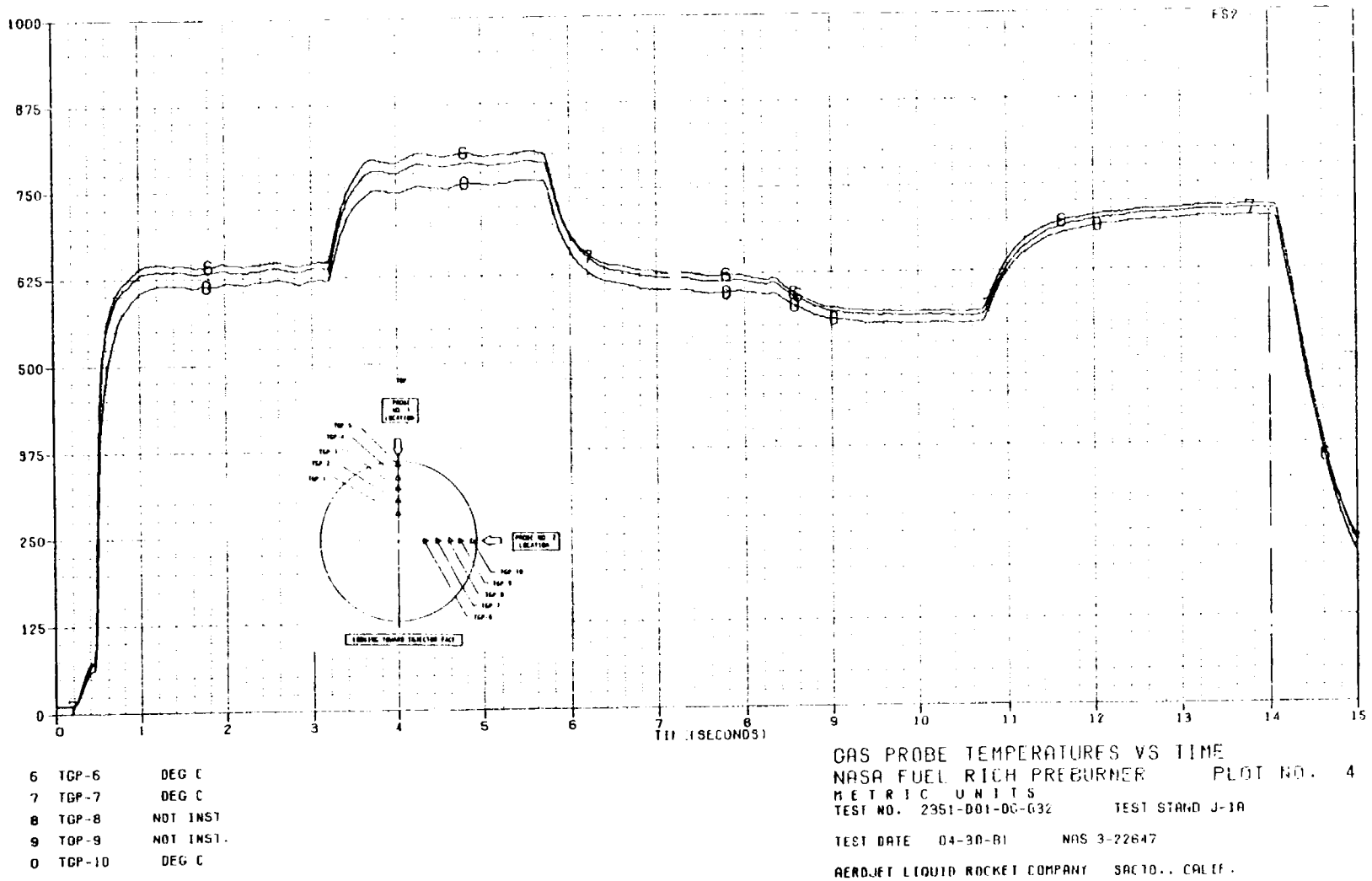

Figure 57. Fuel-Rich Preburner, Gas Probe Temperatures (TGP-6, -10) Versus Time, Test -032 (1 of 2)

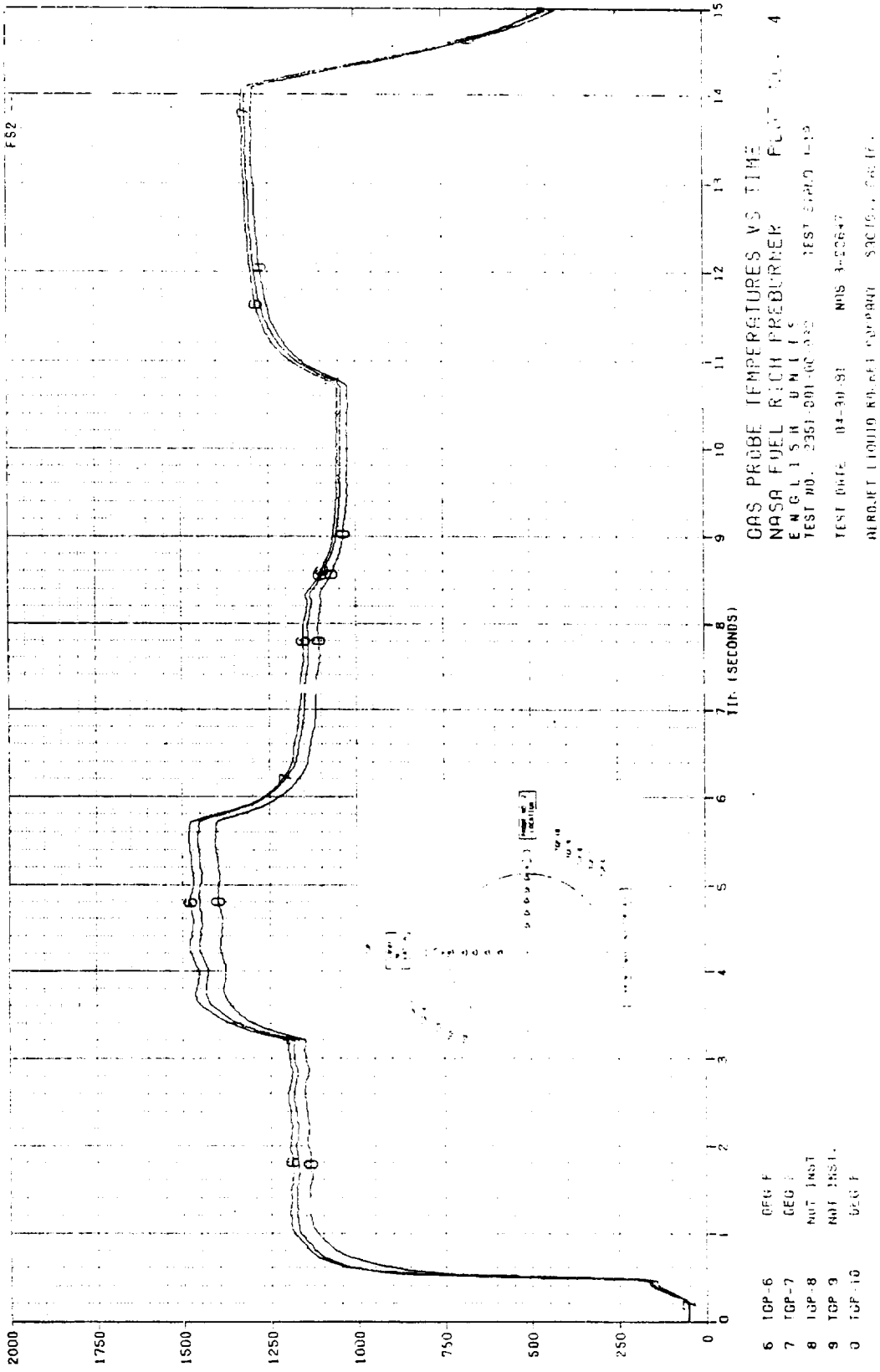

Figure 57. Fuel-Rich Preburner, Gas Probe Temperatures (TGP-6, -10) Versus Time, Test -032 (2 of 2)

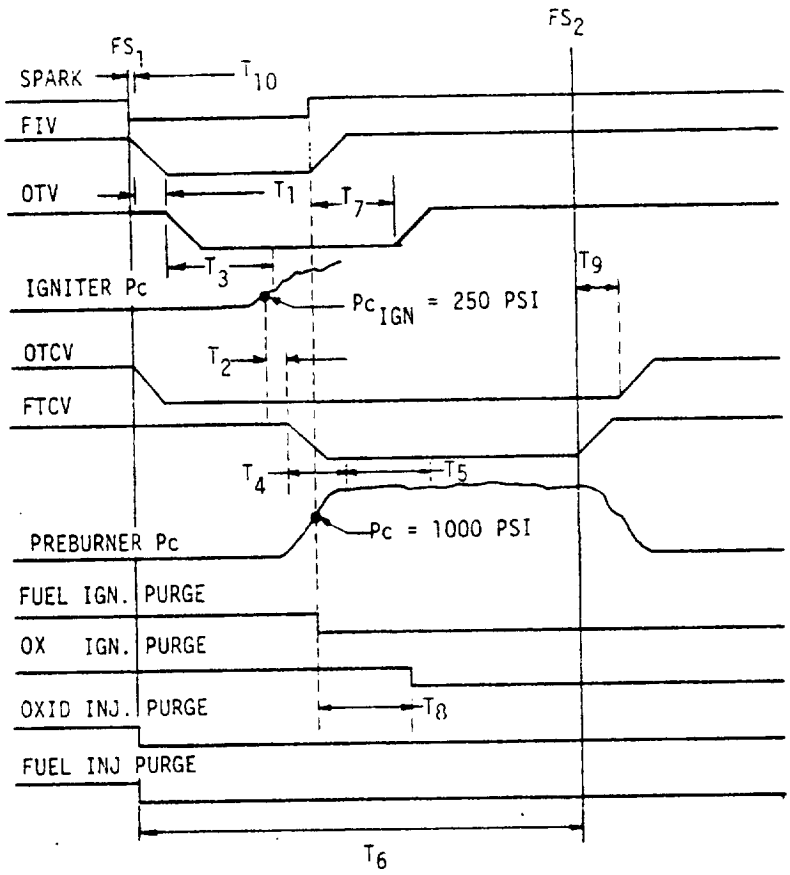

TIMER FUNCTIONS:	TIME (MSEC)
T_1 - OX IGNITER VALVE OPENING DELAY. DELAYS OX VALVE OPENING FROM FUEL IGNITER VALVE OPENING.	10
T_2 - FUEL FLOW CONTROL VALVE DELAY. DELAYS VALVE OPENING FROM INITIAL OPENING SIGNAL TO FUEL FLOW CONTROL VALVE.	0
T_3 - IGNITER CHAMBER PRESSURE SHUTDOWN. IF IGNITER PRESSURE IS NOT UP TO 1.7 MN/m^2 (250 psi) PRESSURE BY T_3, A FS_2 SIGNAL IS OBTAINED.	250
T_4 - PREBURNER CHAMBER PRESSURE SHUTDOWN. IF PREBURNER PRESSURE IS NOT UP TO 6.9 MN/m^2 (1000 psi) BY T_4, A FS_2 SIGNAL IS OBTAINED.	250
T_5 - CSM SHUTDOWN LOCKOUT. THE CSM SHUTDOWN WILL NOT BE INITIATED UNTIL AFTER T_5, TO PRECLUDE ANY PRESSURE PERTURBATIONS DURING START TRANSIENT.	30
T_6 - DURATION TIMER. GIVES THE TOTAL DURATION OF THE TEST	500
T_7 - OX IGNITER VALVE CLOSING DELAY.	50
T_8 - OX IGNITER PURGE VALVE OPENING DELAY.	50
T_9 - OX FLOW CONTROL VALVE CLOSING DELAY.	150
T_{10} - FUEL IGNITER VALVE & SPARK DELAY.	0

Figure 58. Oxidizer-Rich Preburner Test Sequence

ensures that the preburner mixture ratio remains oxidizer-rich from startup to shutdown, thus avoiding temperature spikes due to adverse mixture ratio transients. The igniter was initially orificed to provide an oxidizer-rich (MR = 40) rather than a fuel-rich torch to avoid the possibility of erosion around the igniter exit. The igniter was subsequently run fuel-rich with the platelet injector.

The test results are summarized in Table X on page 142. The oxidizer- rich test series is designated 2351-D02-0G-XXX.

Test -013

This was to have been the first oxidizer-rich EDM injector hot-fire test, but a spark box malfunction terminated the test at the start. The 394-mm (15.5 in.) chamber with a Rokide-Z-coated liner was used. The nozzle plate and nozzle throat reducer were also sprayed with a Rokide Z coating.

Test -014

This was the first hot-fire test with the EDM injector. The chamber pressure, igniter pressure, valve positions, and manifold pressures are plotted in Figures 59 and 60. The test had been scheduled for 1/2 second; however, a computer logic error caused the test to run for 1 second.

The igniter fuel line developed a leak at about 0.750 second, resulting in the loss of the igniter and damage to the injector body and oxidizer manifold. Post-test examination of the hardware indicates that the leak probably developed at the fuel inlet line "B" nut. The failure may have been due to fatigue associated with a high-amplitude 650-Hz 1L mode oscillation. There is also the possibility that oxidizer was forced back into the igniter fuel line by the oscillations. Check valves were subsequently installed at the igniter fuel line inlet to preclude this problem.

Damage to the injector faceplate is shown in Figure 61. The damage is in the igniter mounting port area. As shown in Figure 62, the metal slag deposits on the face are from the resonator ring which suffered some damage when the oxidizer manifold burned through. The chamber and nozzle were undamaged. The test stand sustained minor damage, as shown in Figure 63.

No erosion damage was incurred by the Rokide-Z-coated chamber and nozzle as a result of the injector pattern or the oxidizer-rich environment.

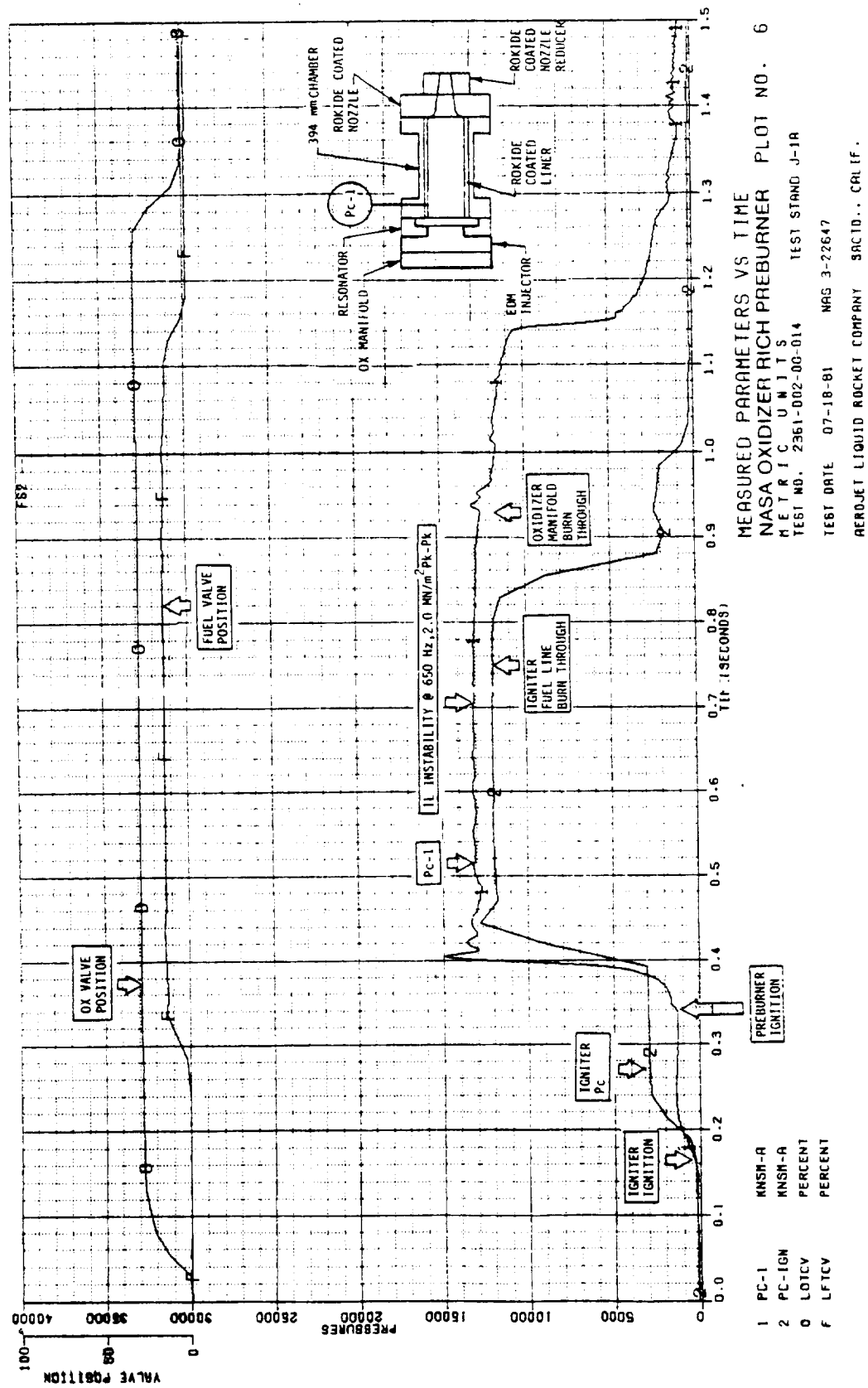

Figure 59. Oxidizer-Rich Preburner, Measured Parameters Versus Time, Test -014 (1 of 2)

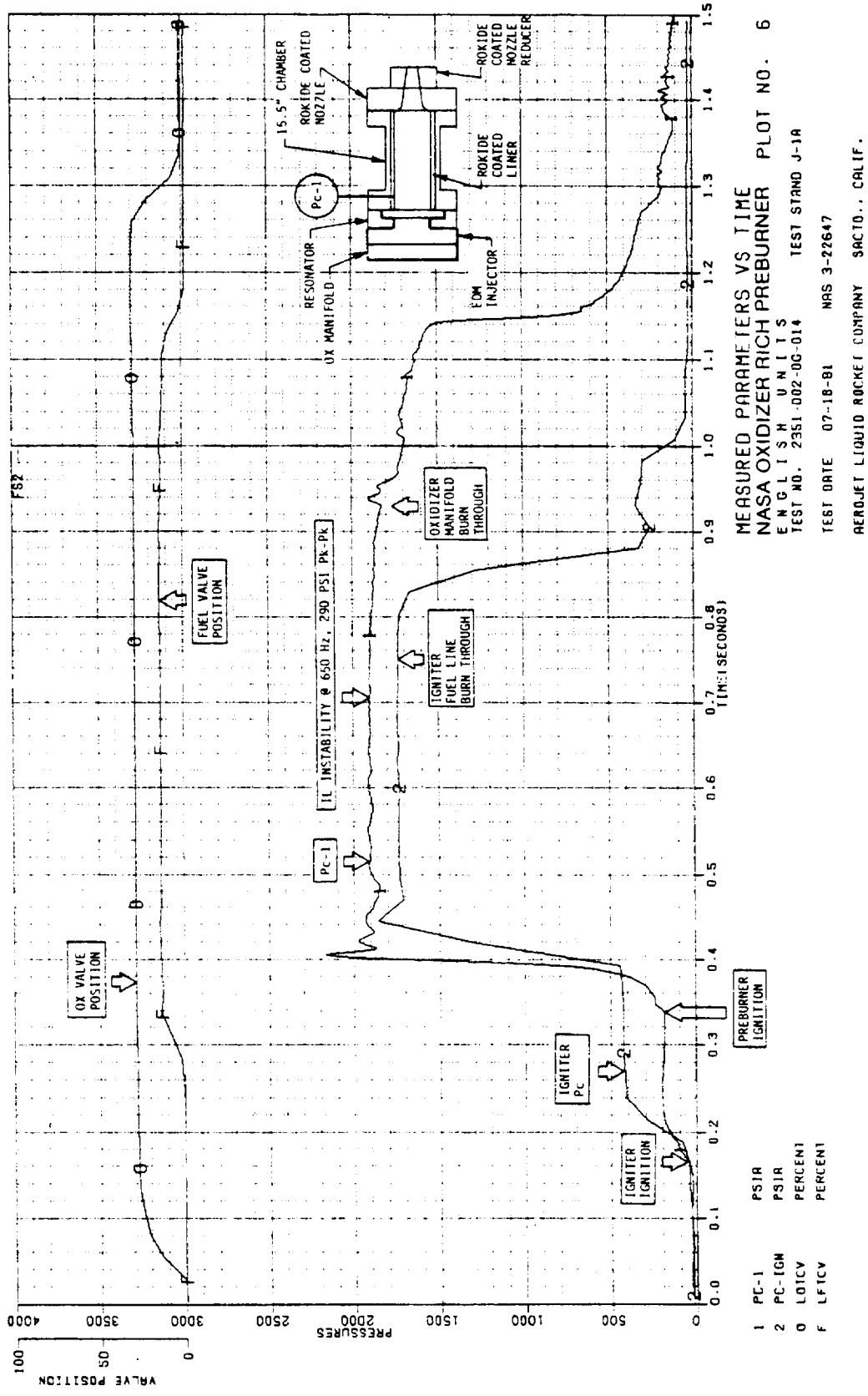

Figure 59. Oxidizer-Rich Preburner, Measured Parameters Versus Time, Test -014 (2 of 2)

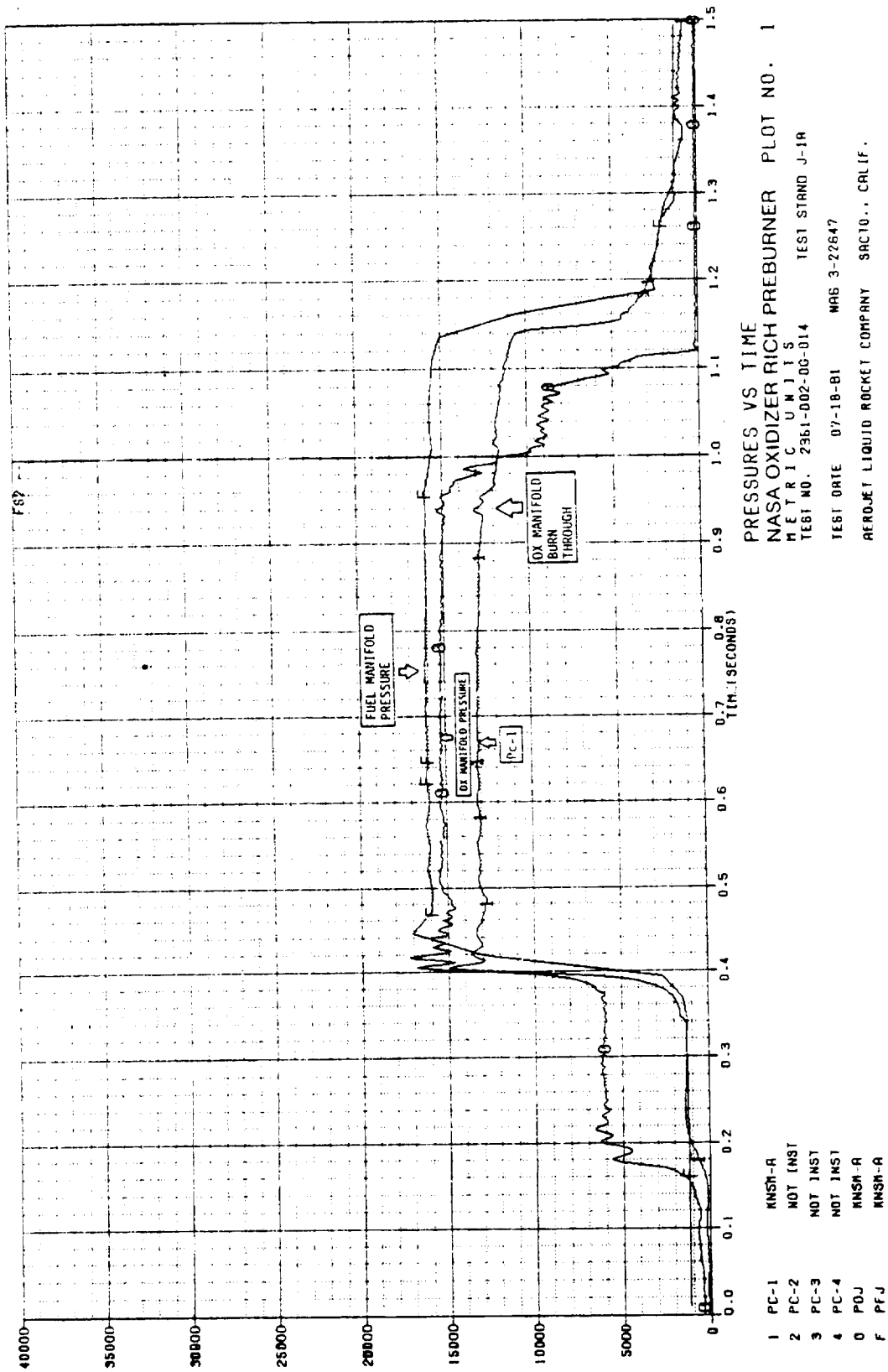

Figure 60. Oxidizer-Rich Preburner, Measured Parameters Versus Time, Test -014 (1 of 2)

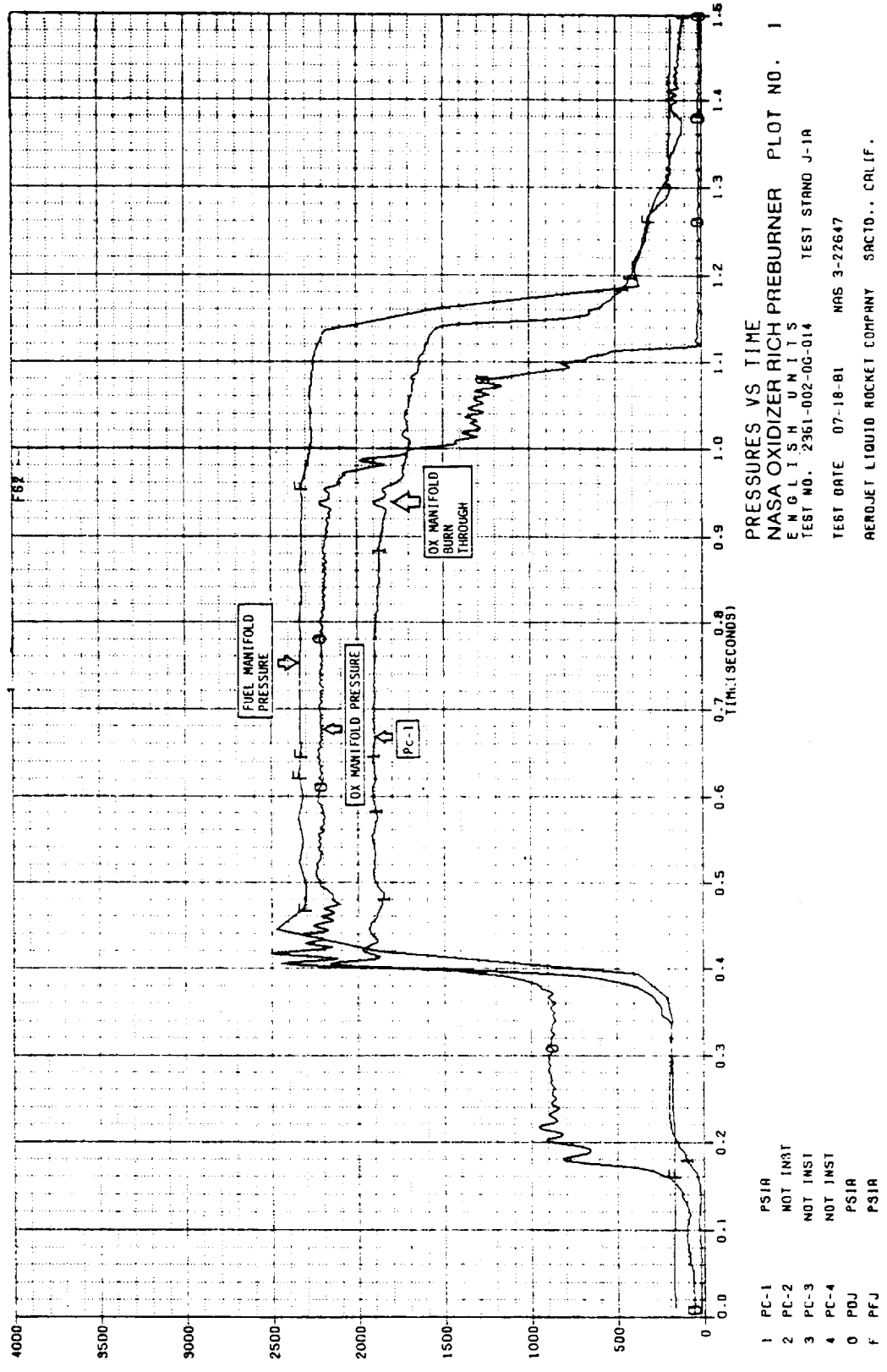

Figure 60. Oxidizer-Rich Preburner, Measured Parameters Versus Time, Test -014 (2 of 2)

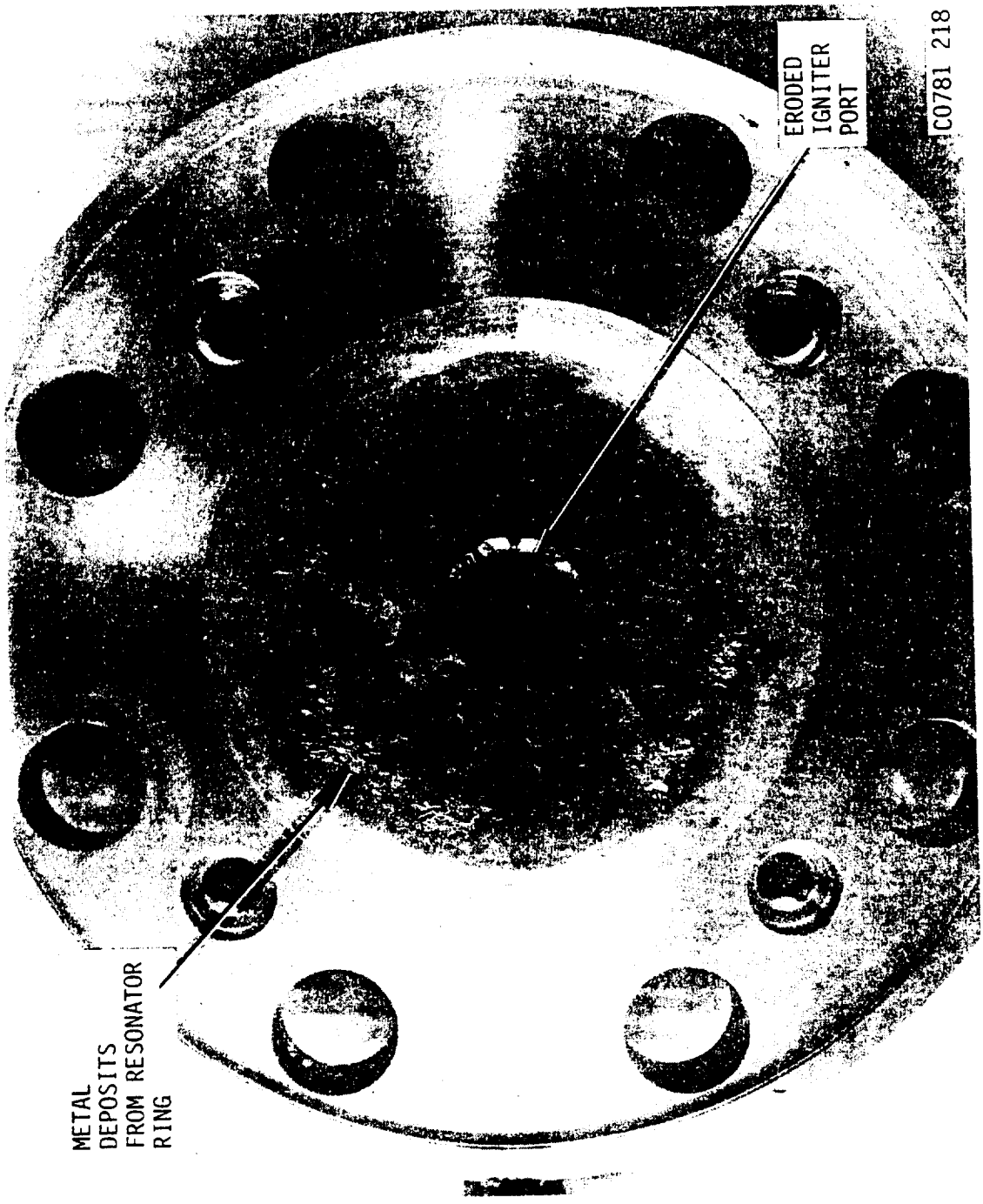

Figure 61. EDM Oxidizer-Rich Injector, Post Test -014

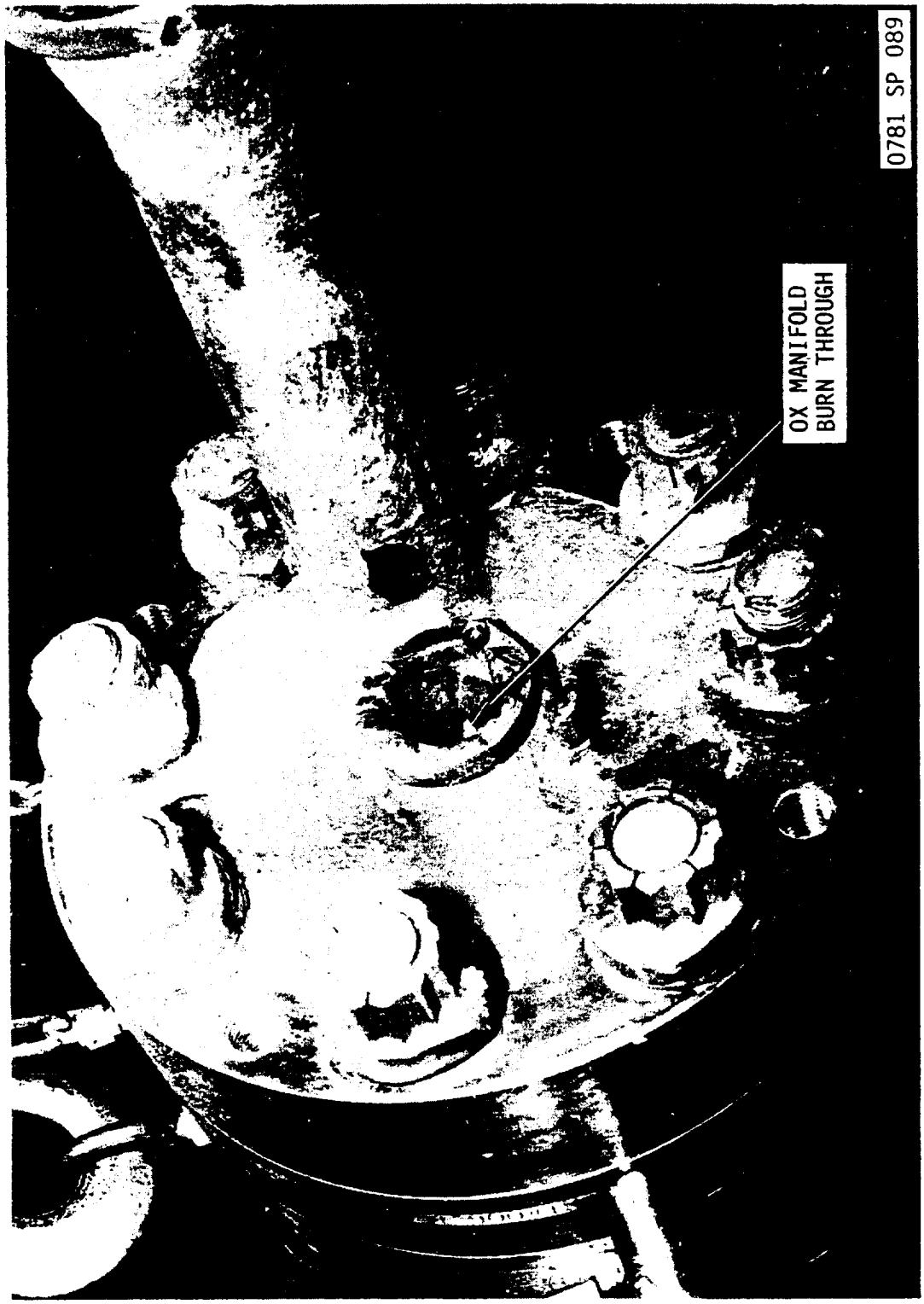

Figure 62. Oxidizer Manifold, Post Test -014

ORIGINAL PAGE
BLACK AND WHITE PHOTOGRAPH

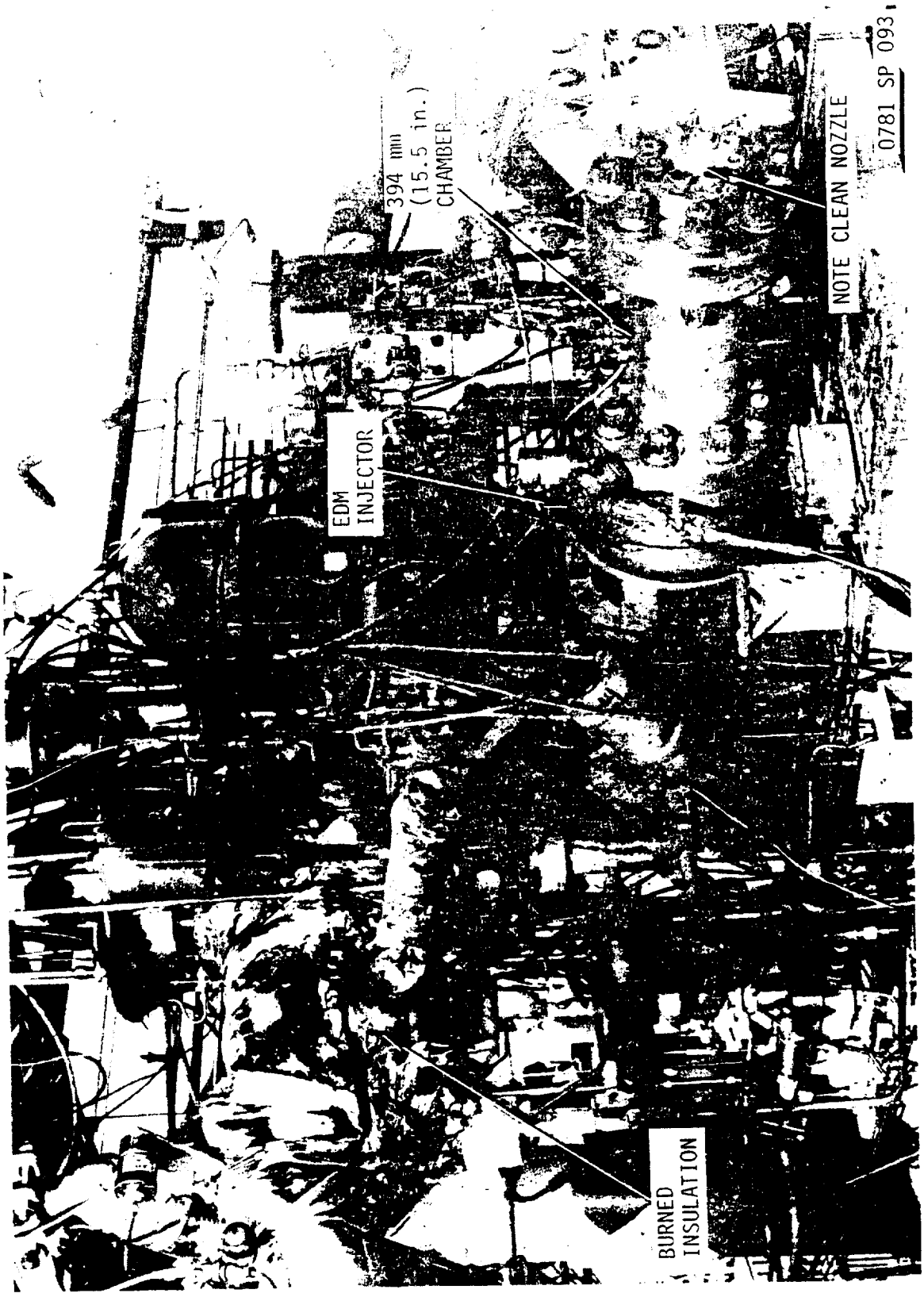

Figure 63. Oxidizer-Rich Preburner Test Setup, Post Test -014

TABLE X

OXIDIZER-RICH PREBURNER TEST SUMMARY

Test No.	Date	Injector	Test Objective	Duration (sec)	P_c MN/m^2 (psia)	MR	$\dot{w}_o$ kg/s (lb/sec)	$\dot{w}_f$ kg/s (lb/sec)	T_G °C (°F)	C* m/s (ft/sec)	Stability	Remarks
-013	7/18/81	EDM	Sequence Checkout	-	-	-	-	-	-	-	-	Igniter spark malfunction
-014	7/18/81	EDM	Sequence Checkout	1	13.1 (1905)	36.8	31.39 (69.2)	0.85 (1.88)	-	787 (2582)	1L @ 650 Hz	Igniter hot gas leak caused damage to injector. No erosion of face, chamber or nozzle.
-015	7/31/81	Platelet	Oxidizer Cold-Flow	1/2	-	-	-	-	-	-	-	
-016	7/31/81	Platelet	Oxidizer Cold-Flow	1/2	-	-	-	-	-	-	-	
-017	7/31/81	Platelet	Sequence Checkout	1/2	-	-	52.21 (115.1)	1.50 (3.30)	-	-	-	No ignition with ox-rich igniter.
-018	7/31/81	Platelet	Sequence Checkout	1/2	12.7 (1844)	37.1	36.74 (81.0)	0.99 (2.18)	-	648 (2127)	1L @ 667 Hz	Hard start with MR = 3.5 igniter. No erosion of hardware.
-019	8/1/81	Platelet	Sequence Checkout	1/2	12.9 (1872)	35.8	37.56 (82.8)	1.05 (2.31)	-	643 (2110)	Stable	Hard start with MR = 1.2 igniter. Injector orifice damage. No erosion of chamber turbulence ring or nozzle.
-020	12/12/81	EDM	Oxidizer Cold-Flow & Igniter Checkout	1/2	-	-	-	-	-	-	-	Igniter Pc too high, fuel orifice left out.
-021	12/14/81	EDM	Performance & Stability	1	13.9 (2023)	47.5	37.69 (83.1)	0.79 (1.75)	-	659 (2163)	1L @ 604 Hz (85 psi) (P-P) 586 kN/m^2	Injector face damaged around igniter port
-022	12/17/81	EDM	Test effect of shorter chamber and high Pc, low MR on 1L stability	1/2	-	-	-	-	-	-	-	Delayed ignition, no data
-023	12/18/81	EDM	Test effect of shorter chamber and high Pc, low MR on 1L stability	1	16.6 (2402)	32.6	36.51 (80.5)	1.12 (2.47)	-	806 (2644)	Stable	Igniter orificed to 1.2 MR. Good ignition.
-024	12/21/81	EDM	Performance & gas temperature uniformity evaluation	1/2	-	-	-	-	-	-	Stable	Rake & turbine simulator failure, no S.S. Data.

NOTES: 1. Pc-1 is injector face pressure.

2. C* based on nozzle inlet pressure.

IV, B, Test Results (cont.)

Test -017

This was the first attempt at a hot-fire test with the platelet injector. The 394-mm (15.5-in.) lined chamber was used with the 86-mm (3.4-in.) diameter turbulence ring. The turbulence ring was installed to provide damping of longitudinal mode oscillations. The test duration was 0.5 second as scheduled. The igniter fired, and the fuel valve opened, but no ignition occurred as can be seen from Figures 64 and 65.

Ignition did not occur because the oxidizer-rich igniter torch was quenched below the ignition temperature before the fuel spray could penetrate the oxidizer spray cones. This is illustrated in Figure 66. The fuel spray was totally encapsulated within the oxidizer spray cone, such that the torch did not contact the ignitable mixture before it had cooled to below the ignition temperature. No combustion occurred between the torch exhaust and the oxidizer spray since the torch was oxidizer-rich (MR = 40).

By contrast, good ignition was achieved with the EDM injector and the oxidizer-rich igniter (MR = 40) since the injector is designed with 10 small fuel orifices around the igniter port. The oxidizer-rich torch exhaust ignites with the fuel from these orifices and provides adequate energy for a smooth ignition. The igniter torch was reorificed to a mixture ratio of 3.5 prior to Test -018 to induce combustion between the torch exhaust and the oxidizer-rich spray.

Test -018

This was the first successful oxidizer-rich platelet hot-fire test. The test parameters are plotted in Figures 67 and 68. Ignition of the fuel-rich igniter exhaust with the oxidizer-rich spray occurred as planned. This is evidenced by the chamber pressure rise prior to ignition. The fuel-rich torch generated a chamber pressure of about 2.4 MN/m^2 (350 psia) as compared to 1.4 MN/m^2 (200 psia) generated with the oxidizer-rich torch on Test -017. However, ignition of the fuel spray was delayed about 40 msec from fuel entry into the chamber, resulting in a pressure spike approaching 27.6 MN/m^2 (4000 psia). The fuel does not adequately penetrate the oxidizer spray until it achieves sufficient momentum or injector pressure drop. The quantity of fuel which enters the chamber prior to the time this condition is reached is sufficient to cause the large overpressure.

Post-test inspection did not reveal any external damage to the injector although some of the fuel orifices appeared to be darkened by soot. The resonator seal retainer ring was damaged and seal leakage was evident. The ring was easily restored to its original shape, and a new seal

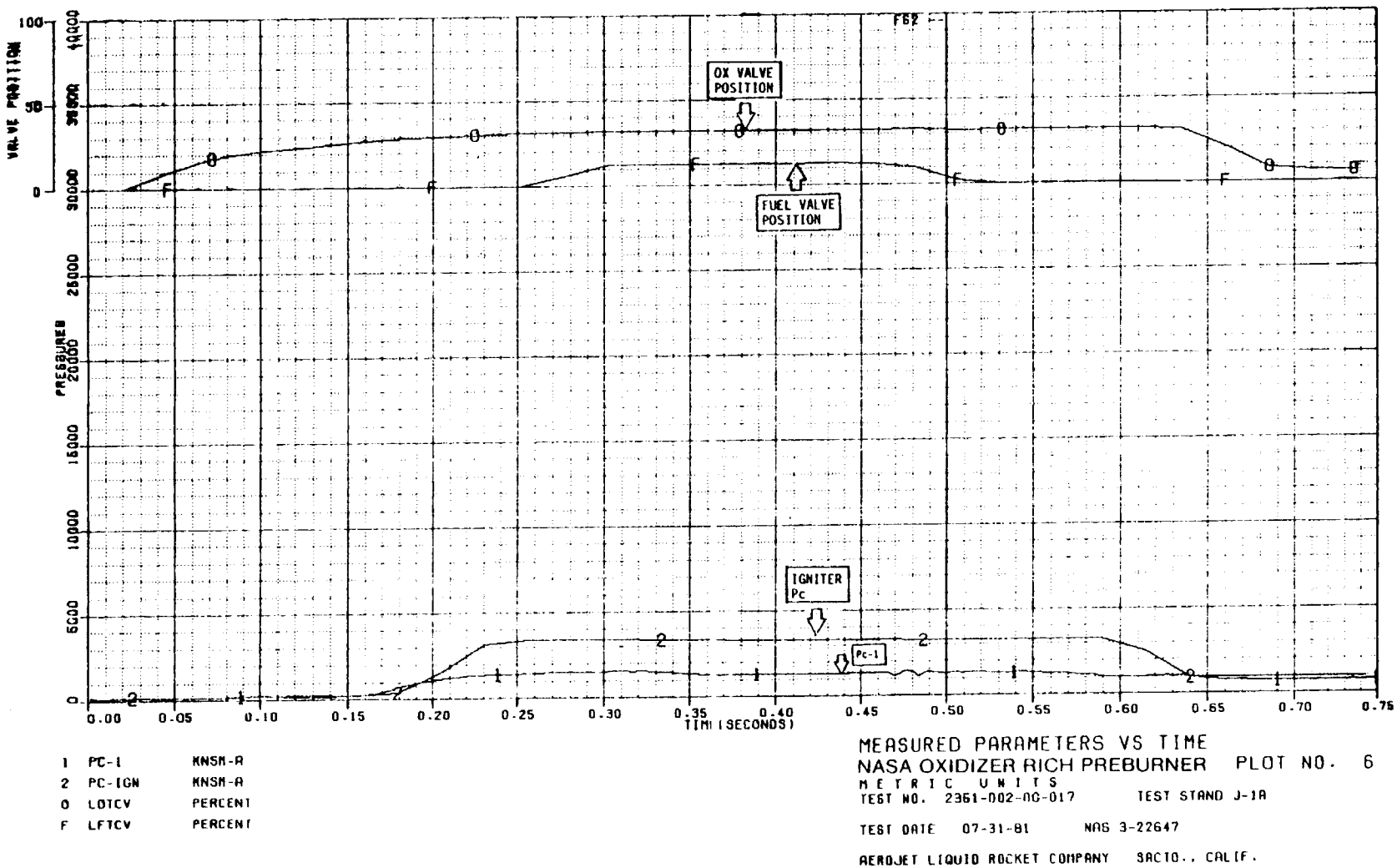

Figure 64. Oxidizer-Rich Preburner, Measured Parameters Versus Time, Test -017 (1 of 2)

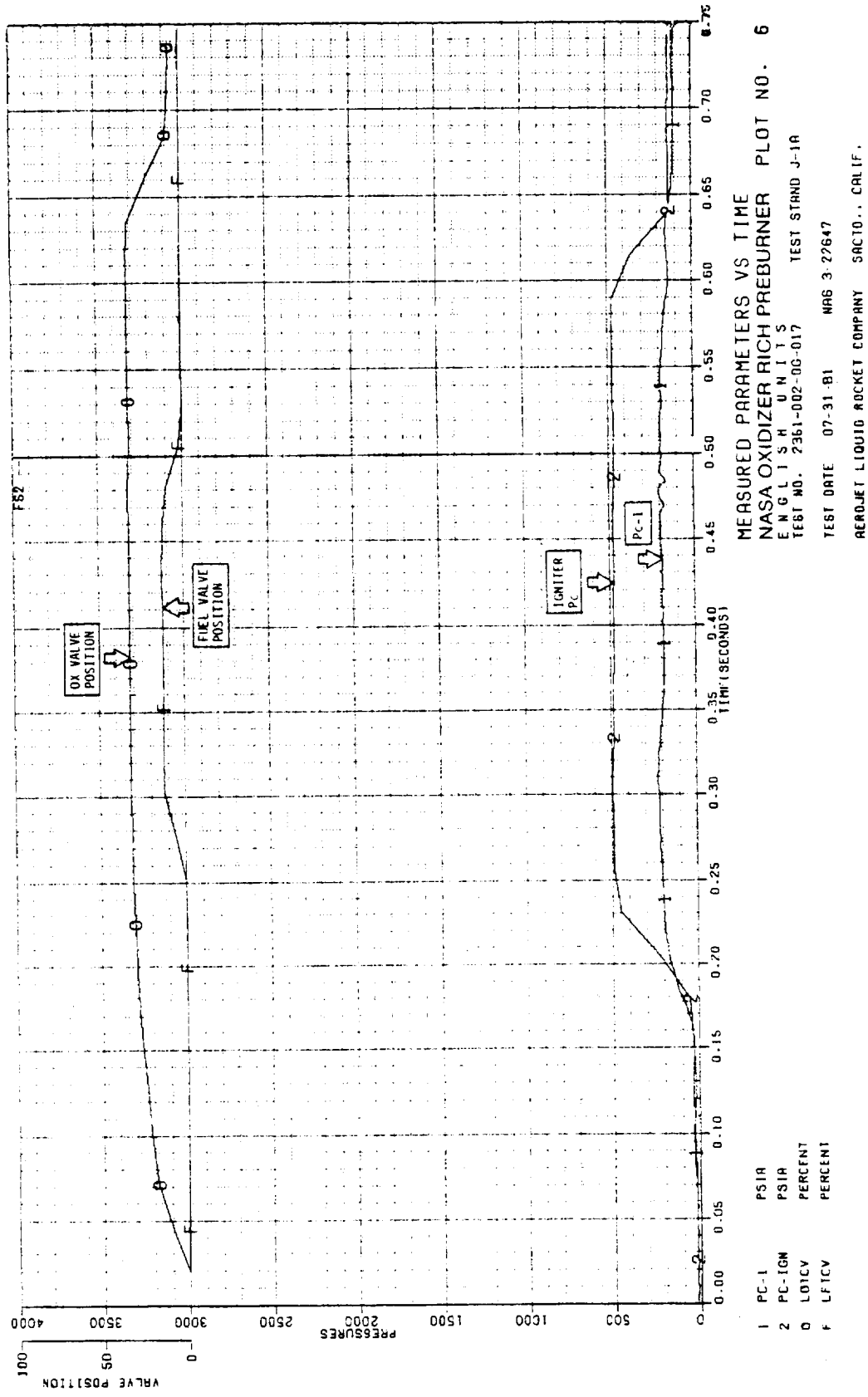

Figure 64. Oxidizer-Rich Preburner, Measured Parameters Versus Time, Test -017 (2 of 2)

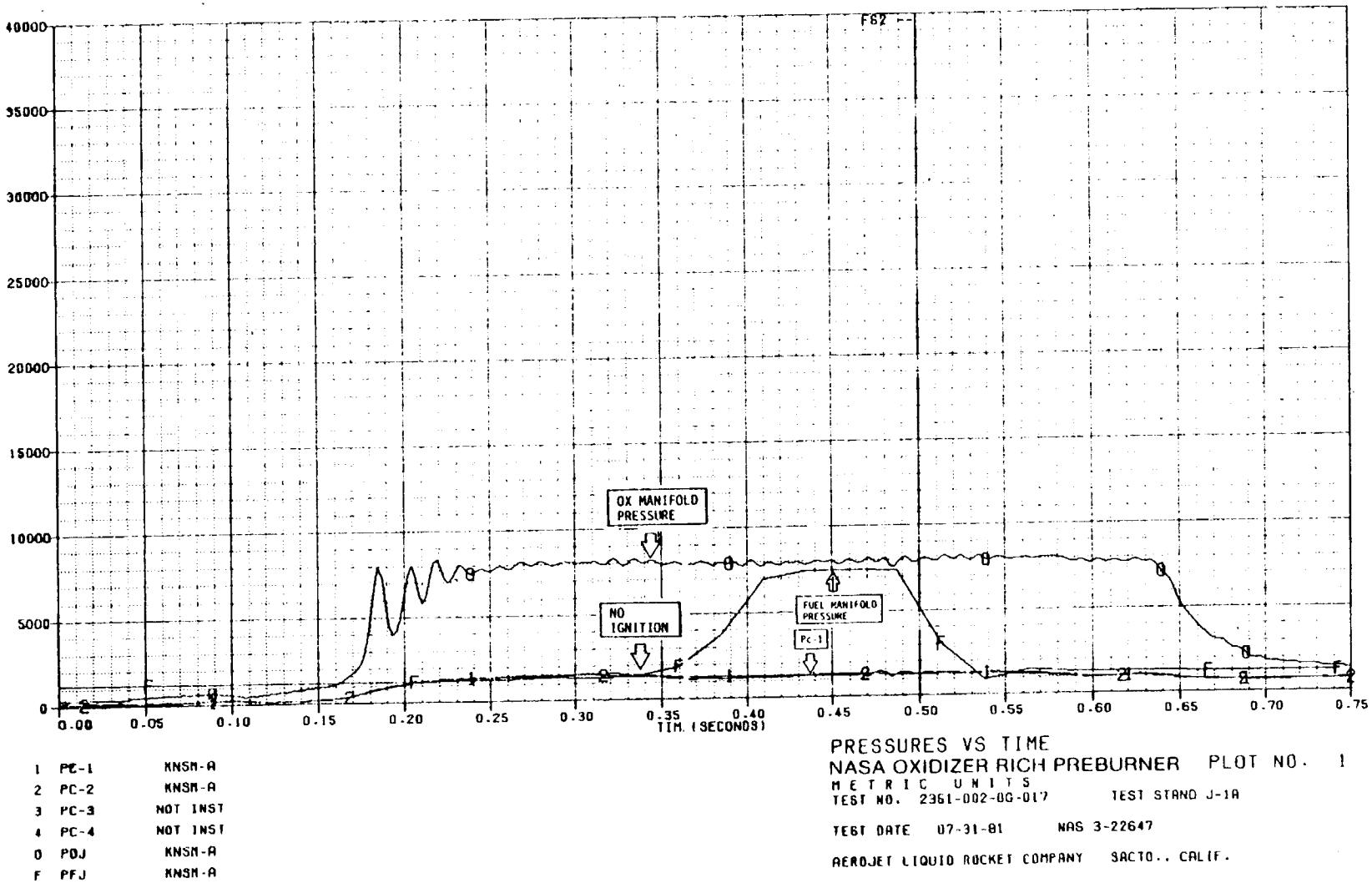

Figure 65. Oxidizer-Rich Preburner, Measured Parameters Versus Time, Test -017 (1 of 2)

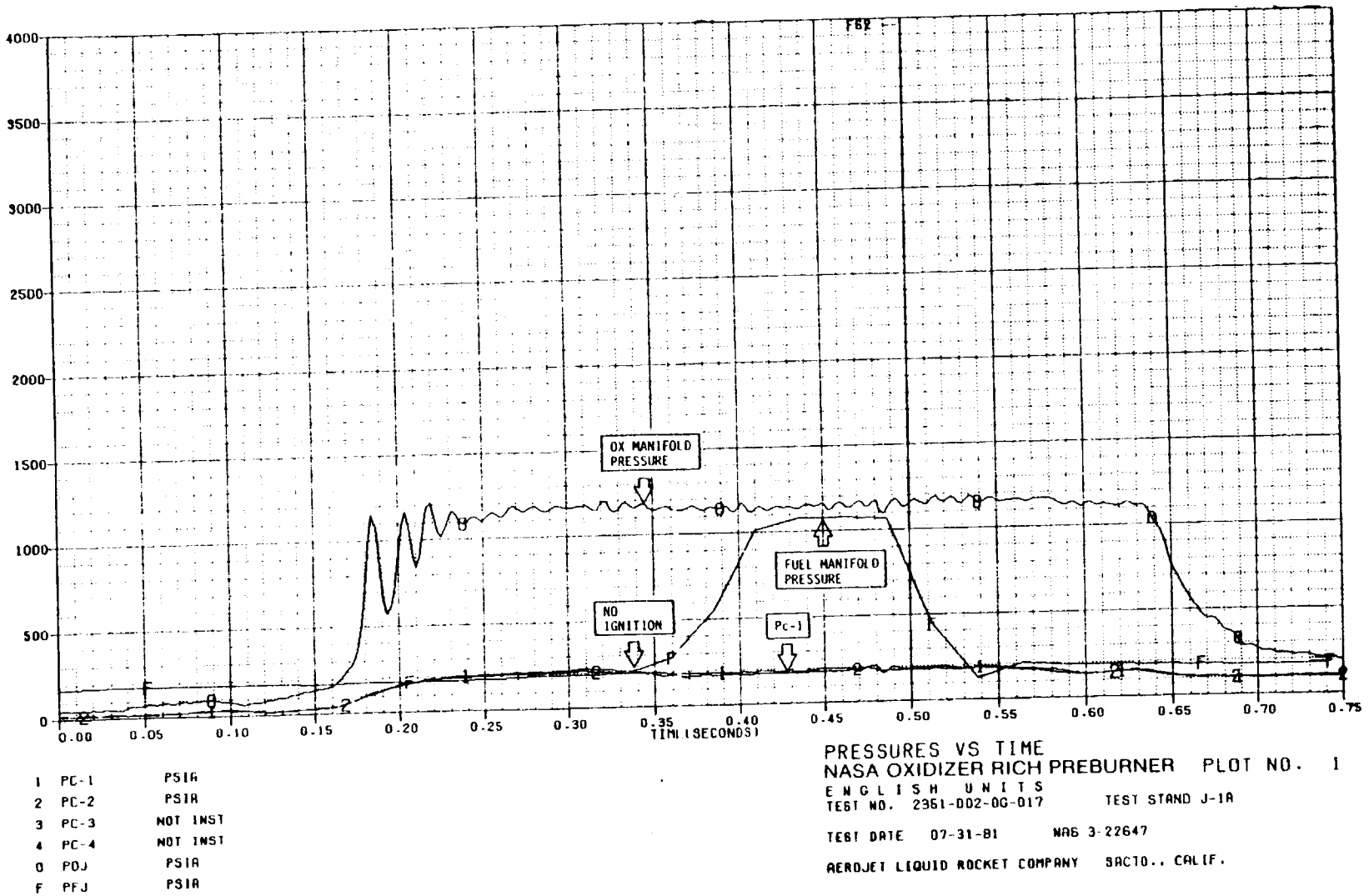

Figure 65. Oxidizer-Rich Preburner, Measured Parameters Versus Time, Test -017 (2 of 2)

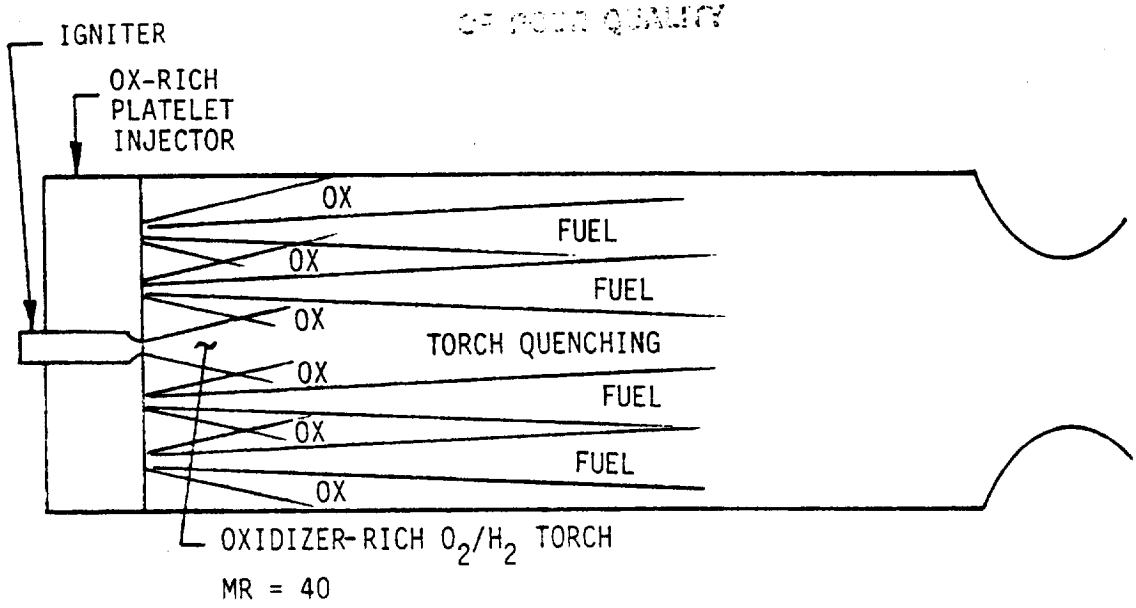

TEST -017

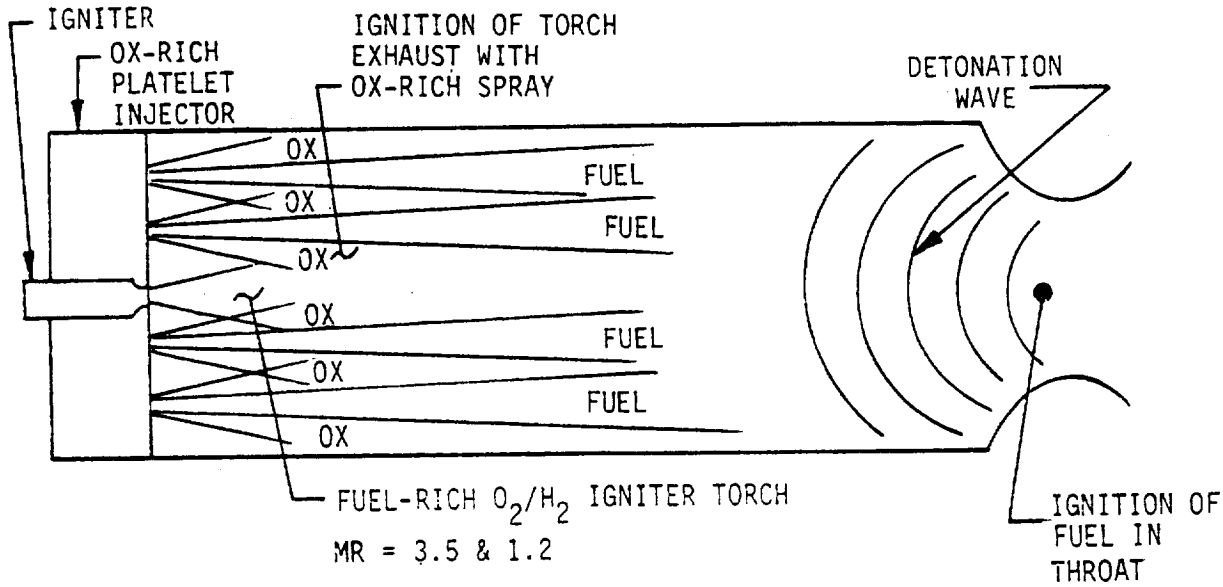

TESTS -018 & -019

Figure 66. Effect of Igniter Torch Mixture Ratio on Oxidizer-Rich Platelet Injector Ignition

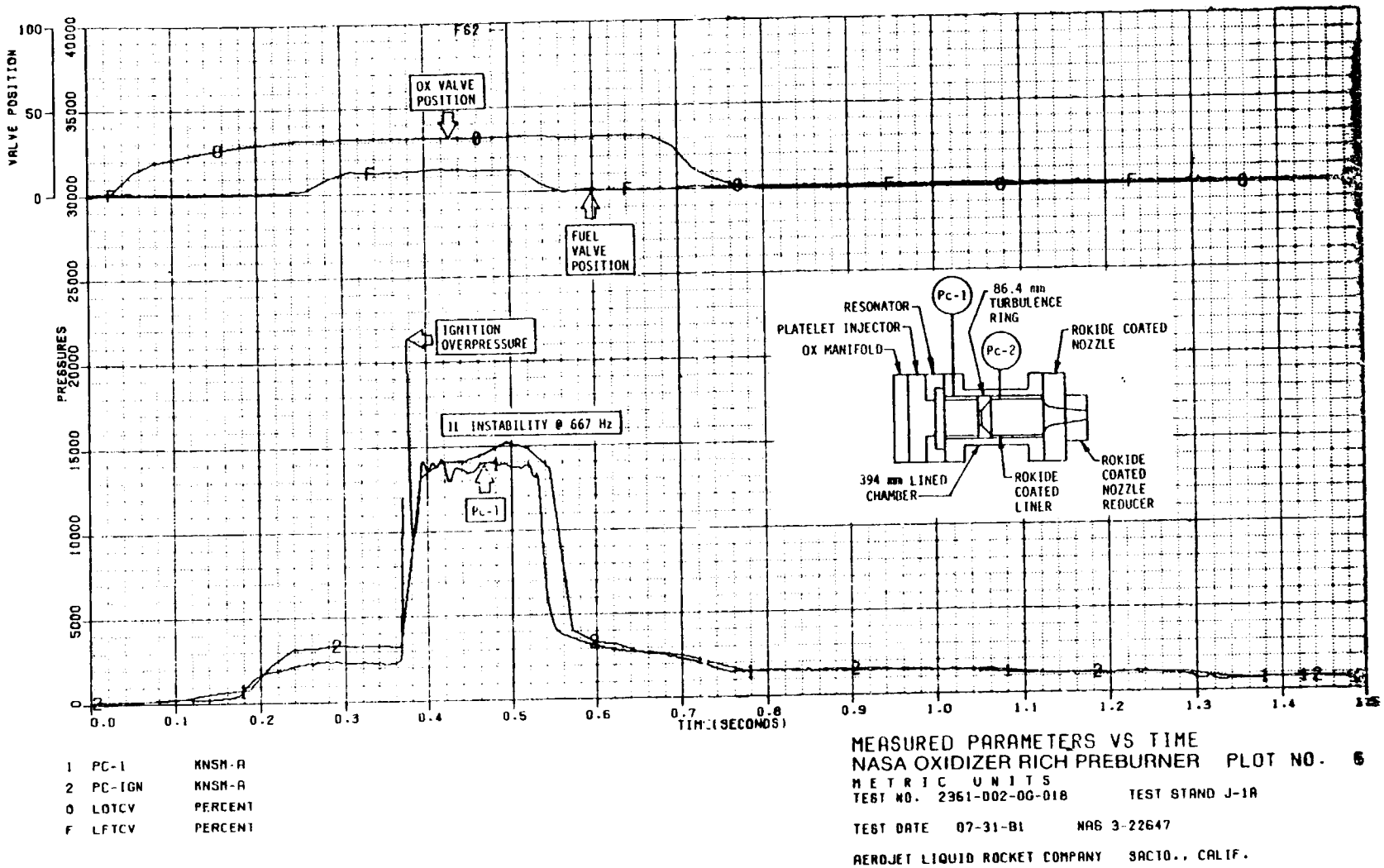

Figure 67. Oxidizer-Rich Preburner, Measured Parameters Versus Time, Test -018 (1 of 2)

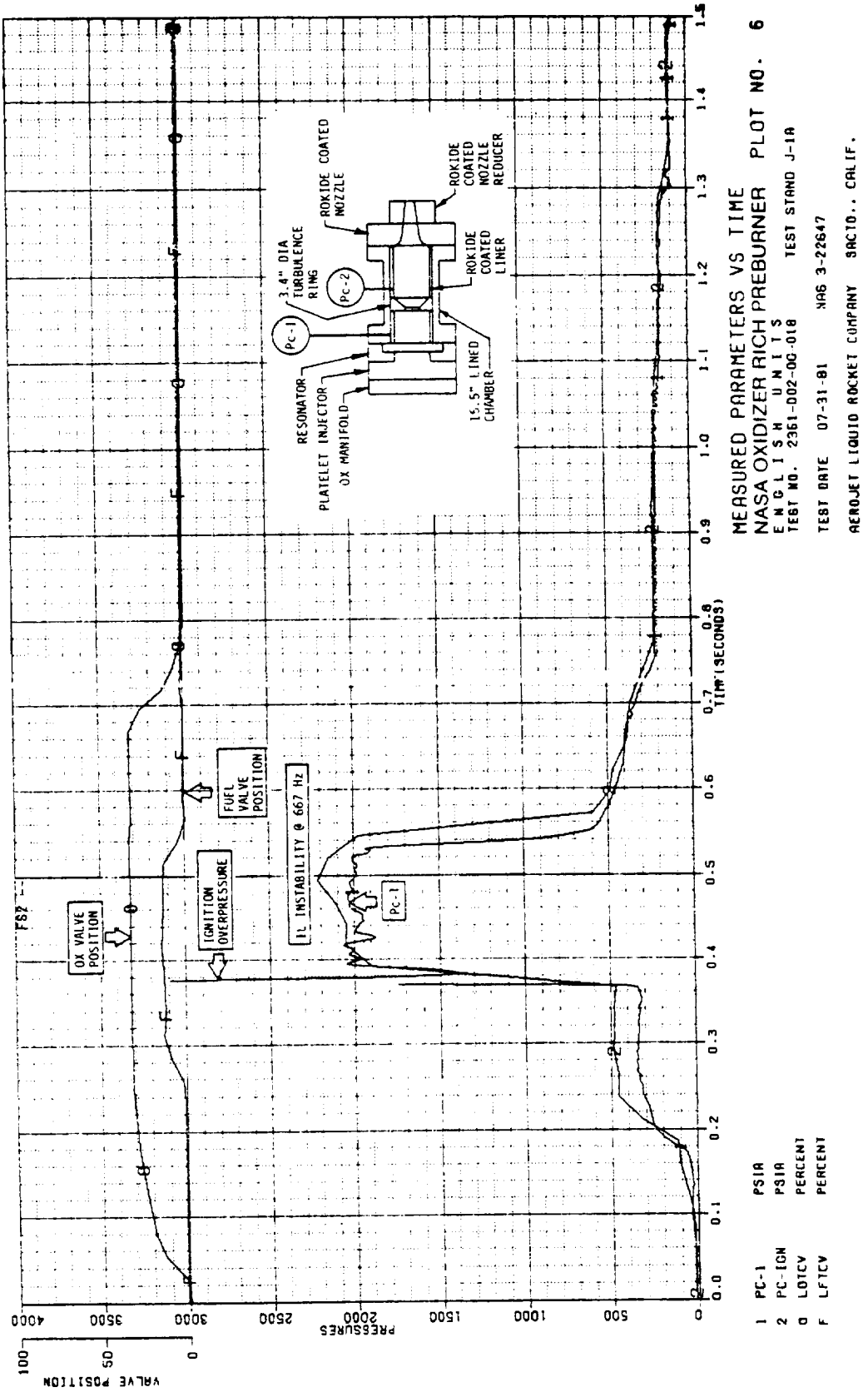

Figure 67. Oxidizer-Rich Preburner, Measured Parameters Versus Time, Test -018 (2 of 2)

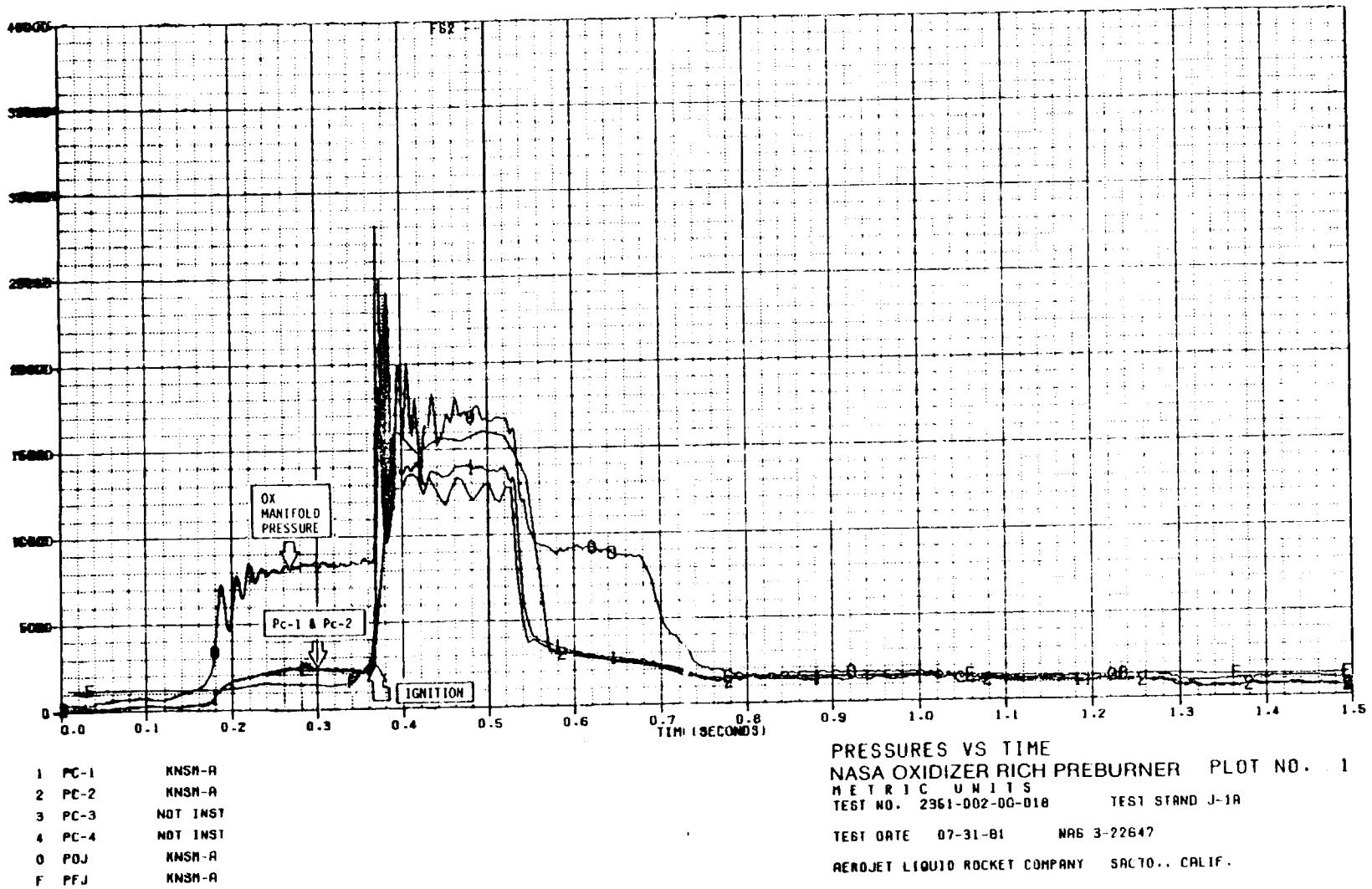

Figure 68. Oxidizer-Rich Preburner, Measured Parameters Versus Time, Test -018 (1 of 2)

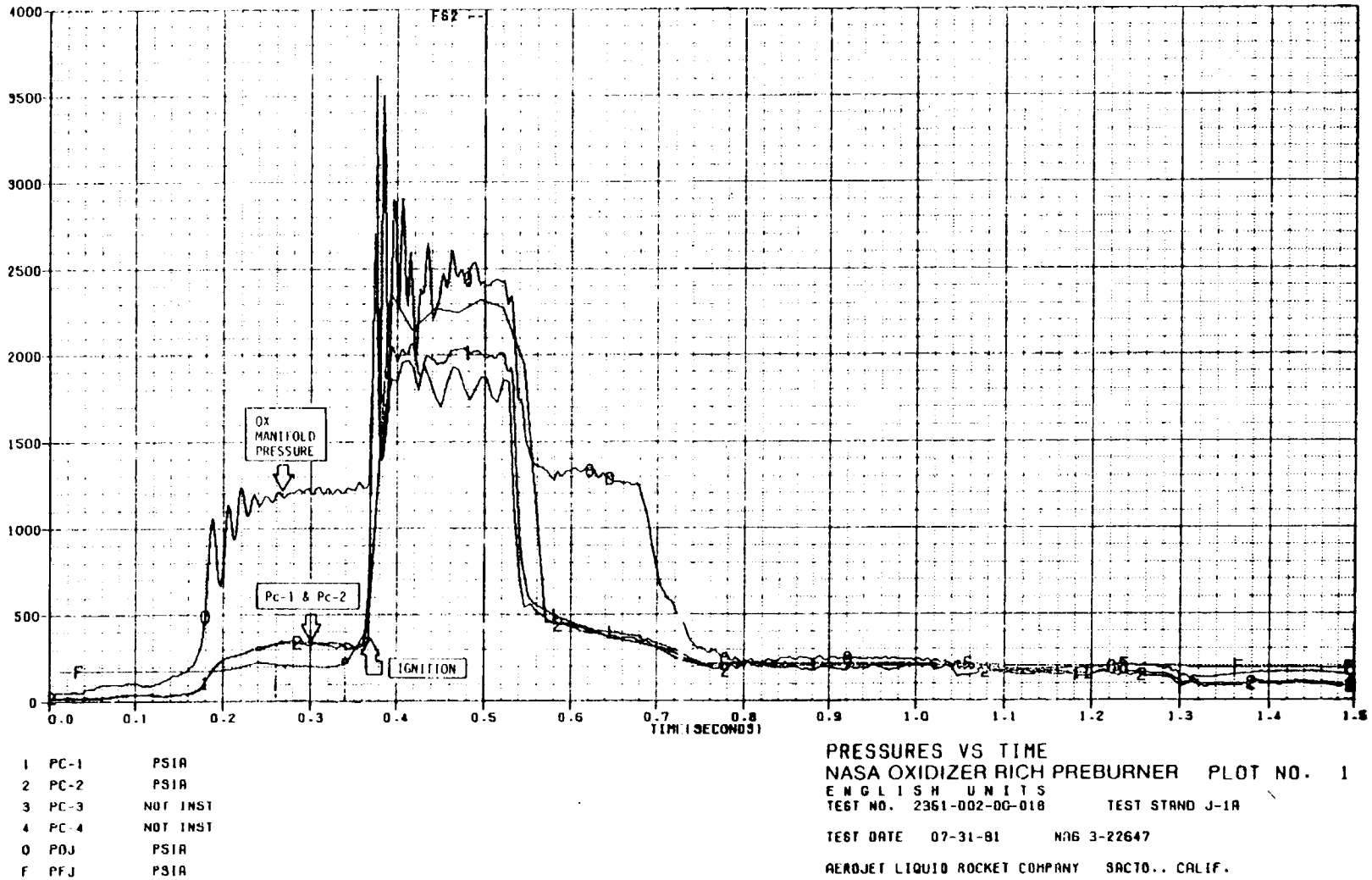

Figure 68. Oxidizer-Rich Preburner, Measured Parameters Versus Time, Test -018 (2 of 2)

was installed. The chamber liner had expanded into the outer housing and had to be forced out.

The turbulence ring, chamber liner, and nozzle were all clean, with no evidence of erosion resulting from the oxidizer-rich environment. The turbulence ring was replaced with a smaller-diameter 76-mm (3.0-in.) turbulence ring to increase the 1L damping for Test -019.

Test -019

In an attempt to improve the ignition characteristics, the igniter was reorificed to a mixture ratio of 1.2 to increase the amount of combustion between the torch and oxidizer-rich spray. The test parameters are plotted in Figures 69 and 70. Ignition of the fuel-rich torch occurred as planned. The pre-ignition Pc was about 2.8 MN/m^2 (400 psia), indicating higher torch energy, as desired. However, ignition was again delayed, resulting in a pressure spike in excess of 27.6 MN/m^2 (4000 psia). The combustion was smooth during the steady-state portion, with no evidence of 1L mode instability. This indicates that the smaller-diameter turbulence ring is an effective damper.

The shutdown was abnormal in that the chamber pressure remained high for about 150 msec following fuel valve closure. Post-test examination showed severe erosion of eight adjacent fuel orifices and minor erosion of several other orifices. The damage had the appearance of intermanifold leakage since the major damage was localized. It is not clear when the damage occurred, but it is reasonable to believe it occurred during the ignition overpressure. The internal damage precluded further firings with the platelet injector.

The Rokide-Z-coated chamber, turbulence ring, and nozzle were intact, showing no evidence of erosion. The resonator seal was damaged and significant leakage was evident.

Test -020

Test -020 was an oxidizer cold-flow and igniter checkout firing test with the repaired EDM injector. The valve sequence was identical to that used previously and is shown in Figure 58. Initially, the igniter was to have been orificed to provide an oxidizer-rich mixture ratio of 40:1. However, post- test examination showed that the igniter fuel orifice had been left out of the line, causing the igniter to run fuel-rich and at a higher chamber pressure than anticipated. The igniter lit and functioned without incurring damage. The igniter was orificed to the proper MR prior to Test -021. The oxidizer cold-flow pressures and manifold fill times were as anticipated.

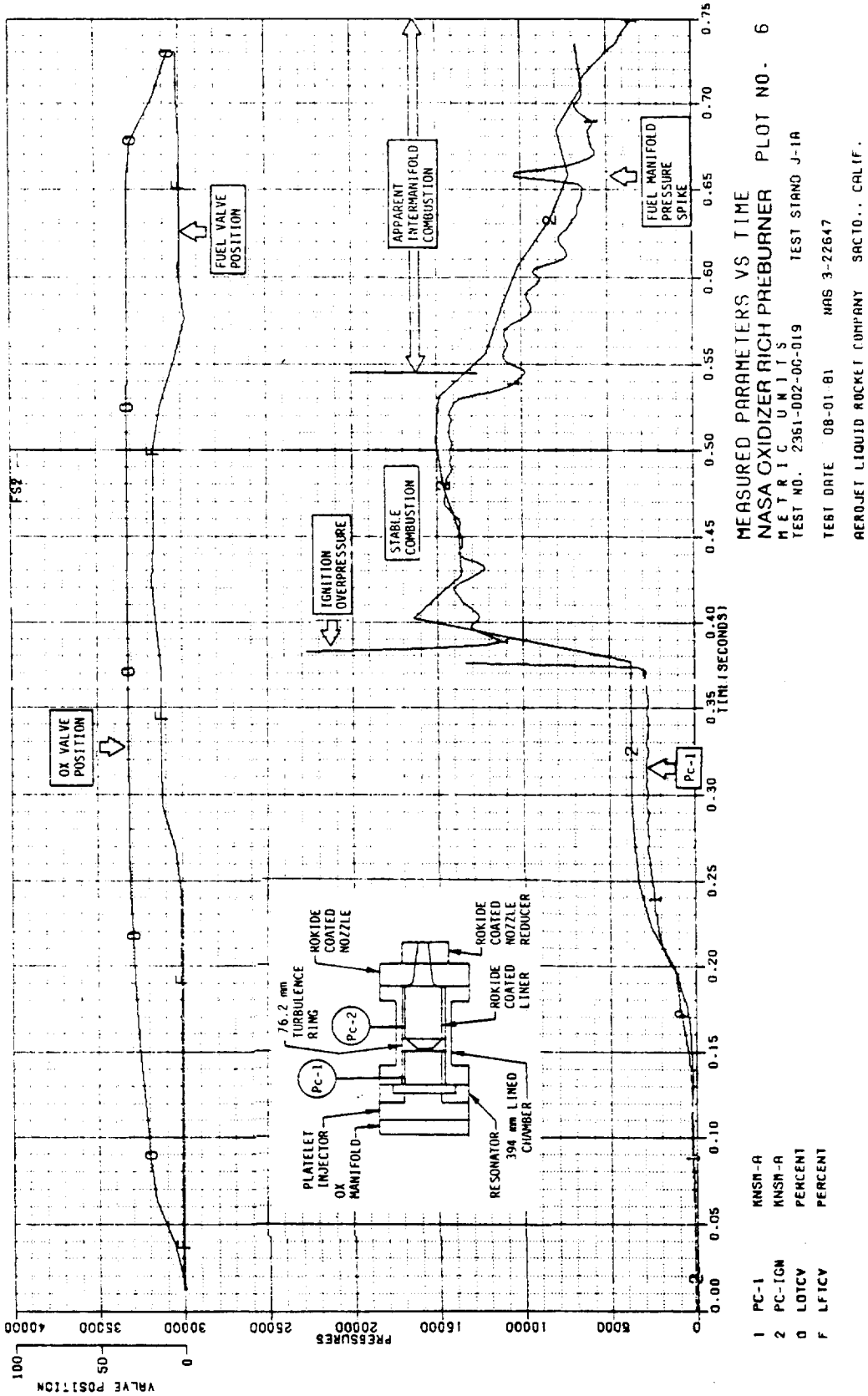

Figure 69. Oxidizer-Rich Preburner, Measured Parameters Versus Time, Test -019 (1 of 2)

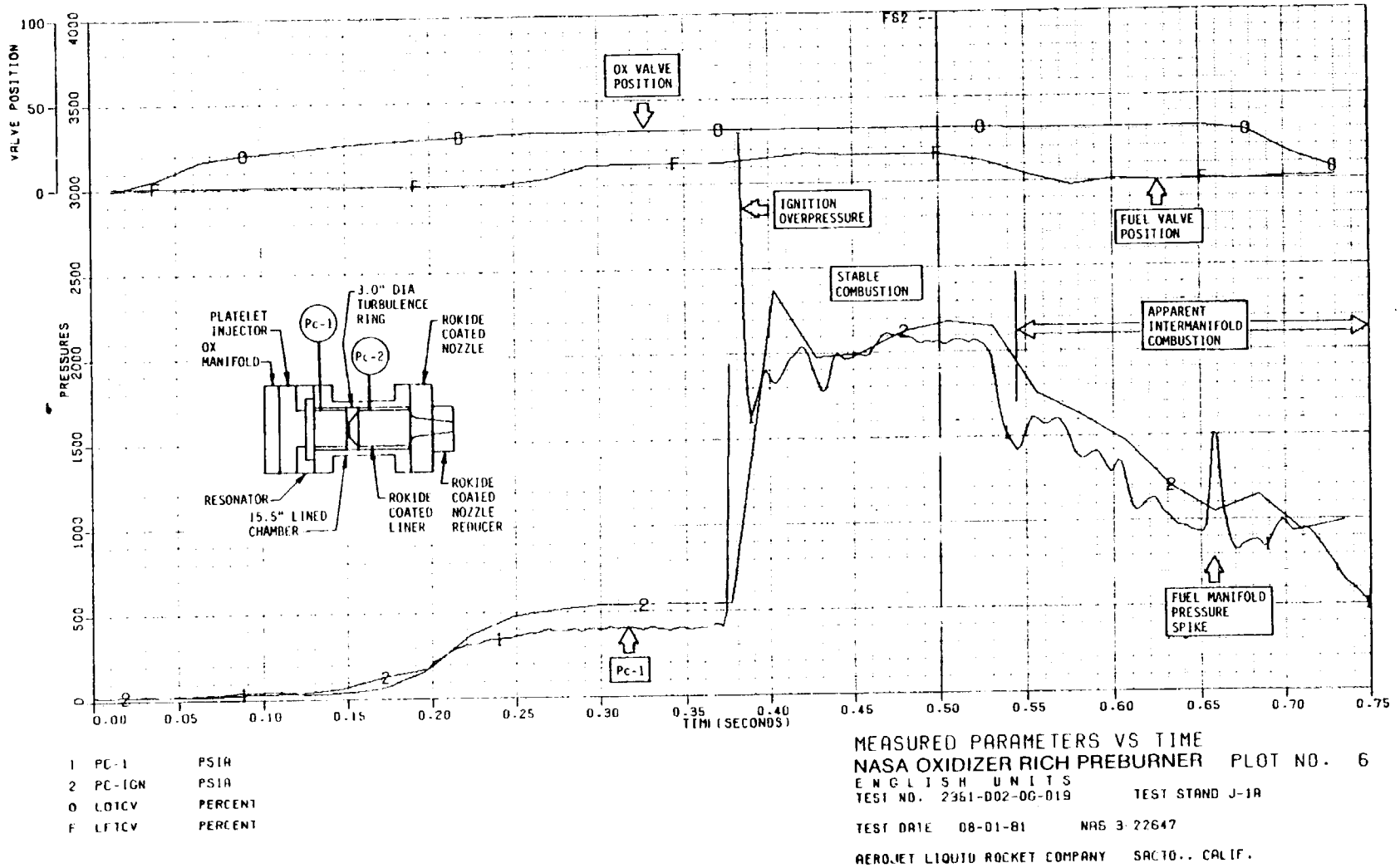

Figure 69. Oxidizer-Rich Preburner, Measured Parameters Versus Time, Test -019 (2 of 2)

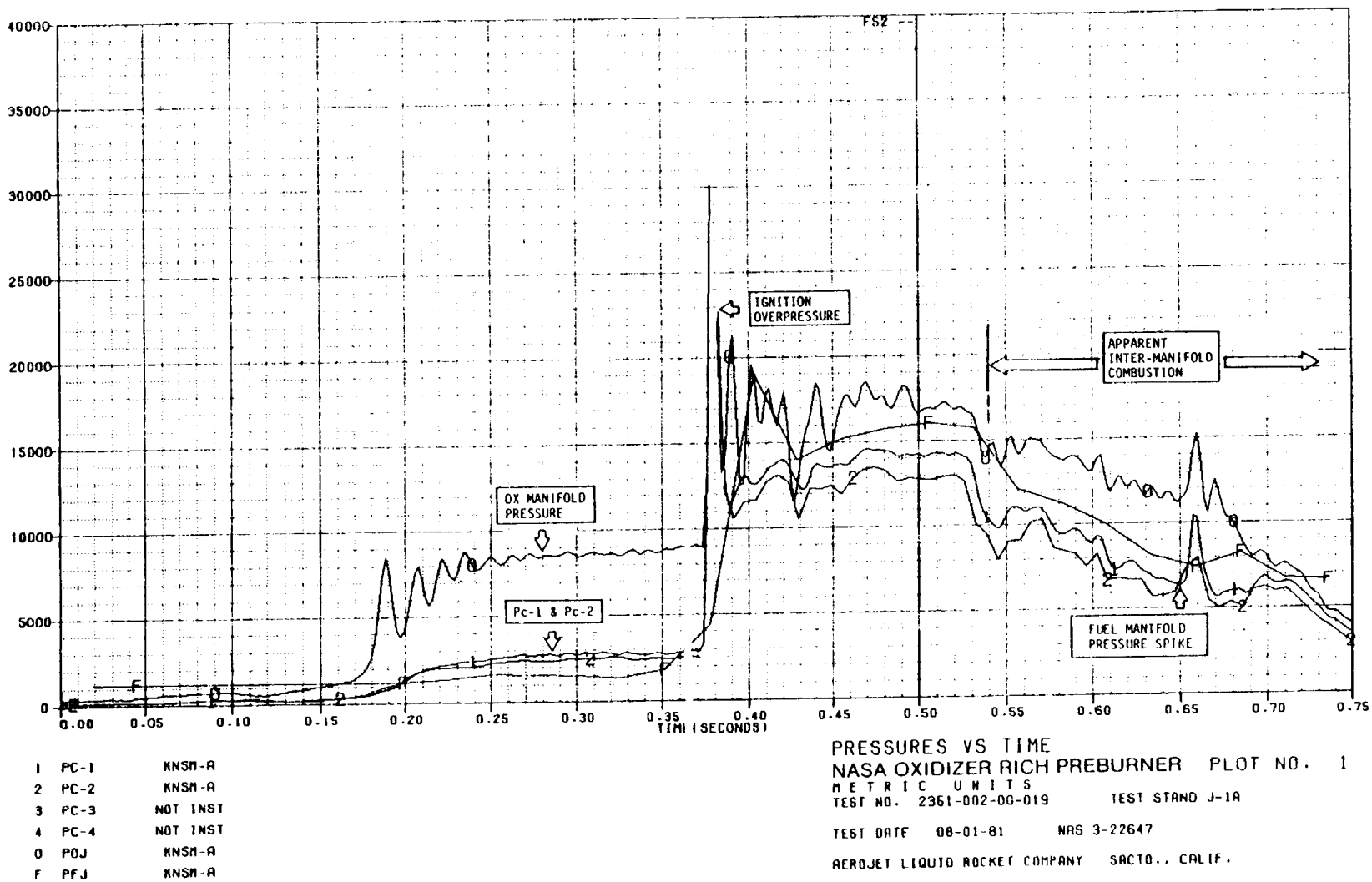

Figure 70. Oxidizer-Rich Preburner, Measured Parameters Versus Time, Test -019 (1 of 2)

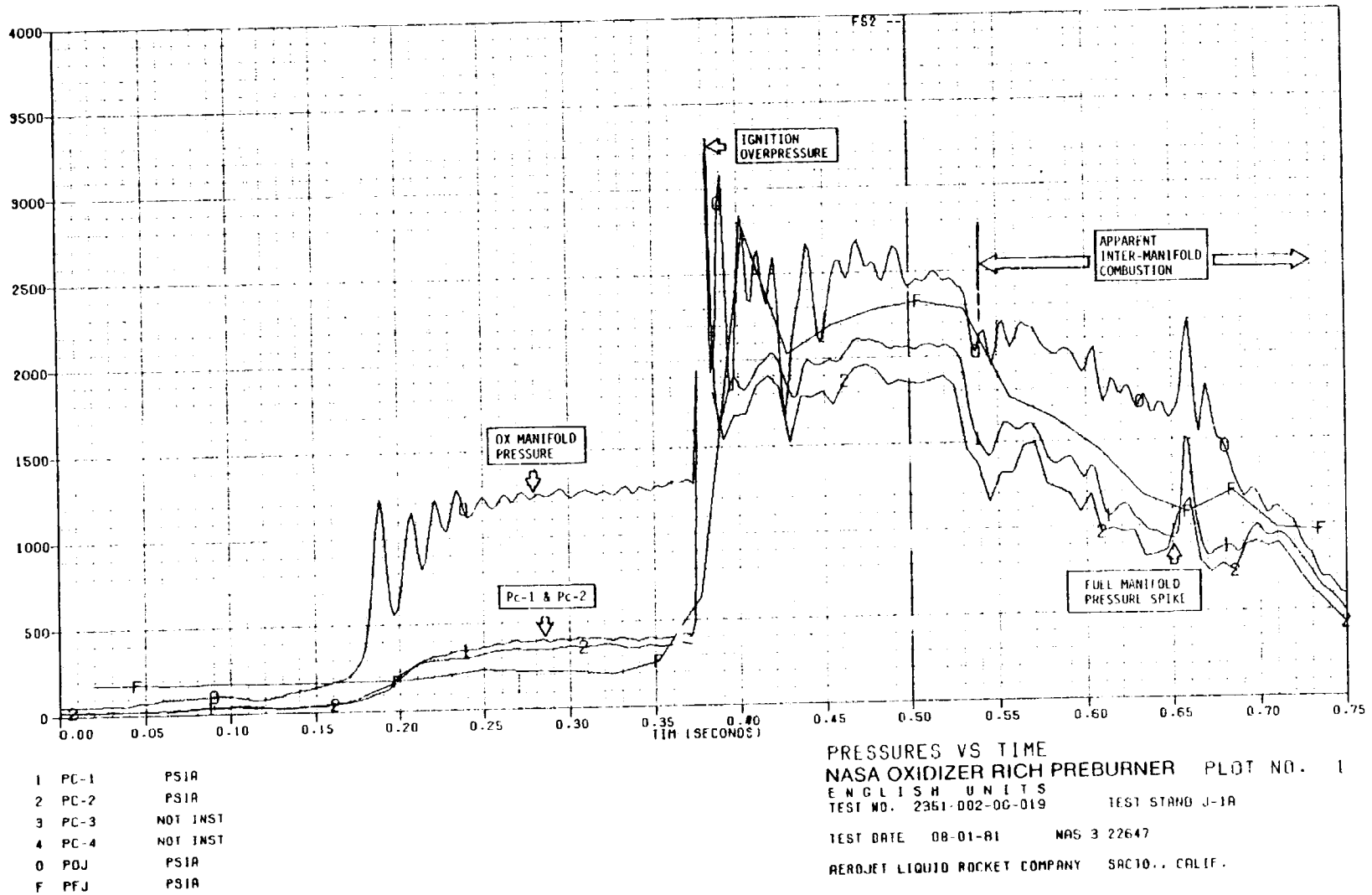

Figure 70. Oxidizer-Rich Preburner, Measured Parameters Versus Time, Test -019 (2 of 2)

Test -021

The objective of this test was to check out the performance and stability of the repaired EDM injector. The injector and chamber were set up as shown in the schematic of Figure 71. The 394-mm (15.5-in.) length chamber was used with the Rokide-Z-coated liner. The effective chamber length is 447 mm (17.6 in.). The 76-mm (3.0-in.) diameter Rokide-Z-coated turbulence ring was installed to provide acoustic damping since the first EDM injector test (Test -014) had experienced 1L instability.

The ignition and shutdown were smooth, as shown in Figure 71. However, post-test examination showed some damage to the injector face and resonator ring due to a 600 Hz 1L mode instability. The amplitude as measured in the resonator cavity was 565 kN/m^2 (82 psia) PK-PK. The major damage occurred in the center area of the injector around the igniter port, as shown in Figure 72. It is theorized that the longitudinal instability caused near-stoichiometric burning to occur on the injector face, resulting in face metal ignition and burning. The area around the igniter port is lower in MR than the overall MR due to the 10 small fuel holes surrounding the igniter port that are used to augment ignition. The result is a hotter MR and hence greater damage in this area.

Examination of the Rokide-Z-coated chamber liner, turbulence ring, and nozzle showed no damage, except for minor erosion of the liner leading edge adjacent to the resonator ring (Figure 73). Erosion of the resonator ring is apparently caused by fuel being driven back into the cavities by the longitudinal pressure waves.

The EDM injector face was repaired on the test stand by heliarc welding prior to Test -022. The orifices surrounding the igniter port were welded shut to avoid the locally hotter MR condition.

Test -022

This was the first test following the EDM injector face repair. The chamber length was reduced from 394 to 292 mm (15.5 to 11.5 in.). The instrumentation rake was installed as shown in Figure 74 to measure gas temperature uniformity. The effective chamber length was 389 mm (15.3 in.).

Analysis of the longitudinal instability showed that greater stability could be achieved by going to a shorter chamber length and changing the operating point from low Pc/high MR to high Pc/low MR. Based on this analysis, the chamber was shortened from 394 to 292 mm (15.5 to 11.5 in.) and an operating point of Pc = 17.2 MN/m^2 (2500 psia), MR = 35 was selected.

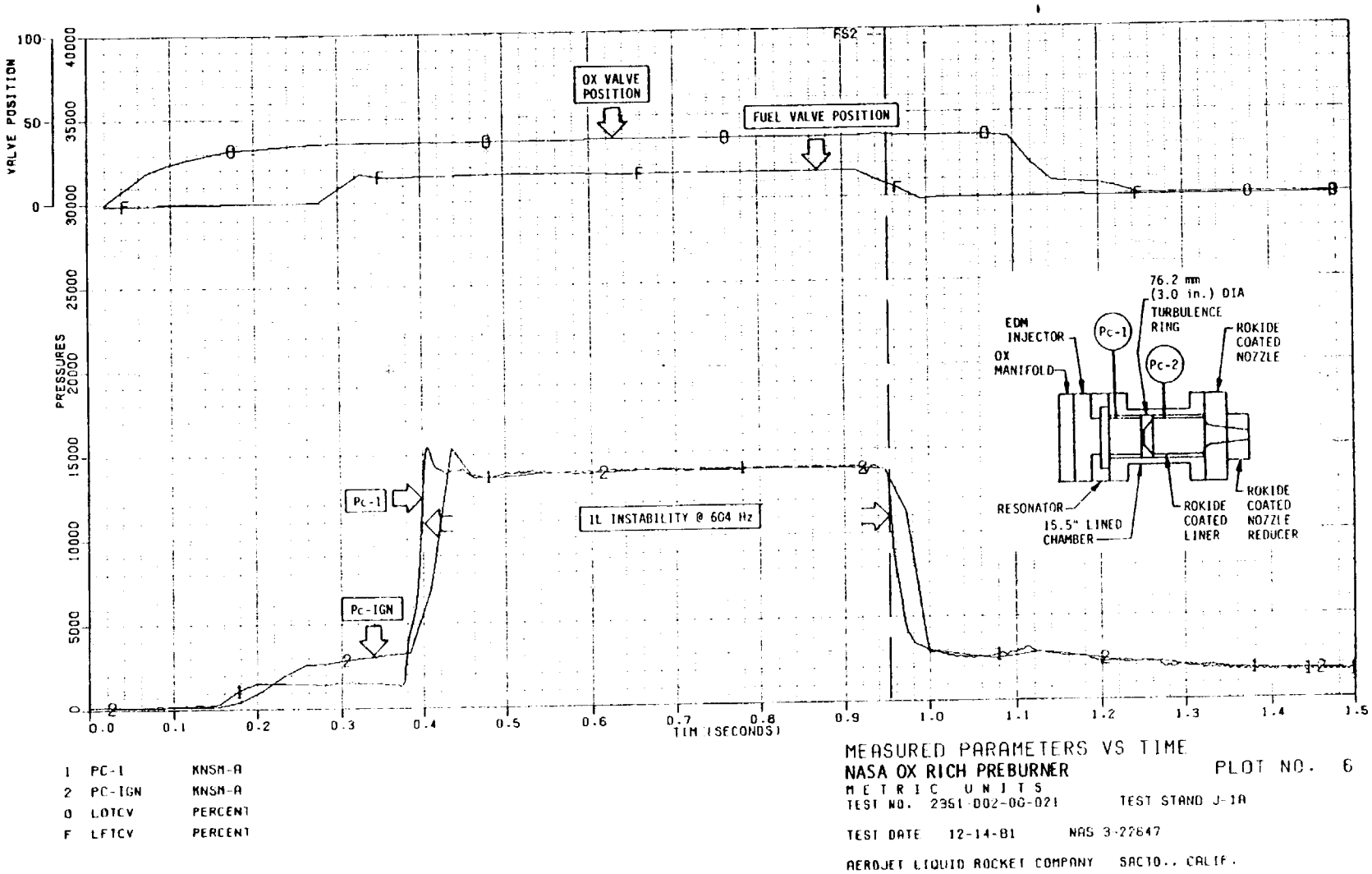

Figure 71. Oxidizer-Rich Preburner, Measured Parameters Versus Time, Test -021 (1 of 2)

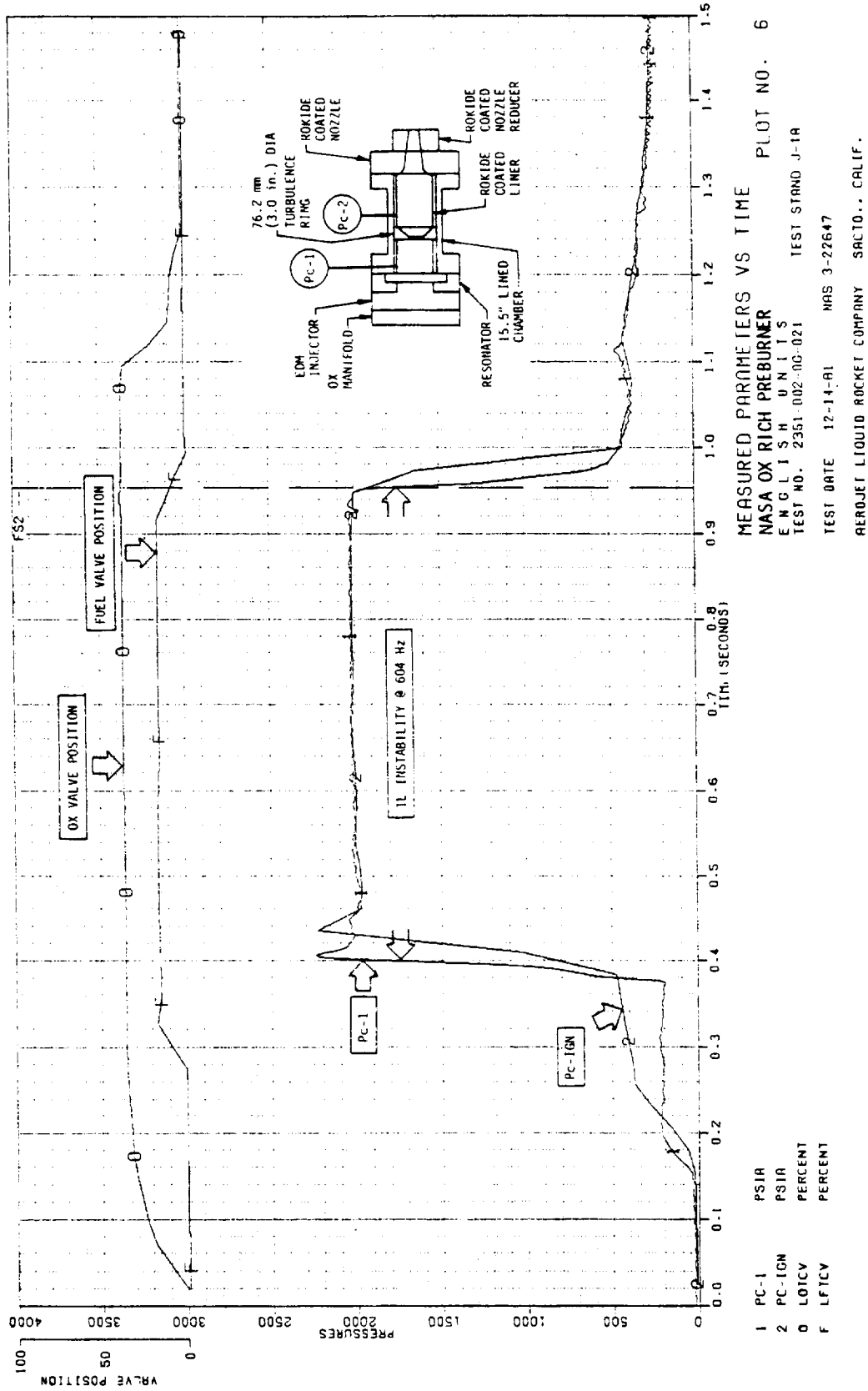

Figure 71. Oxidizer-Rich Preburner, Measured Parameters Versus Time, STest -021 (2 of 2)

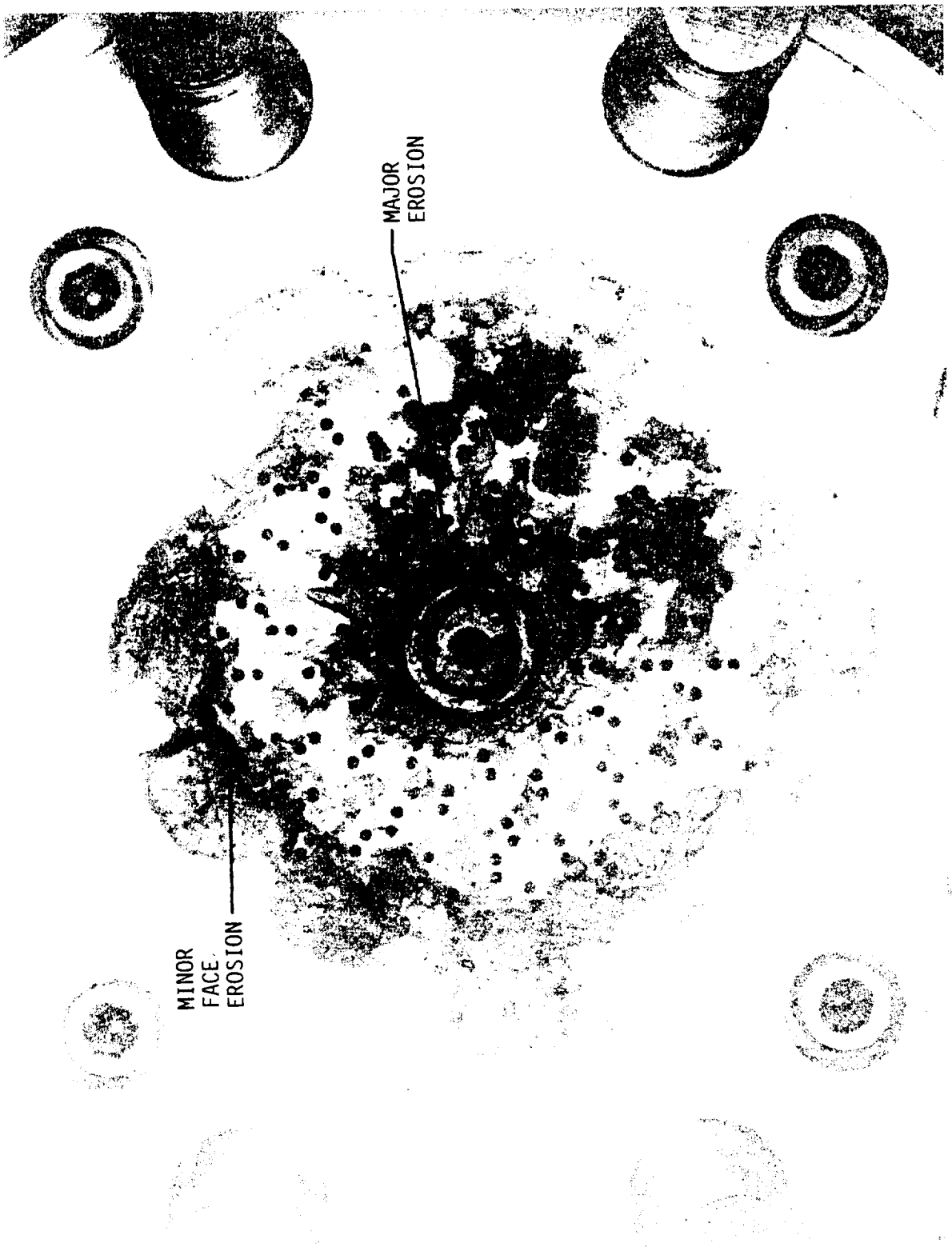

Figure 72. Injector Face Erosion, Post Test -021

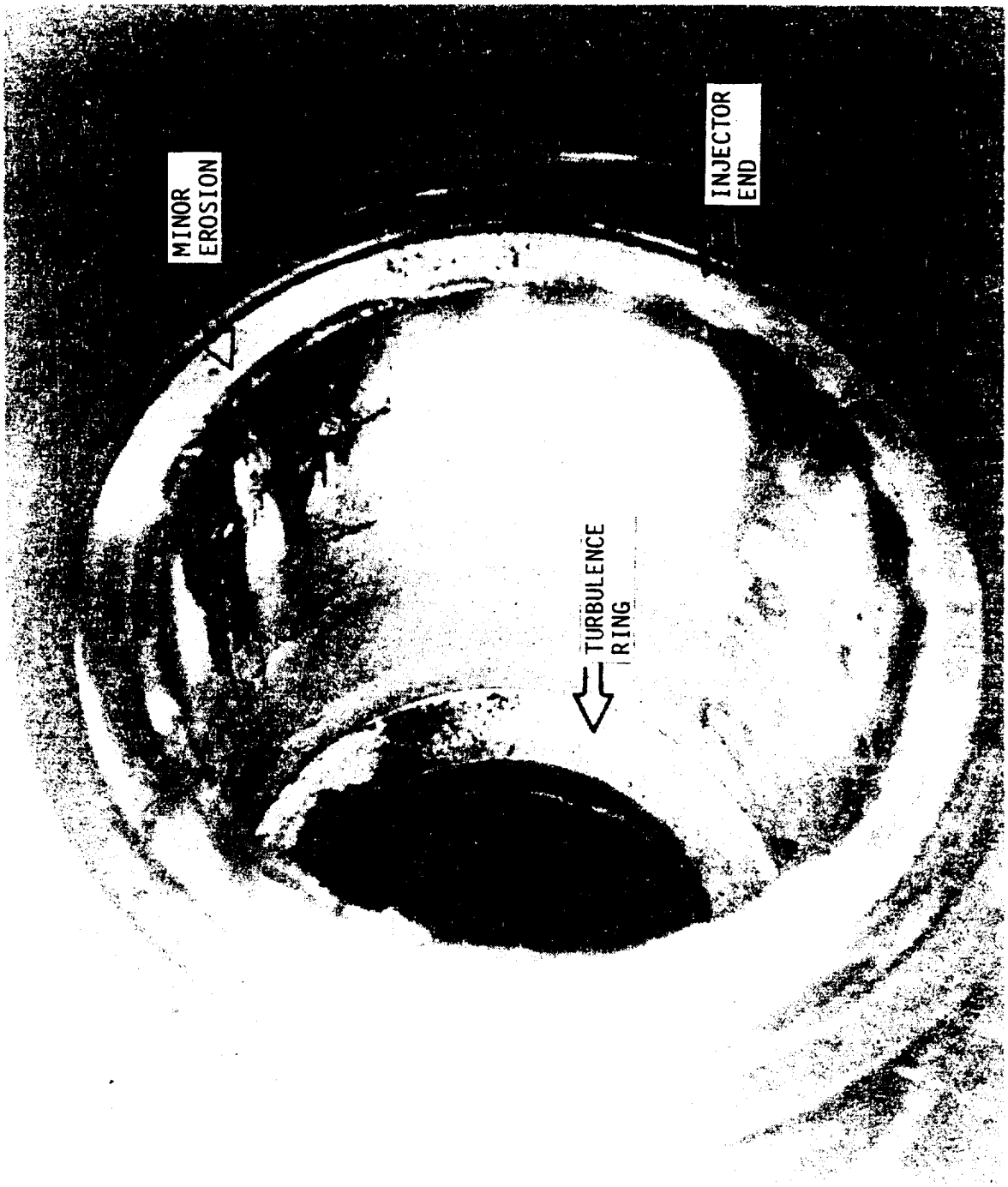

Figure 73. Minor Liner Erosion, Post Test -021

Both shortening the chamber and increasing chamber pressure (i.e., flowrate) are stabilizing factors. Shortening the chamber detunes the chamber acoustics from the combustion response by going to a higher resonant frequency. Increasing the flowrate increases the injector resistance. The shift in MR from 45 to 35 also shifts the chamber tune to a higher frequency through an increase in sound speed.

As shown in Figure 74, preburner ignition failed to occur until after the fuel valve was closed. The delayed ignition caused an overpressure which damaged the instrumentation rake assemblies and the nozzle flange sealing surface. The delayed ignition is attributed to the small fuel orifices around the igniter post being welded shut. The local mixture surrounding the torch does not contain sufficient fuel for reliable oxidizer-rich torch ignition, as was the case before the fuel holes were welded shut.

The igniter was reorificed to provide a fuel-rich torch at a mixture ratio of 1.2. The fuel-rich torch provided smooth reliable ignition on subsequent Test -023 and Test -024.

Test -023

Test -023 was a repeat of the Test -022 operating conditions. The damaged instrumentation rake and Rokide-Z-coated nozzle flange were removed for repair. The uncoated fuel-rich nozzle flange was machined open to 63.5 mm (2.5 in.) and used in place of the damaged coated flange. The hardware assembly is shown schematically in Figure 75.

As seen in Figure 75, ignition was smooth, with some overshoot in Pc with the fuel-rich torch. Combustion was stable, as anticipated. Nozzle erosion began at about 0.8 second after FS-1, as can be seen in Figure 75. Severe damage was incurred by the nozzle flange and nozzle throat reducer, as shown in Figure 76. It occurred as a result of the uncoated nozzle wall reacting with the high-velocity oxygen at the inlet to the throat. A study of the reactivity of uncoated metals with flowing oxygen needs to be made.

No damage was sustained by the injector, resonator, turbulence ring, or liner.

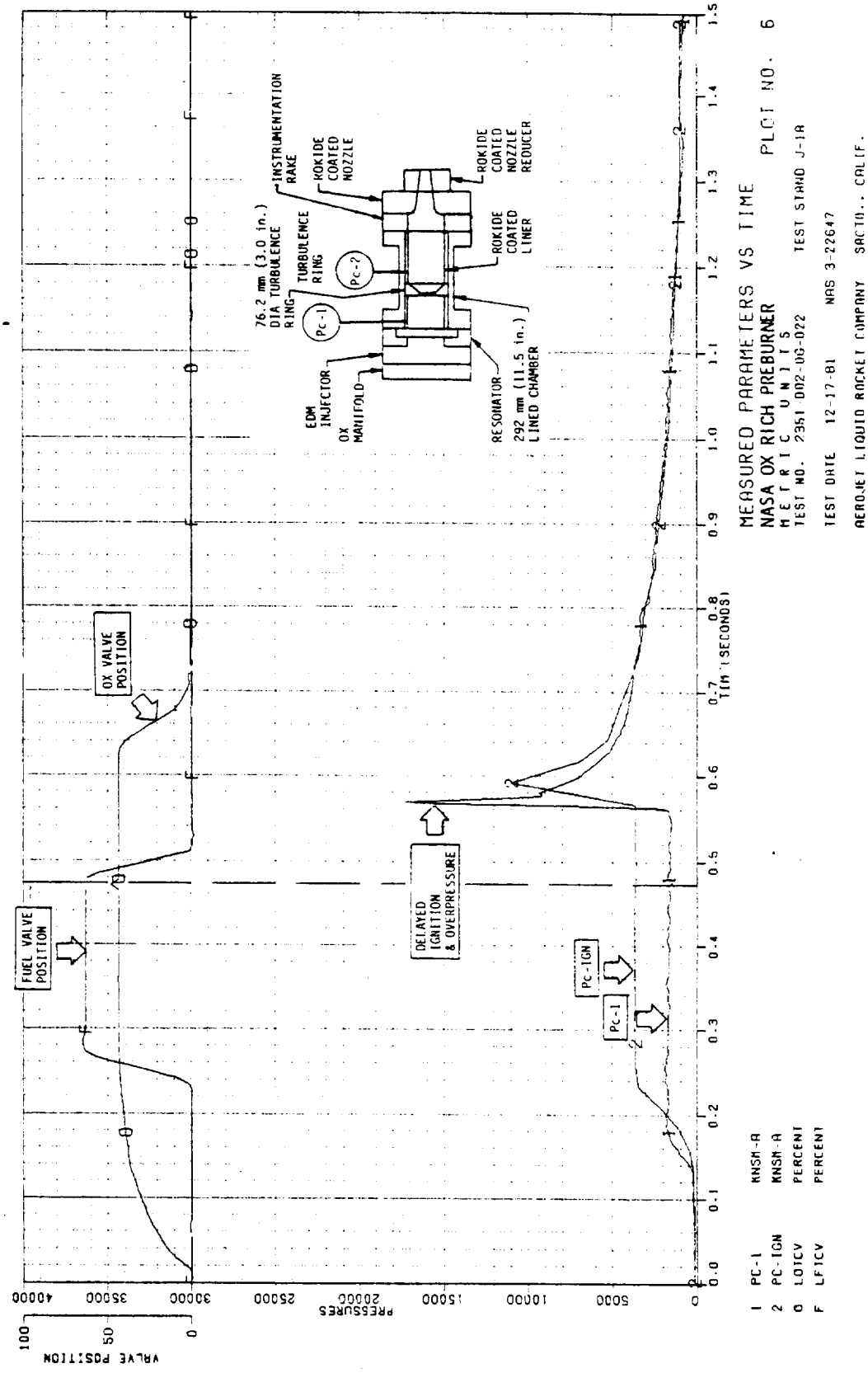

Figure 74. Oxidizer-Rich Preburner, Measured Parameters Versus Time, Test -022 (1 of 2)

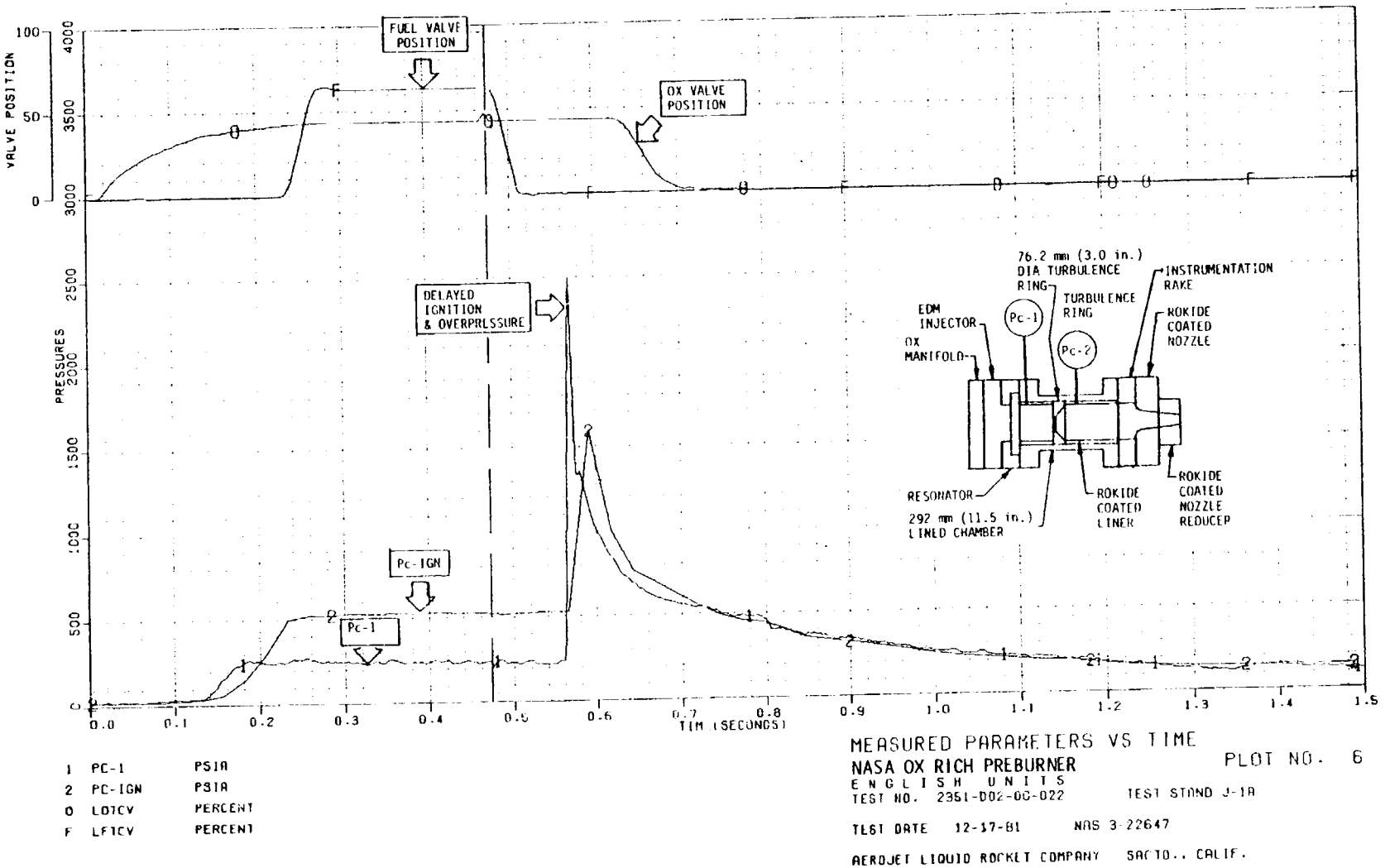

Figure 74. Oxidizer-Rich Preburner, Measured Parameters Versus Time, Test -022 (2 of 2)

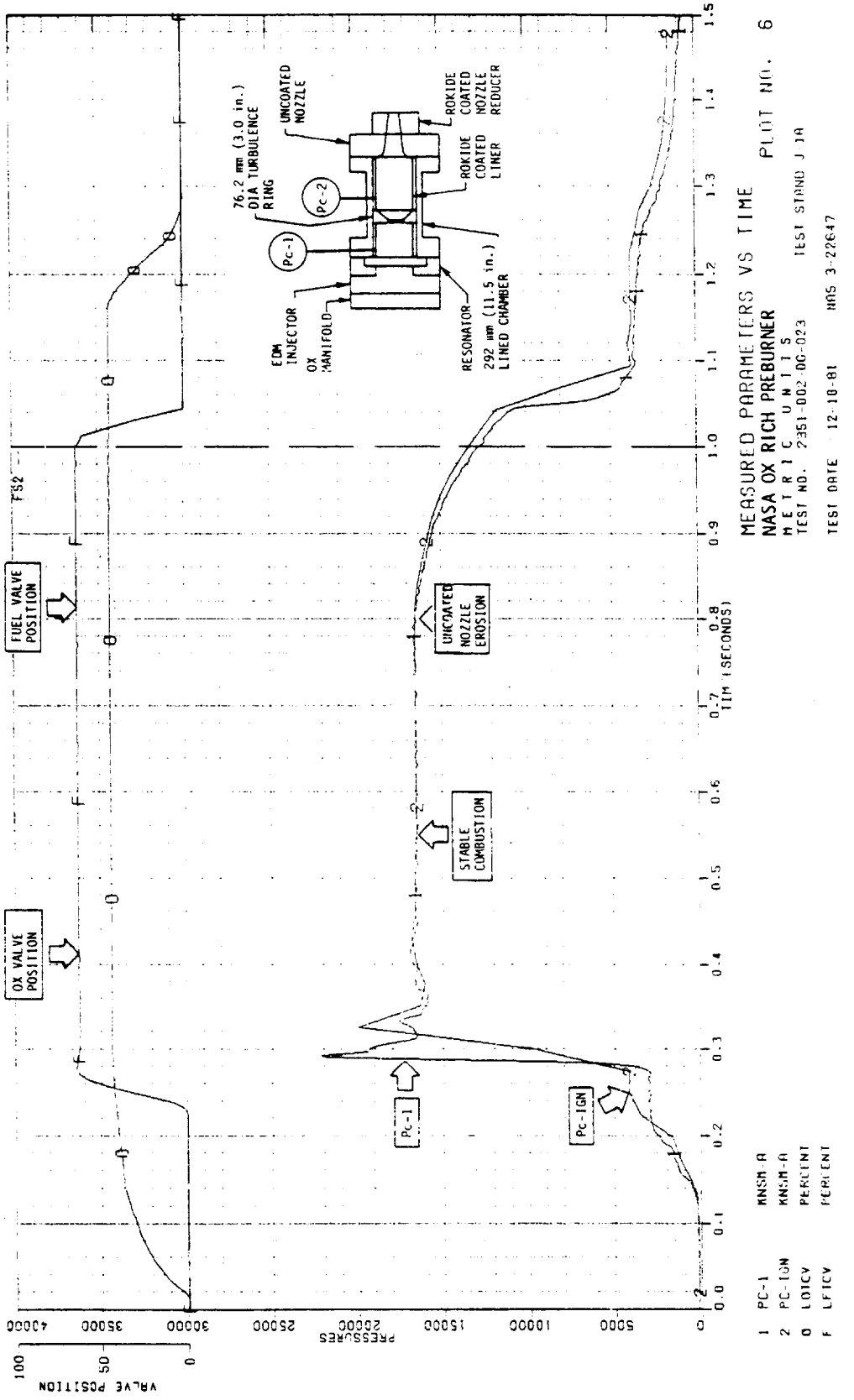

Figure 75. Oxidizer-Rich Preburner, Measured Parameters Versus Time, Test -023 (1 of 2)

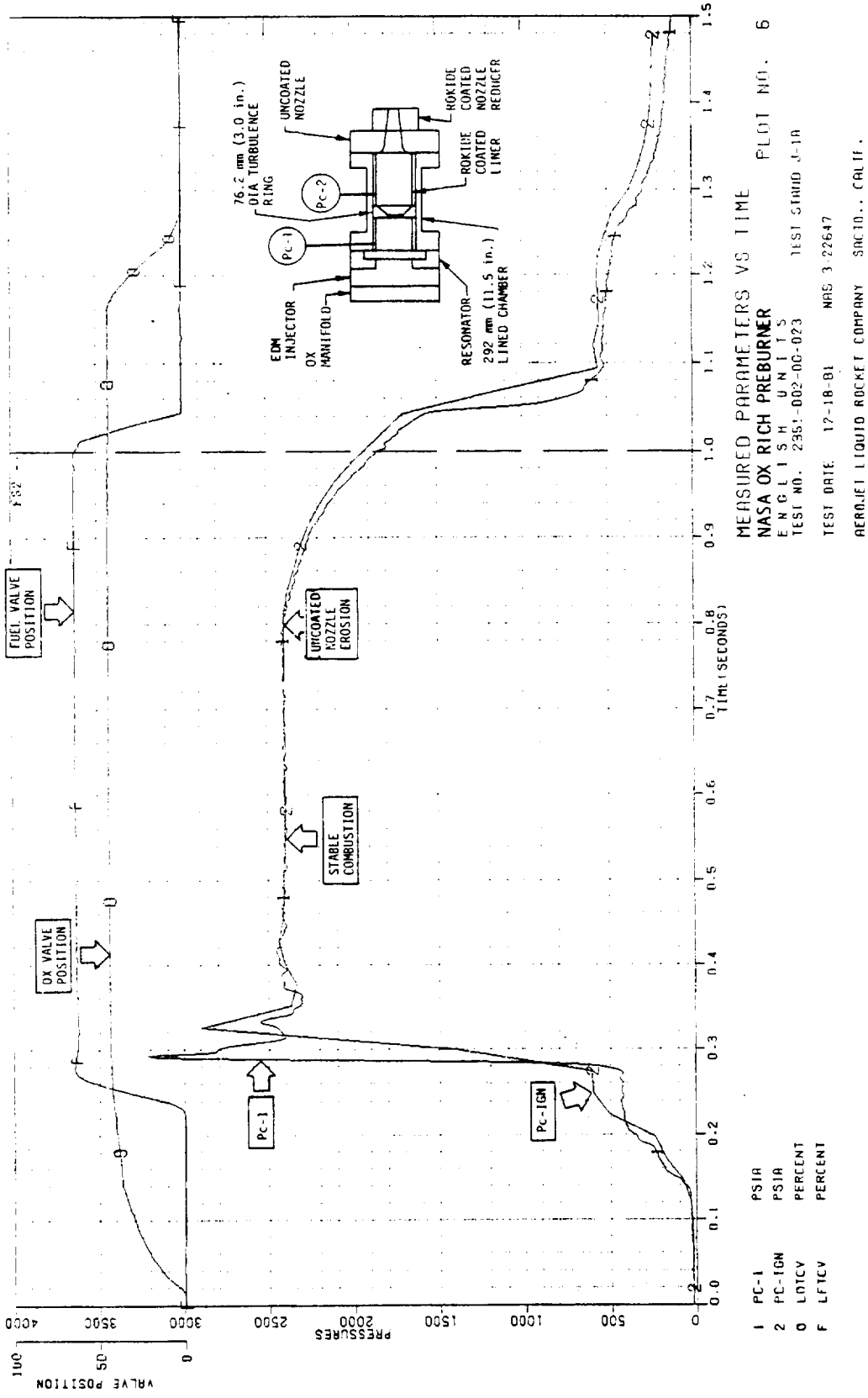

Figure 75. Oxidizer-Rich Preburner, Measured Parameters Versus Time, Test -023 (2 of 2)

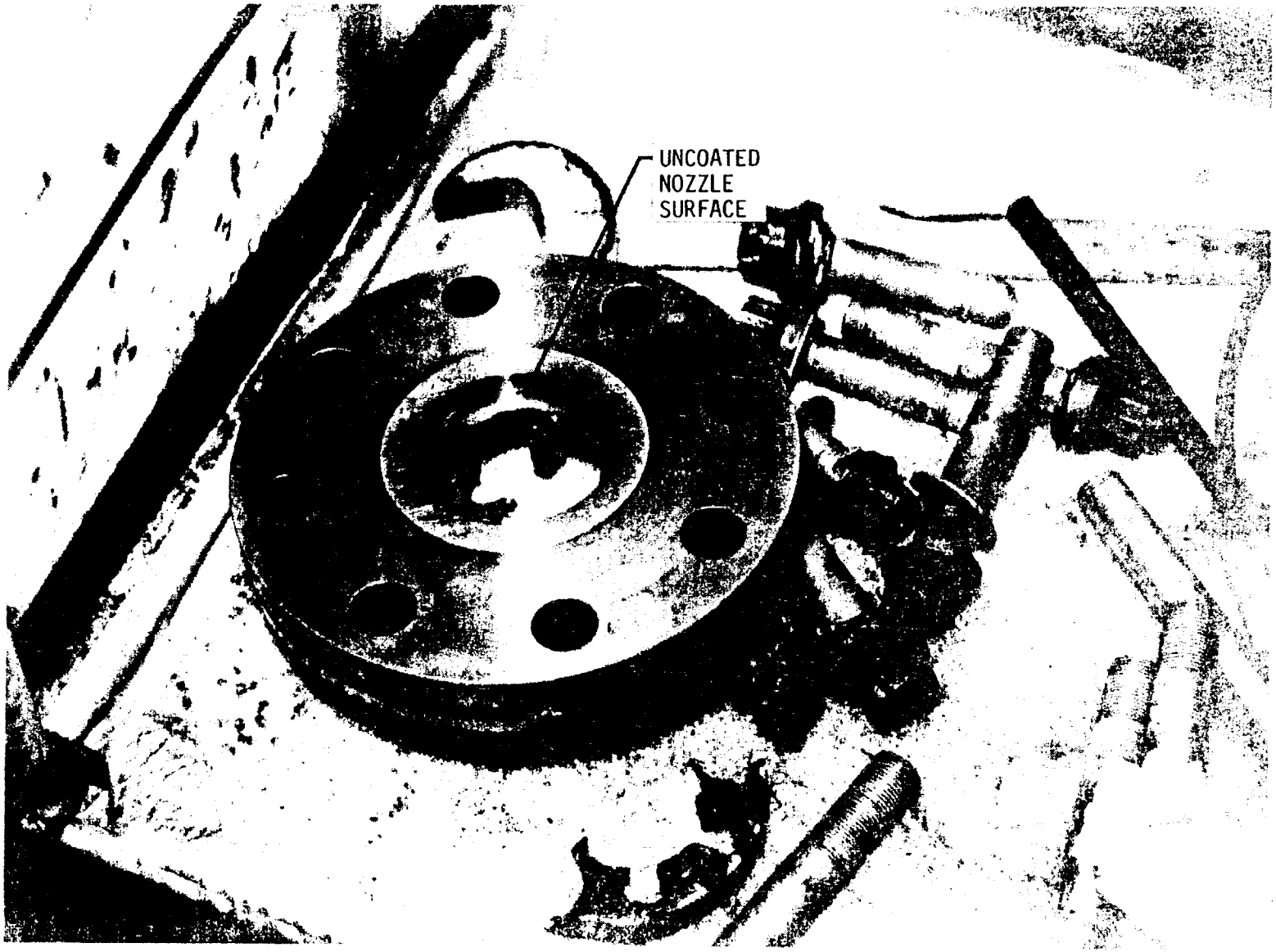

Figure 76. Uncooled Nozzle Erosion, Post Test -023

Test -024

The instrumentation rake and turbine simulator were installed on Test -024 to evaluate gas temperature uniformity. The test conditions were the same as for Test -023. The test duration was set for 9 seconds. The test was planned to run 3 sec each at MR 35, 40, and 45 at a chamber pressure of 17.2 MN/m^2 (2500 psia).

Ignition and overpressure were about the same as on Test -023. Even though the test was stable, severe erosion of the turbine simulator, instrumentation rake, and nozzle occurred at about 0.4 sec from FS-1, as indicated in Figure 77. The erosion probably started at the instrumentation rake since no damage was sustained upstream of the rake and everything downstream was severely eroded.

Figure 78 shows the nozzle erosion sustained on Test -024. Internal erosion occurred, starting from the instrumentation rake flange downstream to the nozzle. The rake mounting flange and the turbine simulator flange were not coated internally, although the rakes and the turbine blade simulators had been coated with Rokide Z. The leading edge of the rake and the thermocouples were not coated. Oxygen reaction with the uncoated components is the most probable cause for component erosion.

No erosion occurred upstream of the rake, as shown in Figure 79. The injector face, turbulence ring, and liner remained intact as shown in Figure 80. All of these components are made of nickel, whereas the chambers, flanges, nozzles, and rakes are made of 304 stainless steel. The turbine simulator blades are made of 17-4 ph CRES. The reactivity of uncoated metals in flowing oxygen needs to be understood better if oxygen-rich preburners are to be successful.

C. DATA ANALYSIS

This section of the report discusses the results of both the fuel-rich and the oxidizer-rich data analysis. Performance and stability data correlations are presented for both the fuel-rich and oxidizer-rich preburners. Gas temperature uniformity data are presented for the fuel-rich preburner only. Carbon deposition (coking) and hardware erosion observed with the fuel-rich preburner are also discussed. The fuel-rich gas sample analysis and results are discussed in Section IV.D.

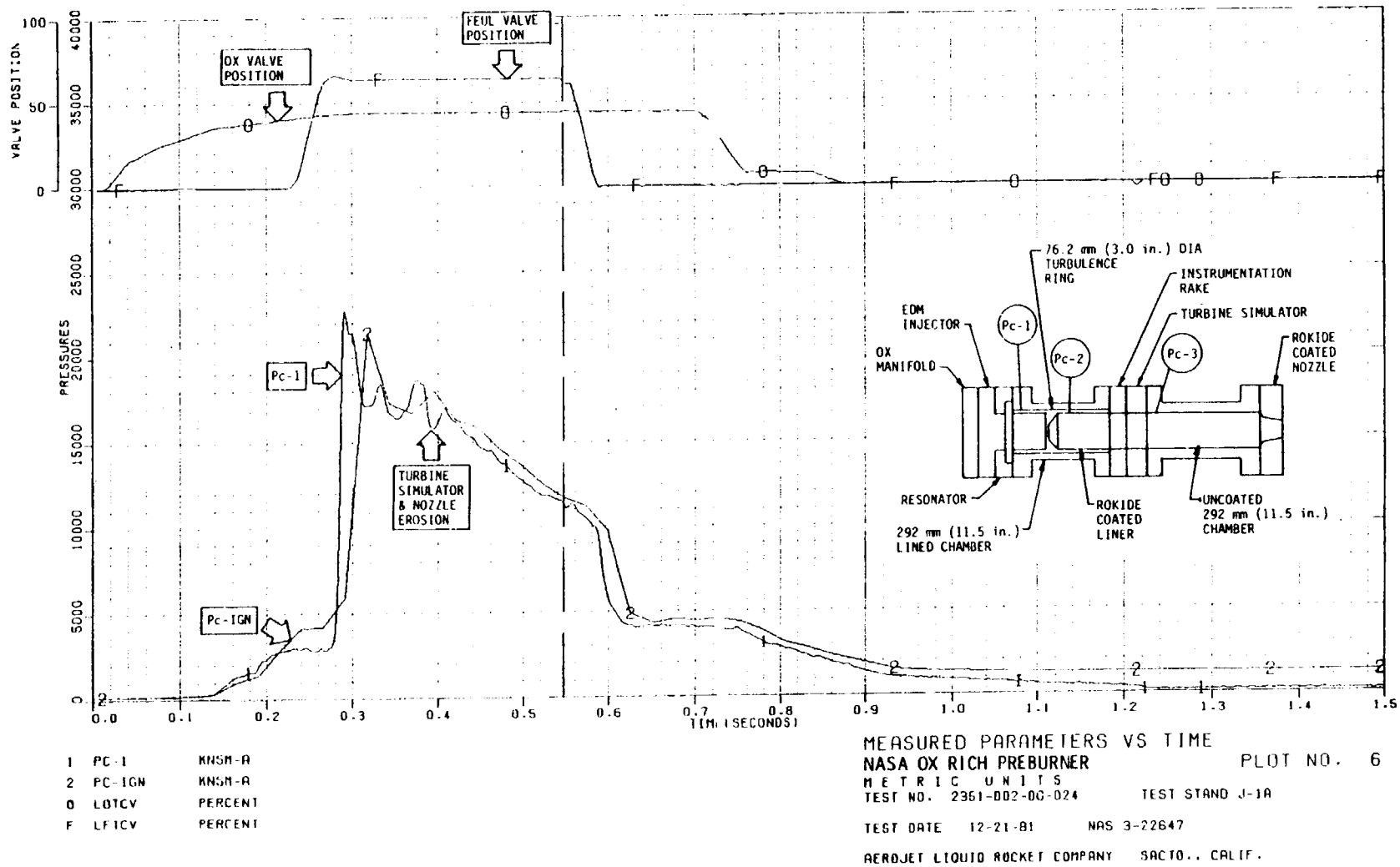

Figure 77. Oxidizer-Rich Preburner, Measured Parameters Versus Time, Test -024 (1 of 2)

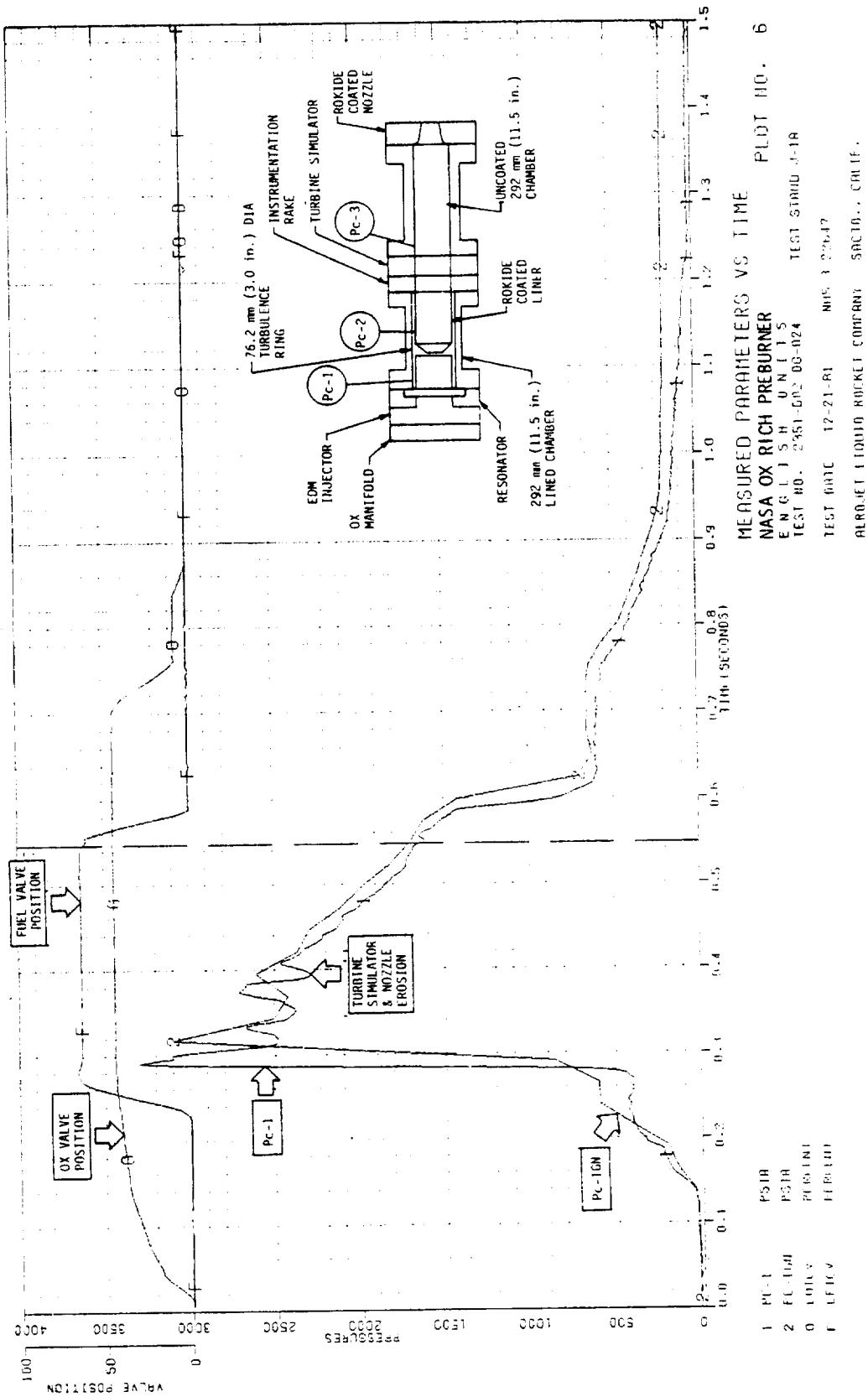

Figure 77. Oxidizer-Rich Preburner, Measured Parameters Versus Time, Test -024 (2 of 2)

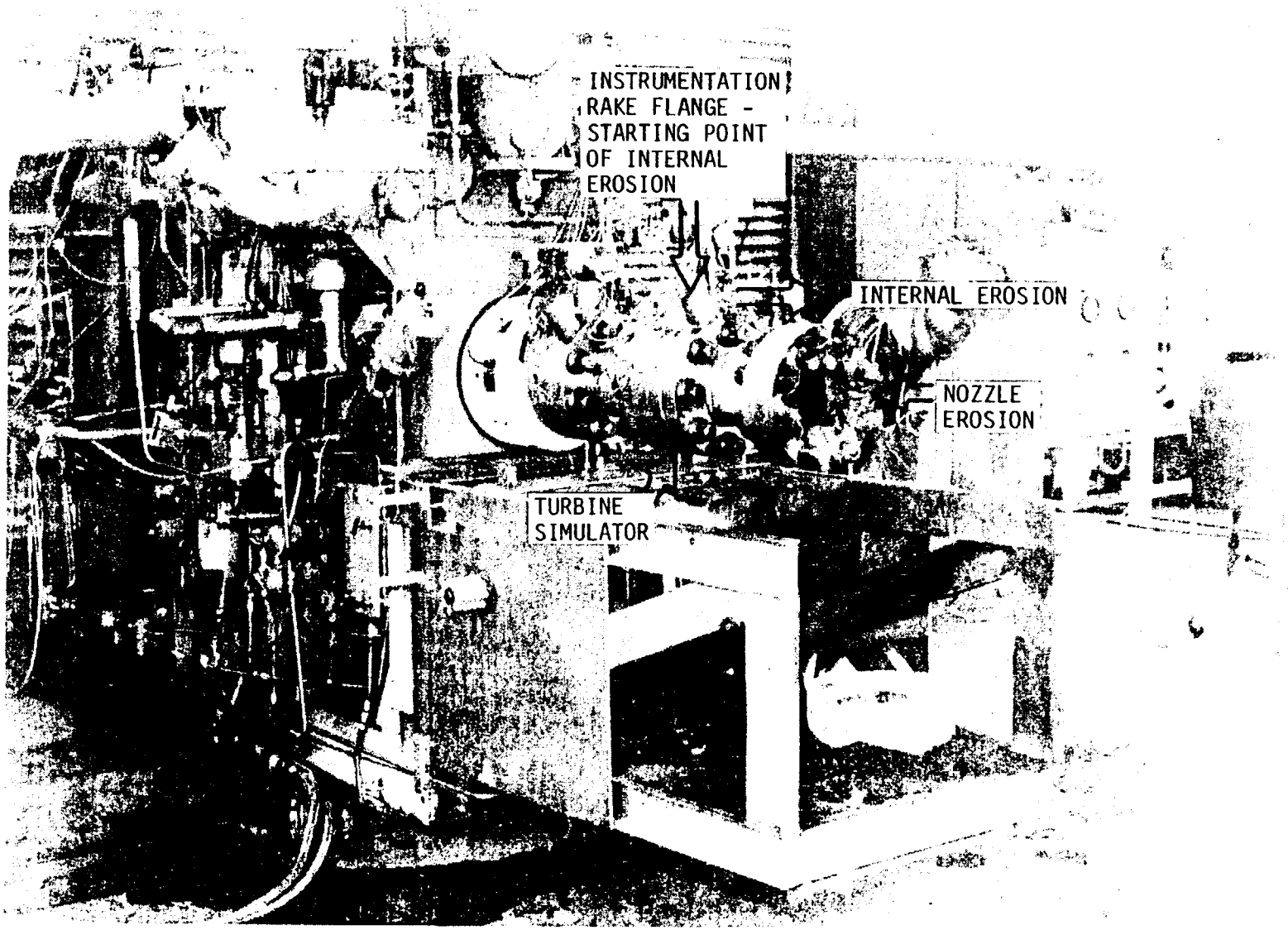

Figure 78. Nozzle Erosion, Post Test -024

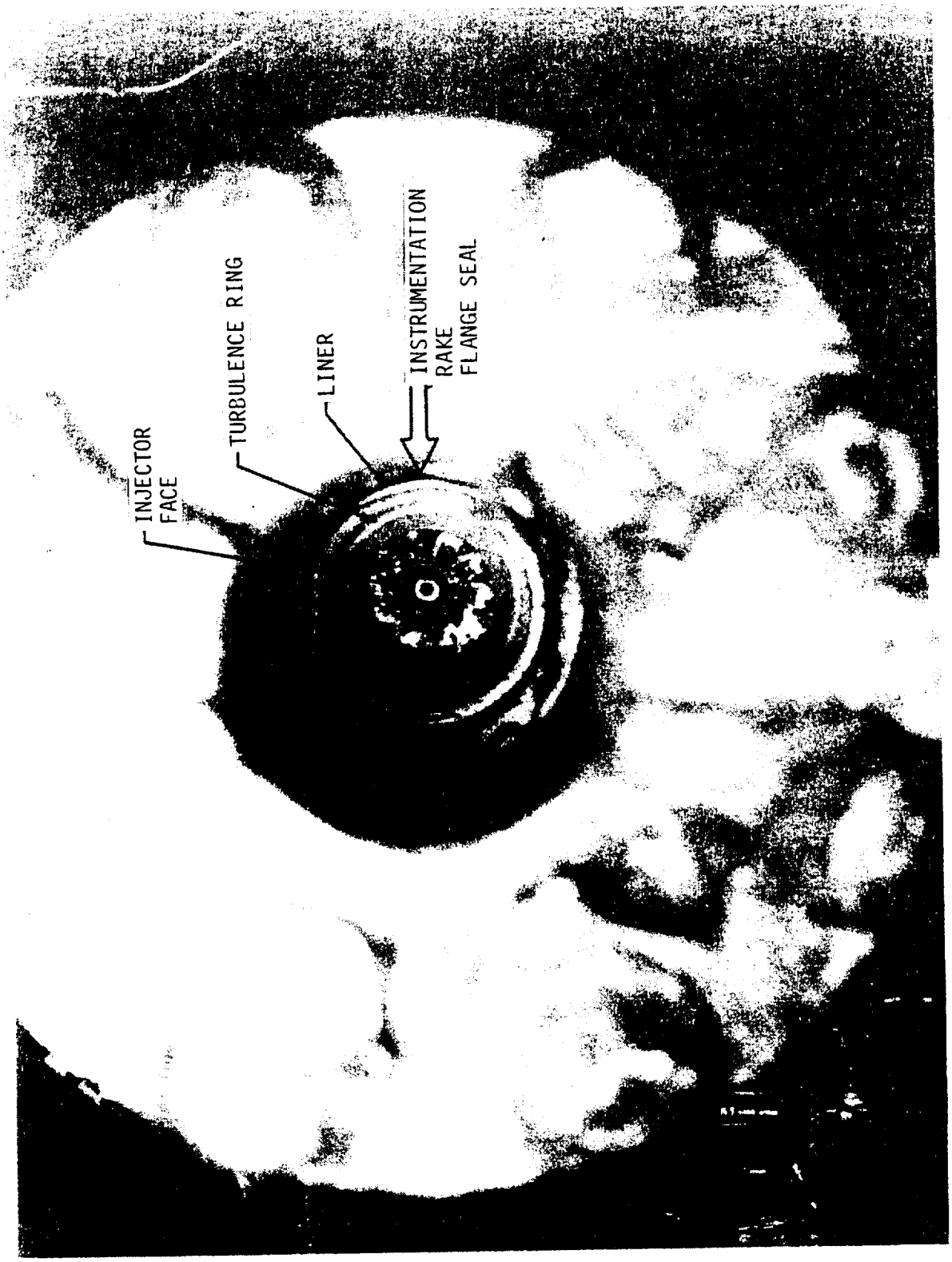

Figure 79. Injector Face Turbulence Ring and Liners, Post Test -024

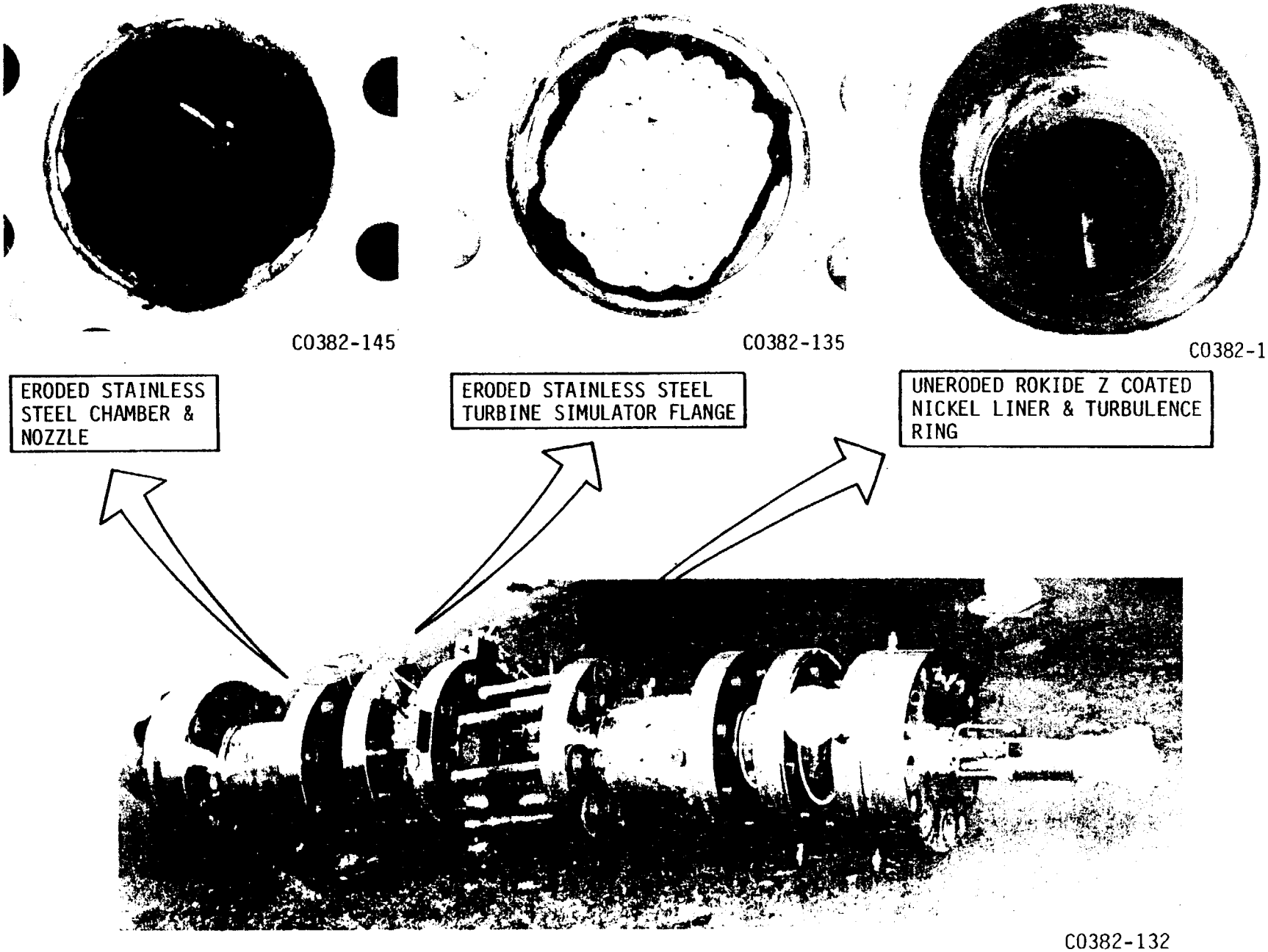

Figure 80. Oxidizer-Rich Preburner Hardware, Post-test, -024

IV, C, Data Analysis (cont.)

1. Fuel-Rich Preburner Data Analysis

a. Performance

Preburner combustion performance is indicated by the energy release efficiency (ERE) which accounts for losses due to incomplete propellant vaporization and mixture ratio maldistributions. The ERE for the preburners was determined by comparing the measured C* with theoretical C* predictions made using the JANNAF Standardized One-Dimensional Equilibrium (ODE) computer program. C* predictions were also made with the fuel-rich combustion model (FRCM). The FRCM predicts the effect of kinetically limited fuel decomposition reactions on the C* performance of fuel-rich preburners. The FRCM is discussed in Section IV, D. Comparison of the measured C*, gas temperature, and gas composition values to those predicted by the FRCM indicates the model's validity. The FRCM theoretical C* predictions were used to compare injector and other hardware effects. These predictions were made before the model was updated (see Section IV, D).

The measured C* data for the fuel-rich preburner are summarized in Tables XI and XII for the EDM and platelet injectors, respectively. These C* data are compared to the ODE and FRCM theoretical C* predictions in Figures 81 and 82. It is apparent that the FRCM prediction best describes fuel-rich preburner performance.

Energy release efficiencies (ERE) were found to vary from about 62 to 81% of ODE depending on mixture ratio. Efficiencies significantly greater than these are not achievable as evidenced by the close correspondence between the measured C* and the FRCM predicted C*. The measured C* varies from 92 to 99% of the FRCM predicted C*. The C* is limited by slow fuel decomposition kinetics and vaporization. The effects of the hardware variables on measured C* is best illustrated by comparing it to the FRCM C*.

The performance was evaluated as functions of injector design, chamber pressure, mixture ratio, chamber length, the use of turbulence ring mixing devices, and chamber contraction ratio. The chamber pressure varied over a range of 8.9 to 17.5 MN/m^2 (1,292 to 2,540 psia), as indicated in the data summaries. The data show the performance to have little pressure dependence over this range of pressures. This is in agreement with the FRCM model predictions. As seen in Figures 81 and 82, the mixture ratio exhibits the single largest effect on C* level, which is also in agreement with the FRCM predictions (see Section IV, D). The mixture ratio was varied over a range from 0.238 to 0.367. Although there is no significant performance difference between injectors, the EDM injector has a slightly higher average C* performance than the platelet injector.

TABLE XI

FUEL-RICH PREBURNER PERFORMANCE DATA EDM INJECTOR

Test No.	Pc-1 MN/m^2 (psia)	MR	C* m/s (ft/sec)	ERE_{ODE} (%)	C^*/C^*_{FRCM} (%)	L' mm (in.)	Turb. Ring	Contr. Ratio	Turbine Simulator	Stability
-009	17.5 (2540)	0.305	792 (2598)	72.9	97.3	736.6 (29)	No	9.4	No	Stable
-011	15.6 (2265)	0.331	838 (2750)	76.0	97.5	736.6 (29)	No	9.4	No	Stable
-012	13.5 (1960)	0.238	655 (2150)	63.8	96.0	787.4 (31)	No	9.4	No	Stable
-012	16.7 (2424)	0.318	815 (2675)	74.6	97.3	787.4 (31)	No	9.4	No	Stable
-012	16.4 (2381)	0.239	659 (2163)	64.0	96.1	787.4 (31)	No	9.4	No	Stable
-013	15.6 (2257)	0.327	834 (2737)	75.9	97.8	787.4 (31)	No	9.4	No	Stable
-013	15.2 (2201)	0.271	718 (2355)	68.0	95.7	787.4 (31)	No	9.4	No	Stable
-013	16.0 (2320)	0.367	915 (3002)	81.1	98.9	787.4 (31)	No	9.4	No	Stable
-013	17.5 (2535)	0.332	844 (2770)	76.5	97.9	787.4 (31)	No	9.4	No	Stable
-013	13.6 (1972)	0.312	794 (2605)	72.9	96.1	787.4 (31)	No	9.4	No	Stable
-030	11.3 (1643)	0.283	749 (2458)	70.3	97.1	787.4 (31)	Yes	7.3	No	Stable
-030	14.0 (2037)	0.343	862 (2827)	77.5	97.6	787.4 (31)	Yes	7.3	No	Stable
-030	14.3 (2067)	0.262	714 (2343)	68.1	97.6	787.4 (31)	Yes	7.3	No	Stable
-030	9.3 (1350)	0.243	675 (2214)	65.4	97.3	787.4 (31)	Yes	7.3	No	Stable
-030	9.1 (1316)	0.332	828 (2718)	75.0	96.2	787.4 (31)	Yes	7.3	No	Stable
-031	14.6 (2122)	0.288	729 (2392)	68.1	93.2	787.4 (31)	Yes	9.4	No	Stable
-031	17.8 (2578)	0.355	867 (2844)	77.4	95.7	787.4 (31)	Yes	9.4	No	Stable
-031	17.4 (2530)	0.271	700 (2298)	66.4	93.4	787.4 (31)	Yes	9.4	No	Stable
-031	12.6 (1826)	0.240	641 (2102)	62.2	93.2	787.4 (31)	Yes	9.4	No	Stable
-031	12.4 (1795)	0.321	782 (2565)	71.3	96.2	787.4 (31)	Yes	9.4	No	Stable
-032	14.8 (2151)	0.298	742 (2434)	68.8	92.5	533.4 (21)	Yes	9.4	No	Stable
-032	17.5 (2535)	0.360	870 (2853)	77.5	95.1	533.4 (21)	Yes	9.4	No	Stable
-032	17.5 (2543)	0.278	708 (2324)	66.7	92.9	533.4 (21)	Yes	9.4	No	Stable
-032	12.8 (1863)	0.254	662 (2173)	63.5	92.4	533.4 (21)	Yes	9.4	No	Stable
-032	12.7 (1841)	0.341	811 (2662)	73.1	92.5	533.4 (21)	Yes	9.4	No	Stable

NOTES:

1. Pc-1 measured at injector face
2. C* based on nozzle inlet pressure

TABLE XII

FUEL-RICH PREBURNER PERFORMANCE DATA PLATELET INJECTOR

Test No.	Pc-1 MN/m^2 (psia)	MR	C* m/s (ft/sec)	ERE_{ODE} (%)	C^*/C^*_{FRCM} (%)	L' mm (in.)	Turb. Ring	Contr. Ratio	Turbine Simulator	Stability
-014	15.1 (2185)	0.303	778 (2551)	71.9	96.1	787.4 (31)	No	9.4	No	Stable
-015	15.1 (2193)	0.300	768 (2521)	71.2	95.5	787.4 (31)	No	9.4	No	Stable
-015	17.2 (2492)	0.350	871 (2858)	78.1	97.2	787.4 (31)	No	9.4	No	Stable
-015	17.3 (2513)	0.263	707 (2318)	67.3	96.6	787.4 (31)	No	9.4	No	Unstable
-015	13.5 (1958)	0.255	679 (2228)	65.1	94.4	787.4 (31)	No	9.4	No	Unstable
-015	13.0 (1881)	0.320	803 (2636)	73.4	95.5	787.4 (31)	No	9.4	No	Stable
-016	15.2 (2204)	0.305	778 (2552)	71.9	95.6	787.4 (31)	No	9.4	No	Stable
-016	15.2 (2208)	0.255	687 (2255)	65.9	96.0	787.4 (31)	No	9.4	No	Unstable
-016	15.1 (2197)	0.349	863 (2830)	77.3	96.6	787.4 (31)	No	9.4	No	Stable
-016	17.4 (2520)	0.319	806 (2645)	71.7	96.2	787.4 (31)	No	9.4	No	Stable
-018	15.2 (2208)	0.304	773 (2535)	71.4	95.3	533.4 (21)	No	9.4	No	Unstable
-018	17.3 (2502)	0.365	888 (2915)	78.9	96.5	533.4 (21)	No	9.4	No	Unstable
-018	17.5 (2545)	0.271	723 (2372)	68.5	96.6	533.4 (21)	No	9.4	No	Stable
-018	13.7 (1991)	0.261	698 (2290)	66.7	95.8	533.4 (21)	No	9.4	No	Unstable
-018	12.7 (1842)	0.335	805 (2641)	72.8	92.7	533.4 (21)	No	9.4	No	Unstable
-019	15.2 (2200)	0.303	751 (2465)	69.5	92.8	533.4 (21)	Yes	9.4	No	Stable
-019	17.2 (2490)	0.353	841 (2760)	75.2	93.4	533.4 (21)	Yes	9.4	No	Stable
-019	17.3 (2515)	0.269	693 (2273)	65.7	93.0	533.4 (21)	Yes	9.4	No	Stable
-019	13.6 (1972)	0.257	673 (2209)	64.5	93.4	533.4 (21)	Yes	9.4	No	Stable
-019	12.8 (1851)	0.327	782 (2564)	71.1	91.6	533.4 (21)	Yes	9.4	No	Unstable
-020	14.9 (2158)	0.299	735 (2411)	68.2	91.5	787.4 (31)	Yes	9.4	No	Stable
-020	17.0 (2470)	0.354	842 (2762)	75.2	93.3	787.4 (31)	Yes	9.4	No	Stable
-020	17.3 (2506)	0.264	685 (2249)	65.2	93.3	787.4 (31)	Yes	9.4	No	Stable
-020	13.5 (1964)	0.260	675 (2214)	64.5	92.8	787.4 (31)	Yes	9.4	No	Stable
-020	12.8 (1860)	0.330	787 (2581)	71.4	91.7	787.4 (31)	Yes	9.4	No	Stable
-021	14.6 (2115)	0.301	798 (2617)	73.9	98.9	1143.0 (45)	Yes	7.3	Yes	Stable
-022	15.8 (2292)	0.350	883 (2897)	79.1	98.2	1143.0 (45)	Yes	7.3	Yes	Stable
-025	16.2 (2351)	0.262	723 (2373)	68.9	98.9	1143.0 (45)	Yes	7.3	Yes	Stable
-027	12.3 (1786)	0.256	711 (2334)	68.1	98.1	1143.0 (45)	Yes	7.3	Yes	Stable
-028	12.1 (1748)	0.369	892 (2926)	78.9	96.0	1143.0 (45)	Yes	7.3	Yes	Stable
-029	13.9 (2015)	0.350	907 (2975)	81.3	100	1143.0 (45)	Yes	7.3	Yes	Stable

NOTES:

1. Pc-1 measured at injector face
2. C* based on nozzle inlet pressure

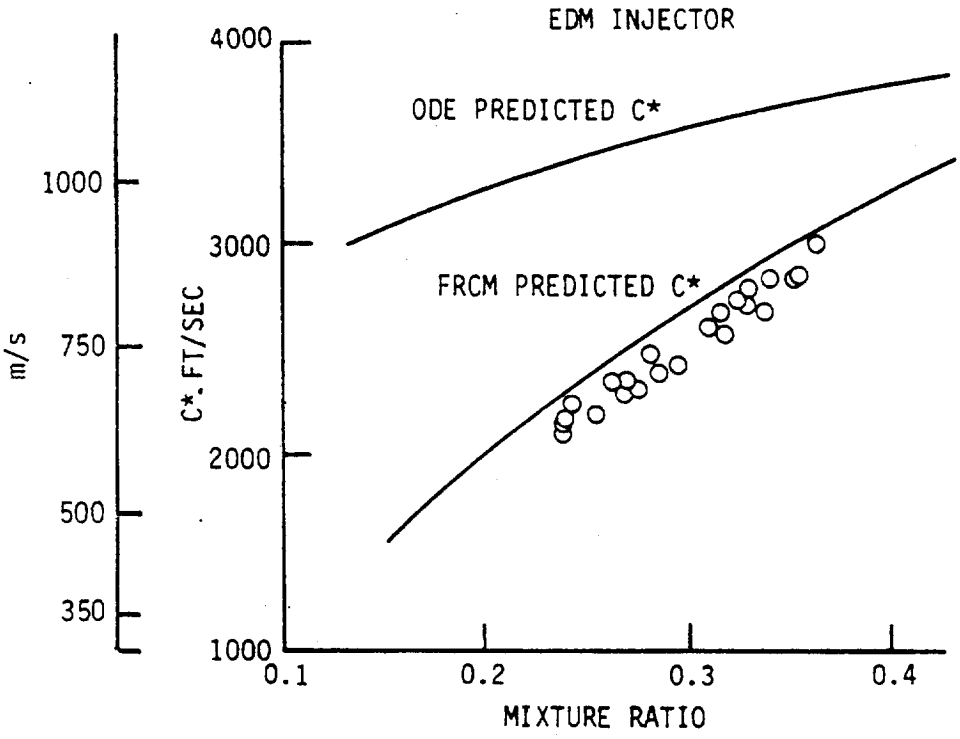

Figure 81. Measured Versus Predicted C* - EDM Injector

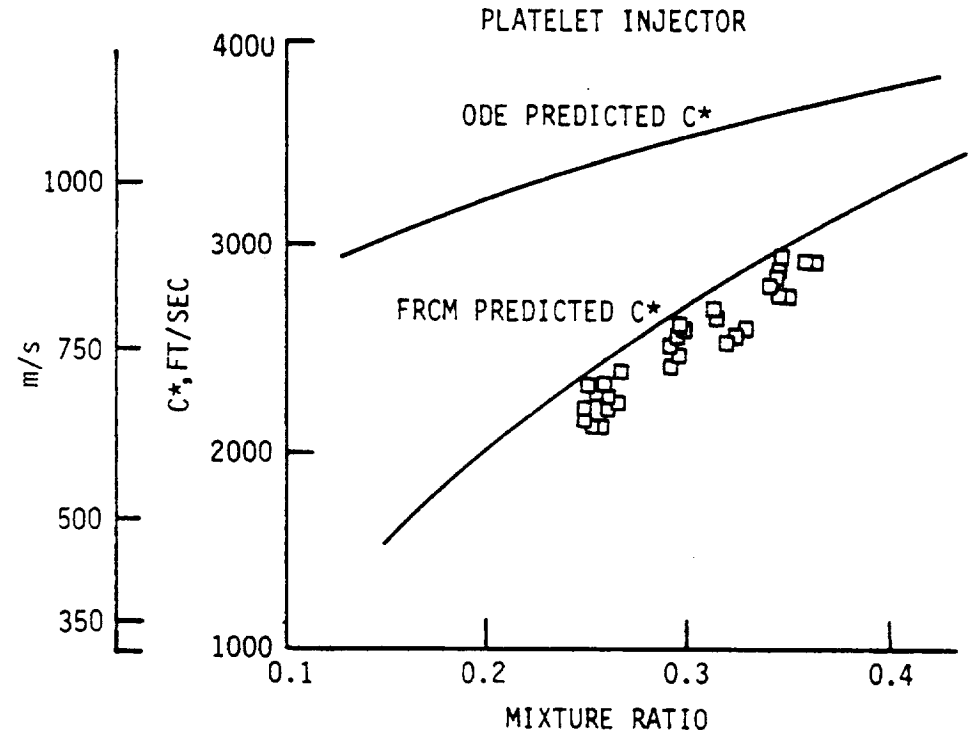

Figure 82. Measured Versus Predicted C* - Platelet Injector

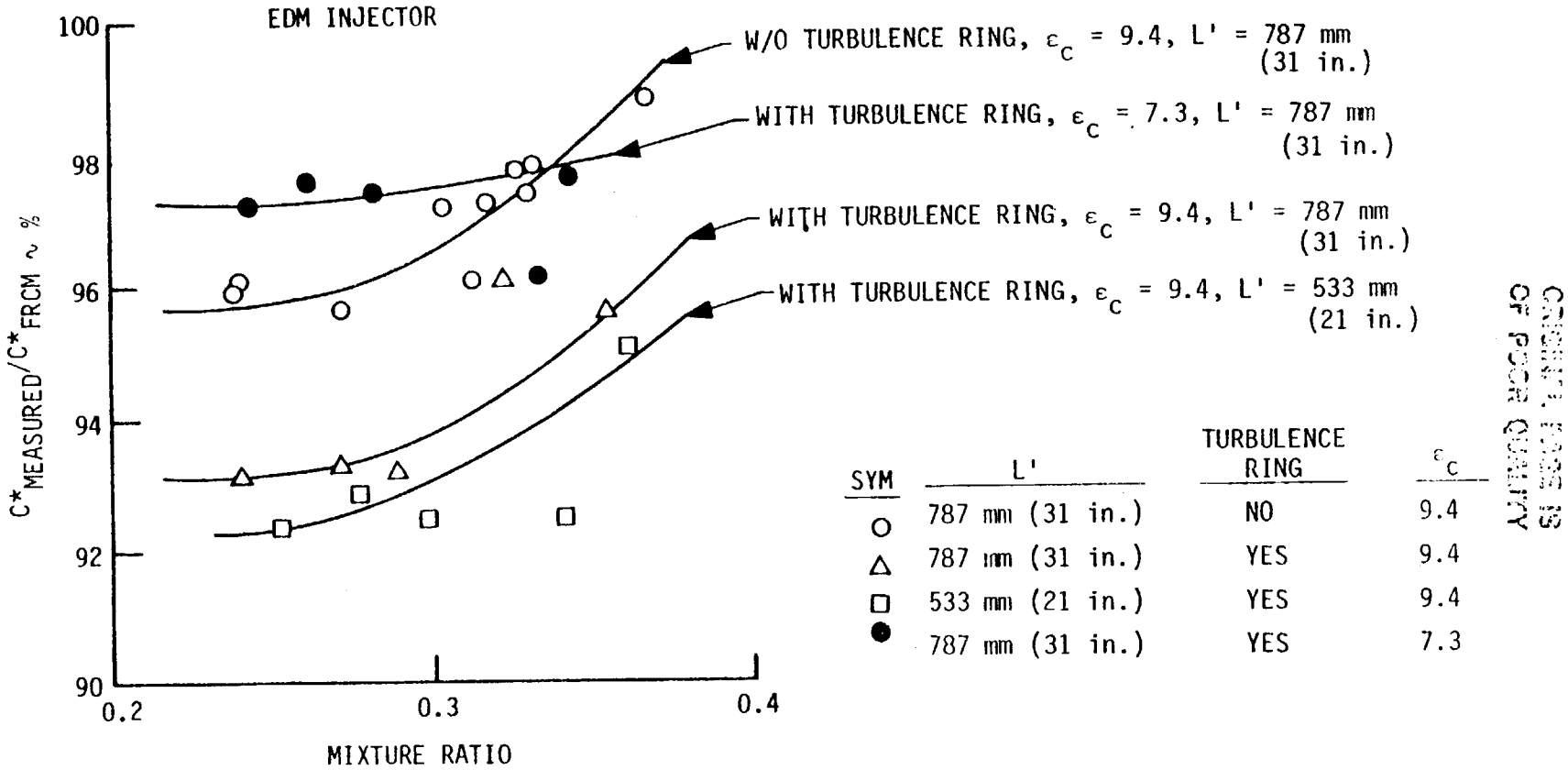

Figure 83. EDM Injector C* Efficiency

The effect of the hardware variables on C* performance is best illustrated by comparing the measured and FRCM predicted C*, as shown in Figure 83 for the EDM injector. Comparison of the measured C* to the FRCM predicted C* provides a comparison of the measured vaporization efficiency with that predicted. The predicted vaporization efficiency is shown in Figure 84 as a function of mixture ratio. A chamber length of 787 mm (31 in.) was selected for comparison. Chamber length effects are expected to be small since the predicted vaporization efficiency does not change appreciably with chamber length beyond 457 to 508 mm (18 to 20 in.) (see Section IV, D).

As shown in Figure 83, the effect of the turbulence ring is to reduce C* performance. The uniform gas temperature (discussed in the following section) that is achieved with the turbulence ring apparently slows the vaporization, as compared to the nonuniform gas obtained without the turbulence ring. Apparently, the higher temperature zones provide faster vaporization.

The effect of reducing contraction ratio is to increase the vaporization efficiency and C* performance. The higher chamber gas velocity results in higher gas-to-droplet relative velocities and thus faster vaporization. The increase in vaporization apparently more than offsets the reduction in gas residence time. This would indicate that, for these chamber lengths, vaporization is limiting the C* performance. This is in agreement with the FRCM predictions discussed in Section IV.D.

The platelet C* performance data are plotted in Figure 85. The general level of C* performance is lower at the higher MR than for the EDM injector but about equal at the low MR end. The shape of the C* curve apparently reflects the swirler injector effects on atomization and vaporization. The effect of adding a turbulence ring is the same for the platelet injector as for the EDM injector; performance is reduced for either injector. The effect of contraction ratio and turbine simulator is to increase performance. It would appear that the vaporization is somewhat enhanced in passing through the turbine simulator. Heating the fuel from ambient temperature to approximately 379°K (223°F) increased the C* efficiency by about 2%.

b. Gas Temperature Uniformity

The combustion gas temperatures were measured using the instrumentation rakes described in Section IV.A.2. Two rakes with five (5) thermocouples each were mounted 1.57 rad (90°) apart and positioned to face toward the injector face, as shown in Figure 21. The gas temperature thermocouple data are summarized in Table XIII which lists the maximum and minimum

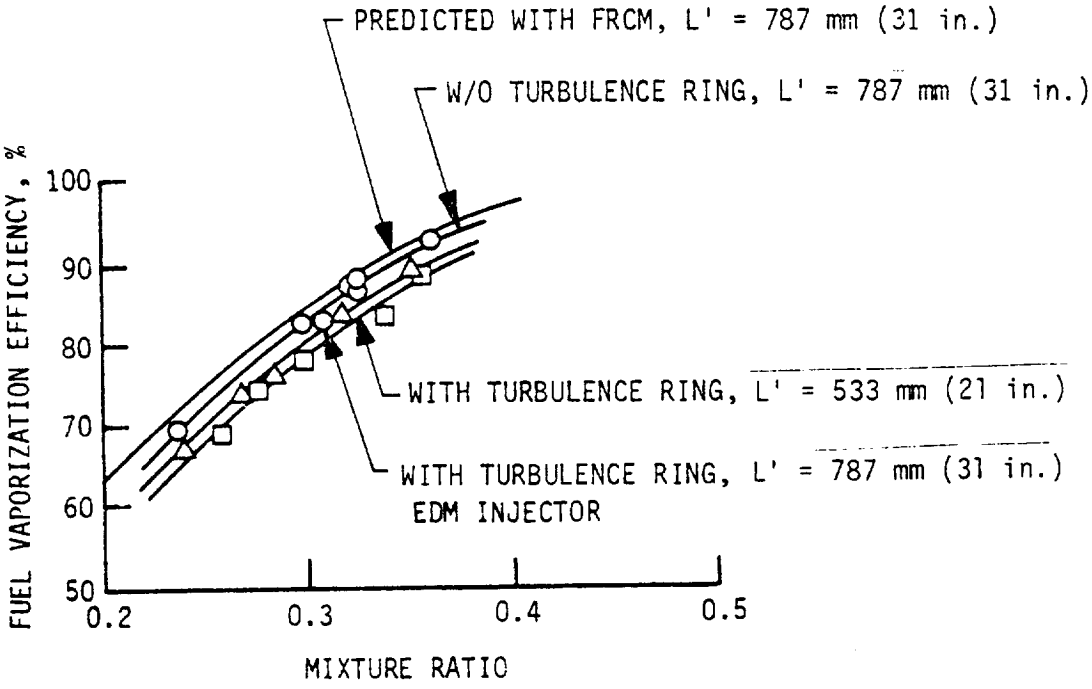

Figure 84. EDM Injector Fuel Vaporization Efficiency

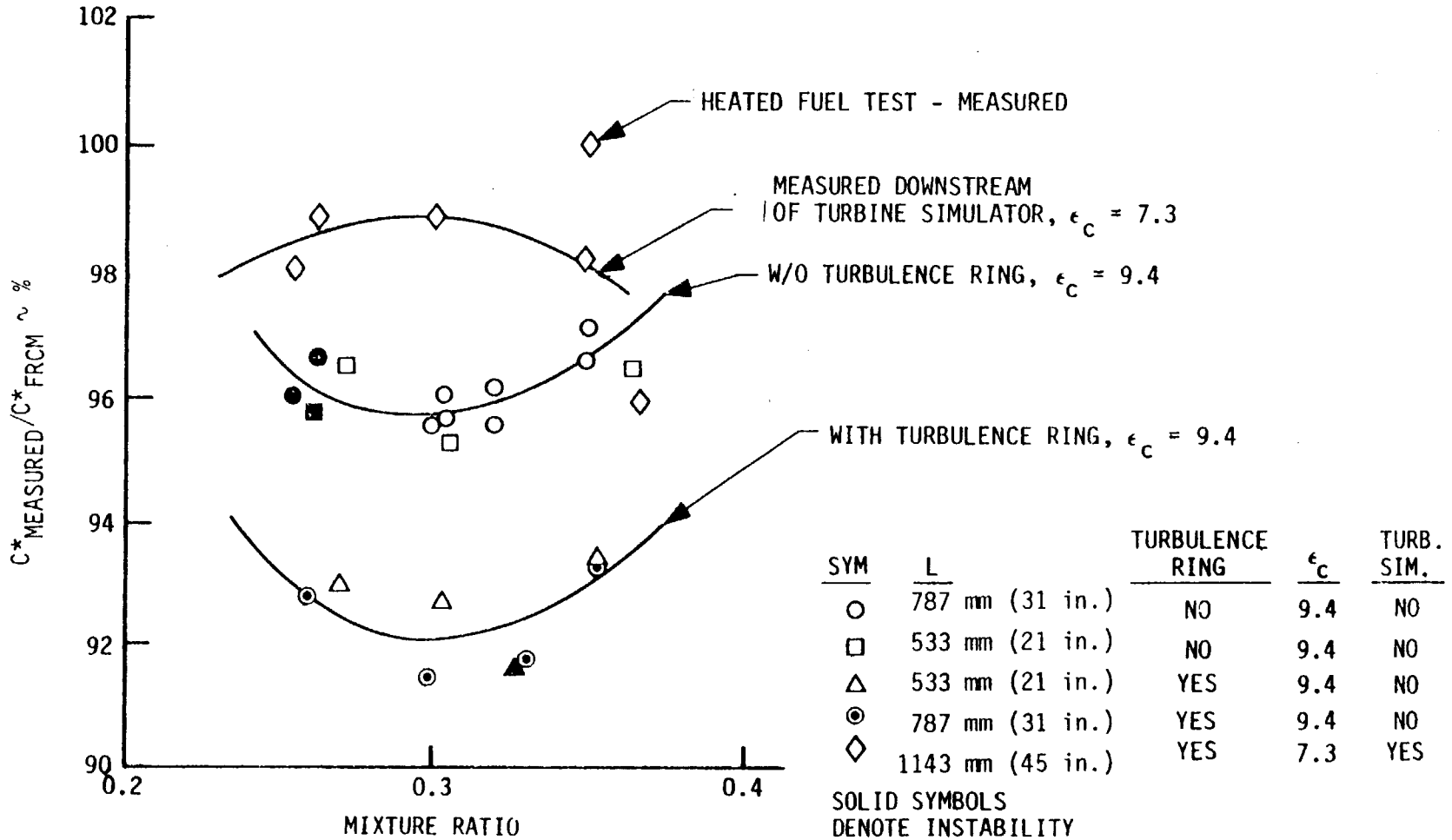

Figure 85. Platelet Injector C* Efficiency

TABLE XIII

GAS TEMPERATURE DATA SUMMARY

Test No.	Data Point	Injector	MR	Stability	L' mm (in.)	Turbulence Ring	T_{max} °C (°F)	T_{min} °C (°F)	T_{avg} °C (°F)	ΔT_{max} °C (°F)
-012	1	EDM	0.238	S	787.4 (31)	No	566 (1050)	419 (787)	499 (930)	146 (263)
	2	EDM	0.318	S	787.4 (31)	No	768 (1415)	524 (975)	643 (1190)	244 (440)
	3	EDM	0.239	S	787.4 (31)	No	577 (1070)	446 (835)	513 (955)	131 (235)
-013	1	EDM	0.327	S	787.4 (31)	No	771 (1420)	543 (1010)	657 (1215)	228 (410)
	2	EDM	0.271	S	787.4 (31)	No	635 (1175)	474 (885)	554 (1030)	161 (290)
	3	EDM	0.367	S	787.4 (31)	No	910 (1670)	596 (1105)	743 (1370)	314 (565)
	4	EDM	0.332	S	787.4 (31)	No	813 (1495)	554 (1030)	688 (1270)	258 (465)
	5	EDM	0.312	S	787.4 (31)	No	714 (1318)	532 (990)	638 (1180)	182 (328)
-015	1	Platelet	0.300	S	787.4 (31)	No	696 (1285)	613 (1135)	654 (1210)	83 (150)
	2	Platelet	0.350	S	787.4 (31)	No	843 (1550)	710 (1310)	774 (1425)	133 (240)
	3	Platelet	0.263	Un	787.4 (31)	No	666 (1230)	554 (1030)	610 (1130)	111 (200)
	4	Platelet	0.255	Un	787.4 (31)	No	571 (1060)	532 (990)	552 (1025)	39 (70)
	5	Platelet	0.320	S	787.4 (31)	No	724 (1335)	638 (1180)	685 (1265)	87 (155)
-016	1	Platelet	0.305	S	787.4 (31)	No	699 (1290)	618 (1145)	660 (1220)	81 (145)
	2	Platelet	0.255	Un	787.4 (31)	No	577 (1070)	541 (1005)	566 (1050)	36 (65)
	3	Platelet	0.349	S	787.4 (31)	No	818 (1505)	699 (1290)	749 (1380)	119 (215)
	4	Platelet	0.319	S	787.4 (31)	No	754 (1390)	663 (1225)	704 (1300)	92 (165)
-018	1	Platelet	0.304	Un	533.4 (21)	No	688 (1270)	624 (1155)	657 (1215)	64 (115)
	2	Platelet	0.365	Un	533.4 (21)	No	802 (1475)	760 (1400)	782 (1440)	42 (75)
	3	Platelet	0.271	S	533.4 (21)	No	671 (1240)	549 (1020)	610 (1130)	122 (220)
	4	Platelet	0.261	Un	533.4 (21)	No	593 (1100)	571 (1060)	582 (1080)	22 (40)
	5	Platelet	0.335	Un	533.4 (21)	No	704 (1300)	663 (1225)	682 (1260)	42 (75)
-019	1	Platelet	0.303	S	533.4 (21)	Yes	654 (1210)	643 (1190)	649 (1200)	11 (20)
	2	Platelet	0.353	S	533.4 (21)	Yes	754 (1390)	738 (1360)	749 (1380)	17 (30)
	3	Platelet	0.269	S	533.4 (21)	Yes	599 (1110)	582 (1080)	591 (1095)	17 (30)
	4	Platelet	0.257	S	533.4 (21)	Yes	574 (1065)	563 (1045)	568 (1055)	11 (20)
	5	Platelet	0.327	Un	533.4 (21)	Yes	679 (1255)	660 (1220)	677 (1250)	19 (35)

TABLE XIII (cont.)

Test No.	Data Point	Injector	MR	Stability	L' mm (in.)	Turbulence Ring	T_{max} °C (°F)	T_{min} °C (°F)	T_{avg} °C (°F)	ΔT_{max} °C (°F)
-020	1	Platelet	0.299	S	787.4 (31)	Yes	638 (1180)	632 (1170)	635 (1175)	6 (10)
	2	Platelet	0.354	S	787.4 (31)	Yes	746 (1375)	738 (1360)	743 (1370)	8 (15)
	3	Platelet	0.264	S	787.4 (31)	Yes	588 (1090)	588 (1090)	588 (1090)	0 (0)
	4	Platelet	0.260	S	787.4 (31)	Yes	574 (1065)	574 (1065)	574 (1065)	0 (0)
	5	Platelet	0.330	S	787.4 (31)	Yes	691 (1275)	682 (1260)	688 (1270)	8 (15)
-021	-	Platelet	0.301	S	787.4 (31)	Yes	649 (1200)	643 (1190)	646 (1195)	6 (10)
-022	-	Platelet	0.350	S	787.4 (31)	Yes	738 (1360)	729 (1345)	735 (1355)	8 (15)
-025	-	Platelet	0.262	S	787.4 (31)	Yes	585 (1085)	579 (1075)	582 (1080)	6 (10)
-027	-	Platelet	0.256	S	787.4 (31)	Yes	566 (1050)	560 (1040)	563 (1045)	6 (10)
-028	-	Platelet	0.369	S	787.4 (31)	Yes	749 (1380)	743 (1370)	746 (1375)	6 (10)
-029	-	Platelet	0.350	S	787.4 (31)	Yes	766 (1410)	757 (1395)	763 (1405)	8 (15)
-030	1	EDM	0.283	S	787.4 (31)	Yes	603 (1118)	600 (1112)	602 (1115)	3 (6)
	2	EDM	0.343	S	787.4 (31)	Yes	721 (1329)	718 (1325)	719 (1326)	2 (4)
	3	EDM	0.262	S	787.4 (31)	Yes	571 (1060)	570 (1058)	571 (1059)	1 (2)
	4	EDM	0.243	S	787.4 (31)	Yes	529 (985)	527 (981)	528 (983)	2 (4)
	5	EDM	0.332	S	787.4 (31)	Yes	678 (1252)	673 (1243)	674 (1245)	5 (9)
-031	1	EDM	0.288	S	787.4 (31)	Yes	624 (1156)	619 (1146)	621 (1150)	6 (10)
	2	EDM	0.355	S	787.4 (31)	Yes	766 (1411)	762 (1403)	765 (1409)	4 (8)
	3	EDM	0.271	S	787.4 (31)	Yes	601 (1114)	600 (1112)	601 (1113)	2 (3)
	4	EDM	0.240	S	787.4 (31)	Yes	534 (994)	533 (992)	534 (993)	1 (2)
	5	EDM	0.321	S	787.4 (31)	Yes	678 (1252)	675 (1247)	674 (1246)	3 (5)
-032	1	EDM	0.298	S	533.4 (21)	Yes	646 (1194)	619 (1147)	632 (1170)	28 (50)
	2	EDM	0.360	S	533.4 (21)	Yes	803 (1477)	760 (1400)	782 (1440)	43 (77)
	3	EDM	0.278	S	533.4 (21)	Yes	619 (1147)	596 (1105)	609 (1128)	23 (42)
	4	EDM	0.254	S	533.4 (21)	Yes	567 (1052)	553 (1027)	559 (1038)	14 (25)
	5	EDM	0.341	S	533.4 (21)	Yes	717 (1323)	702 (1295)	709 (1309)	15 (28)

gas temperature, the average temperature, and the maximum temperature differential. The average gas temperature was determined by taking the arithmetic average of the ten thermocouple readings.

The measured average gas temperatures for the EDM and platelet injector, respectively, were compared to the predicted values in Figures 86 and 87. Both ODE and FRCM predictions are shown. It is evident that the FRCM provides the best prediction. The chamber length does not affect the average temperature for either injector. The average temperature versus mixture ratio curves are virtually identical for the two injectors, indicating no significant injector effects on average temperature. The mixture ratio is the most significant factor affecting average gas temperature. No pressure effects were found over the range tested. This agrees with the FRCM predictions.

Gas temperature uniformity is affected by the injector, turbulence ring, and chamber length, as shown in Figures 88 and 89 for the EDM and platelet injector, respectively. Figures 88 and 89 show that both the EDM and platelet injector exhibit large temperature nonuniformities without the aid of a turbulence ring mixing device. Temperature differences of almost 333°K (600°F) were measured with the EDM injector in the 787-mm (31-in.) L' chamber whereas the differences were less than 167°K (300°F) for the platelet injector (see Figure 89). The addition of a turbulence ring dramatically reduces the nonuniformities to less than + 5.6°K (+ 10°F) for both injectors. The platelet injector provides more uniform gas temperatures with the turbulence ring and shorter (533-mm [21-in.]) L' chamber than does the EDM injector. With a turbulence ring, either injector can easily meet the contract temperature uniformity goal of + 27.8°K (+50°F). The influence of the turbulence ring on gas temperature uniformity is dramatic even though the pressure drop across the turbulence ring is only 1 to 2% (20 to 50 psid) of chamber pressure.

c. Combustion Stability

The platelet injector exhibited longitudinal instabilities at certain operating conditions as listed in Table XIV. No transverse high-frequency instabilities were encountered. The 600-Hz oscillation observed on Tests -015 and -016 was identified as the second longitudinal (2L) mode by comparing the measured Kistler pressure amplitude ratios to the predicted pressure amplitude ratios (Figure 90). Further verification of the mode is indicated by the close agreement between the calculated and measured frequencies.

The occurrence of the instability was observed to be primarily dependent on the operating mixture ratio and less dependent on injector stiffness (P_{inj}/Pc), as shown in Figure 91. An analysis was

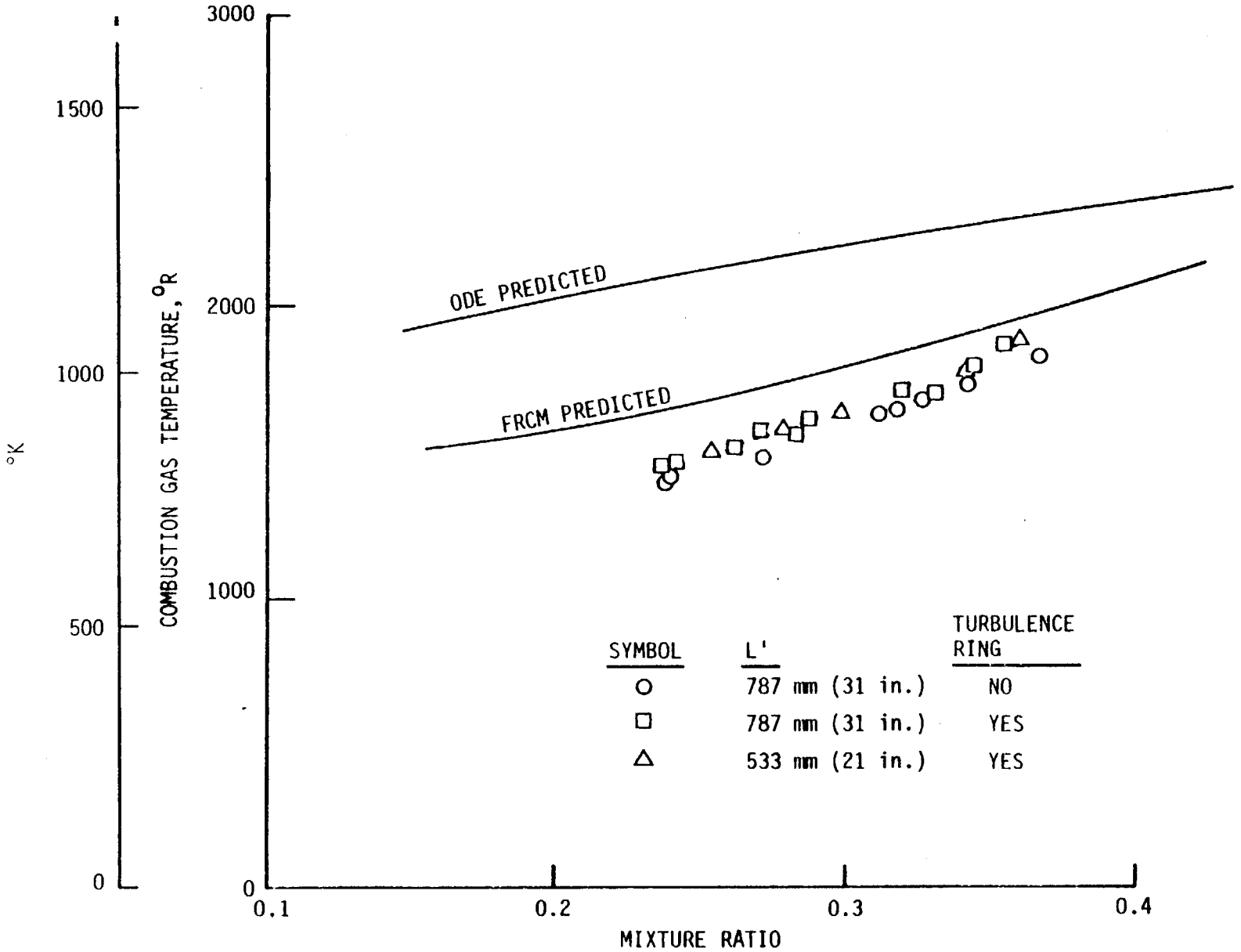

Figure 86. Comparison of Measured to Predicted Gas Temperature - EDM Injector

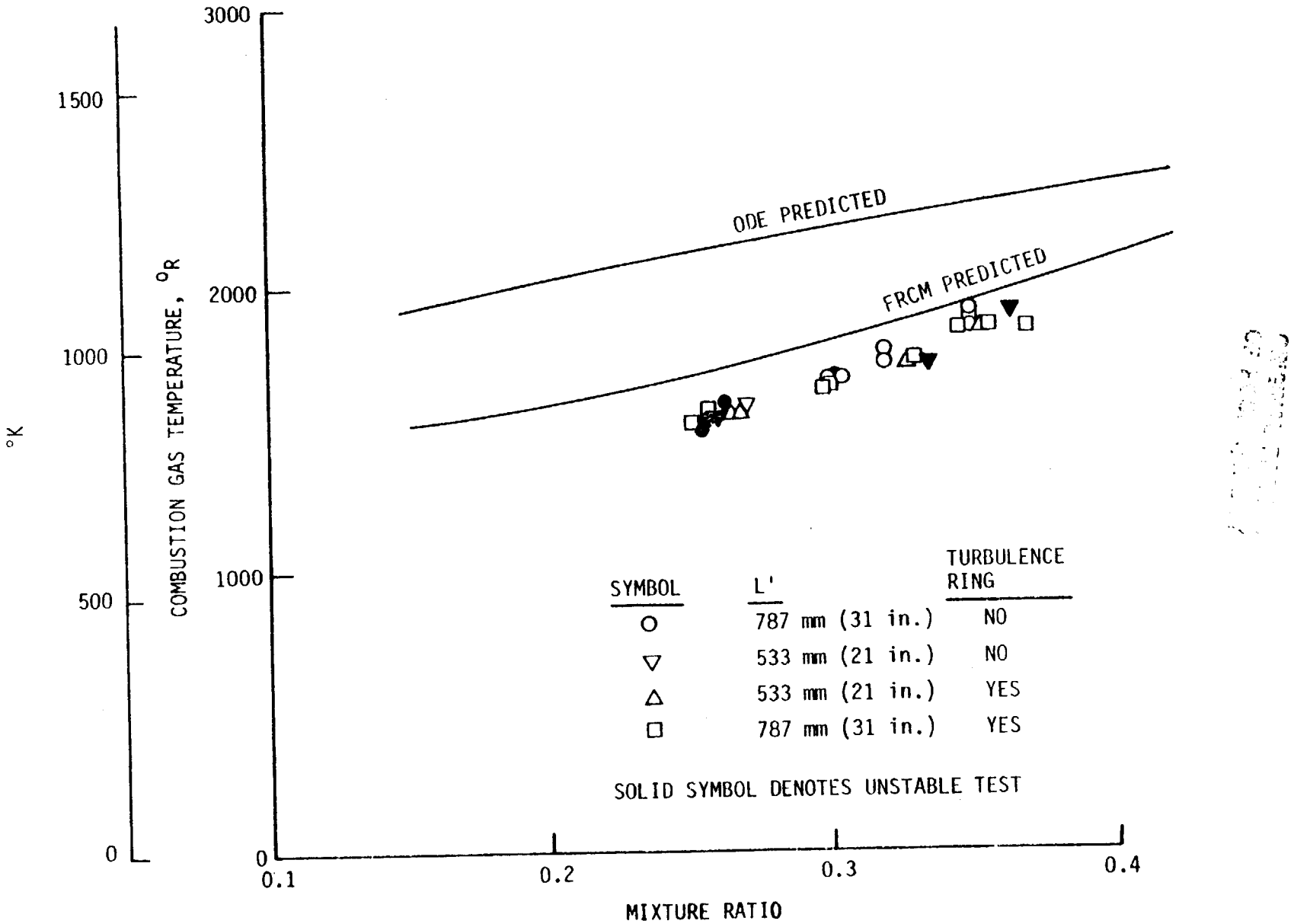

Figure 87. Comparison of Measured to Predicted Gas Temperature - Platelet Injector

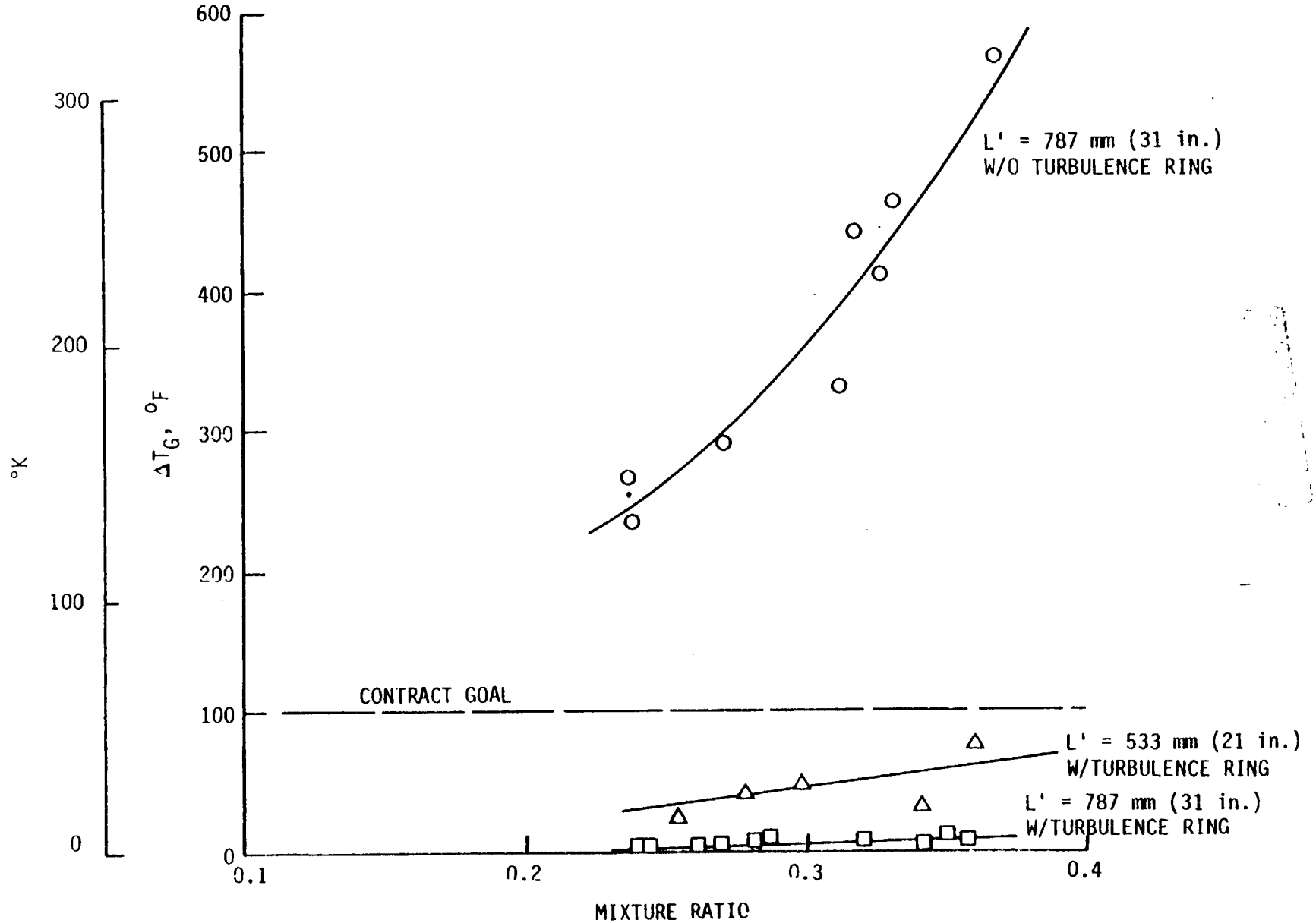

Figure 88. Gas Temperature Uniformity - EDM Injector

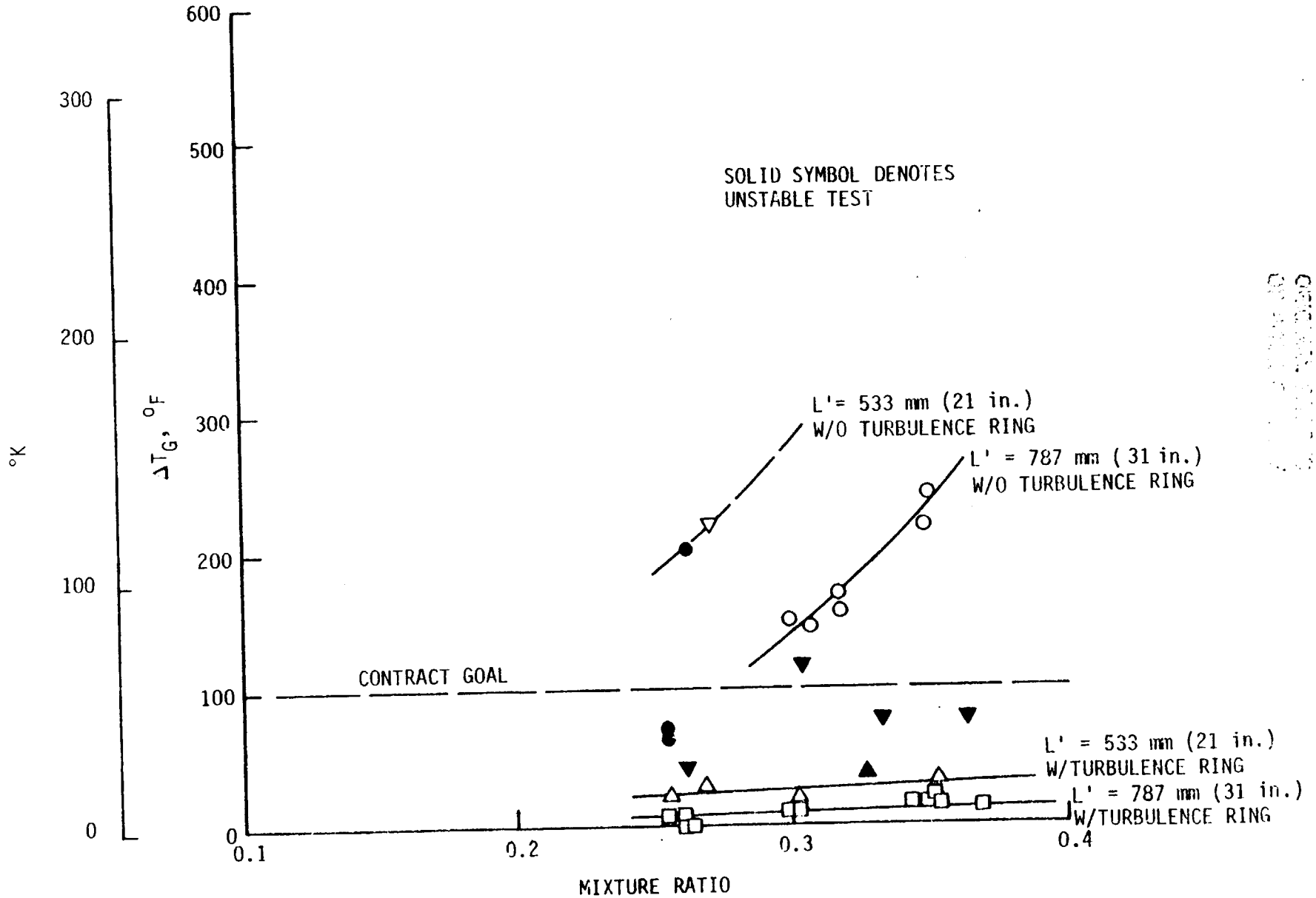

Figure 89. Gas Temperature Uniformity - Platelet Injector

TABLE XIV

FUEL-RICH PREBURNER COMBUSTION STABILITY SUMMARY

Test	Data Point	Injector	L' mm (in.)	Turbulence Ring	Pc MN/m^2 (psia)	MR	Freq. (Hz)	Mode	Amplitude MN/m^2 (psi)
-015	4	Platelet	787.4 (31)	No	13.5 (1958)	0.255	590	2L	2.21 (320)
-016	1	Platelet	787.4 (31)	No	15.2 (2204)	0.304	680	2L	0.69 (<100)
	2	Platelet	787.4 (31)	No	15.2 (2208)	0.255	600	2L	2.21 (320)
-018	1	Platelet	533.4 (21)	No	15.2 (2208)	0.304	540	1L	2.34 (340)
	2	Platelet	533.4 (21)	No	17.3 (2502)	0.365	590	1L	2.34 (340)
	4	Platelet	533.4 (21)	No	13.7 (1991)	0.261	500	1L	1.93 (280)
	5	Platelet	533.4 (21)	No	12.7 (1842)	0.335	520	1L	2.34 (340)
-019	1	Platelet	533.4 (21)	Yes	15.2 (2200)	0.303	550	1L	0.69 (<100)
	4	Platelet	533.4 (21)	Yes	13.6 (1972)	0.257	500	1L	0.69 (<100)
	5	Platelet	533.4 (21)	Yes	12.8 (1851)	0.327	515	1L	2.21 (320)

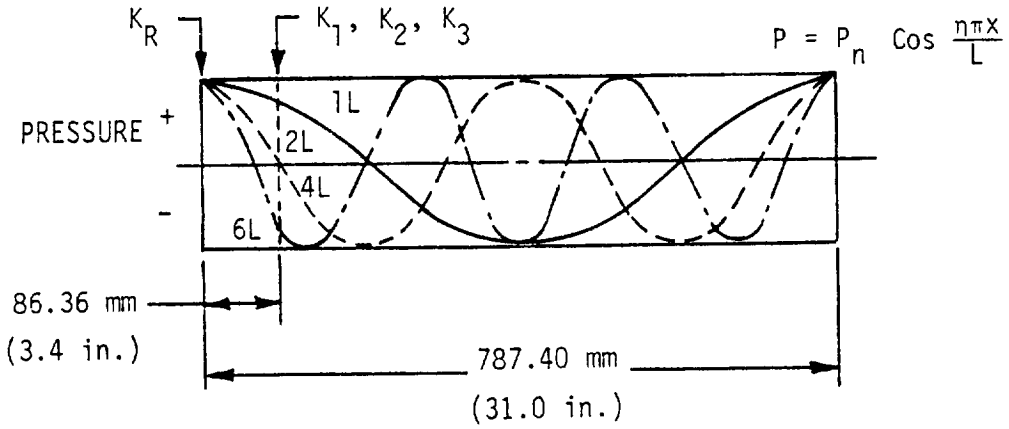

AMPLITUDES MEASURED FROM SPECTRAL DENSITY PLOTS

	2L 600 HZ	4L 1200 HZ	6L 1800 HZ
K_R	84	18	14
K_1	14.5	0.8	2.2
K_3	17.3	0.7	2.5

MEASURED AMPLITUDE RATIOS

	P_{2L}/P_{2L}	P_{4L}/P_{2L}	P_{6L}/P_{2L}
K_R	1.0	0.22	0.17
K_1	1.0	0.056	0.15
K_3	1.0	0.035	0.14

PREDICTED AMPLITUDE RATIOS

K_1, K_3	1.0	0.049	-0.011

Figure 90. Comparison of Measured to Predicted Pressure Amplitude Ratios

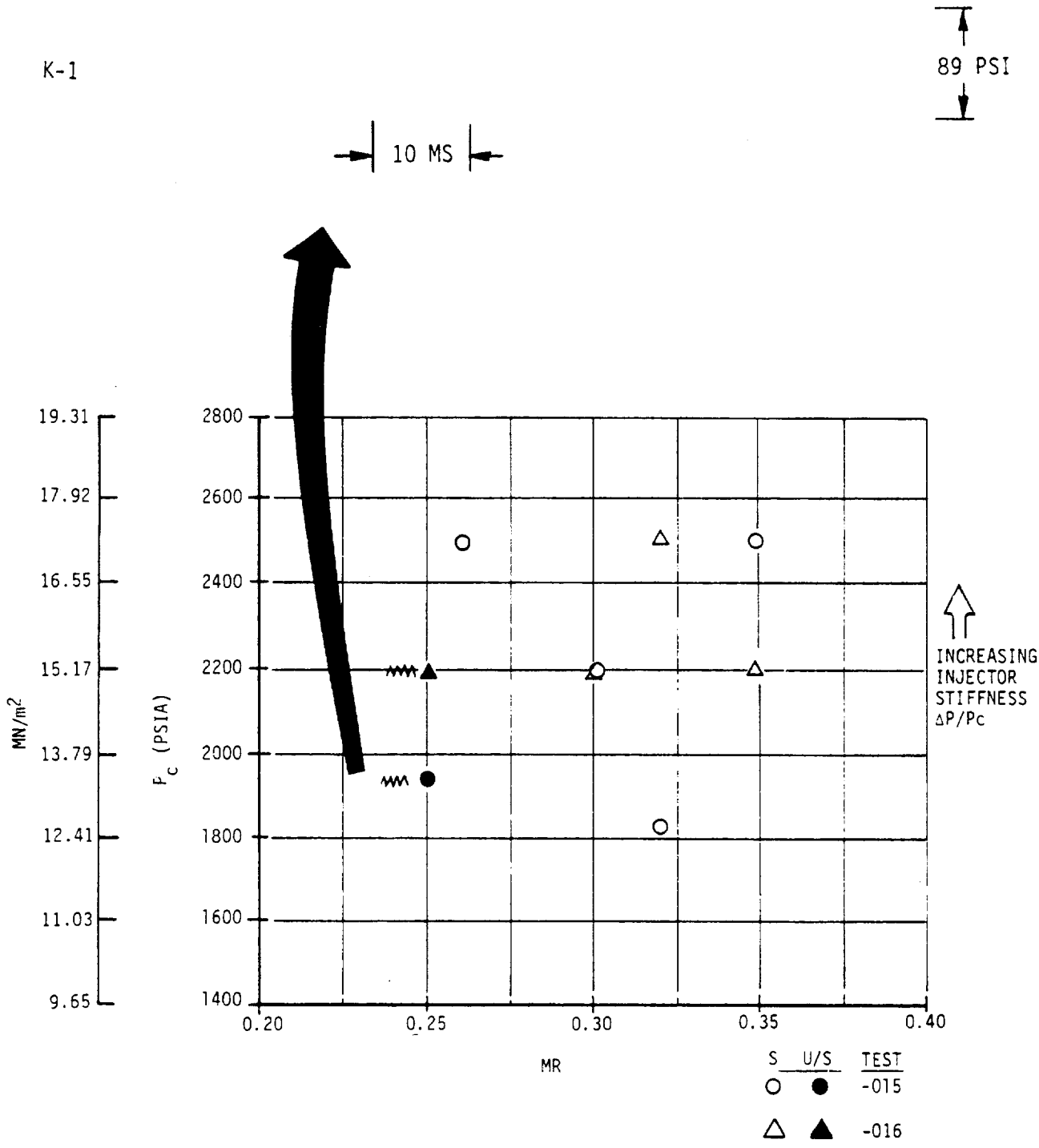

Figure 91. Effect of Mixture Ratio (MR) and Chamber Pressure (Pc) on Longitudinal Stability

made to predict the effect of mixture ratio and chamber length on longitudinal stability. The results are shown in Figure 92. The analysis predicted that reducing the chamber length from 787 mm (31 in.) to 533 mm (21 in.) would shift the instability from a 2L to a 1L mode of instability at the high-MR condition. Test -018 confirmed this prediction.

Further analysis showed that the addition of a turbulence ring would provide damping of the longitudinal mode oscillations. The effect of the turbulence ring on the damping is illustrated in Figure 93. The best damping is achieved by placing the turbulence ring at the velocity antinodes, as illustrated. However, the turbulence ring was designed to be placed 127-mm (5-in.) from the injector face based on thermal compatibility problems. Analysis indicated that impingement of unvaporized propellant would provide adequate cooling of the turbulence ring at the 127-mm (5-in.) chamber length. Placement further downstream may not provide adequate cooling of hot streaks, resulting in thermal compatibility problems. The 787-mm (31- in.) chamber length is predicted to be more stable than the 127-mm (21-in.) chamber length as confirmed by Tests -019 and -020. The 127-mm (21-in.) chamber was more stable with the turbulence ring. The 787-mm (31-in.) chamber was stable at all operating conditions with the turbulence ring. It is concluded that longitudinal mode instabilities can be effectively damped with properly selected turbulence rings and chamber lengths.

d. Carbon Deposition and Hardware Erosion

Tests -021 through -029 were run with the turbine and main injector simulators installed as shown in Figure 94 to evaluate carbon buildup (coking). The preburner was instrumented to measure pressures upstream and downstream of the turbine simulator to detect changes in the simulator effective flow areas. Area reductions are interpreted to be an indication of carbon buildup.

An example of a typical test result is shown in Figure 95 for Test -027. The combustor pressures upstream of the turbine simulator (Pc-1 and Pc-2) are seen to slowly rise in relation to the downstream pressures (Pc-3 and Pc-4). The gas temperature, flowrates, and mixture ratio are steady, indicating a reduction in the simulator flow area. The turbine simulator effective flow areas were calculated by using the measured parameters and the isentropic flow relationships. Adjustments to the measured flow were made to account for the unvaporized fuel. These adjustments were made on the basis of the predicted fuel vaporization efficiency. Multiple points were calculated during each test to determine trends. These results are plotted in Figure 96.

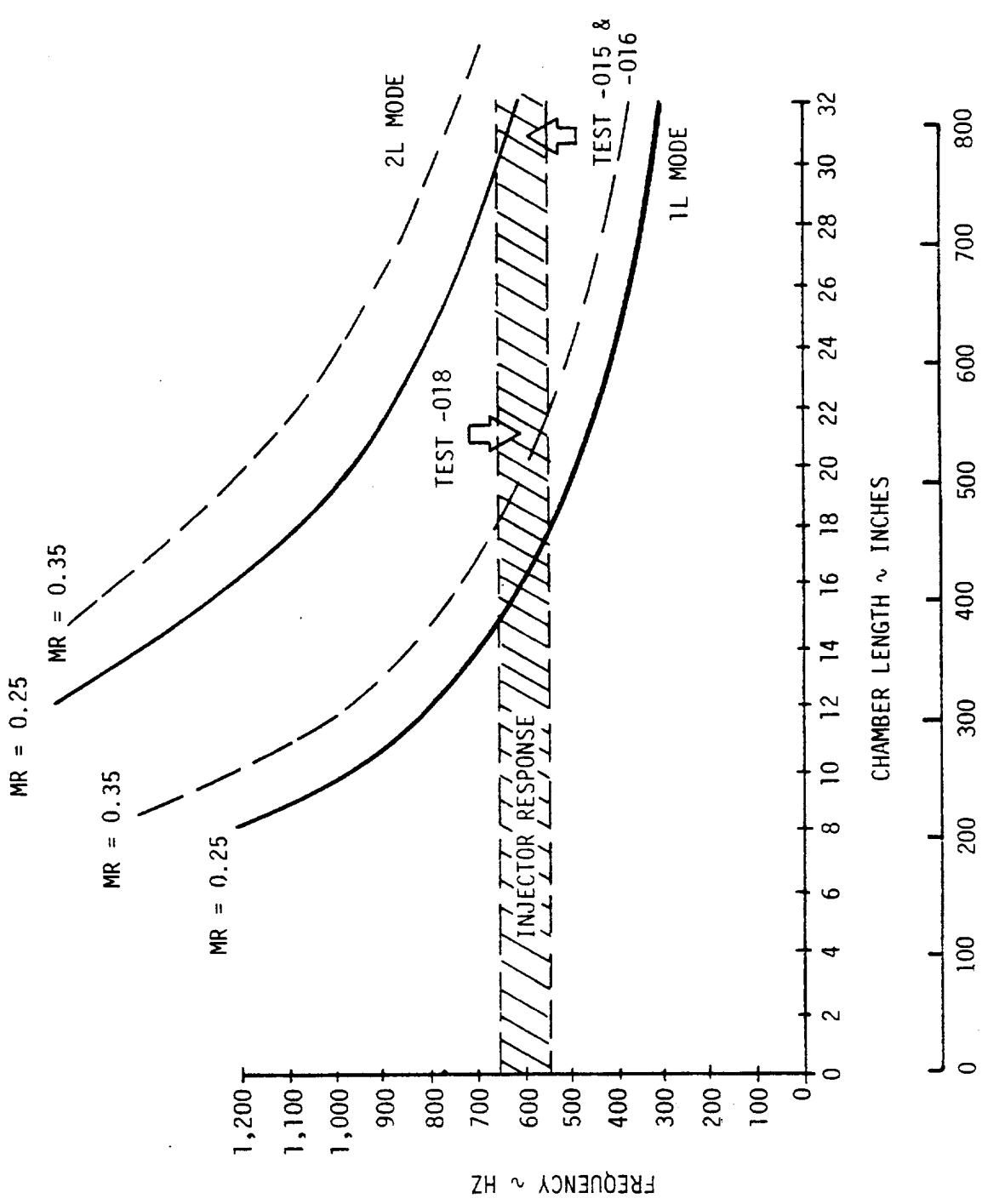

Figure 92. Predicted Effect of Mixture Ratio (MR) and Chamber Length on Longitudinal Stability

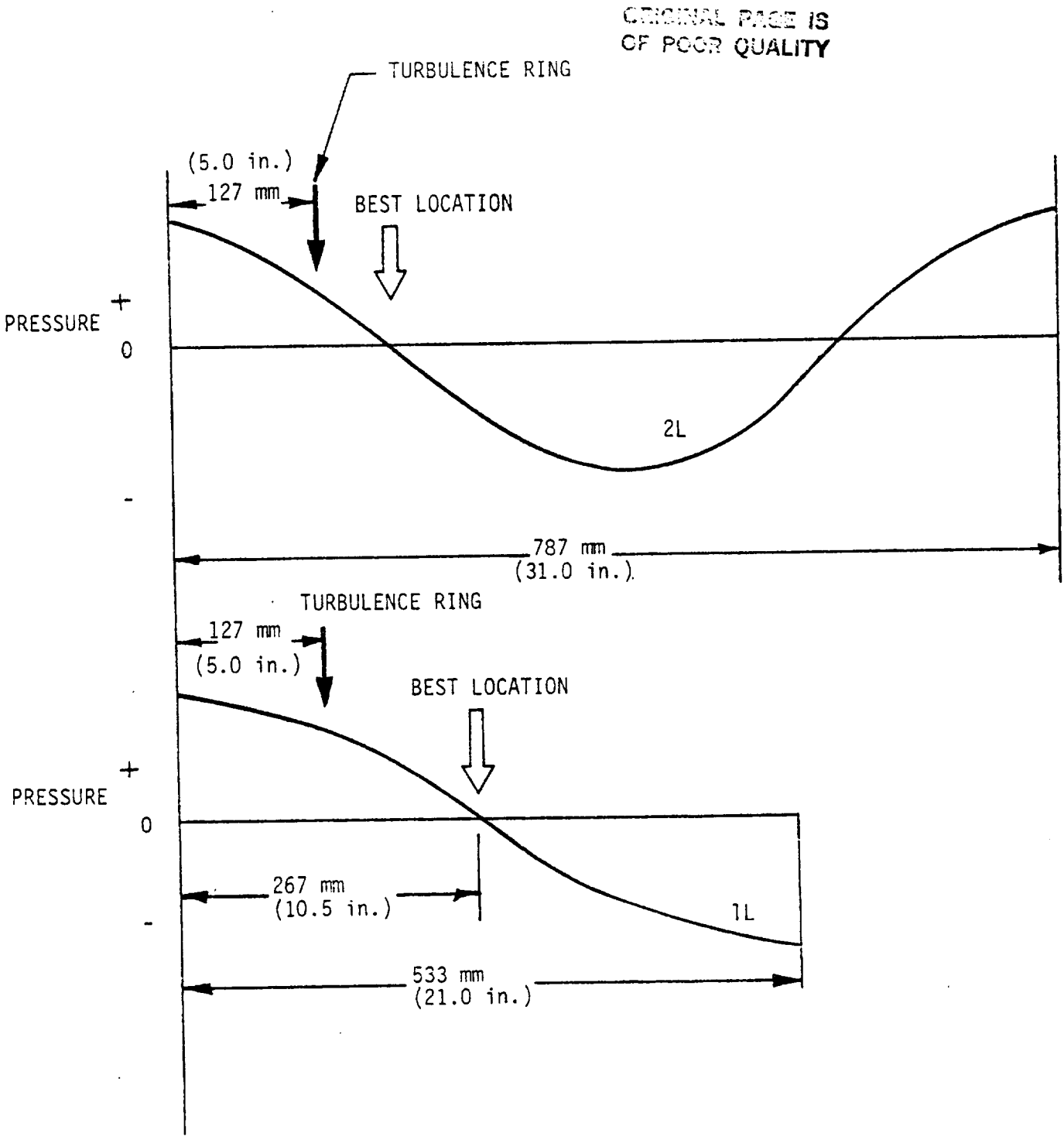

Figure 93. Effect of Turbulence Ring on Longitudinal Mode Damping

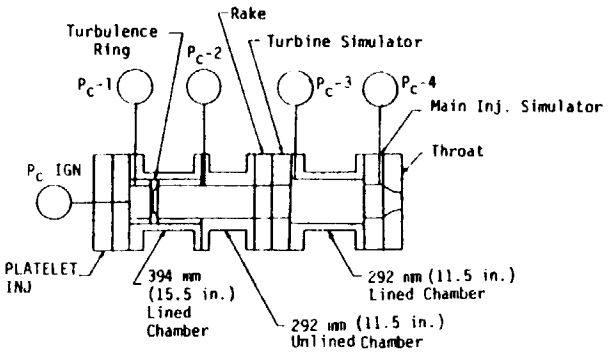

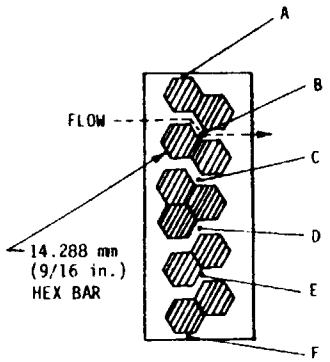

TEST	GAP WIDTH mm (in.) A	B	C	D	E	F
-021	0.127 (0.005)	4.877 (0.192)	3.531 (0.139)	3.556 (0.140)	4.699 (0.185)	0.762 (0.030)
-020,-029	0.127 (0.005)	3.683 (0.145)	3.531 (0.139)	3.556 (0.140)	3.683 (0.145)	0.762 (0.030)

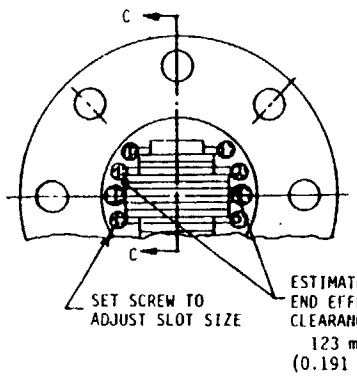

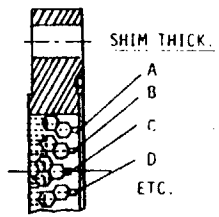

TEST	SHIM THICKNESS mm (in.) A	B	C	D	E
-021	0	0	1.676	0	0
	0	0	(0.066)	0	0
-022,-029	1.905	0	1.676	0	1.905
	(0.075)	0	(0.066)	0	(0.075)

NOMINAL TURBINE SIMULATOR GEOMETRIC FLOW AREA

TEST 21 1512 mm^2 (2.344 in.^{2})

TESTS 22-29 1439 mm^2 (2.231 in.^{2})

Figure 94. Fuel-Rich Preburner Turbine Simulator Test Configurations

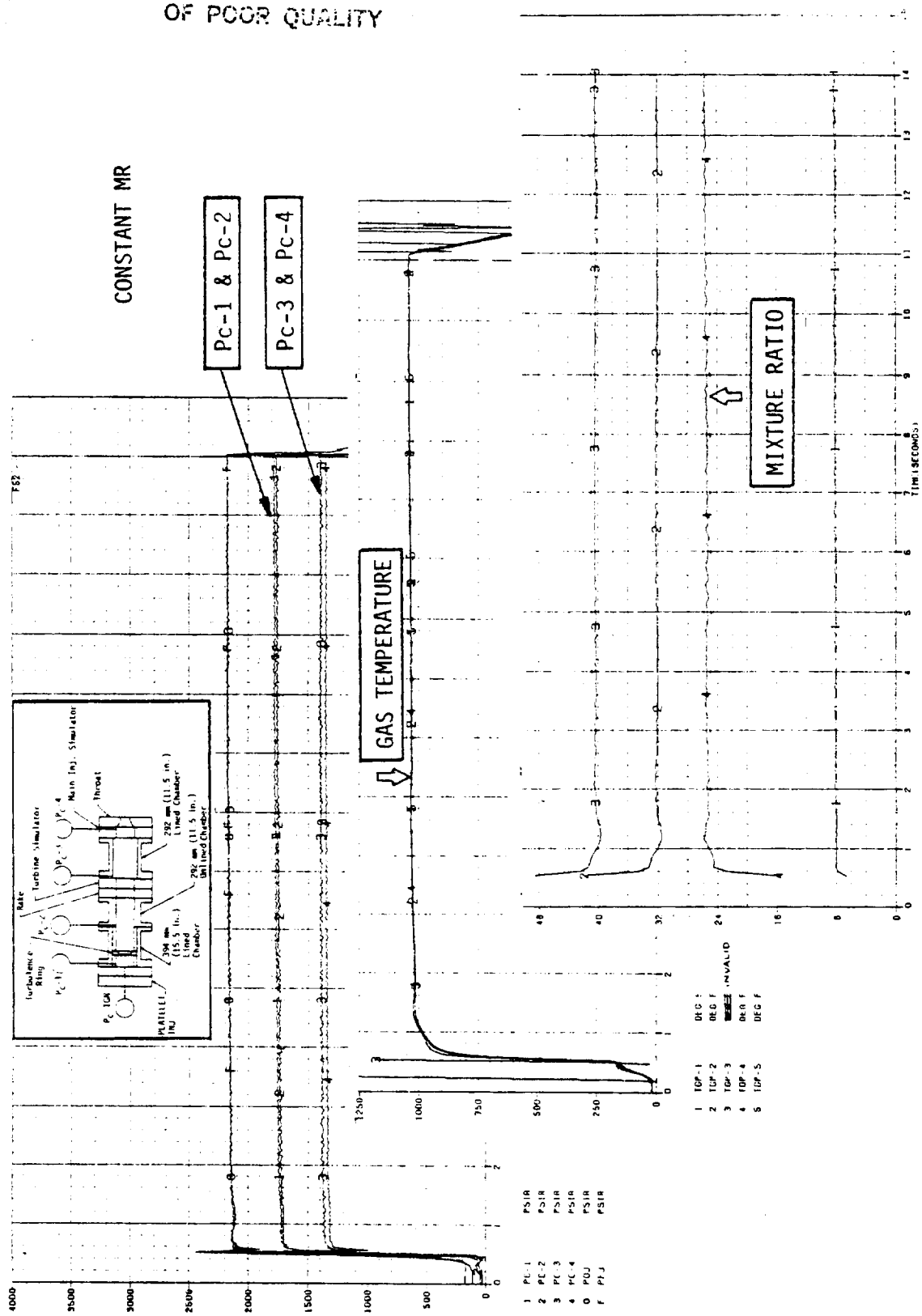

Figure 95. Typical Carbon Formation Test Results

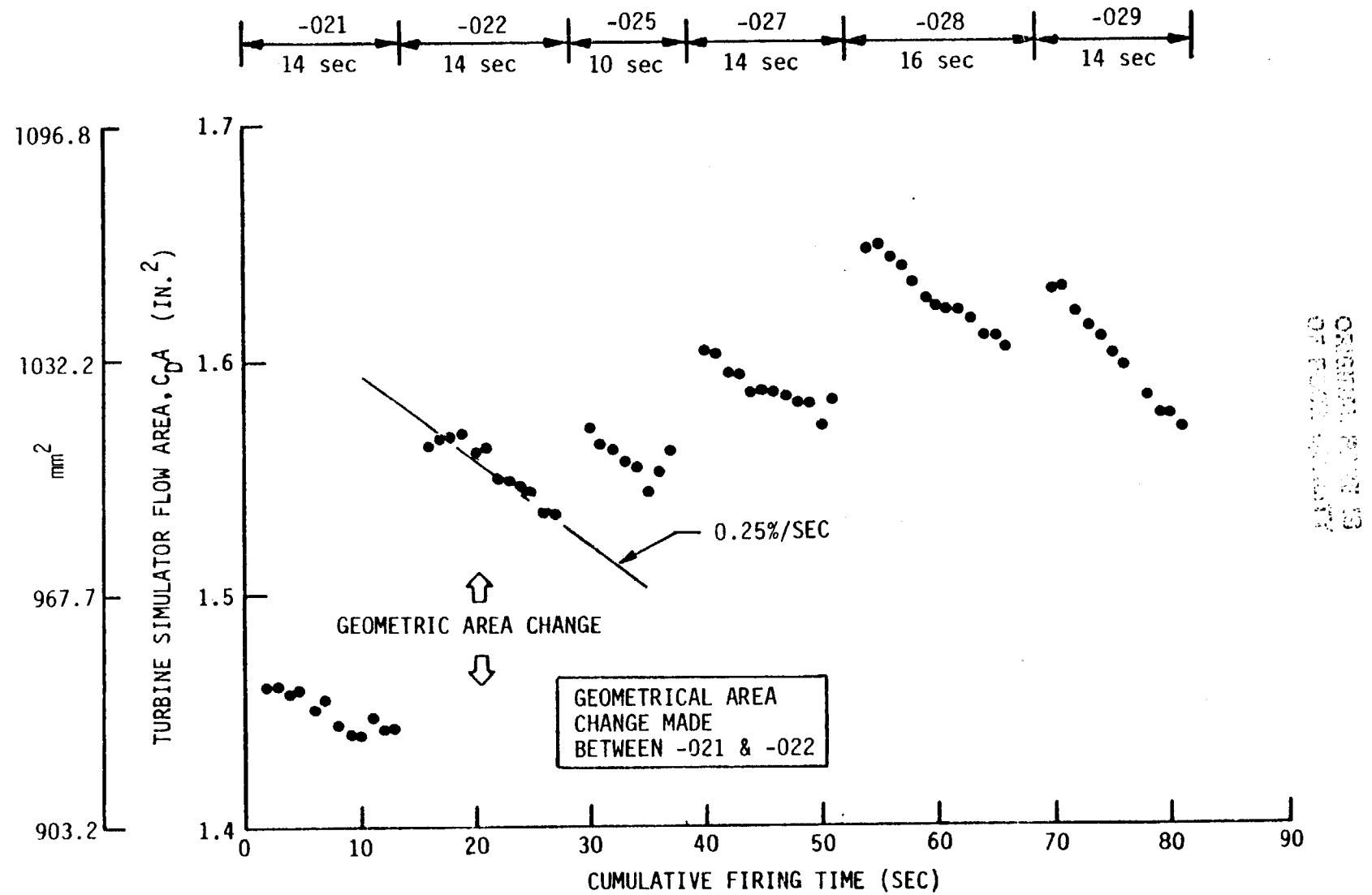

Figure 96. Turbine Simulator Effective Area Time History

IV, C, Data Analysis (cont.)

The data indicate slight reductions in flow area during each firing and an increase in flow area from test to test. The area reductions during the test are due to both carbon buildup and thermal expansion of the turbine simulator blades. It is estimated that the blades should reach thermal equilibrium in about 6 to 7 seconds, i.e., at about half of the test duration. It is estimated that the maximum area reduction due to thermal growth of the simulator blades would be about 2.5% as compared to a maximum measured reduction of 3.5%. It is difficult to differentiate the two effects since no clear-cut change in the slope of flow versus time curve occurs at 6 to 7 seconds. Also, there are no obvious mixture ratio effects, as shown in Figure 97. If the area reduction is due primarily to thermal effects, it is expected that the slope of the flow area versus mixture ratio curve would be negative. As the MR is increased, the flow area would decrease due to higher temperatures and greater expansion. However, the slope appears to be positive, indicating carbon deposition effects similar to those on the Titan I gas generator. The carbon buildup effects are also clouded by the fact that no significant carbon deposits were found during post-test examinations and that erosion of the turbine blades had occurred. If the measured area reductions are due to carbon buildup, then the indicated rates are 2 to 4 times those observed in the Titan I gas generator. The indicated area reductions vary from 0.13 to 0.25%/sec as compared to 0.06%/sec for the Titan I gas generator.

Severe erosion of the turbine simulator blades and housing was observed to occur progressively from Test -021 to Test -029. The main injector simulator and the nozzle were also badly eroded, with the erosion having the appearance of cavitation damage. The turbine blade erosion is evident by comparing the post-test photos of Tests -021 to -029, as shown in Figures 98 and 99. Figure 100 shows the blade areas incurring the most damage. It appears that the areas of high velocity impingement suffer the worst erosion. This effect is also seen in the main injector simulator and nozzle, as shown in Figures 101 and 102. Figure 102 shows that the nozzle plate is severely eroded in 8 areas directly under orifices in the main injector simulator plate. High velocity impact seem to aggravate erosion. As shown in Figure 103, the nozzle throat is also eroded, with the erosion resembling cavitation damage. This form of nozzle throat erosion was observed on all of the fuel-rich testing.

One of the eroded turbine blades was sectioned for metallurgical examination. A photograph of the section is shown in Figure 104, indicating that a definite change in the grain structure has occurred at the blade surface. A micro-hardness test has revealed that the surface layer ($\approx$0.025 mm [0.001 in.]) is softer than the parent material. Softening of the surface indicates a decarburization of the material. Although decarburization was also observed on the surfaces not subjected to high velocity flows, there was no evidence of erosion on the surfaces. It is concluded that the

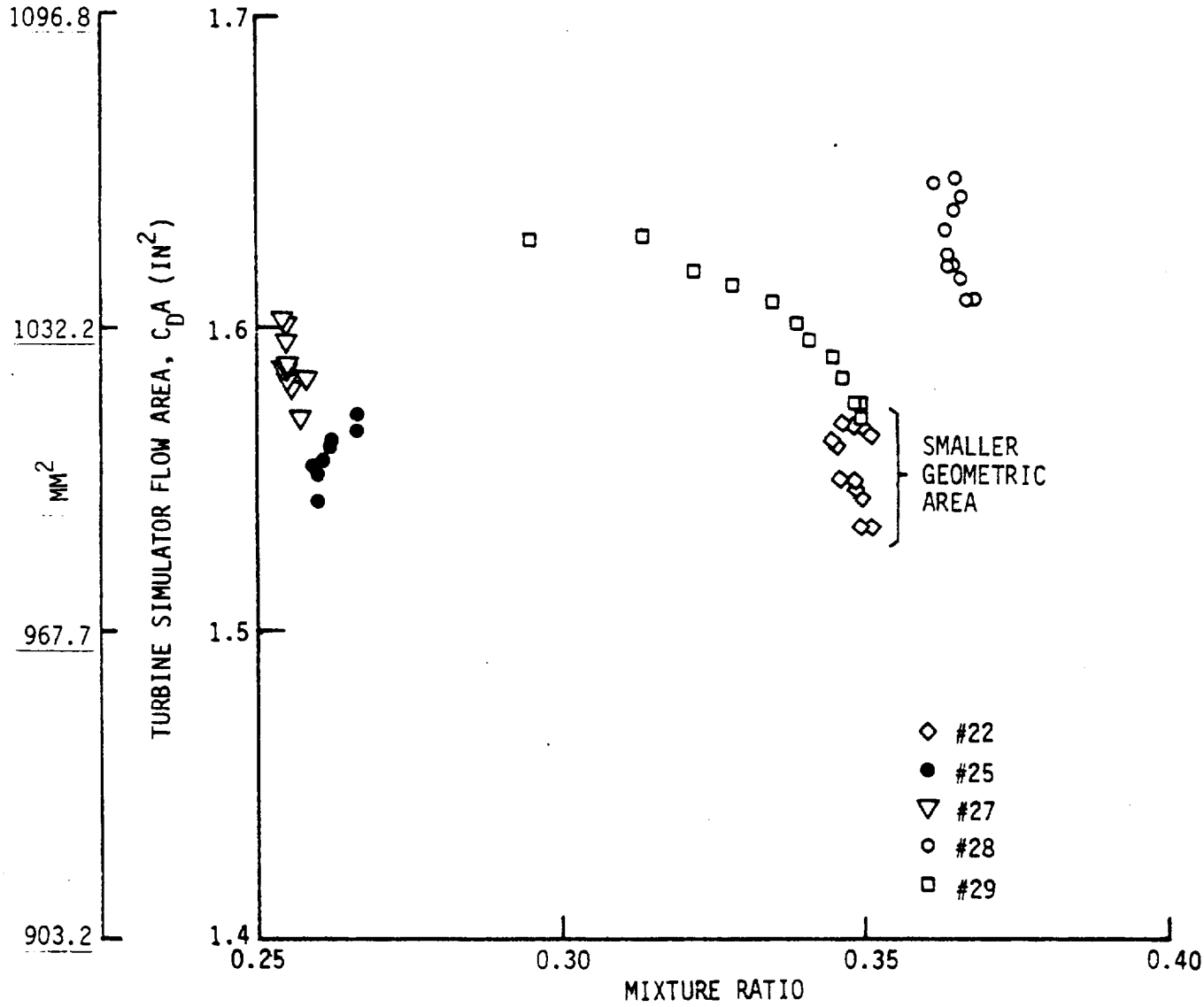

Figure 97. Turbine Simulator Area Versus Mixture Ratio

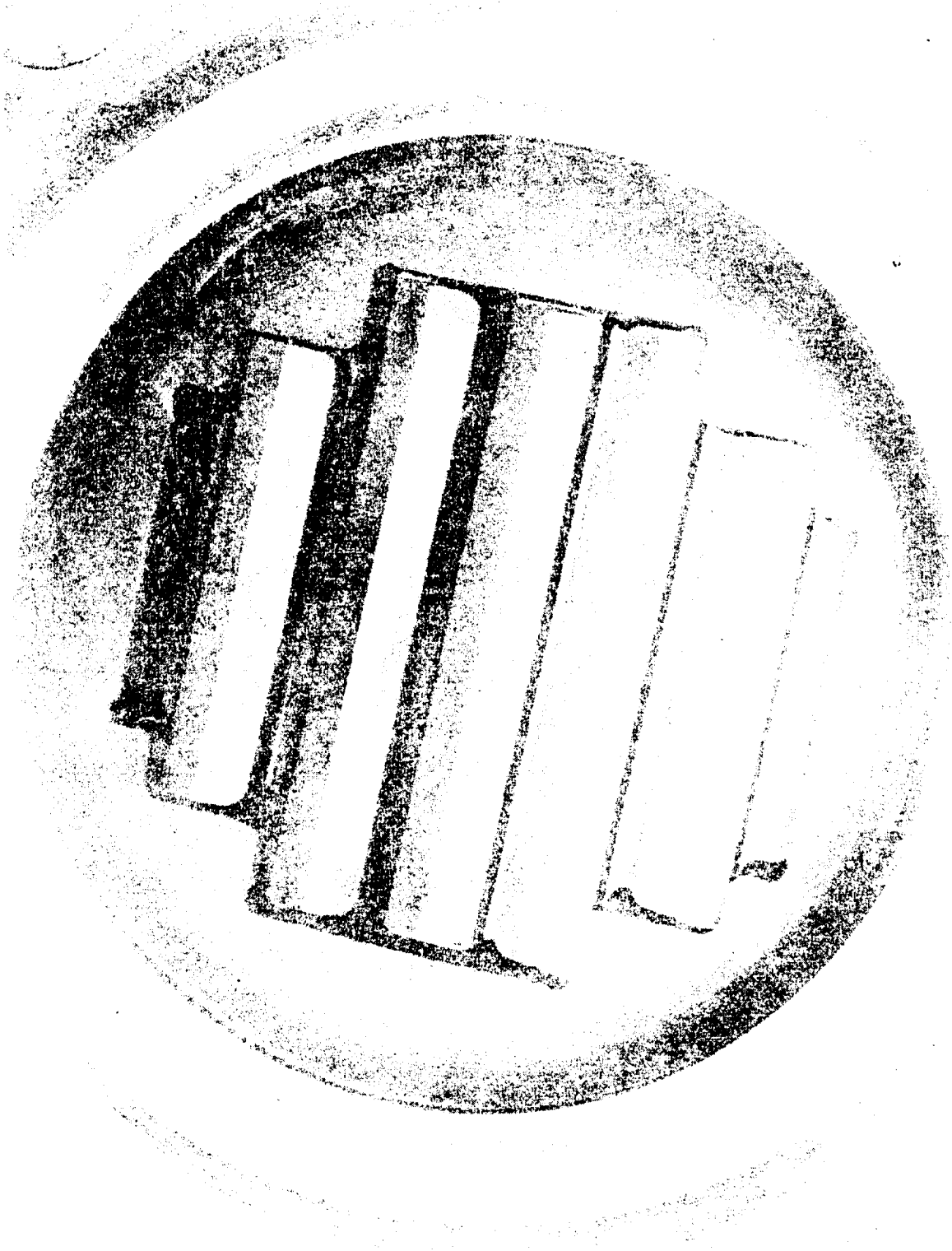

Figure 98. Downstream Side of Turbine Simulator - Post-Test -021

Figure 99. Downstream Side of Turbine Simulator - Post-Test -029

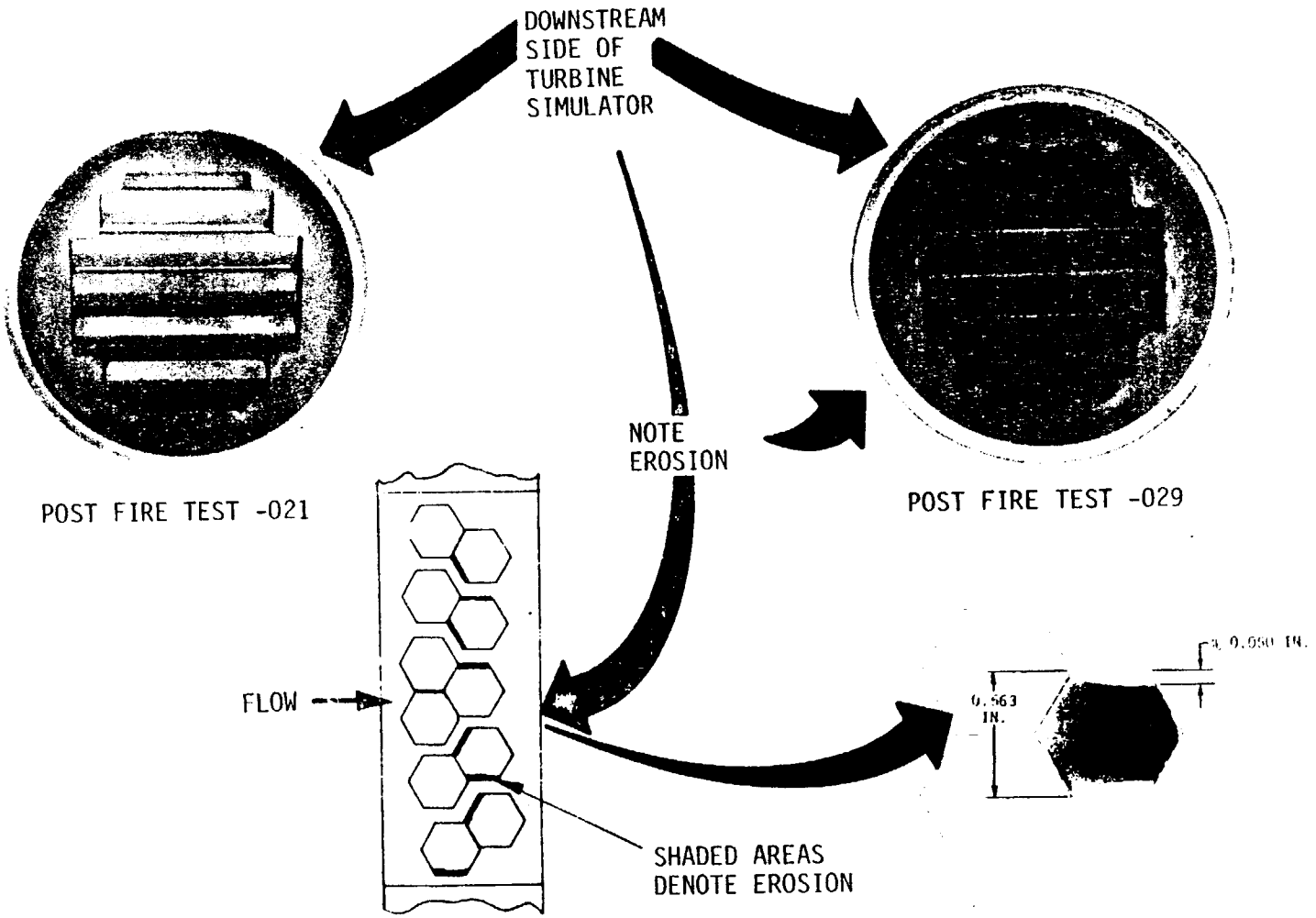

ORIGINAL PAGE
BLACK AND WHITE PHOTOGRAPH

Figure 100. Turbine Simulator Blade Erosion

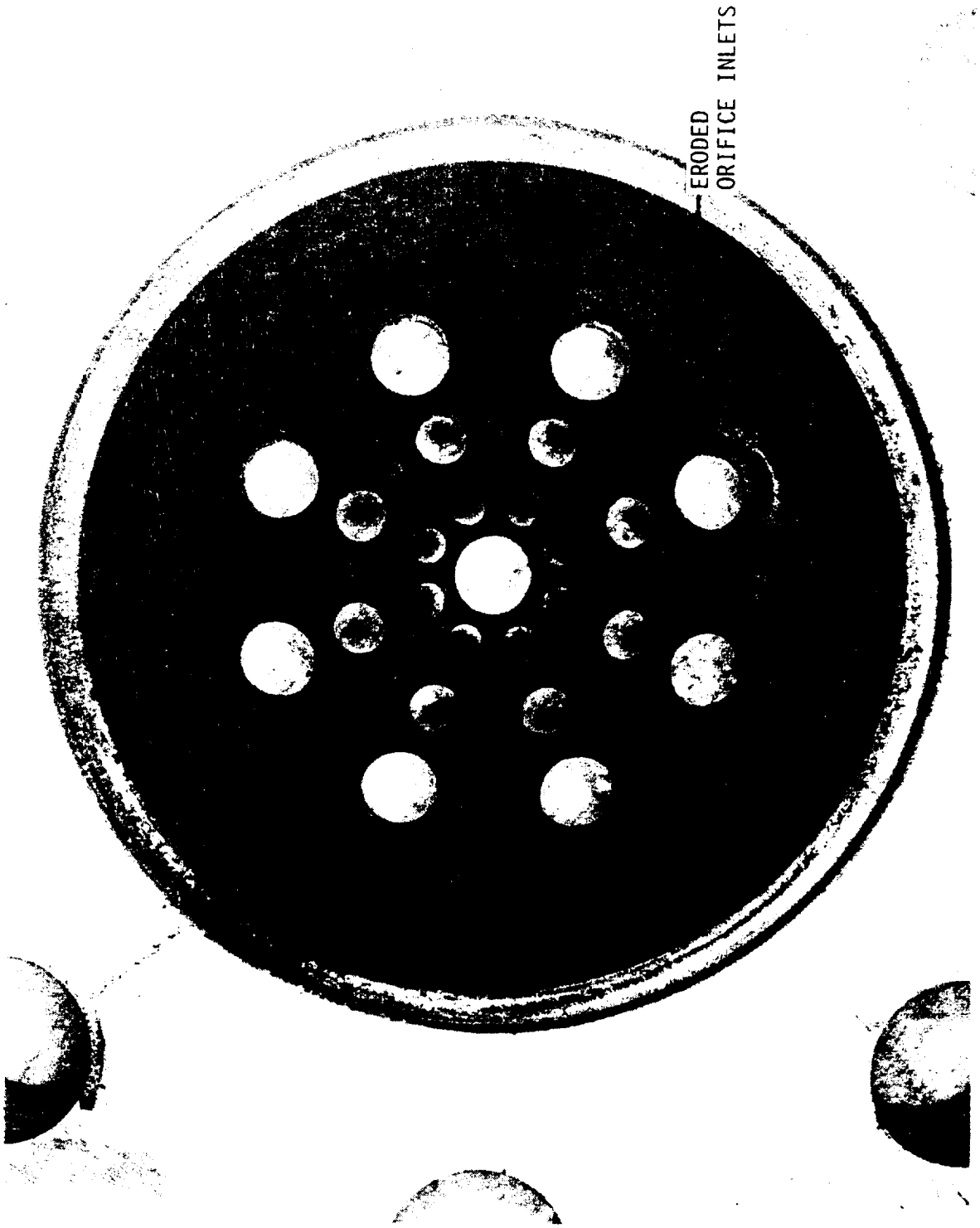

Figure 101. Main Injector Simulator Erosion - Post Test -029

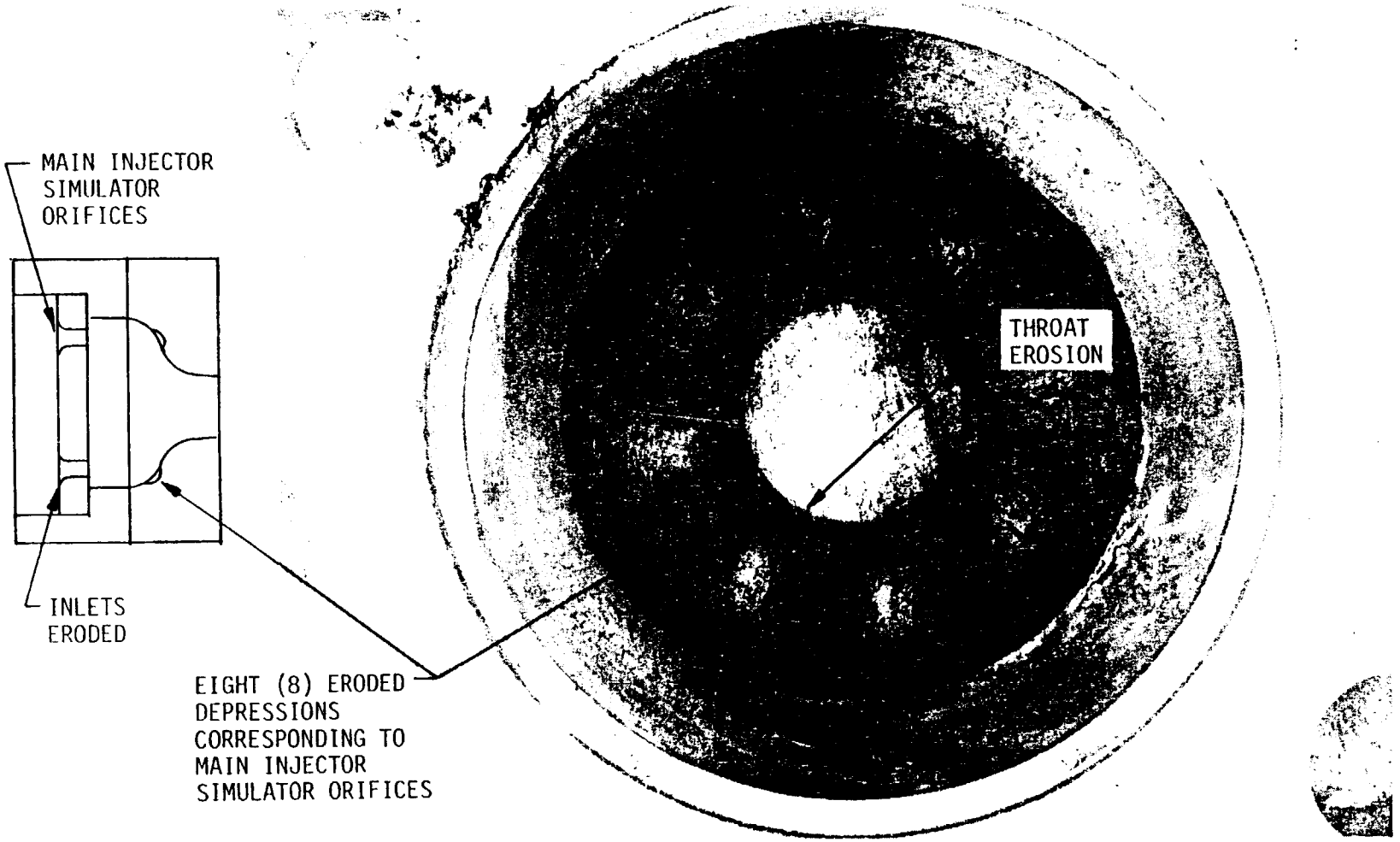

Figure 102. Nozzle Plate Erosion - Post Test -029

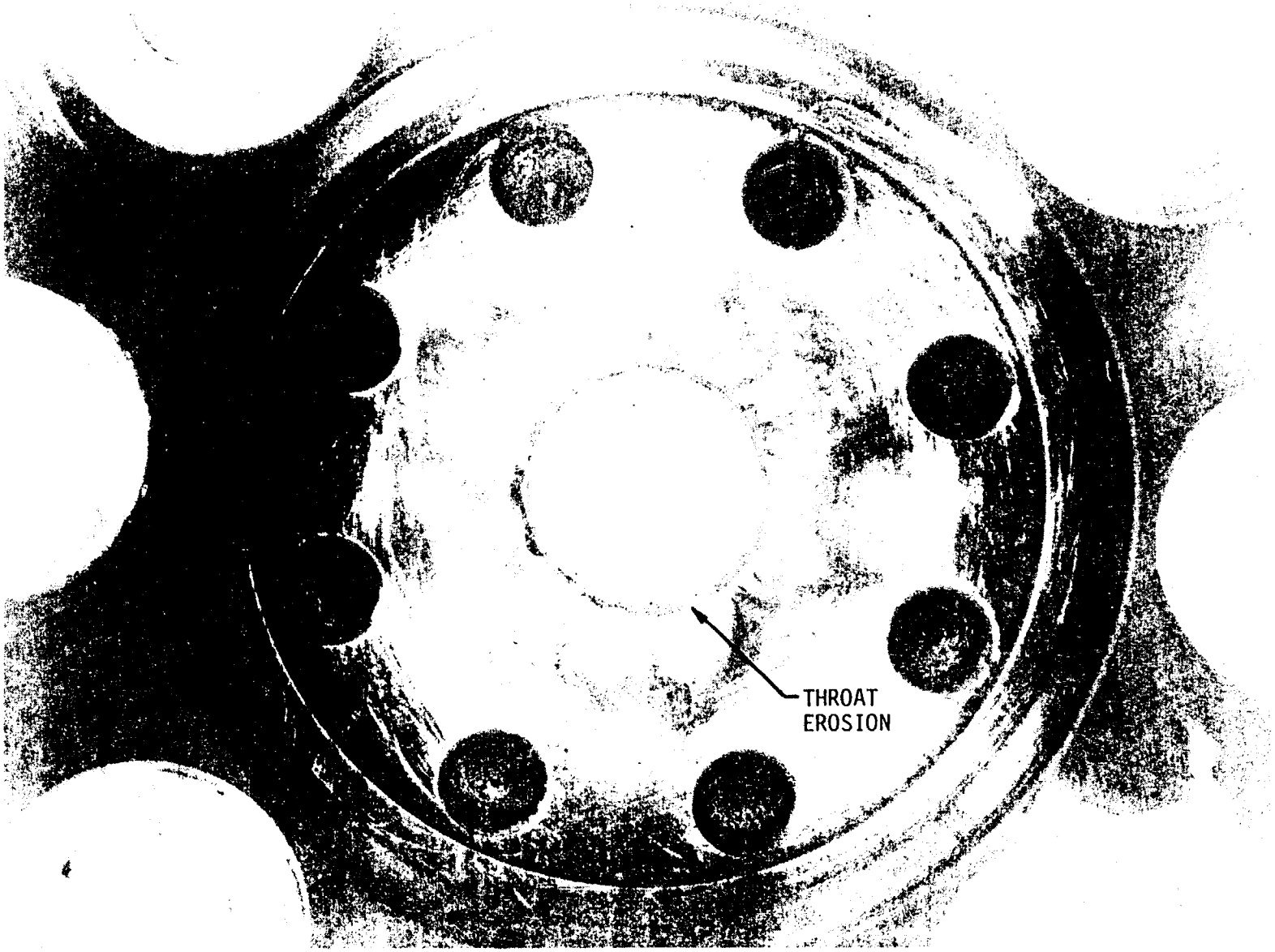

Figure 103. Nozzle Throat Erosion - Post -029

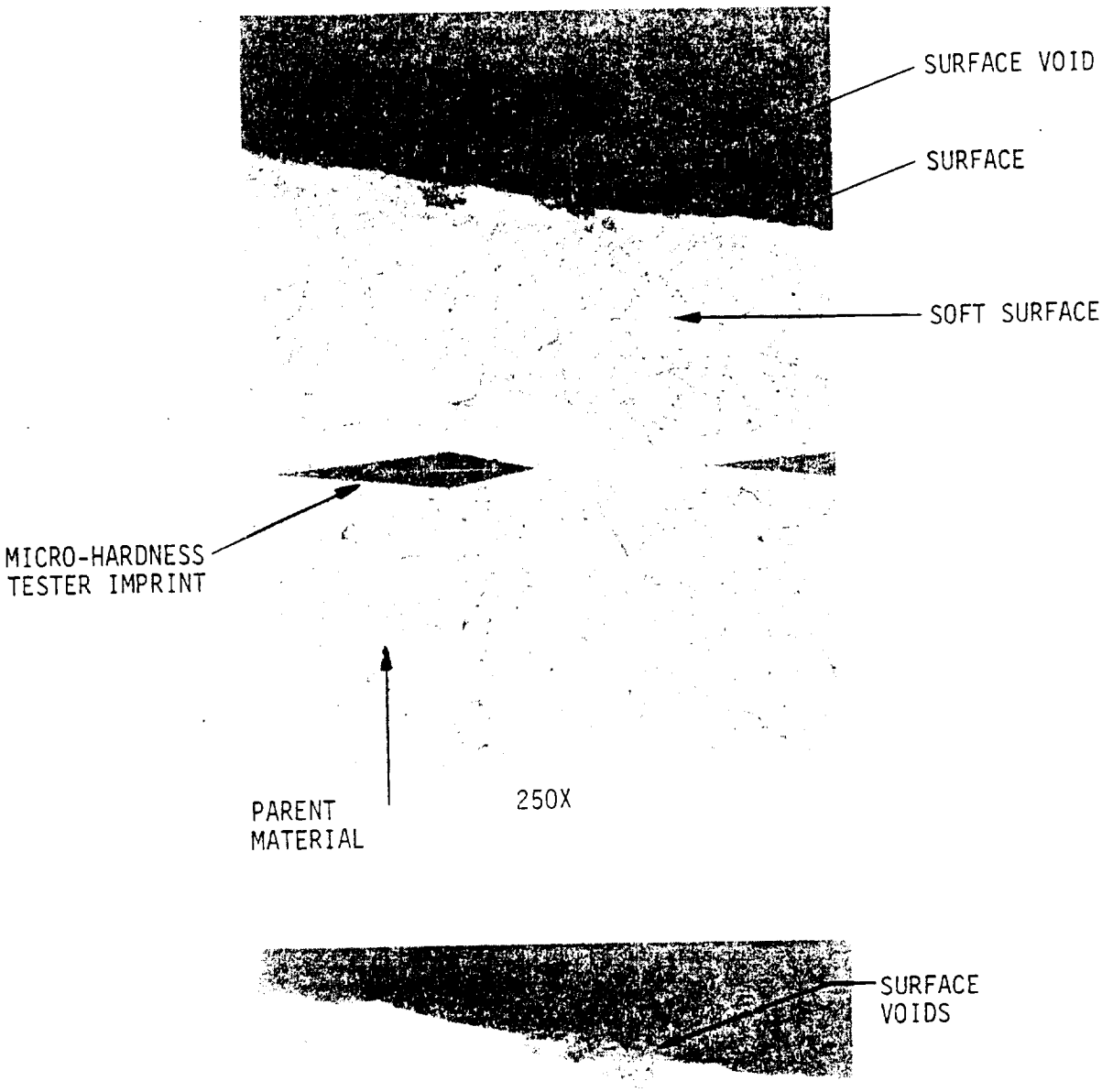

Figure 104. Turbine Simulator Blade Section - Micro Photograph

erosion is a result of the hydrogen-rich (20%) gas reacting with the carbon within the interstitial grain boundaries. The carbon loss reduces strength and causes the material to be vulnerable to unvaporized liquid droplet impact erosion. It is recommended that a laboratory materials study be conducted to identify materials less susceptible to fuel-rich gas erosion.

2. Oxidizer-Rich Preburner Data Analysis

The oxidizer-rich data consist of performance and stability data only. No gas temperature uniformity data were acquired due to probe failure early in the test run. The oxidizer-rich C* performance data are summarized in Table XV.

The C* performance is plotted in Figure 105. It is apparent that the ODE prediction adequately describes the anticipated oxidizer-rich C* performance. The platelet injector C* performance is noticeably lower than that of the EDM injector. This may be a result of the short test durations (≈1/2 sec).

The predicted combustion gas temperature versus mixture ratio is plotted in Figure 106. Also indicated are the operating mixture ratios for each of the oxidizer-rich tests. Serious erosion of an uncoated nozzle on Test -023 and uncoated rake probes and housings on Test -024 would seem to indicate that gas temperatures in excess of 1111°K (2000°R) are to be avoided with uncoated metals. Published metal ignition data are shown in Figure 107. The nozzle wall temperature is predicted to reach a maximum of 1033°K (1860°R) in a 1/2 second test. These published data would indicate that temperatures of up to 1477 to 1533°K (2660 to 2760°R) can be tolerated by uncoated stainless steels. However, these data are for static (nonflowing) oxygen environments. High-oxygen gas velocities appear to significantly reduce metal ignition temperatures. It is recommended that a laboratory materials study be conducted to define the effect of oxygen gas velocity on metal wall ignition.

The stability data are summarized in Table XVI. The EDM injector exhibited 1L mode oscillations at 650 Hz in a 447-mm (17.6-in.) L' chamber without use of a turbulence ring (Test -014). The installation of a 76.2-mm (3.0-in.) turbulence ring 127 mm (5 in.) from the injector face reduced the amplitude (Test -021). Reducing the chamber length from 447 to 345 mm (17.6 to 13.6 in.) stabilized the EDM injector, as had been analytically predicted.

The platelet injector also exhibited 1L mode oscillations in the 447-mm (17.6-in.) L' chambers on Test -018. A 86.4-mm (3.4-in.) diameter turbulence ring had been installed, based on the EDM experience on Test -014.

TABLE XV

OXIDIZER-RICH PREBURNER PERFORMANCE DATA

Test No.	Duration Sec	Pc-1 MN/m^2 (psia)	MR	Injector	L' mm (in.)	Turbulence Ring mm (in.)	C* m/s ft/sec	η_{c^*} (%)
-014	1	13.1 (1905)	36.8	EDM	447 (17.6)	No	787 (2582)	102
-018	1/2	12.7 (1844)	37.1	Platelet	447 (17.6)	86.4 (3.4)	648 (2127)	84.9
-019	1/2	12.9 (1872)	35.8	Platelet	447 (17.6)	76.2 (3.0)	643 (2110)	82.4
-021	1	13.9 (2023)	47.5	EDM	447 (17.6)	76.2 (3.0)	659 (2163)	98.7
-023	1	16.6 (2402)	32.6	EDM	345 (13.6)	76.2 (3.0)	806 (2644)	98.6
-024	1/2	17.2 (2497)	27.2	EDM	396 (15.6)	76.2 (3.0)	-	-

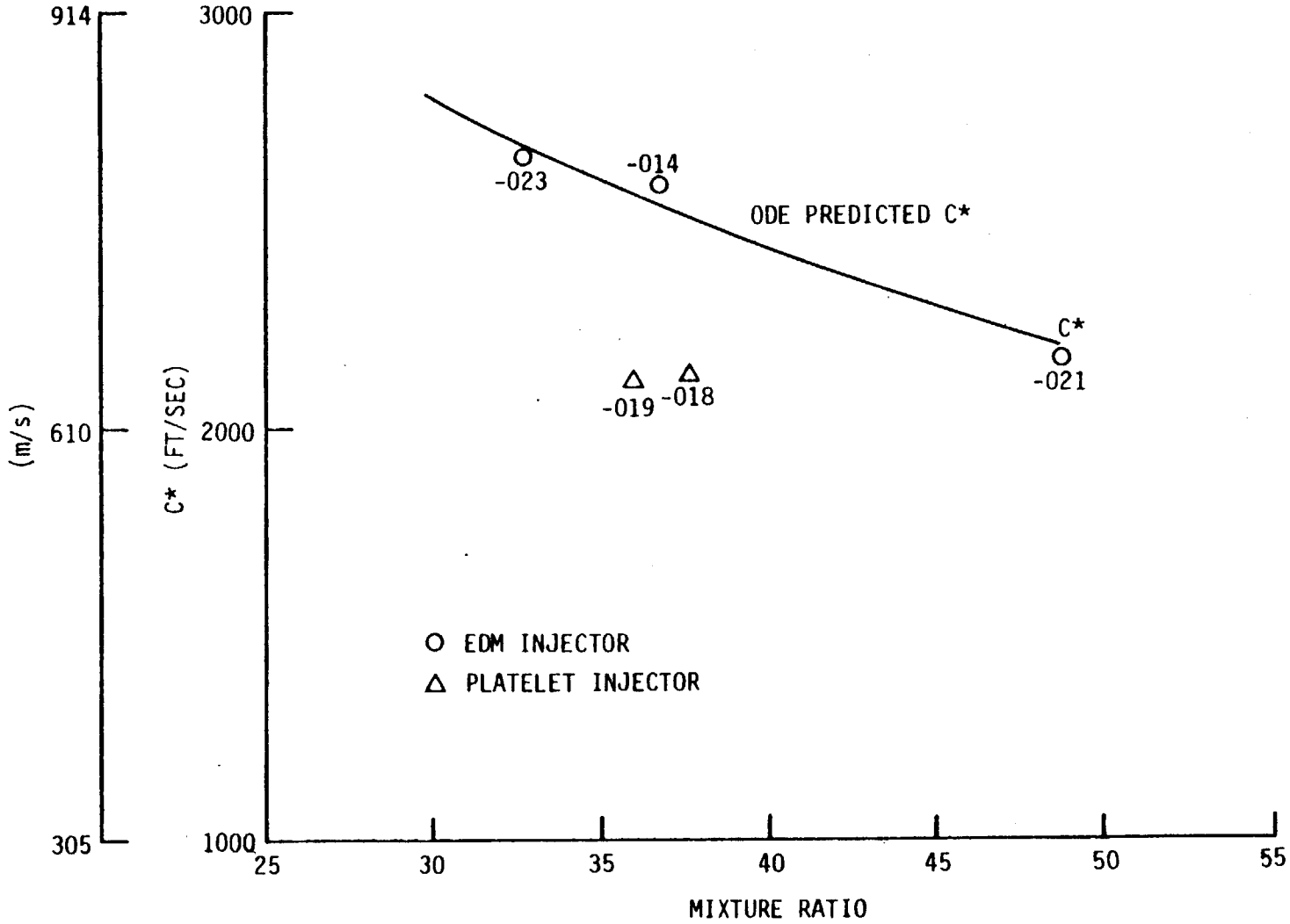

Figure 105. Oxidizer-Rich Preburner, Comparison of Measured to Predicted C*

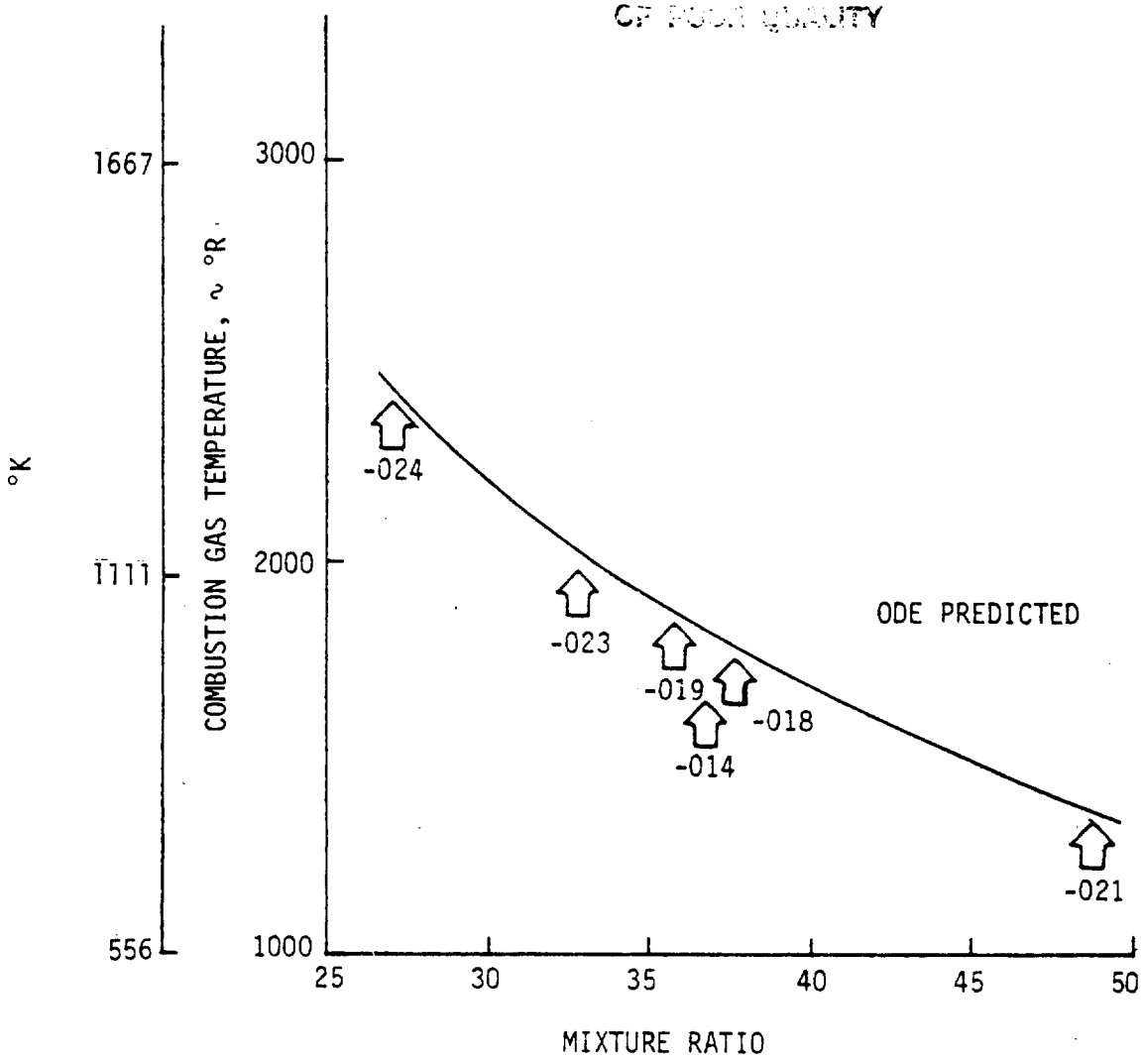

Figure 106. Oxidizer-Rich Preburner, Predicted Combustion Gas Temperatures

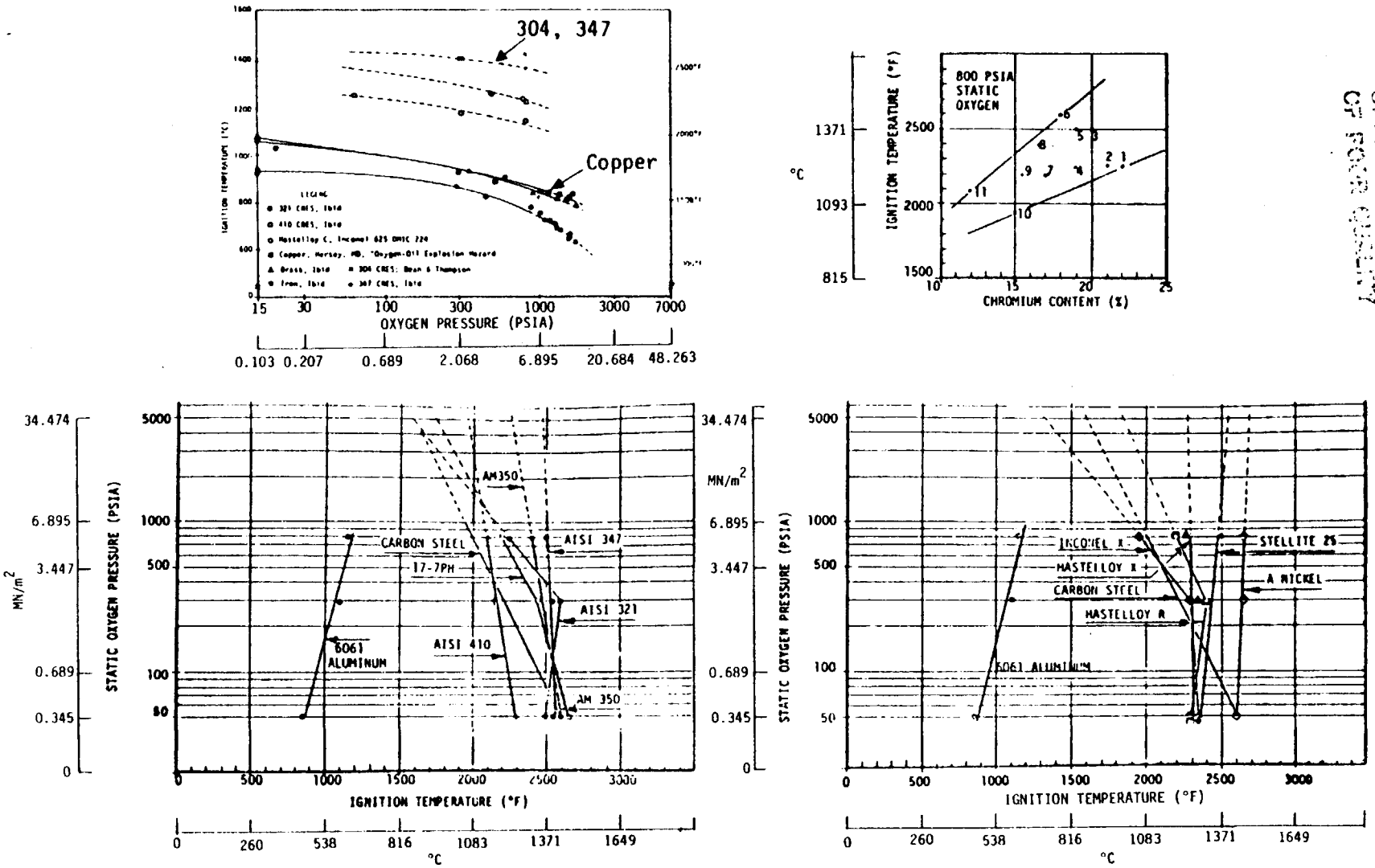

Figure 107. Metal Ignition Temperatures in Static Oxygen

TABLE XVI

OXIDIZER-RICH PREBURNER STABILITY DATA

Test No.	Duration Sec	Pc MN/m^2 (psia)	MR	Injector	L' mm (in.)	Turbulence Ring mm (in.)	Stable	Freq. (Hz)
-014	1	13.1 (1905)	36.8	EDM	447 (17.6)	No	1L	650
-018	1/2	12.7 (1844)	37.1	Platelet	447 (17.6)	86.4 (3.4)	1L	667
-019	1/2	12.9 (1872)	35.8	Platelet	447 (17.6)	76.2 (3.0)	Stable	-
-021	1	13.9 (2023)	47.5	EDM	447 (17.6)	76.2 (3.0)	1L	604
-023	1	16.6 (2402)	32.6	EDM	345 (13.6)	76.2 (3.0)	Stable	-
-024	1/2	17.2 (2497)	27.2	EDM	396 (15.6)	76.2 (3.0)	Stable	-

Reducing the turbulence ring diameter to 76.2 mm (3.0 in.) stabilized the platelet injector (Test -019).

D. FUEL-RICH COMBUSTION MODEL UPDATE

This section of the report discusses the Fuel-Rich Combustion Model (FRCM) and how the measured data are used to update it. The basis for the model, a comparison between predicted and measured results, and model modifications are described.

1. Fuel-Rich Combustion Model Description

The FRCM was developed on Contract NAS 3-21753 and is described in the final report for that contract (Ref. 1). An additional brief description is included herein for the sake of completeness.

Combustion in fuel-rich preburners is presumed to occur as illustrated in Figure 108. The oxidizer is assumed to vaporize and react immediately with a portion of the fuel. The remainder of the fuel undergoes vaporization and thermal decomposition to arrive at the final combustion products. Equilibrium combustion of the oxidizer is assumed such that the starting gas-phase properties are defined by the One-Dimensional-Equilibrium (ODE) combustion products. The gas-phase temperature is higher at the injector-end than at the nozzle-end since the starting gas-phase mixture ratio is higher than the overall mixture ratio. The gas temperature decays as the fuel vaporizes and undergoes kinetically limited thermal decomposition. The net effect is that the gas properties and C* performance are slightly dependent on residence time. The rate of temperature decay depends on the vaporization rate which is modeled as an exponential function (see Figure 109). The appropriate vaporization rate constants are determined from data calibrations.

The model assumes the chemical reaction scheme shown in Figure 110. Both the oxygen and RP-1 are injected into the combustion chamber in the liquid phase. The liquid oxygen rapidly vaporizes, leaving a large amount of unvaporized RP-1. The oxygen vapors quickly react with the available fuel vapors at a mixture ratio that is higher than the overall MR. The oxidation of the RP-1 vapor is assumed to result in equilibrium products due to the higher mixture ratio. With the exception of hydrogen, these products do not undergo further reaction in the chamber. Based on previous calibrations, the appropriate value for the assumed starting mixture ratio has been determined to be on the order of 1.2. The oxidation process provides the heat needed for the vaporization and thermal decomposition processes.

- FUEL RICH COMBUSTION

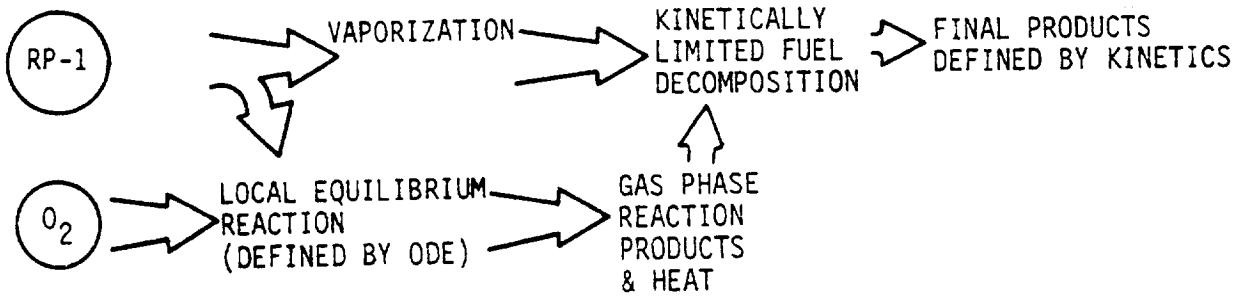

FUEL DECOMPOSITION

KINETIC: $C_{12}H_{26} \longrightarrow H_2 + CH_4 + C_2H_2 + C_2H_4 + C_2H_6 + C_3H_6 + \cdots\cdots$

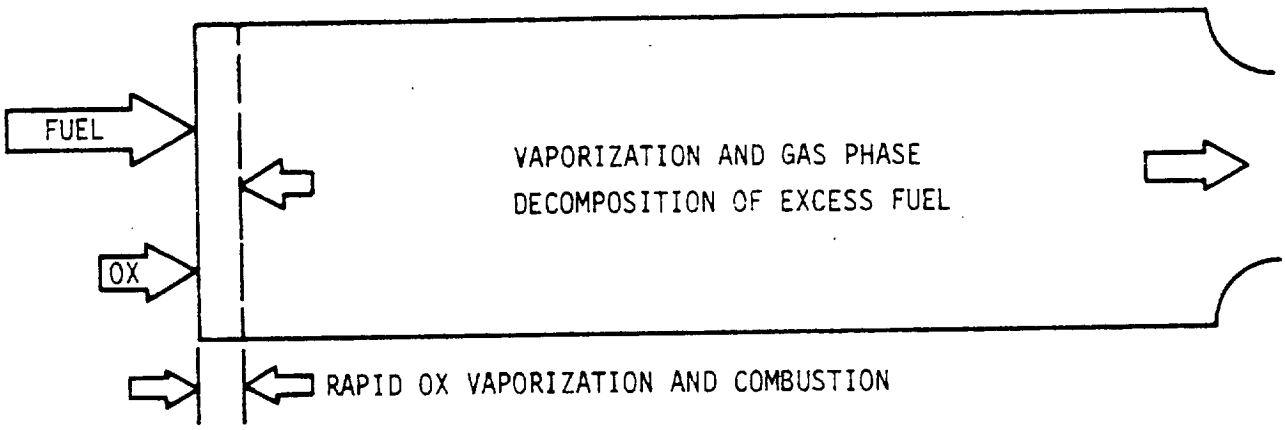

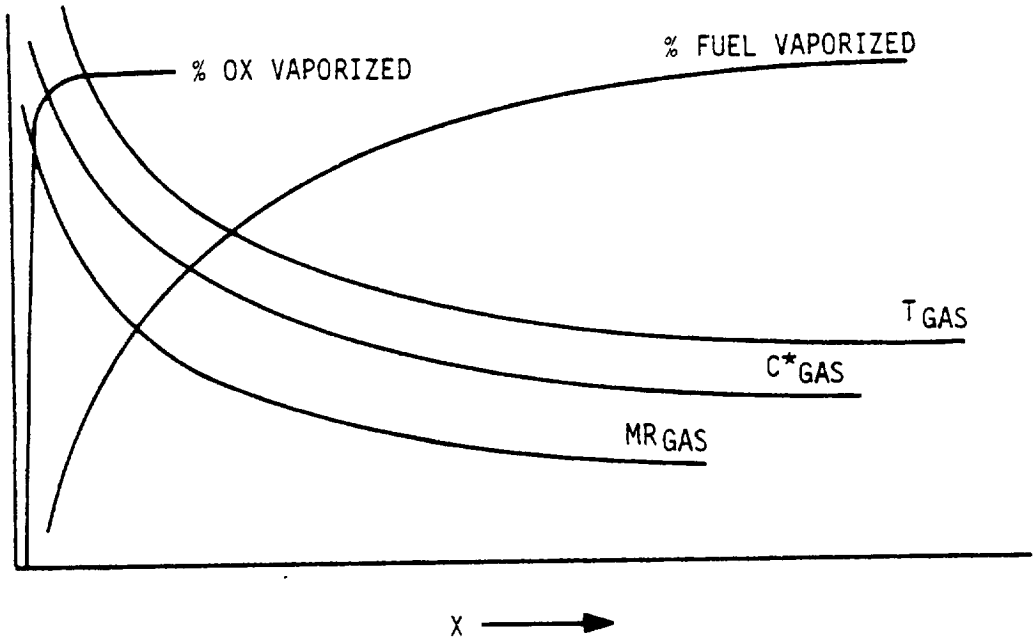

Figure 108. Fuel-Rich LOX/RP-1 Combustion Model

$\eta_{vap} = 1 - C_f/C_i$

$C_f/C_i = e^{-X/V\ (Ae^{-\Delta H/RT})}$

X = LENGTH, INCHES

V = CHAMBER VELOCITY, INCHES/SEC

A = CONSTANT, 1×10^4

ΔH = ACTIVATION ENERGY

R = GAS CONSTANT, 1.987

T = TEMPERATURE, °K (°R)

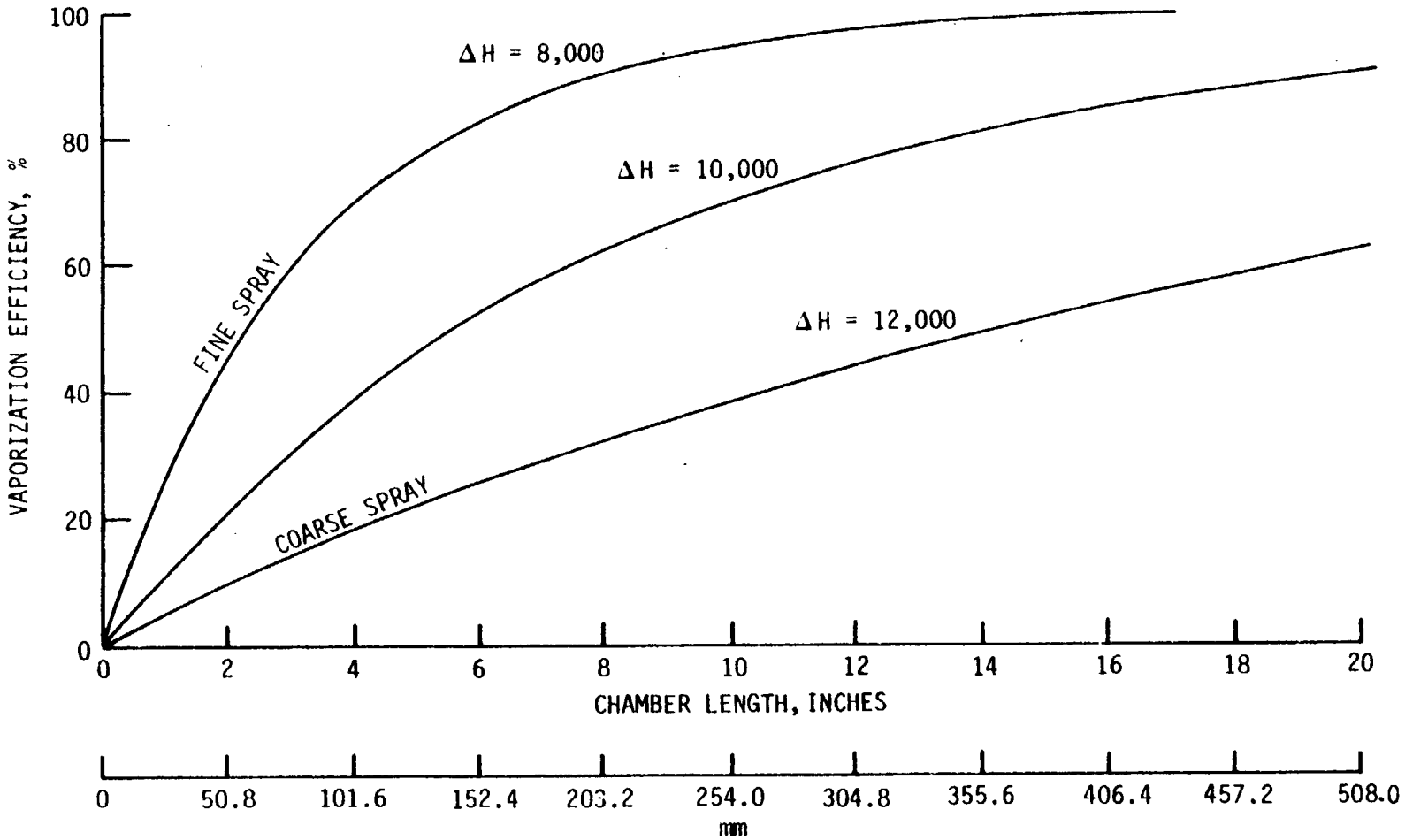

Figure 109. Fuel Vaporization Model

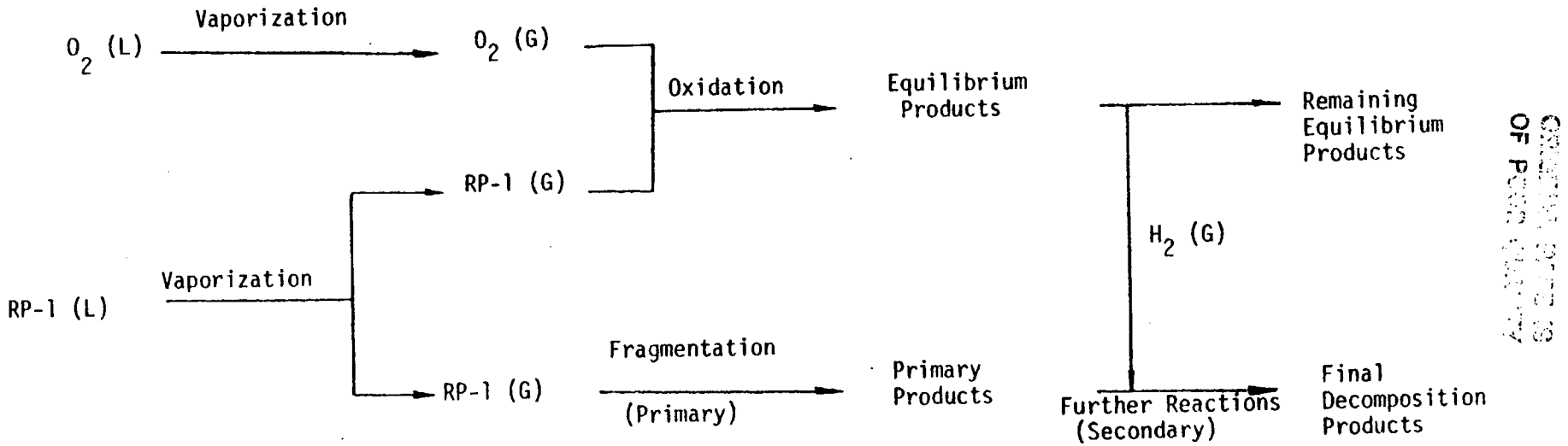

Figure 110. Fuel-Rich Combustion Model Reaction Schematic

The unreacted liquid RP-1 vaporizes and undergoes a two-step gas-phase thermal decomposition. The two steps consist of (1) RP-1 fragmentation (primary reactions) and (2) gas-phase reaction (secondary reactions). The primary reactions fragment the RP-1 into lighter hydrocarbons, such as H_2, CH_4, C_2H_4, C_3H_6, etc. These fragments then undergo secondary reactions with the hydrogen molecules that are produced by the starting RP-1 oxidation reactions. The net effects of the propellant vaporization and RP-1 decomposition are a reduction in gas temperature. As a result, the RP-1 decomposition takes place in a low-temperature environment and thus the decomposition reactions proceed slowly and are limited by the reaction rate.

In its currently existing form, the model does not predict solid carbon formation since an appropriate reaction mechanism has not been identified. It predicts only the precursors, such as C_2H_2. Table XVII is a listing of the chemical reactions considered by the model.

2. Comparison of Original Predictions to Experimental Results

The experimental results and original model predictions were compared to determine the need for modifications. The original model predictions had been made for a chamber pressure of 20.7 MN/m^2 (3000 psia) and a gas residence time of 12 msec whereas the actual test conditions covered a chamber pressure range of 11.7 to 16.5 MN/m^2 (1700 to 2400 psia) and residence times of 17 to 43 msec. However, this presented no problem since both the model and the data indicate that the pressure effects are negligible over this pressure range. Also, the model indicates that residence time effects are negligible above residence times of 5 to 6 msec.

The gas compositions were measured using the gas probe system described in Section IV.A.4. Combustion gas product samples were collected in high-pressure bombs. The physical properties of the samples are listed in Table XVIII. The sample included solid carbon and liquid condensates as well as gas. The condensate included carbon, condensed fuel vapors, and unvaporized fuel. The gas and condensate weight fractions versus mixture ratio are plotted in Figure 111 for comparison with those predicted by the fuel-rich combustion model. The trend with mixture ratio is excellent although the absolute value is slightly lower than the predicted one.

The gas-phase composition was determined by using a Hewlett-Packard Model 5803A gas chromatograph. The measured gas compositions are listed in Table XIX. The gas samples were checked for oxygen/hydrocarbon ratio to verify that there were no leaks in the sample system. The results are plotted in Figure 112, indicating that the agreement is excellent. No injector effects are noted in the measured gas-phase composition.

TABLE XVII

FUEL-RICH COMBUSTION MODEL CHEMICAL REACTIONS


```
$$$$$$$$$$ CURRENT EXECUTION TIME THIS CASE =        .000  (MIN) $$$$$$$$$$

REACTIONS
     1          C12H26(L) = C12H26      ,A=1.0E4,   N=0.,    B=10., DODECANE VAPORIZATION *
     2        C12H26=  H2+   CH4+    C2H4+   C2H6+   C3H6+    C7H14,A=1.4E14,N=0.,B=60,  *
     3          C7H14 = H2+ CH4+ C2H4+ C2H6+ C3H6+ C2F2,          A=1.413E13,N=0.,B=55.,  *
     4     CH4          = CH3 + H        ,A=1.E17    ,N=0      ,B=85.8,  TABAYASH/BLR(1979)  9
     5     C2H5         = C2H4 + H       ,A=6.8E17   ,N=0      ,B=31.8,  TABAYASH/BLR(1979) 35
     6     C2H6         = C2H2 + H2      ,A=2.09E17  ,N=0      ,B=79.1,  TABAYASH/BLR(1979) 37
     7     C2H3         = C2H2 + H       ,A=7.94E14  ,N=0      ,B=31.5,  TABAYASH/BLR(1979) 39
END TBR REAX
     8     CH4 + H      = CH3 + H2       ,A=6.310E13,N=0       ,B=11.9,  ENGLEMAN (1976)    15
     9     CH3 + C2H6   = C2H5 + CH4     ,A=5.0E14   ,N=0      ,B=21.5,  TABAYASH/BLR(1979) 30
    10     CH3 + CH4    = C2H6 + H       ,A=8.0E13   ,N=0      ,B=40.,   TABAYASH/BLR(1979) 31
    11     CH3 + CH4    = C2H5 + H2      ,A=1.0E13   ,N=0      ,B=23.,   TABAYASH/BLR(1979) 32
    12     CH3 + C2H4   = C2H3 + CH4     ,A=5.0E12   ,N=0      ,B=13.,   TABAYASH/BLR(1979) 33
    13     C2H4+H       = C2H3 + H2      ,A=7.E14    ,N=0      ,B=14.5,  TABAYASHI(1979)    38
    14     C2H3+ H      = C2H2 + H2      ,A=4.571E12,N=0       ,B=2.5,   EHRENIUS      (1973) 40
    15     C2H6+ H      = C2H5 + H2      ,A=1.672E14,N=0       ,B=9.23,  TABAYASH/BLR(1979) 47
    16          C3H6    = C2H3 + CH3     ,A=7.9E17   ,N=0.     ,B=95.,   SUNDARAM-FRUMONT   71
    17     C2H4 + C2H4  = C2H3 + C2H5    ,A=8.9E16   ,N=0.     ,B=65.,   SUNDARAM-FRUMONT   74
    18        C2H2 + H  = C2H3           ,A=4.E13    ,N=0.     ,B=1.5,   SUNDARAM-FRUMONT   76
    19        C2H3 + H  = C2H4           ,A=1.E13    ,N=0.     ,B=0.,    SUNDARAM-FRUMONT   77
LAST REAX
THIRD BODY REAX RATE RATIOS
SPECIES C12H26,1.,1.,0.,
 1.,1.,1.,1.,1.,1.,1.,1.,1.,1.,1.,
SPECIES H2,0.,.05,.09,
 1.,1.,1.,1.,1.,1.,1.,1.,1.,1.,1.,
SPECIES CH4,0.,.51,.11,
 1.,1.,1.,1.,1.,1.,1.,1.,1.,1.,1.,
SPECIES C2H4,0.,1.07,.9,
 1.,1.,1.,1.,1.,1.,1.,1.,1.,1.,1.,
SPECIES C2H6,0.,.44,.07,
 1.,1.,1.,1.,1.,1.,1.,1.,1.,1.,1.,
SPECIES C3H6,0.,.49,1.47,
 1.,1.,1.,1.,1.,1.,1.,1.,1.,1.,1.,
SPECIES C7H14,0.,1.,1.,
 1.,1.,1.,1.,1.,1.,1.,1.,1.,1.,1.,
SPECIES C2H2,0.,0.,.27,
 1.,1.,1.,1.,1.,1.,1.,1.,1.,1.,1.,
SPECIES C12H26(L),1.,0.,0.,
 1.,1.,1.,1.,1.,1.,1.,1.,1.,1.,1.,
LAST CARD
```

TABLE XVIII

COMBUSTION PRODUCT SAMPLE PHYSICAL PROPERTIES

	Run Number											
	-012	-013	-015	-016	-018	-019	-021*	-022	-025	-027	-028	-029
Sample Pressure MN/m^2 (psia)	5.93 (860.5)	7.10 (1029.6)	6.17 (894.7)	5.55 (804.7)	6.38 (925.8)	6.11 (886.8)	1.50 (217.8)	6.02 (872.7)	6.22 (901.7)	4.77 (691.6)	3.514 (509.64)	5.58 (809.
Temperature °C (°R)	16.85 (522)	16.85 (522)	16.85 (522)	16.85 (522)	16.57 (521.5)	16.57 (521.5)	16.85 (522)	16.85 (522)	17.96 (524)	19.63 (527)	19.63 (527)	19.0 (526
Condensate Weight (GR)	13.4	6.8	8.1	7.0	8.3	8.9	8.3	4.8**	14.0	9.6	4.0	4.1
Gas Fraction Weight (GR)	14.81	18.49	16.28	13.81	16.17	15.29		15.51	15.62	11.74		14.4
Condensate Mass Fraction %	47.50	26.89	33.22	33.64	33.92	36.79		23.63	47.27	44.99		22.0
Gas Molecular Weight	20.86	21.77	22.05	20.80	21.15	20.88	22.22	21.54	21.08	20.77	21.81	21.8
Preburner O/F Ratio	0.240	0.310	0.318	0.317	0.335	0.327	0.300	0.330	0.260	0.257	0.368	0.35
Sample O/F Ratio	0.278	0.328	0.293	0.329	0.336	0.327		0.368	0.267	0.290		0.34

*Valve Leaking

**Solid Condensate = 0.3188 Grams

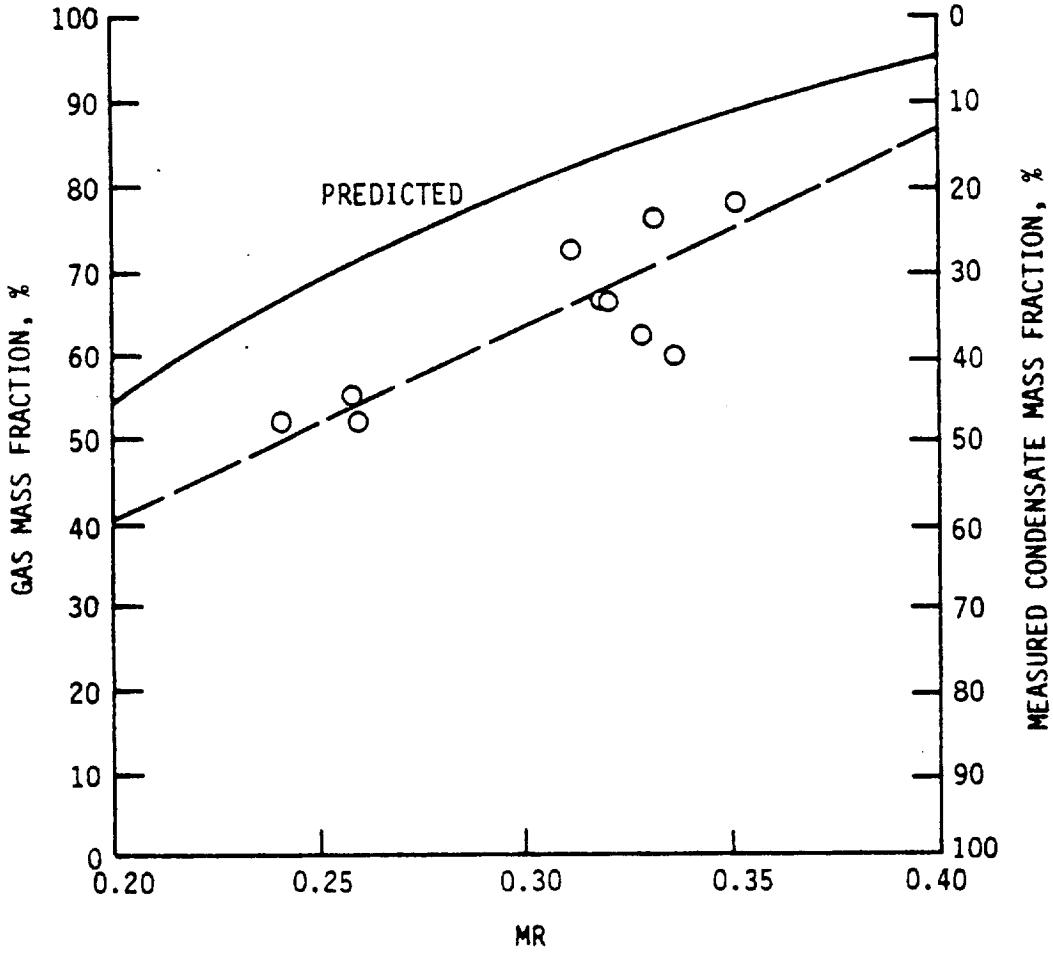

Figure 111. Fuel-Rich Combustion Product Sample Phase Distribution

TABLE XIX

MEASURED FUEL-RICH COMBUSTION PRODUCT GAS COMPOSITION

	EDM Injector		Platelet Injector									
Run Number	-012	-013	-015	-016	-018	-019	-021	-022	-025	-027	-028	-029
Propylene	1.72 vol%	3.26 vol%	3.56 vol%	2.59 vol%	2.59 vol%	2.25 vol%	3.21 vol%	3.47 vol%	2.03 vol%	1.98 vol%	4.29 vol%	4.19 vol%
Butane	0.38	0.76	0.88	0.051	0.57	0.48	1.04	0.66	0.47	0.48	1.09	0.82
Heptylene (C_6^+)	0.05	0.74	0.77	0.08	0.14	0.04	0.23	0.16	0.08	0.02	0.12	0.37
Ethylene	7.16	5.98	7.06	6.32	6.73	6.39	6.73	5.97	6.99	7.68	6.90	6.47
Ethane	1.44	3.45	3.34	2.24	1.93	1.98	2.35	4.02	2.05	1.71	4.02	4.74
Acetylene	0.40*	0.38	0.39	0.48	0.32	0.40	2.44	0.35	0.21	0.37	0.37	0.59
Methane	14.34	22.79	20.11	20.38	19.27	18.80	18.01	21.26	16.50	13.45	18.38	22.37
Carbon Monoxide	44.02	37.62	37.83	39.36	40.82	41.19	40.01	38.50	42.38	42.11	37.82	36.49
Hydrogen	25.50	20.86	21.58	23.45	22.90	23.65	20.71	21.13	24.16	26.73	22.37	19.79
Carbon Dioxide	4.99	4.16	4.48	4.59*	4.73	4.82	5.27	4.48	5.13	5.47	4.64	4.17

*Assumed values, not actually determined

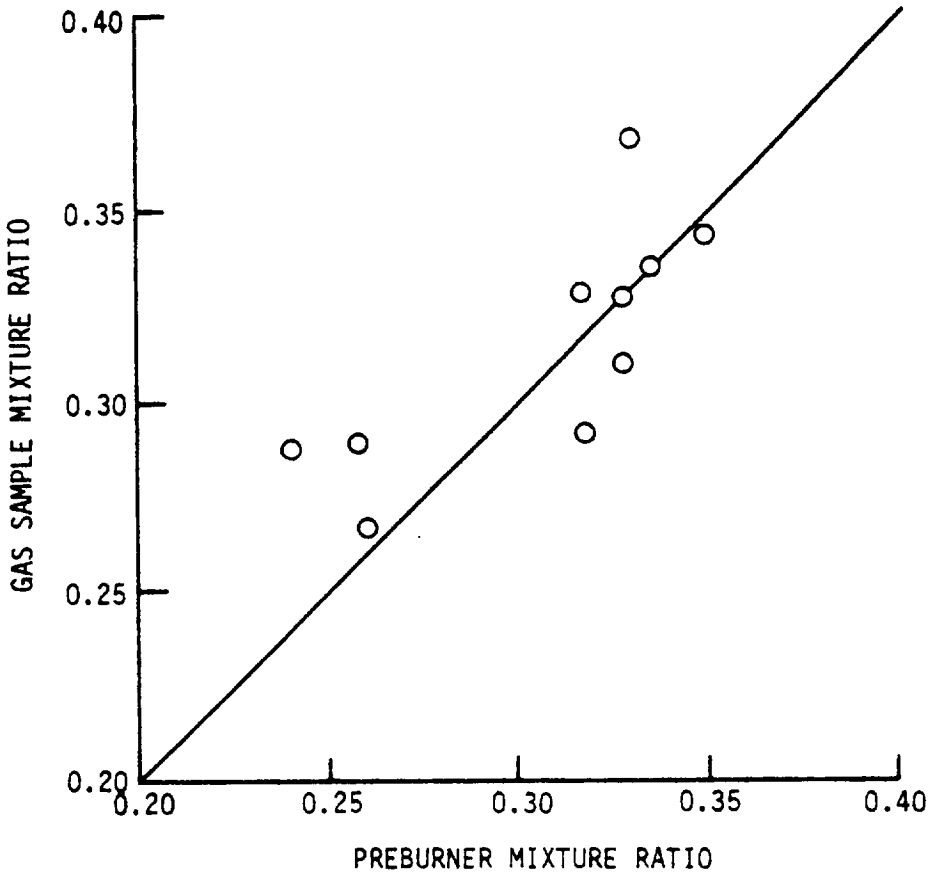

Figure 112. Comparison of Gas Sample Mixture Ratio to Preburner Mixture Ratio

The vapor pressure of the condensate was measured to further characterize its properties. The results are plotted in Figure 113 for comparison with several known hydrocarbons. Vapor pressures for RP-1, heptane, hexane, and butane are plotted. The condensate appears to consist of "cracked" RP-1. Its molecular weight lies between 86 for hexane and 58 for butane as compared to 172 for RP-1.

Figure 114 shows the predicted and measured combustion gas compositions as a function of the overall mixture ratio. The starting mixture ratio used for the prediction is 1.2. All but the hydrogen and methane species original predictions show good agreement with the experimental data. The data trends clearly show that, as the mixture ratio increases, the hydrogen content decreases and the methane content increases. The hydrogen content is underpredicted while the methane content is overpredicted, indicating that the production of one is accompanied by destruction of the other.

Figure 115 shows the measured and predicted apparent molecular weight and specific heat ratio for the gas fraction of the combustion products. The molecular weight is overpredicted while the specific heat ratio is underpredicted. This indicates that the model predicts heavier hydrocarbon gas constituents than the combustion actually generates. Figure 116 shows the molecular weight and specific heat ratio for the entire mixture of gaseous and condensed phase combustion products. The model does not predict solid phase products and therefore the predicted condensed phase constituent contains only unvaporized fuel. The experimental condensed phase constituent was also assumed to contain only liquid RP-1, despite the fact that a small amount ($\approx$1%) of solid particles was collected in the gas samples.

Figures 86 and 87 show plots of the measured and predicted gas temperature as a function of overall propellant mixture ratio for the EDM and platelet injectors. The model overpredicts the temperatures by approximately 65.5°C (150°F). The C* variation with the mixture ratio is shown in Figures 82 and 84 for the EDM and platelet injector, respectively. The predicted and measured values are shown to be in good agreement. It should be noted that the measured C* does not significantly vary with chamber length.

3. Model Modification

The model updating work was initially focused on finding a chemical reaction set that would predict carbon formation as well as H_2 and CH_4 gas compositions in agreement with the experimental data. The work followed the sequence of events illustrated in Figure 117. The first modification involved replacing the entire secondary gas- phase reaction set with

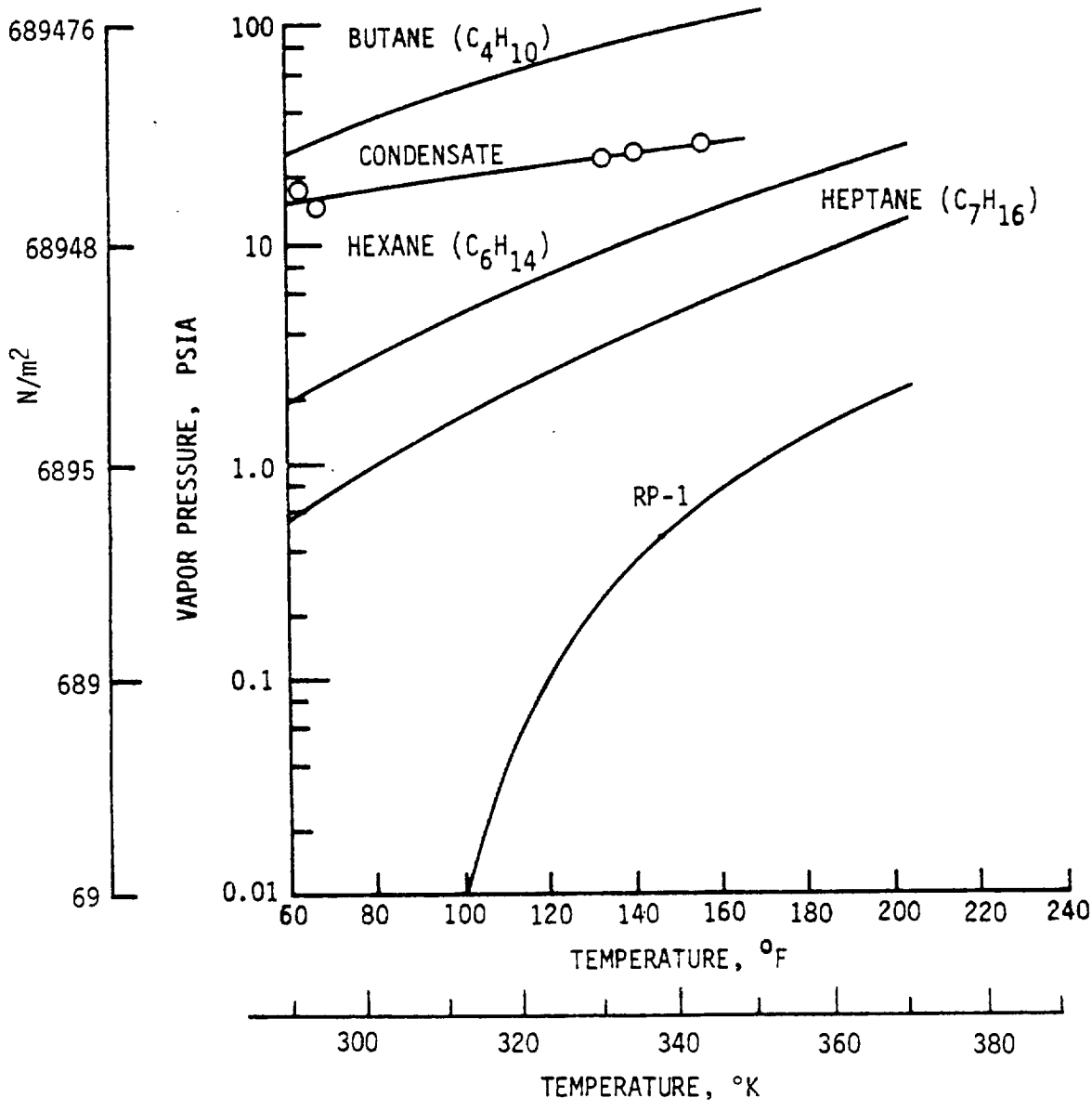

Figure 113. Measured Condensate Vapor Pressure

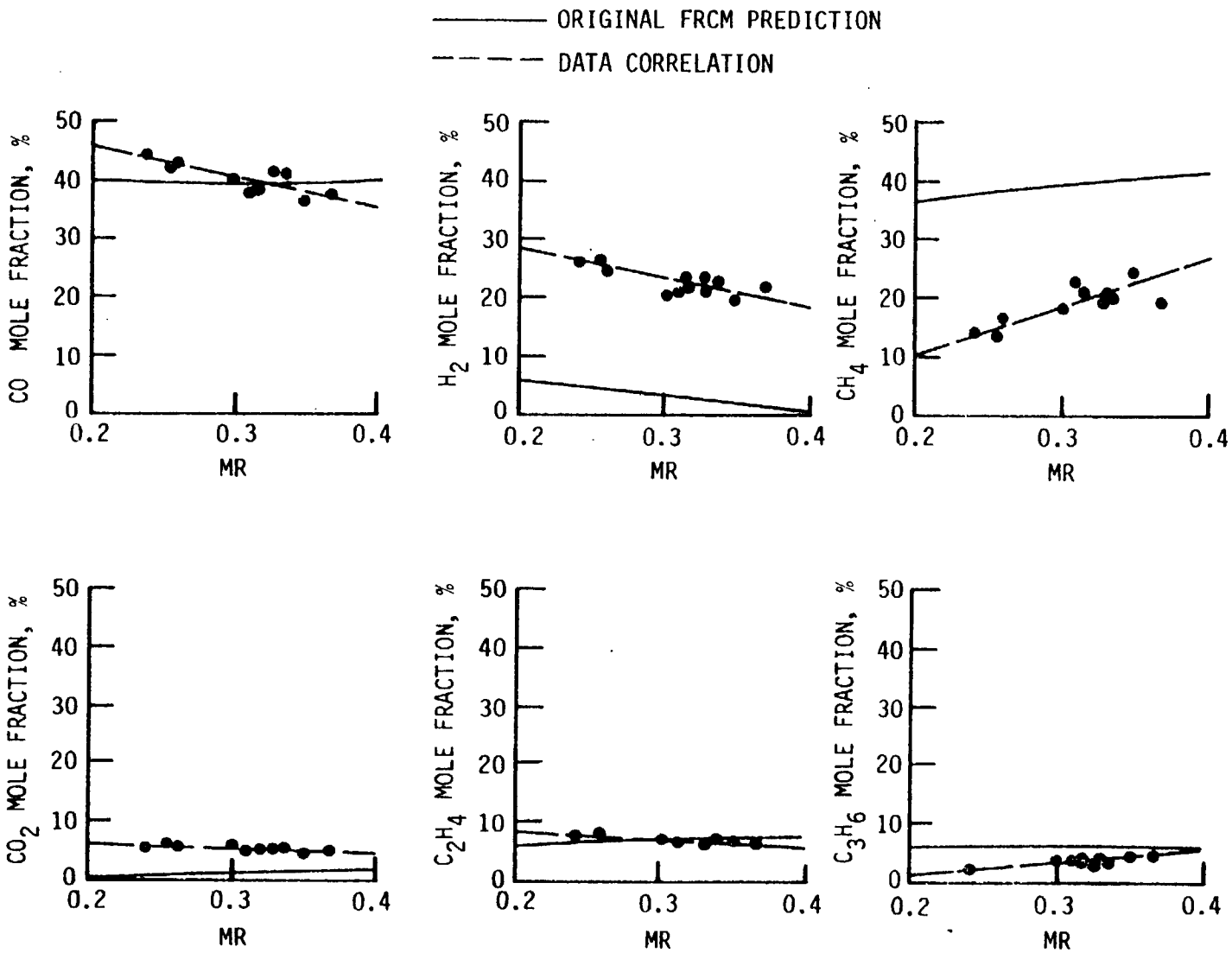

Figure 114. Comparison of Measured Gas Compositions to Original FRCM Predicted Compositions

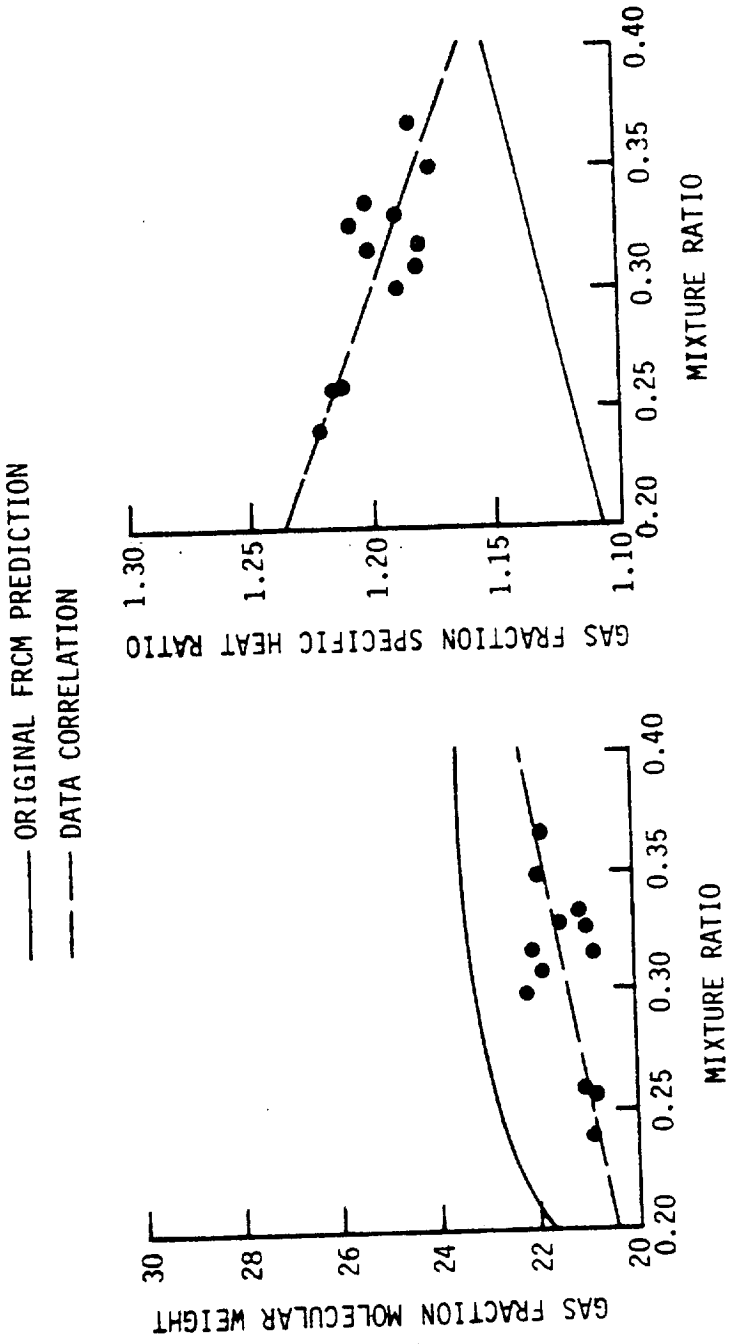

Figure 115. Comparison of Measured Original FRCM Predicted Gas Fraction Properties

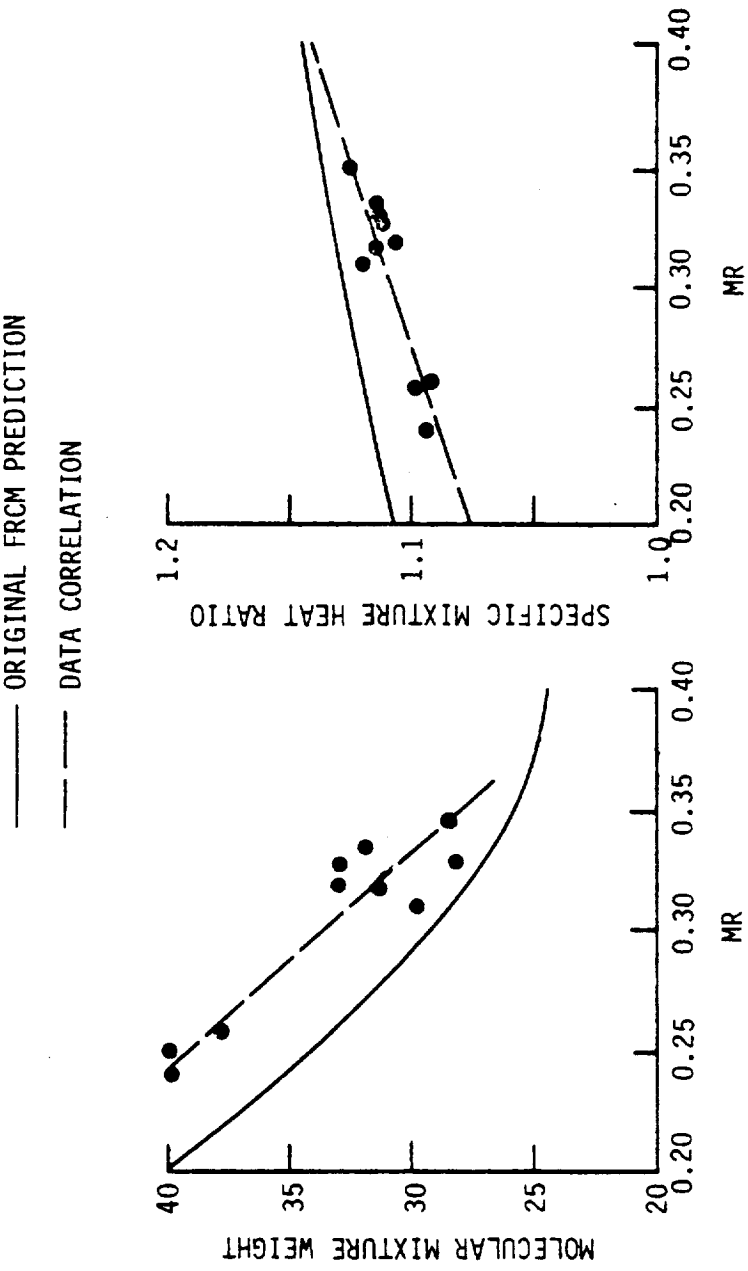

Figure 116. Comparison of Measured Original FRCM Predicted Mixture Properties

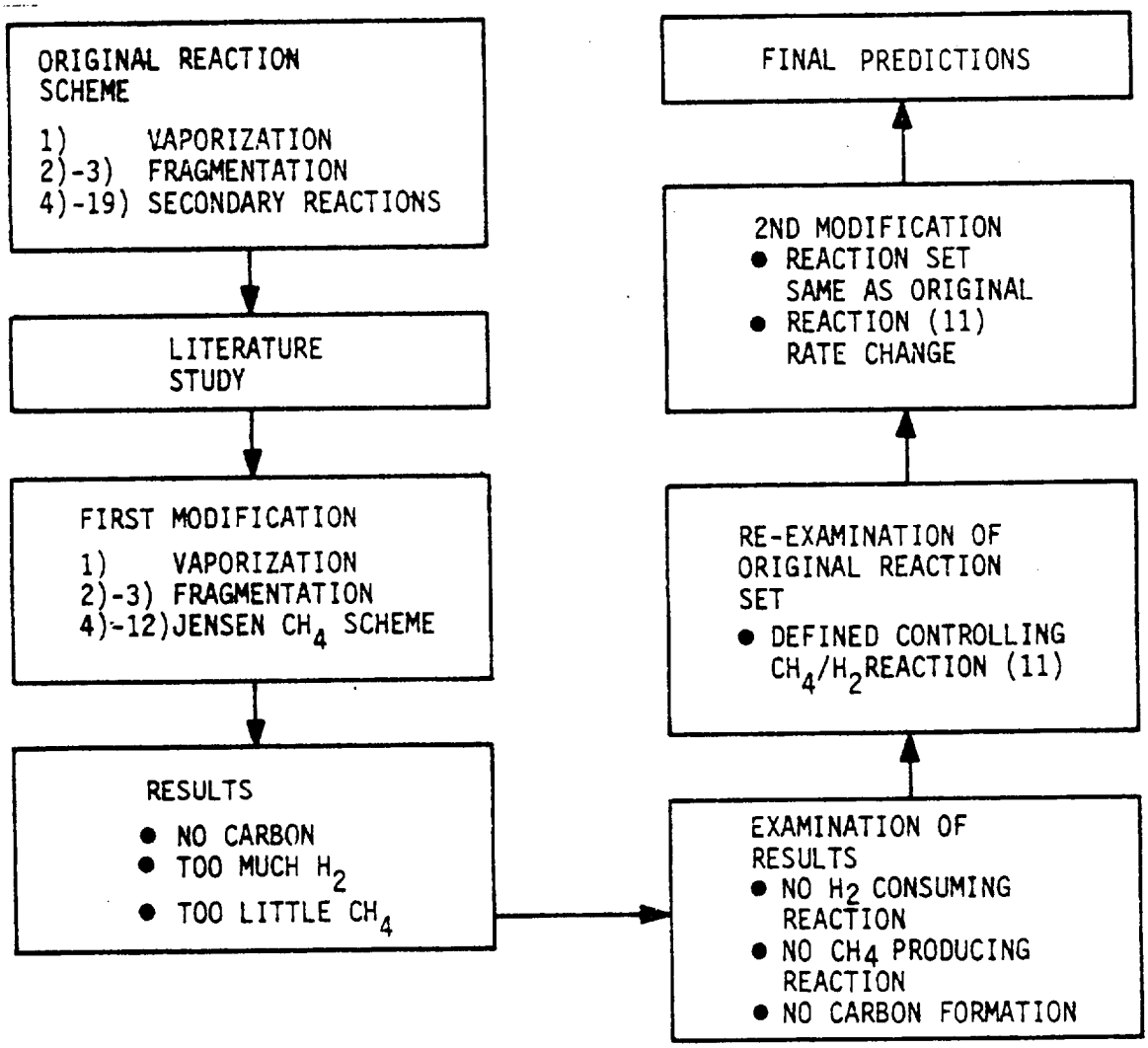

Figure 117. Fuel-Rich Combustion Model Modification Sequence

the methane soot-formation reaction scheme proposed by Jensen (Ref. 2) shown in Table XX. Several computer runs were made using this set without reaction (12) (Table XX) which is the mechanism for solid particle growth. Reaction (12) was not included due to uncertainties in selecting active growth species and since solid carbon is produced by reaction (11). The results of the Jensen scheme were an overprediction of the hydrogen content and an underprediction of the methane content. Further examination showed that hydrogen is produced both by the starting equilibrium oxidation reaction and by the primary thermal decomposition reaction while the Jensen set provides no reactions to consume the hydrogen. Also, methane is formed only in the primary fragmentation decomposition process and is destroyed in the soot-formation process. The result is an overprediction of hydrogen and an underprediction of methane.

In retrospect, it is apparent that the Jensen scheme should have been added to the original reaction set instead of replacing it. However, the effort was redirected to a modification of the original reaction set to achieve better H_2 and CH_4 gas composition correlation. Subsequent detailed analysis revealed that reaction (11) of the original reaction set (Table XVII) produces CH_4 at such a high rate that it consumes almost the entire H_2 generated by the oxidation and fragmentation processes:

$CH_3 + CH_4 \rightleftharpoons C_2H_5 + H$	Reaction (11)
$k_{11} = 10^{13}\ e^{-(23{,}000/RT)}$	Original Rate Constant
$k_{11} = 10^{12}\ e^{-(23{,}000/RT)}$	Updated Rate Constant

This explains why the original prediction indicated too much CH_4 and too little H_2. It was therefore decided to change the rate constant to obtain the appropriate amount of H_2 and CH_4. The pre-exponential constant was changed from 10^{13} to 10^{12}. With this modification, the major products of the primary reactions are CO and H_2 by the oxidation, and C_2H_4 and C_3H_6 from the fragmentation. The H_2 and C_2H_4 undergo further reaction (secondary reactions) to product CH_4, as shown in Figure 118.

4. New Model Predictions

Several computer runs were made with the updated model for comparison with the experimental data and to develop a better understanding of fuel-rich preburner combustion. These predictions were made at a chamber pressure of 13.8 MN/m^2 (2000 psia) and 33.5 m/s (110 ft/sec) chamber gas velocity. The starting mixture ratio was taken to be 1.2 for both the EDM

TABLE XX

JENSEN'S GAS-PHASE REACTION MECHANISM FOR METHANE SOOT FORMATION

	reaction	rate coefficient	equilibrium constant	uncertainty factor
(3)	$\wedge \cdot CH_3 + H \rightleftharpoons CH_4 \cdot \wedge$	1.7×10^{-11}	$1.7 \times 10^{-36} \exp(51300/T)$	30
(4)	$CH_4 + H \rightarrow CH_3 + H_2$	$3 \times 10^{-10} \exp(-6000/T)$	$24 \exp(-30/T)$	10
(5)	$CH_3 + CH_3 \rightarrow C_2H_6$	$1 \times 10^{-10} \exp(-1400/T)$	$2.1 \times 10^{-27} \exp(43600/T)$	10
(6)	$C_2H_6 + H \rightarrow C_2H_5 + H_2$	$2 \times 10^{-10} \exp(-5000/T)$	$9.4 \exp(1360/T)$	3
(7)	$C_2H_5 \rightarrow C_2H_4 + H$	$2.8 \times 10^{13} \exp(-20400/T)$	$9.3 \times 10^{22} \exp(-17000/T)$	5
(8)	$C_2H_4 + H \rightarrow C_2H_3 + H_2$	$3 \times 10^{-11} \exp(-3460/T)$	$6.3 \exp(-590/T)$	10
(9)	$C_2H_3 + M \rightarrow C_2H_2 + H + M$	$3.6 \times 10^{-9} \exp(-15600/T)$	$3.6 \times 10^{24} \exp(-20400/T)$	30
(10)	$C_2H_3 + H \rightarrow C_2H + H_2$	$3 \times 10^{-10} \exp(-9500/T)$	$4.5 \exp(-2600/T)$	100
(11)	$C_2H + H \rightarrow C_2 + H_2$	$1 \times 10^{-10} \exp(-16000/T)$	$2.3 \exp(-16600/T)$	30
(12)	$N_i + G \rightarrow C_\Delta (+ \frac{1}{2}\nu H_2)$	1×10^{-10}	—	—

N_i, initial nucleus; G, growth species; ν is integral; $N_i \equiv C_2$ or C_2H; G ≡ C_2, C_2H or C_2H_2.

Origins of rate coefficients are given in the appendix.

Units of rate coefficients: one molecule reactions, s^{-1}; two molecule reactions, ml molecule^{-1} s^{-1}; three molecule reactions, ml^2 molecule^{-2} s^{-1}.

Uncertainty factors u are such that ku and k/u provide rough upper and lower bounds respectively to rate coefficients k.

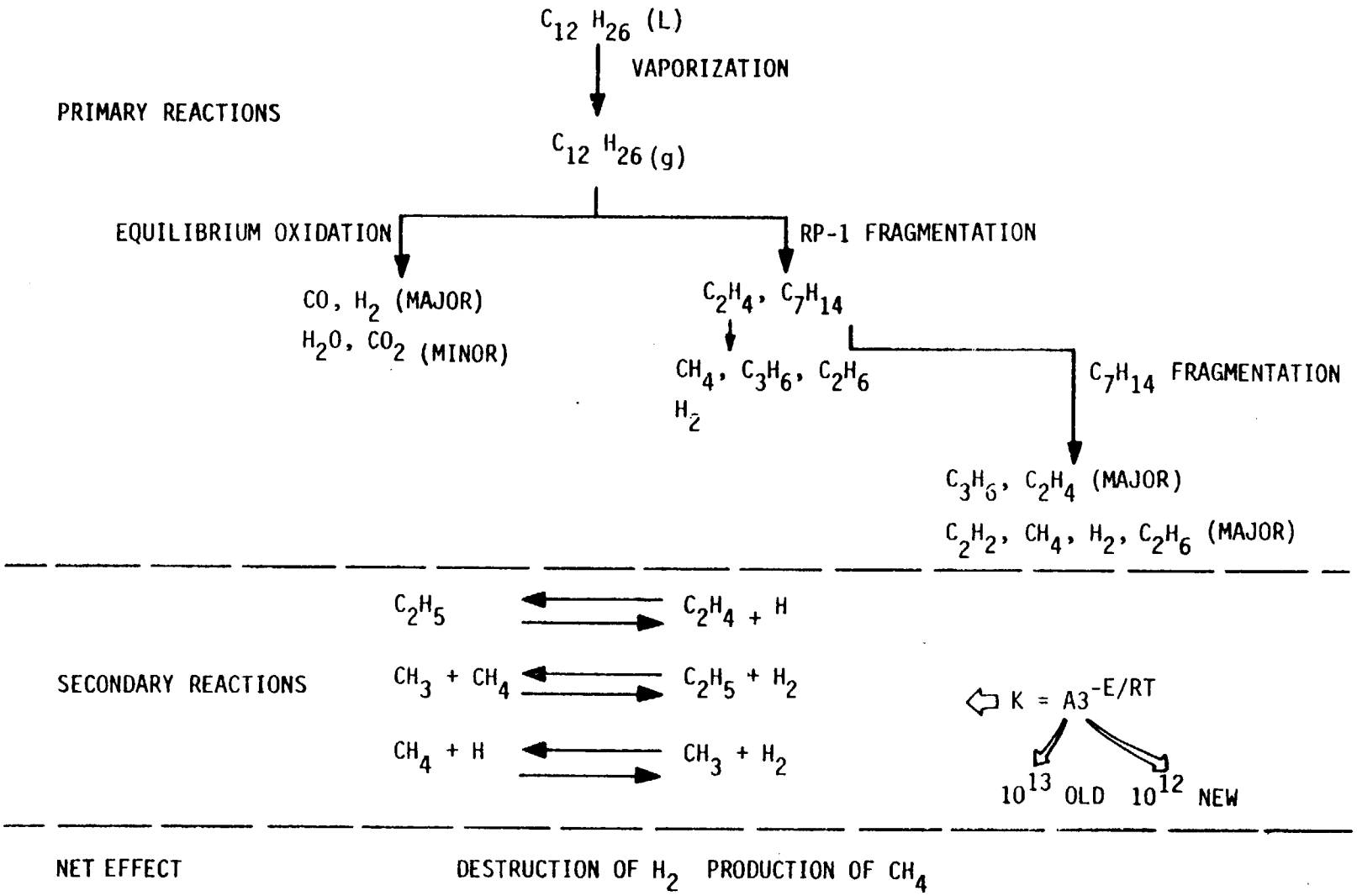

Figure 118. RP-1 Decomposition Reaction Scheme

and the platelet injector. The overall propellant mixture ratios used were 0.2, 0.3, and 0.4.

Figure 119 shows the predicted percent fuel vaporization versus chamber axial distance for the three different mixture ratios. The vaporization rate is quite low compared to those usually observed in main combustors. The fuel almost stops vaporizing at approximately 508 mm (20 in.) from the face. Higher overall mixture ratios have higher fuel vaporization rates because of the higher combustion flame temperatures.

Figure 120 shows the predicted gas temperature variation with chamber axial distance. The same initial gas temperature is predicted for the three different mixture ratios because the same starting mixture ratio is used. The gas temperature quickly drops with axial distance due to fuel vaporization and endothermic RP-1 fragmentation reactions. Higher overall mixture ratios produce both higher end-gas temperatures and higher fuel vaporization efficiencies. The predictions show that the temperature drops very rapidly near the face because of the high fuel vaporization rate resulting from the higher gas temperature. Once the gas temperature drops to a certain range, the fuel vaporization becomes very slow, as shown in Figure 119. Both the temperature and vaporization curves are almost flat at chamber lengths beyond 457 to 508 mm (18 to 20 in.)

Figure 121 shows the predicted gas-phase C* based on the gas fraction of combustion products only. The gas-phase C* curves have trends similar to those of the predicted gas temperature curves since C* is proportional to the square root of the gas temperature. Figure 122 shows the predicted mixture C* that takes the unvaporized fuel into account. The mixture C* is always less than the gas-phase C* unless the vaporization is complete. A noticeable difference between the two sets of C* curves is that the gas C* decreases as the chamber axial distance increases due to the gas temperature reduction caused by the fuel vaporization and chemistry effects, whereas the mixture C* increases due to the gas mass fraction increase resulting from the excess fuel vaporization.

Figure 123 shows the predicted mass fractions of CO, H_2, CH_4, and RP-1 for a mixture ratio of 0.3. The carbon monoxide mass fraction remains constant because the model assumes no further chemical reactions for the oxides once they are formed in the starting oxidation reaction. The hydrogen fraction declines and the methane fraction increases as the chamber axial distance increases because the latter, as discussed earlier, is formed at the cost of the former. These results indicate that the gas composition ceases to change significantly beyond chamber lengths of 152.4 mm (6 inches). Fuel vaporized beyond this point does not thermally decompose due to the low temperature environments, as illustrated in Figure 124. The sum of the

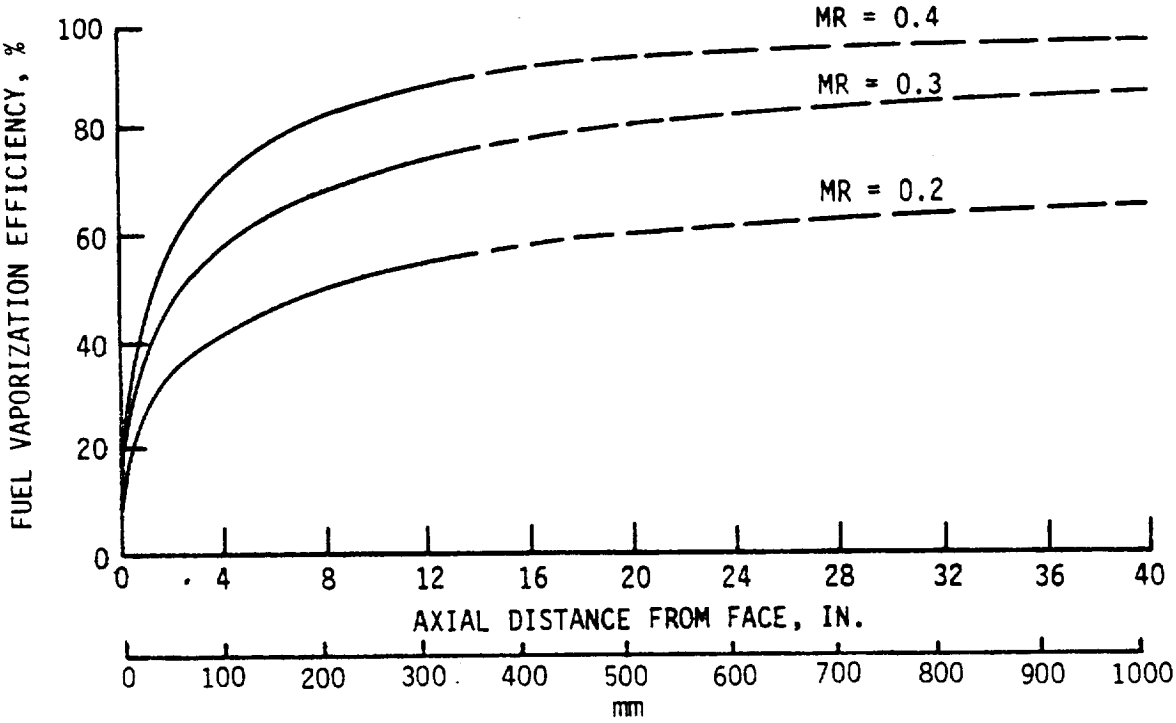

Figure 119. Predicted Fuel Vaporization Profile - Updated Model

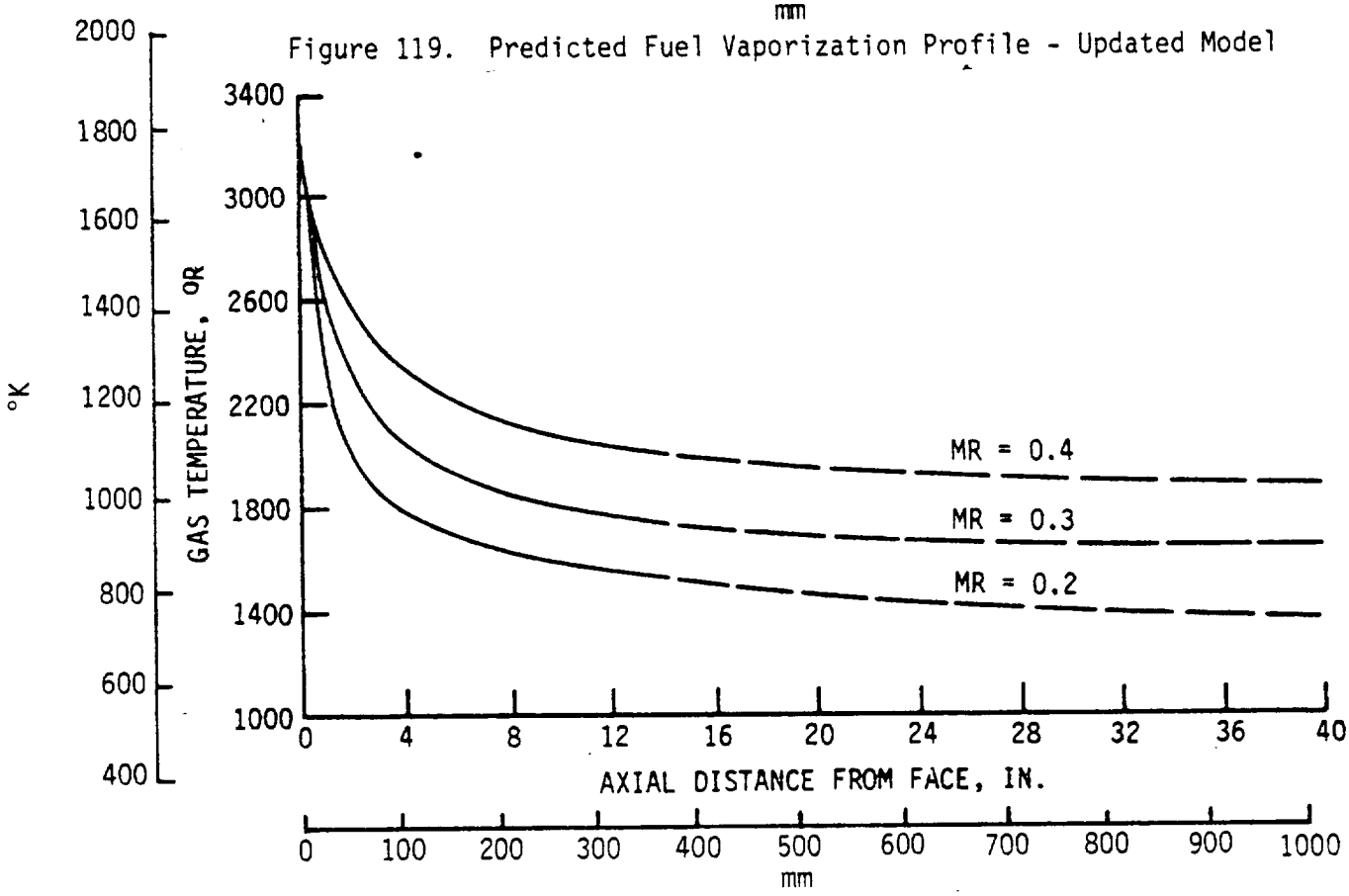

Figure 120. Predicted Gas Temperature Profile - Updated Model

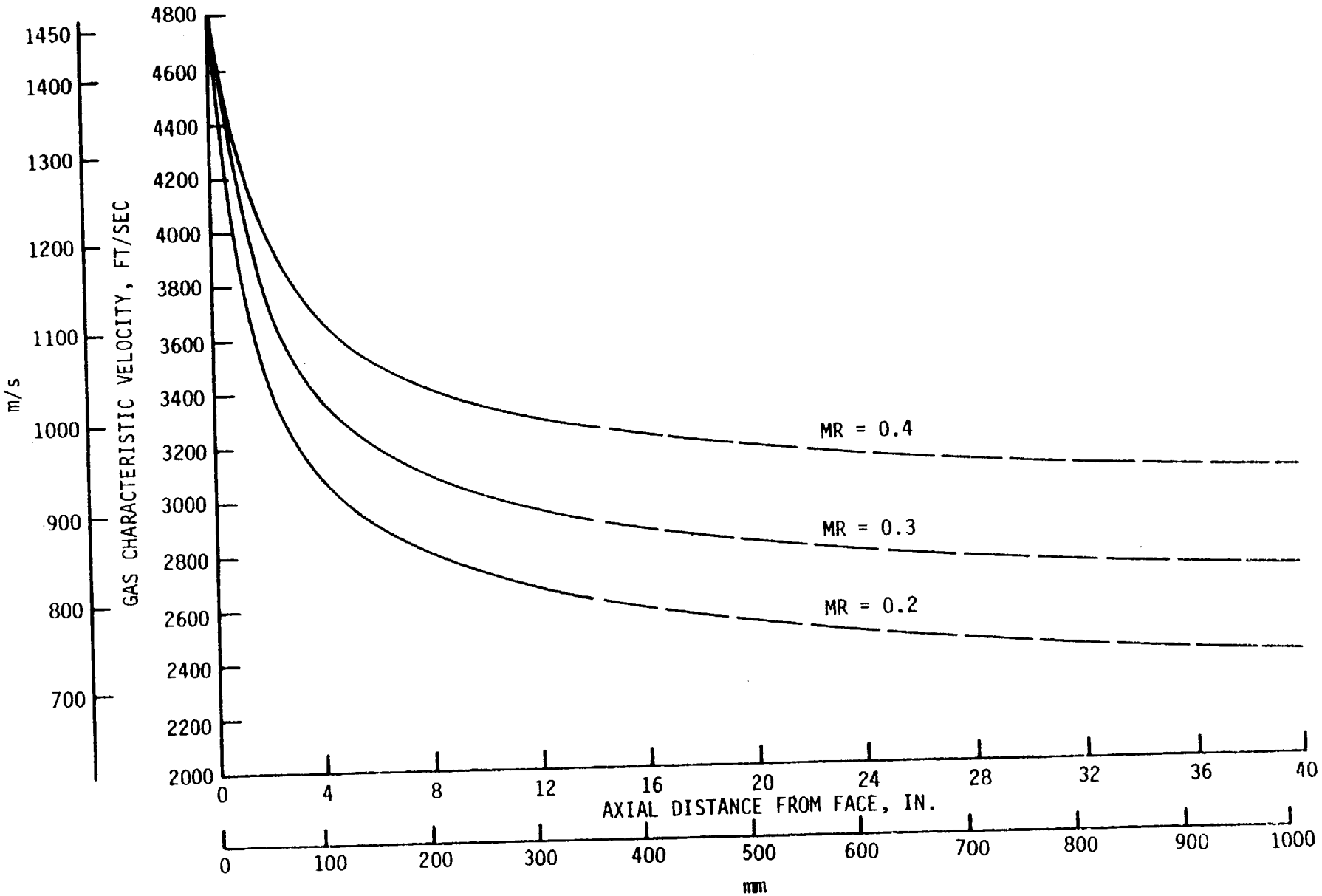

Figure 121. Predicted Gas-Phase C* Profile - Updated Model

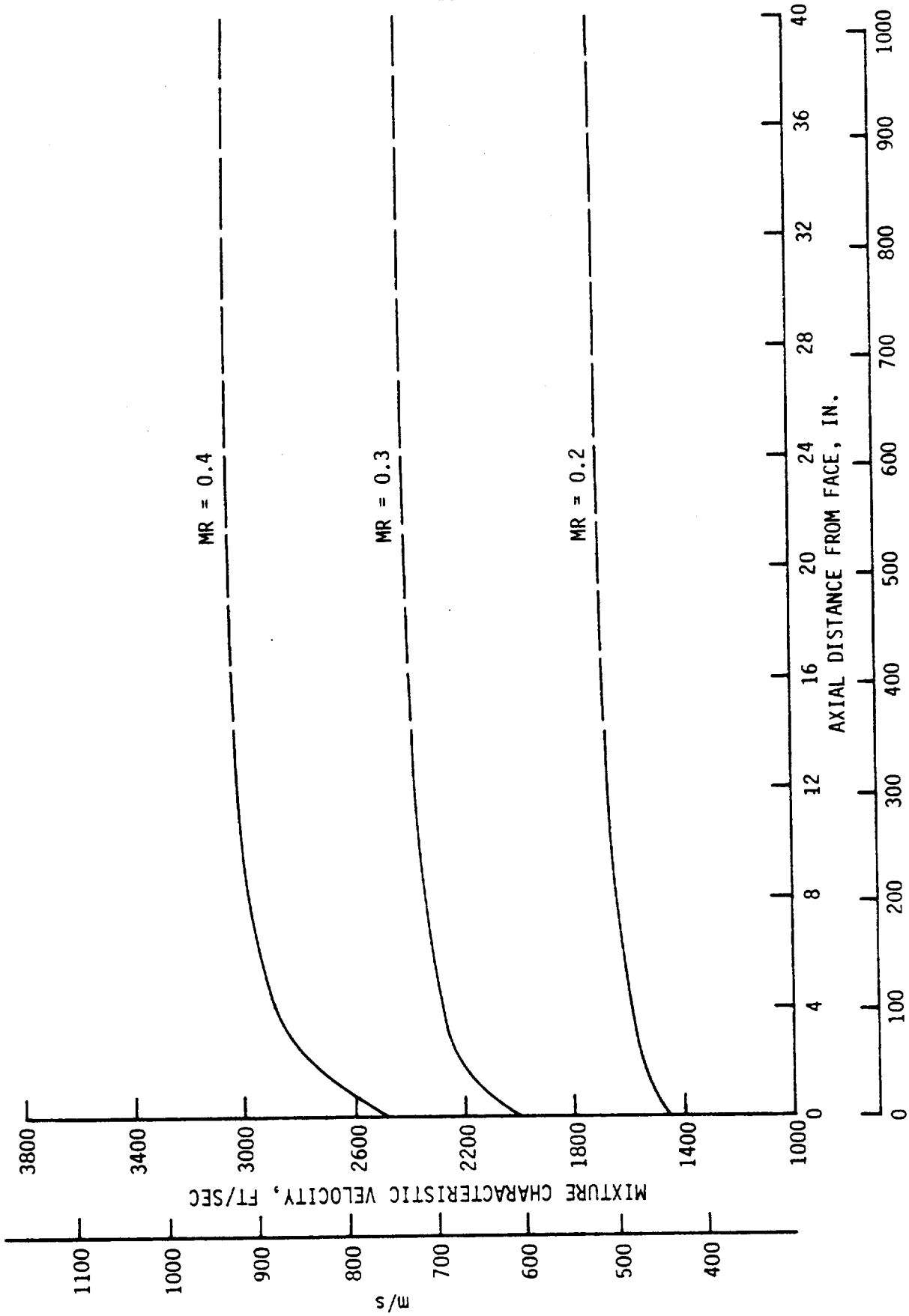

Figure 122. Predicted Mixture C* Profile - Updated Model

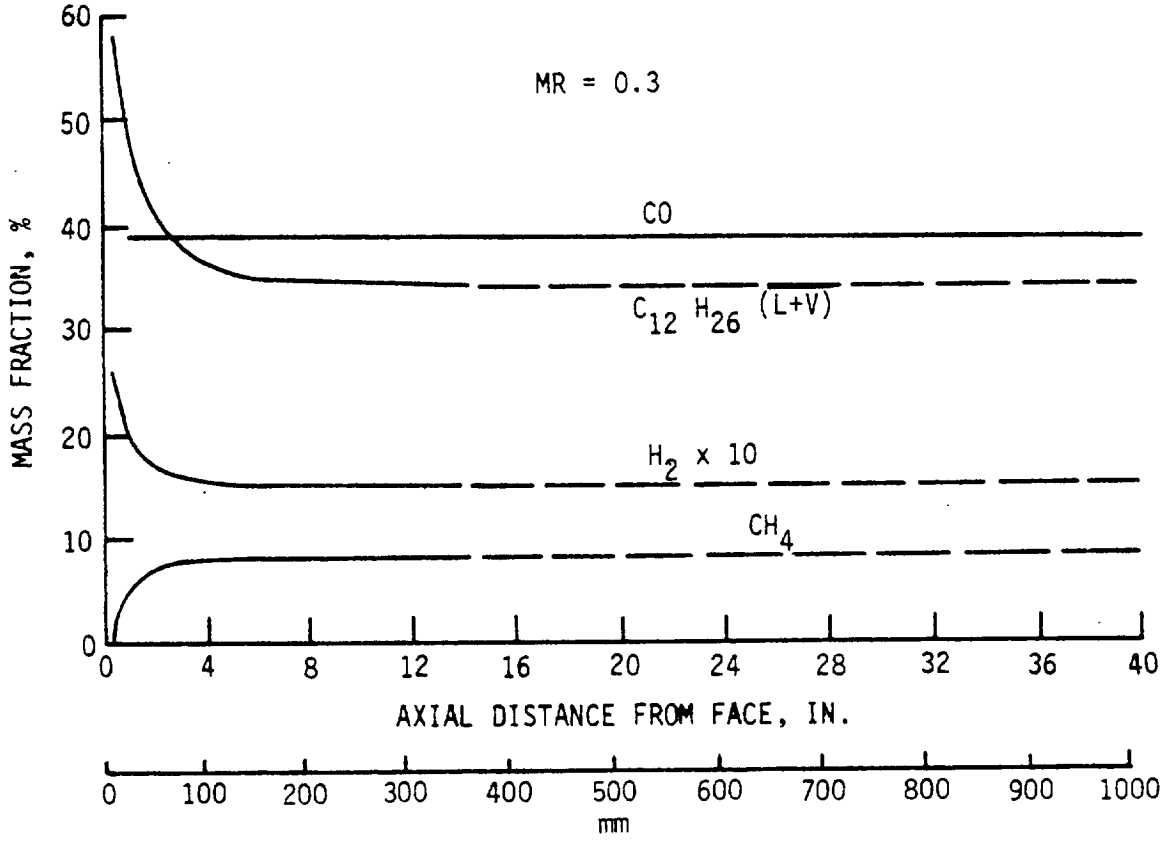

Figure 123. Predicted Major Species Mass Fractions - Updated Model

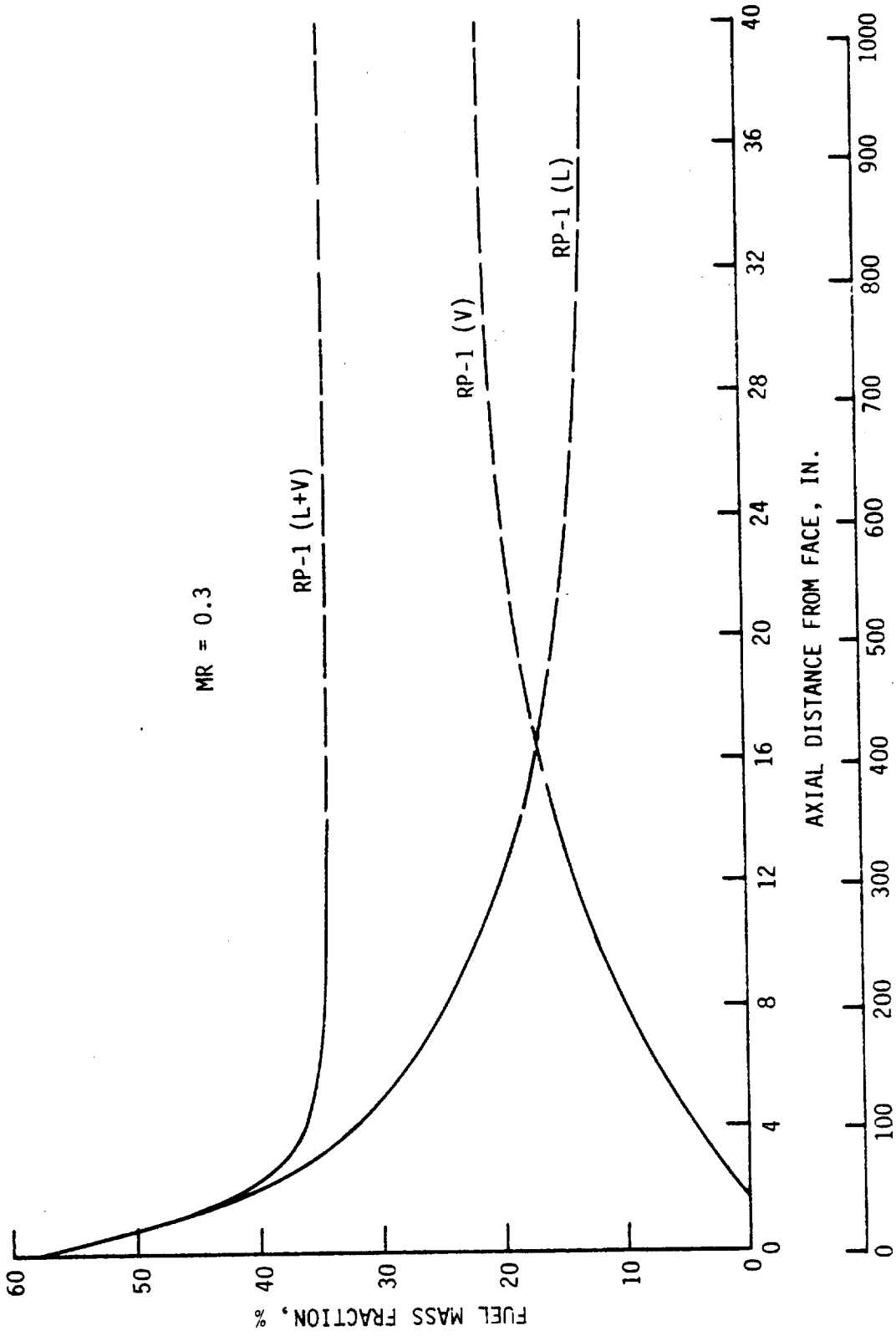

Figure 124. Predicted Fuel-Phase Distribution - Updated Model

liquid-phase and vapor-phase fuel remains unchanged beyond the 152.4-mm (6-in.) point due to the freezing of the thermal decomposition reactions.

Based on the analytical predictions and C* performance results, it can be assumed that the gas composition and gas temperature have achieved steady values at the gas sample location (533 mm [21 in.]) from the face). Cross plots of predicted gas composition, gas temperature, and mixture C* were made at this location for comparison with the experimental data.

Figure 125 compares the newly predicted mole fractions of the major species with both the original predictions and the experimental data. The new predictions are generally in better agreement with the experimental data than the original predictions. Obviously, the most striking improvement is in the agreement of H_2 and CH_4 mole fractions.

Figure 126 shows the C*, temperature, molecular weight, and specific heat ratio comparisons. All except the C* show better agreement with the data obtained with the updated model. The C* is underpredicted about 3 to 4% due to a 6 to 8% error in underpredicting the molecular weights. Closer agreement could be achieved with more effort but is not deemed warranted at this time.

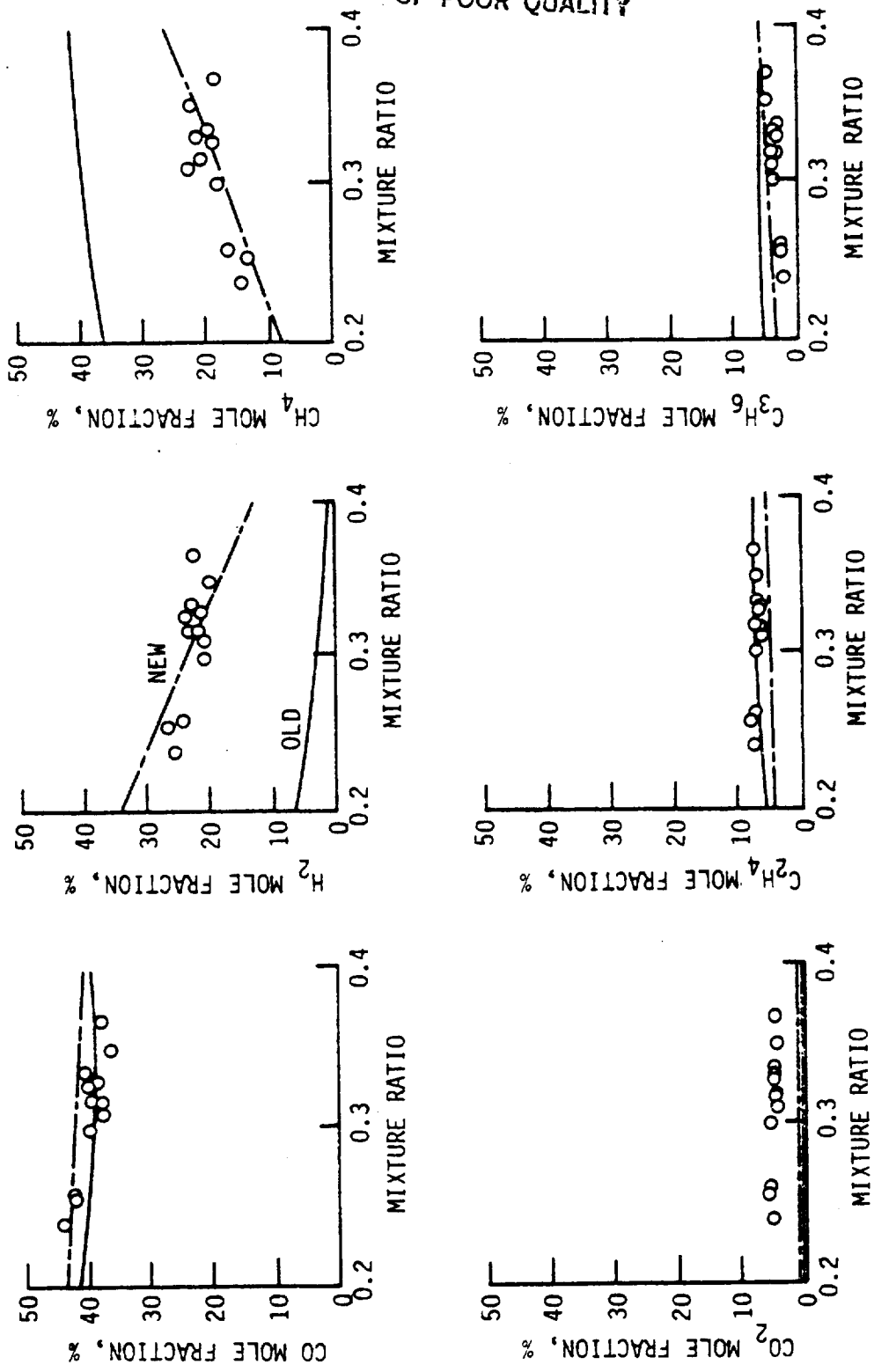

Figure 125. Comparison of Predicted and Measured Gas Compositions - Updated Model

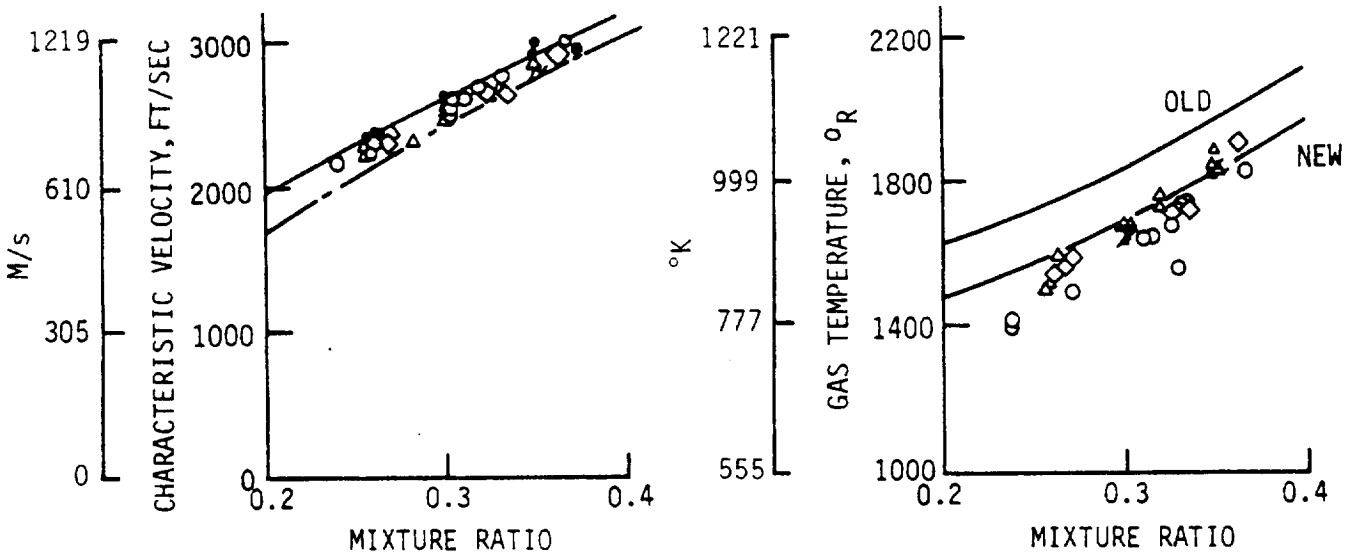

SYMBOL	INJECTOR	LENGTH	T.R.	T.S.	M.I.S.
○	EDM-LOL	787 mm (31 in.)	NO	NO	NO
△	SWIRL	787 mm (31 in.)	NO	NO	NO
◇	SWIRL	533 mm (21 in.)	NO	NO	NO
⊘	SWIRL	533 mm (21 in.)	YES	NO	NO
⋈	SWIRL	787 mm (31 in.)	YES	NO	NO
●	SWIRL	1168 mm (46 in.)	YES	YES	YES

SOLID LINE - OLD PREDICTION
CENTER LINE - NEW PREDICTION

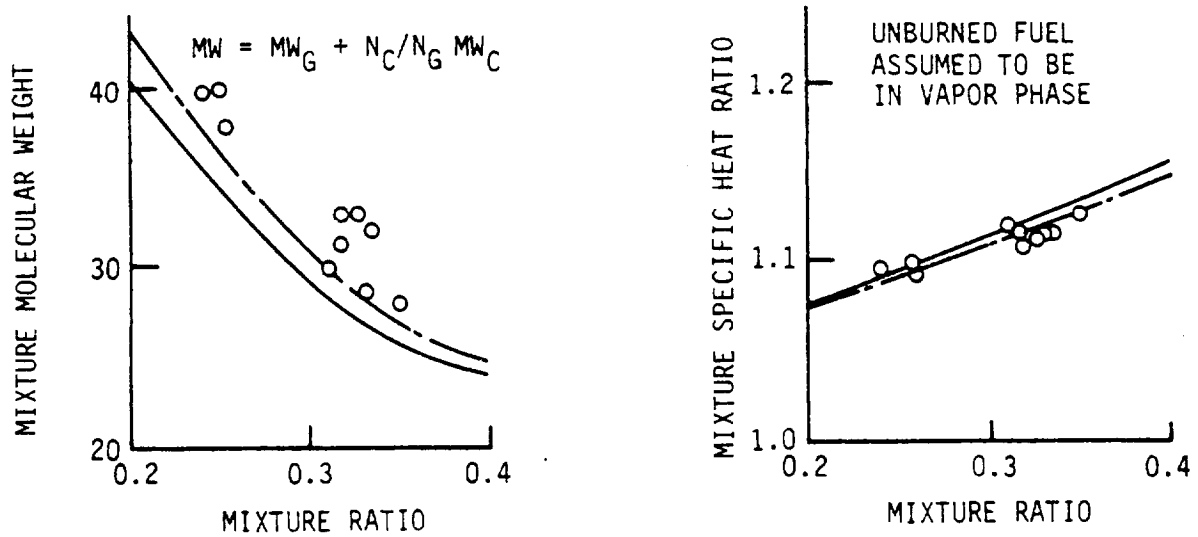

Figure 126. Comparison of Predicted to Measured Performance - Updated Model

REFERENCES

1. Schoenman, L. "Fuel/Oxidizer-Rich High-Pressure Preburners," Final Report, NASA CR-16544, NASA/Lewis Research Center, October 1981.

2. Jensen, D.E., "Soot Formation in Liquid Propellant Rocket Motors; A Basic Modeling Approach," Combustion Institute/European Symposium, 1973.

DISTRIBUTION LIST FOR FINAL REPORT - CR-165609
CONTRACT NAS 3-22647

Name	No. of Copies
National Aeronautics & Space Administration Lewis Research Center 21000 Brookpark Road Cleveland, Ohio 44135	
Attn: Contracting Officer, MS 500-306	1
Technical Utilization Office, MS 7-3	1
Technical Report Control Office, MS 5-5	1
AFSC Liaison Office, MS 501-3	2
Library, MS 60-3	2
Office of Reliability & Quality Assurance, MS 500-211	1
N. T. Musial, MS 500-318	1
H. J. Price, Project Manager, MS 501-6	10
E. A. Bourke, MS 501-5	5
T. Brabbs, MS 86-5	1
National Aeronautics & Space Administration Headquarters Washington, D.C. 20546	
Attn: Office of Aeronautics & Space Technology	
RS/Director, Manned Space Technology	1
RP/Director, Space Propulsion & Power	1
RW/Director, Materials & Structures	1
RTP-6/F. W. Stephenson	1
Attn: Office of Manned Space Flight MT/Director, Advanced Manned Mission	1
Attn: Office of Space Science	
SG/Director, Physics & Astronomy Programs	1
SL/Director, Planetary Programs	1
SV/Director, Launch Vehicles & Propulsion	1
Attn: Office of Technology Utilization Division KT/Director, Technology Utilization	1
National Aeronautics & Space Administration Ames Research Center Moffett Field, CA 94035 Attn: Library	1
National Aeronautics & Space Administration Flight Research Center P.O. Box 273 Edwards, CA 93523 Attn: Library	1
National Aeronautics & Space Administration Goddard Space Flight Center Greenbelt, MD 20771 Attn: Library	1
National Aeronautics & Space Administration George C. Marshall Space Flight Center Marshall Space Flight Center, AL 35812	
Attn: Library	1
J. L. Sanders/PD13	1
R. Richmond/EP24	1
J. A. Lombardo/EP21	1
C. R. Bailey/EP23	1
D. E. Pryor/EP23	1
National Aeronautics & Space Administration John F. Kennedy Space Center Kennedy Space Center, FL 32899 Attn: Library	1
National Aeronautics & Space Administration Lyndon B. Johnson Space Center Houston, TX 77058	
Attn: Library	1
EP2/M. F. Lausten	1
National Aeronautics & Space Administration Langley Research Center Hampton, VA 23665	
Attn: Library	1
J. A. Martin, MS 365	1

Name	No. of Copies
NASA Scientific & Technical Information Facility P.O. Box 8757 Baltimore-Washington Intnl. Airport Baltimore, MD 21240 Attn: Accessioning Department	10
Office of the Director of Defense Research & Engineering Washington, D.C. 20301 Attn: Office of Assistant Director (Chemical Technology)	1
Jet Propulsion Laboratory 4800 Oak Grove Drive Pasadena, CA 91103 Attn: Library	1
Defense Documentation Center Cameron Station, Bldg 5 5010 Duke St. Alexandria, VA 22314 Attn: TISIA	1
Advanced Research Projects Agency Washington, D.C. 20525 Attn: Library	1
Aeronautical Systems Division Air Force Systems Command Wright-Patterson Air Force Base Dayton, Ohio 45433	
Attn: Library	1
E. E. Bailey	1
Air Force Rocket Propulsion Laboratory (RPM) Edwards, CA 93523 Attn: Library	1
Air Force FTC (FTAT-2) Edwards Air Force Base, CA 93523 Attn: Library	1
Air Force Office of Scientific Research 1400 Wilson Blvd. Arlington, VA 22209 Attn: Library	1
U.S. Air Force, Office of Information Office of Sec. of Air Force The Pentagon Washington, D.C. 20333 Attn: Library	1
Air Force Aero Propulsion Laboratory Research & Technology Division U.S. Air Force Systems Command Wright Patterson AFB, Ohio 45433 Attn: Library (APRP)	1
Arnold Engineering Development Center Air Force Systems Command Tullahoma, TN 37388 Attn: Library	1
Bureau of Naval Weapons Department of the Navy Washington, D.C. Attn: Library	1
U.S. Naval Research Laboratory Washington, D.C. 20390 Attn: Library	1
U.S. Army Research Office (Durham) Box OM, Duke Station Durham, NC 27706 Attn: Library	1

DISTRIBUTION LIST FOR FINAL REPORT - CR 165609
CONTRACT NAS 3-22647

Name	No. of Copies
U.S. Army Missile Command Redstone Scientific Information Center Redstone Arsenal, AL 35808 Attn: Document Section	1
U.S. Naval Missile Center Point Mugu, CA 93041 Attn: Technical Library	1
U.S. Naval Weapons Center China Lake, CA 93557 Attn: Library	1
Aro Incorporated Arnold Engineering Development Center Arnold AF Station, TN 37389 Attn: Library	1
Battelle Memorial Institute 505 King Avenue Columbus, Ohio 43201 Attn: Library	1
Bell Aerosystems Inc. Box 1 Buffalo, NY 14240 Attn: Library	1
Boeing Company, Space Division P.O. Box 868 Seattle, WA 98124 Attn: Library	1
Chemical Propulsion Information Agency Applied Physics Laboratory 8621 Georgia Avenue Silver Spring, MD 20910	1
Chrysler Corporation Space Division P.O. Box 29200 New Orleans, LA 70129 Attn: Library	1
General Dynamics/Convair P.O. Box 1128 San Diego, CA 92112 Attn: Library	1
General Electric Company Missiles & Space Systems Center Valley Forge Space Tech. Center P.O. Box 8555 Philadelphia, PA 19101 Attn: Library	1
Grumman Aerospace Corp. Bethpage, L.I., NY 11714 Attn: Library	1
Ling-Temco-Vought Corporation P.O. Box 5907 Dallas, TX 75222 Attn: Library	1
Lockheed Missiles & Space Co. P.O. Box 504 Sunnyvale, CA 94088 Attn: Library	1
Marquardt Corporation 16555 Saticoy Street Box 2013 South Annex Van Nuys, CA 91409 Attn: Library	1
Martin-Marietta Corp. P.O. Box 179 Denver, CO 80201 Attn: Library	1
McDonnell Douglas Astronautics 5301 Bolsa Avenue Huntington Beach, CA 92547 Attn: Library	1
Philco-Ford Corporation Aeronautics Div. Ford Rd. Newport Beach, CA 92663 Attn: Library	1
Purdue University Lafayette, IN 47907 Attn: Library	1
Rocketdyne A Div. of Rockwell Corp. 6633 Canoga Avenue Canoga Park, CA 91304 Attn: Library G. Bremer F. M. Kirby	1 1 1
Rocket Research Corporation Willow Road at 116th Street Redmond, WA 98052 Attn: Library	1
Thiokol Chemical Corporation P.O. Box 1000 Newton, PA 18940 Attn: Library	1
TRW Systems, Inc. 1 Space Park Redondo Beach, CA 90278 Attn: Library	1
United Aircraft Corporation Pratt & Whitney Division Florida Research & Development Center P.O. Box 2691 West Palm Beach, FL 33402 Attn: Library	1
United Technologies Research Center East Hartford, CT Attn: Library	1